MASTER RESEARCH PROJECT
ASTRONOMY, MATHEMATICS AND PHYSICS
21 AUGUST 2014

STATISTICS OF CAUSTICS IN LARGE-SCALE STRUCTURE FORMATION

KAPTEYN ASTRONOMICAL INSTITUTE

JOHAN BERNOULLI INSTITUTE

& CENTRE FOR THEORETICAL PHYSICS

UNIVERSITY OF GRONINGEN
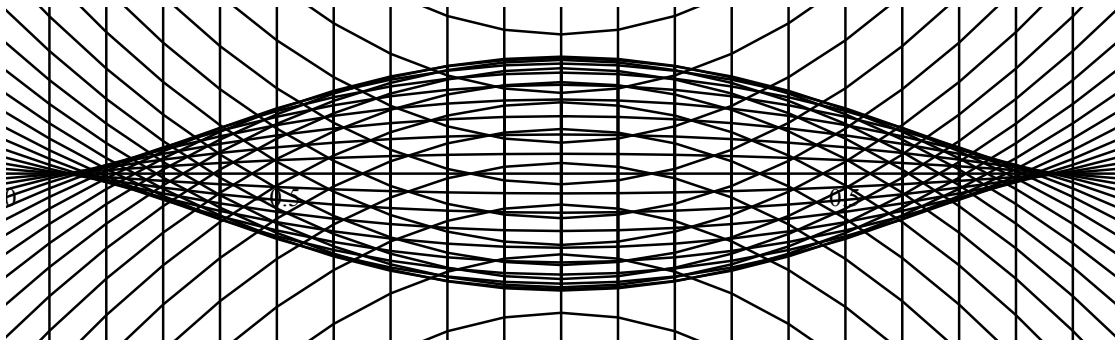
Author:
Job Feldbrugge

Supervisors:
Prof. dr. M.A.M. van de Weygaert, Kapteyn Astronomical Institute
Prof. dr. A.C.D. van Enter, Johann Bernoulli Institute
Dr. D. Roest, Centre for Theoretical Physics

Statistics of Caustics in Large-Scale Structure Formation

Job Feldbrugge

*Kapteyn Astronomical Institute, Johann Bernoulli Institute &
Center for Theoretical Physics*

University of Groningen

21 August 2014

Abstract

There have been many attempts to explain how the large-scale structure of our cosmos has formed and is developing. We are, however, still unable to make an unambiguous classification of features of the cosmic web or make qualitative predictions. The usual approach to model large-scale structure formation is to assume that in the very early universe, the baryonic and dark matter was distributed in a certain way and that this matter distribution then evolved according to certain mechanics into the universe as we observe it now. In my thesis, I assume that the initial matter distribution can be modeled by Gaussian random fields. For the evolutionary mechanics, I use Lagrangian fluid dynamical approximations. In these approximations, layers of matter will flow through each other, a process called shell-crossing, which creates regions of infinite density, called caustics. These caustics can be seen as a skeleton of the cosmic web, both in the initial conditions as in the current large-scale structure. In my thesis, I look at the role of these caustics in structure formation, compare the caustics skeleton to numerical simulations of the cosmic web and try to make qualitative predictions of the skeleton as function of the initial distribution of the perturbations. We first concentrate on the linear Lagrangian approximation, known as the Zel'dovich approximation, and subsequently extend our approach to higher corrections and effective field theories. In particular, I try to estimate the length of lines and density of vertices in the skeleton in the early and present day universe.

Contents

Acknowledgements

Chapter 1

Introduction

Mankind has always been fascinated by questions about its own origin. Where do we come from and how did the universe come about? Did time start at some instant and is there an end of time? Until the start of the twentieth century, answers to these questions remained merely philosophical. Newton's law of gravitation was simply not sufficient to model the evolution of the universe. However, since the discovery of general relativity by Albert Einstein in 1916, this has dramatically changed. Cosmology has developed into an exciting science with many revolutionary new insights, often rewarded with Nobel Prizes.

Using Einstein's theory of general relativity, the Russian physicist Alexander Friedmann derived equations that describe the expansion of space in homogeneous and isotropic models of the universe. In such models, a universe can expand and contract; it can have a beginning and an ultimate end. Final proof in favor of a universe with a beginning – a Big Bang – was found by Arno Penzias and Robert Wilson. They observed the afterglow emitted by some hot medium, present at some earlier epoch. For this (accidental!) observation Penzias and Wilson were awarded with a Nobel Prize. The afterglow, or radiation field, they observed is nowadays known as the cosmic microwave background. It is a relic of the early universe. Many more detailed studies followed. The most recent complete survey was performed with the Planck satellite and its observation is depicted in figure 1.1. This figure shows the density fluctuations in the early universe or, to be more precise, at the moment the universe became neutral.

Not only the past, but also the present universe can nowadays be observed in great detail. The Sloan Digital Sky Survey (SDSS) and the two-degree-Field Galaxy Redshift Survey (2dF) are, at the moment, the most complete surveys of the galaxy distribution at the mega parsec scale (see figure 1.2). In the depicted observations we can distinguish a very striking structure: the cosmic web (or large-scale structure). This web contains points, lines and surfaces, that are commonly referred to as clusters, filaments and walls. These structures are largely in agreement with simulations of the current universe, as predicted based on the early universe density fluctuations, mentioned earlier (see for example the Millennium simulation in figure 1.3).

In the last decades, analyses of the cosmic microwave background have led to many
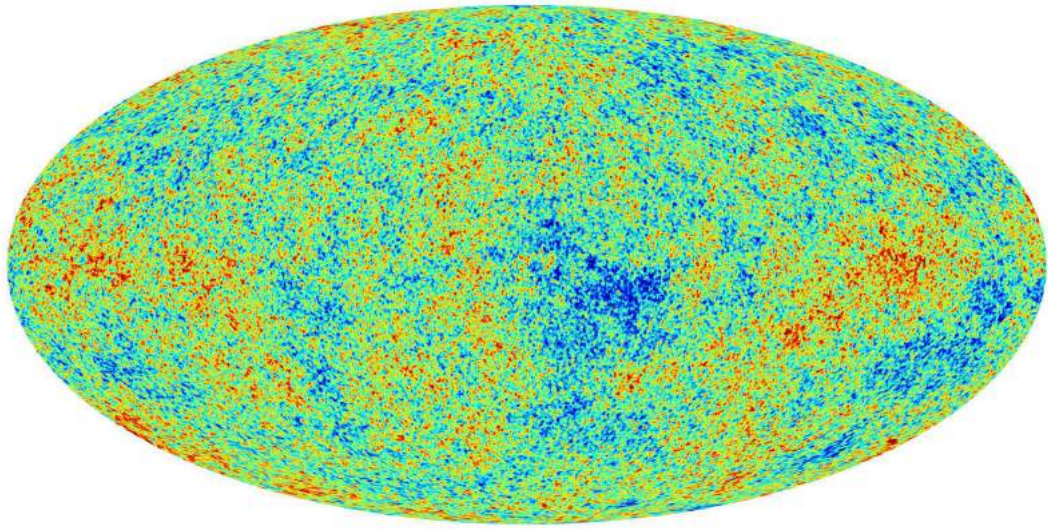
Figure 1.1: The cosmic microwave background observed with the Planck satellite
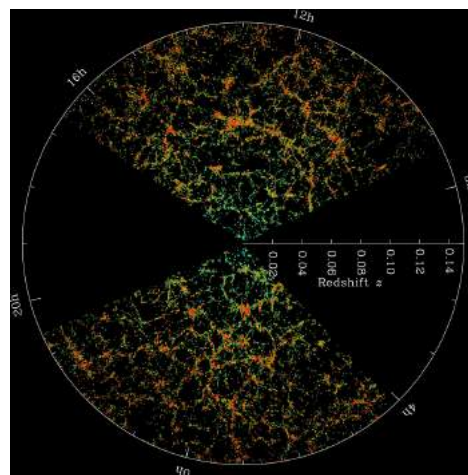
(a) Slices through the SDSS 3-dimensional map of the distribution of galaxies
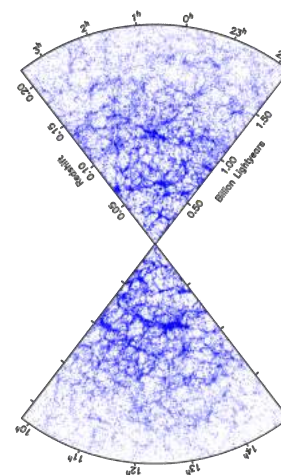
(b) Slices through the two-degree-Field Galaxy Redshift Survey

Figure 1.2: Large scale structure surveys
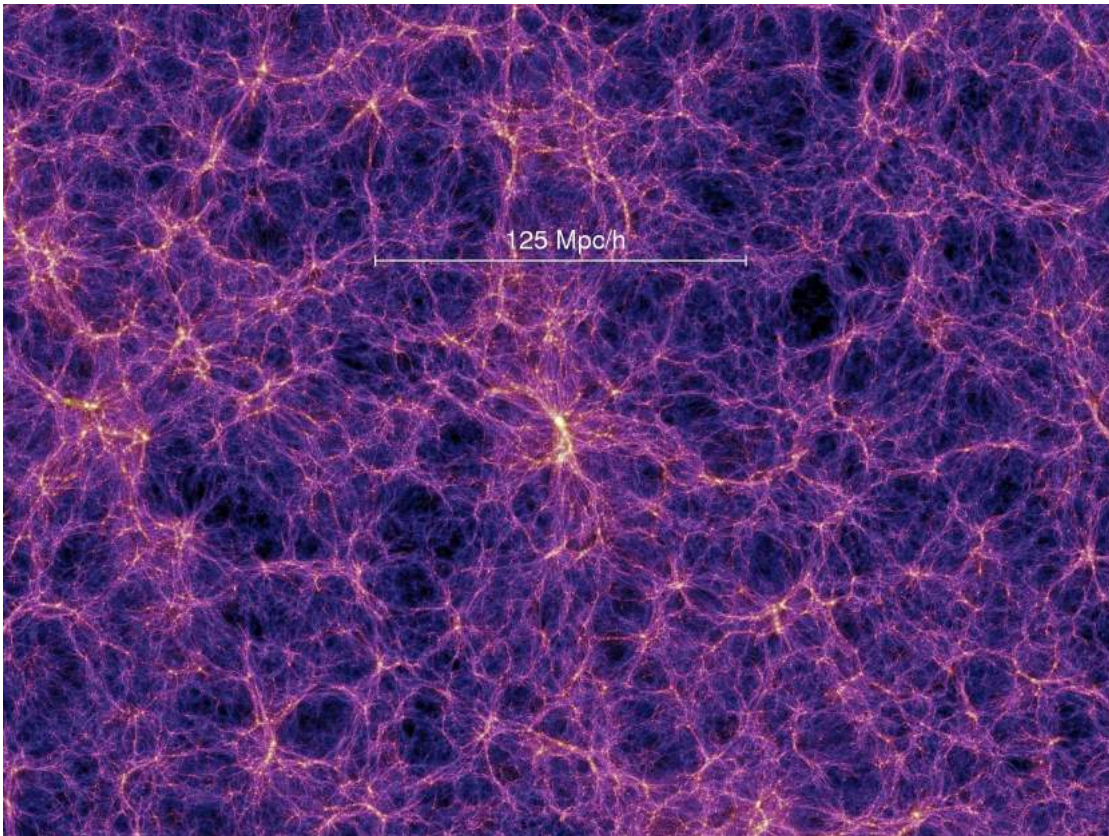
Figure 1.3: A slice through the Millennium simulation

insights in the physics of the early universe; our universe originated at the Big Bang, expanded and cooled down. In this process tiny fluctuations were generated that have led to the large-scale structure we observe today. Although the formation of this cosmic web is a nonlinear process, in principle these structures still contain information about the early universe. Hence, a detailed analysis of the cosmic web may give us clues about the physics just after the Big Bang. In this thesis, we try to recover this information by estimating the number density of clusters and the length of filaments, as a function of the initial fluctuations in the cosmic microwave background. This may in the end tell us about the current universe as well as about its beginning.

In this initial investigation we use the Zel'dovich approximation to model large-scale structure formation. The Zel'dovich approximation is a linear Lagrangian fluid dynamical approximation proposed in 1970 by Zel'dovich [72]. It assumes that the fluid elements move in straight lines with directions and velocities determined at the initial time and do not feel the gravitational force of its environment at later points in time. This approximation of nature is adequate up to the mildly non-linear regime, when clusters and filaments start to form. During the further evolution of clusters and filaments it however becomes invalid, since in nature matter is supposed to turn around and stick to a filament or cluster.

It furthermore predicts the location and time at which filaments or clusters starts to form. Structures are supposed to form in regions where matter flows pass through each other, resulting in so-called caustics. This process is completely analogous to the creation of caustics in optical systems and can be analyzed and classified by Lagrangian catastrophe theory developed by Vladimir Arnol'd. In 1982 Arnol'd, Shandarin and Zel'dovich [6] found conditions on the initial gravitational field for the formation of caustics.

In this thesis we combine these caustics conditions with geometric statistics of the initial density perturbations modeled by Gaussian random fields. Geometric statistics of stationary random processes were first investigated in 1936 by Stephen Rice. He analyzed level crossings of noise in communication devices. Here we use an extended analysis in which time is replaced by $\mathbb{R}^2$, or $\mathbb{R}^3$, and the random process is called a Gaussian random field. Under certain conditions we can ensure the field to be smooth and calculate number densities of point statistics and average lengths of level sets. In this way we calculate statistics of the caustics predicted by the Zel'dovich approximation.

Although the Zel'dovich approximation can serve as a first investigation of the role of caustics in large-scale structure formation, it has its limitations in collapsed regions. In this thesis we determine the role of caustics in Eulerian and Lagrangian effective field theory. This new perturbation scheme in the study of large-scale structure formation is an approach commonly used in high energy physics. We model the small scale physics as an imperfect fluid, and in this way include the influence of the small scale on the large scale, reaching more accurate results than obtained through standard perturbation theory.

The research that has led to this thesis has been supervised by professor Rien van der Weygaert (cosmology), professor Aernout van Enter (statistical mechanics) and dr.

Diederik Roest (string cosmology). This thesis has a clear astronomical, mathematical and physical component.

- In chapters 2, 3, 4, 5, 6, 9, and 14 we discuss the process of large scale structure formation and the creation of caustics in the Zel'dovich approximation. Numerically determined statistics are presented in chapter 14. These chapters are mainly on the topic of astronomy.

- In chapters 7, 8, 10, 11, 12, and 13 we formally discuss catastrophe theory, Gaussian random field theory, and geometric statistics on them. We furthermore present analytic statistics of caustics in Gaussian random fields. These chapters are primarily mathematical.

- Finally, in chapters 15, 16, 17, 18, and 19 we discuss the application of effective field theory to the study of large scale structure and, in specific, caustics. These chapters are mostly about physics.

This division of the chapters is far from absolute, as is the division between the sciences. The chapters should be seen as a unit: the mathematical and physical chapters are intertwined with the astronomy chapters. Combined, they tell the story of my exploration of the role and use of caustics in the study of the cosmic web.

Chapter 2

Cosmology

Cosmology is one of the oldest branches of science. For centuries, mankind has been trying to understand the origin, nature and eventually the end of our universe. For a long time, cosmology remained in the realm of religion and philosophy. However, in 1916, Albert Einstein changed this for good by publishing his theory of general relativity [25]. General relativity became the framework in which precise cosmological predictions could be made, making cosmology a physical discipline.

According to Einstein, space and time are dynamical quantities. According to the work of Alexander Friedmann in 1922, this also made the universe itself dynamic [28]. The universe could be expanding or contracting, originating, and even ending at some definite time. The dynamics of large scales satisfies the so called Friedmann equations. However, the scientific community was not yet ready for a dynamical universe when general relativity appeared. Einstein introduced a cosmological constant to stabilize his universe and remove the dynamics. In 1929, Edwin Hubble published a paper in which he presented observations of the redshift of several stars as function of their distance [36]. This indicated a systematic velocity of galaxies moving away from us. The Roman Catholic priest Georges Lemaître had already two years earlier interpreted such a distance-redshift relation as proof of the expansion of the universe [41]. After some years Einstein removed his cosmological constant and declared it to be his greatest blunder. This became the starting point of a physical debate about the evolution of the universe. Is the universe a stable object which has always existed, or did it have a beginning and would it someday even end?

The debate about the evolution of the universe was finally decided in 1965 by accidental observations of the two radio astronomers Arno Penzias and Robert Wilson [52]. George Gamow studied dynamic universes under Friedmann in the years before his death. Gamow continued his scientific career by studying tunneling in alpha- and beta-decay. In 1948 he revisited his study of the universe with Ralph Alpher by analyzing the matter content produced during the early universe. This lead to the α-β-γ-paper [3] describing the production of the light elements in the universe. Shortly afterwards Ralph Alpher and Robert Herman predicted an afterglow of a hot early epoch of the universe currently present as a black body spectrum with a temperature of $T = 5K$ [2]. This

work remained ignored for many years. Around 1964, Penzias and Wilson had started the construction of a radio telescope to perform satellite communication experiments. During these observations they observed an excess noise of about 3 Kelvin, which they could not remove or account for. After a telephone call with professor Robert Dicke at Princeton University, the noise was found to be a remnant of an early hot phase of the universe, for which Robert Dicke was looking. Penzias, Wilson and Dicke wrote two separate papers describing the observation [69] and explanation [22]. This remnant is nowadays called the Cosmic Microwave Background radiation (CMB). This discovery led to a Nobel prize in physics for Penzias and Wilson in 1974.

From these early observations of the CMB, the astronomical community concluded that the CMB contains a vast amount of information about our Universe. Many more detailed observations of the CMB followed. The most recent measurements were made with the European Space Agency (ESA) Planck satellite. Extensive measurements of the CMB have unleashed a revolution in cosmology. It is the earliest observable image of our universe and has had a great influence on the development of the Big Bang theory and structure formation models. In this chapter we give a description of cosmology. We start with general relativity, derive the Friedman equations and study some cosmological models. We finish with the concordance model, which is a Friedmann model with good agreement with observational data. In this chapter we largely follow 'A short course in General Relativity' by James Foster and J. David Nightingale [27] and an 'Introduction to Cosmology' by Barbara Ryden [60].

2.1   Einstein field equations

In 1905 Einstein published his famous theory of special relativity. According to special relativity the speed of light in vacuum is universal and therefore independent of the velocity of an observer. This is in clear conflict with Newtonian physics, in which one has to add the observer's speed to the speed of light. Special relativity therefore forms a correction to Newton's dynamics when velocities close to the speed of light are considered. Special Relativity has so far been in perfect agreement with observations in which gravity is relatively weak. However, the introduction of these corrections also led to the inescapable conclusion that space and time, now called spacetime, can be mixed in a very special way and that the speed of light c is the maximum speed at which information can travel.

After the triumph of special relativity a new problem appeared. Einstein's new theory was in conflict with Newton's law of gravitation. According to Newton, a change in the mass of an object and thus in its gravitational field, would instantaneously be effective throughout space, whereas special relativity predicted a finite speed limit on information. In order to resolve this issue Einstein proposed his theory of general relativity to replace Newton's law of gravitation.

According to general relativity, energy, momentum and pressure densities described in the energy momentum tensor $T_{\mu\nu}$ (as illustrated in figure 2.1) possess the power to bend spacetime. To be more precise, the curvature of space-time can be described by
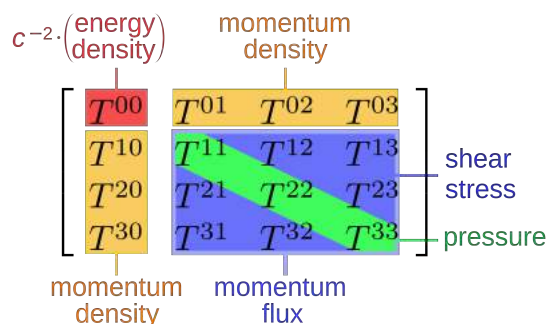
Figure 2.1: The Stress Energy Tensor

the metric tensor $g_{\mu\nu}$ which defines the distance $\mathrm{d}s$ between points via

$$\mathrm{d}s^2 = \sum_{\mu\nu} \mathrm{d}x_\mu \mathrm{d}x_\nu g^{\mu\nu} = \mathrm{d}x_\mu \mathrm{d}x_\nu g^{\mu\nu}.$$

This definition should be seen as a generalization of the Pythagorean theorem. Starting from the metric tensor $g_{\mu\nu}$ we can compute the Ricci tensor $R_{\mu\nu}$ defined as

$$R_{\mu\nu} = \Gamma^\sigma_{\mu\sigma,\nu} - \Gamma^\sigma_{\mu\nu,\sigma} + \Gamma^\rho_{\mu\sigma}\Gamma_{\rho\nu}\sigma - \Gamma^\rho_{\mu\nu}\Gamma^\sigma_{\rho\sigma},$$

with the Christoffel symbol

$$\Gamma_{\sigma\mu\nu} = \frac{1}{2}(g_{\sigma\mu,\nu} + g_{\sigma\nu,\mu} - g_{\mu\nu,\sigma}).$$

Finally, the Ricci curvature scalar is given by

$$R = g^{\mu\nu}R_{\mu\nu}.$$

In these equations, we use the shorthand $g_{\mu\nu,\sigma} = \frac{\partial g_{\mu\nu}}{\partial x_\sigma}$ and use the Einstein summation convention which states that all dummy indices are summed over.

The bent spacetime in turn influences the movement of objects and therefore influences the energy distribution. The exact interplay between energy and spacetime is described by the Einstein field equations

$$R_{\mu\nu} - \frac{1}{2}Rg_{\mu\nu} = \frac{8\pi G}{c^4}T_{\mu\nu}, \text{ with } \mu,\nu = 0,1,2,3,$$

where G is Newton's gravitational constant and c is the speed of light in vacuum.

2.2   Friedmann equations

The Einstein field equations form a complicated system of nonlinear differential equations. These equations are valid for slow moving particles with weak gravitational fields

as well as physical situations with object approaching the speed of light in strong gravitational fields such as black holes. However, Einstein's field equations can also model the evolution of the universe as a whole. Assuming a completely homogeneous and isotropic universe, nowadays part of the cosmological principle, Alexander Friedmann, in 1922 [28], and later independently Georges Lemaître, in 1927 [41], derived expressions for such models of the universe.

The imposed symmetry on space kand time restricts the freedom of the metric $g_{\mu\nu}$ considerably. Roberson and Walker proved that the metric in a universe satisfying the cosmological principle in polar coordinates r, θ, ϕ must be of the form of the Robertson-Walker metric

$$\mathrm{d}s^2 = g_{\mu\nu}x^\mu x^\nu = \mathrm{d}t^2 - R(t)^2 \left((1 - kr^2)^{-1}\mathrm{d}r^2 + r^2\mathrm{d}\theta^2 + r^2 \sin^2\theta\mathrm{d}\phi^2\right),$$

with $R(t)$ the curvature radius, $x^\mu = (t, r, \theta, \phi)$ the space-time coordinates and $k = -1, 0, 1$ describing the geometry of the universe, respectively hyperbolic, flat and spherical space. In this expression and the expressions that will follow we chose dimensions such that the speed of light $c = 1$. Friedmann furthermore assumed that the universe is filled with a perfect fluid, free of shear-viscosity, bulk-viscosity or heat-conducting properties. The energy-momentum tensor of such a fluid is

$$T_{\mu\nu} = (\rho + p)u_\mu u_\nu - pg_{\mu\nu},$$

with ρ the density, p the pressure, $g_{\mu\nu}$ the metric and u_μ the velocity of the fluid.

Using the differential geometry machinery we can compute the corresponding Christoffel symbols. The nonzero components with implied symmetry $\Gamma^\mu_{\nu\sigma} = \Gamma^\mu_{\sigma\nu}$ are

$$\begin{aligned}
&\Gamma^0_{11} = R\dot{R}/(1 - kr^2), &&\Gamma^0_{22} = R\dot{R}r^2, &&\Gamma^0_{33} = R\dot{R}r^2 \sin^2\theta, \\
&\Gamma^1_{11} = kr/(1 - kr^2), &&\Gamma^1_{22} = -r(1 - kr^2), &&\Gamma^1_{33} = -r(1 - kr^2)\sin^2\theta, \\
&\Gamma^2_{12} = \Gamma^3_{13} = 1/r, &&\Gamma^2_{33} = -\sin\theta\cos\theta, &&\Gamma^3_{23} = \frac{1}{\tan\theta}, \\
&\Gamma^1_{01} = \Gamma^2_{02} = \Gamma^3_{03} = \dot{R}/R,
\end{aligned}$$

with $\dot{R} = \frac{\partial R}{\partial t}$. These Christoffel symbols can be used to compute the Ricci tensor, whose nonzero components are

$$\begin{aligned}
R_{00} &= 3\ddot{R}/R, \\
R_{11} &= -(R\ddot{R} + 2\dot{R}^2 + 2k)/(1 - kr^2), \\
R_{22} &= -(R\ddot{R} + 2\dot{R}^2 + 2k)r^2, \\
R_{33} &= -(R\ddot{R} + 2\dot{R}^2 + 2k)r^2 \sin^2\theta.
\end{aligned}$$

Since all diagonal terms of the Ricci tensor are zero, we are only interested in the trace of the energy-momentum tensor for the Einstein field equations

$$T = T^\mu_\nu g^\nu_\mu = (\rho + p)u_\mu u_\nu g^{\mu\nu} - 4p = \rho - 3p,$$

since from special relativity we know that $u_\mu u_\nu g^{\mu\nu} = 1$. After substitution of these expressions in the Einstein field equations we obtain two independent differential equations

$$3\ddot{R}/R = -4\pi G(\rho + 3p)$$
$$R\ddot{R} + 2\dot{R}^2 - 16\pi G = 4\pi G(\rho - p).$$

Eliminating $\ddot{R}$ from these equations and writing R in terms of the Hubble parameter H and the normalized scale parameter a

$$a = \frac{R(t)}{R_0},$$
$$H(t) = \frac{\dot{R}}{R} = \frac{\dot{a}}{a},$$

with R_0 the current curvature, we obtain the Friedmann equations

$$H^2 = \left(\frac{\dot{a}}{a}\right)^2 = \frac{8\pi G}{3}\rho - \frac{kc^2}{R_0^2 a^2},$$
$$\frac{\ddot{a}}{a} = -\frac{4\pi G}{3}\left(\rho + \frac{3P}{c^2}\right).$$

The second equation is often combined with the first to obtain the conservation of energy

$$0 = \dot{\rho} + 3\frac{\dot{a}}{a}(\rho + Pc^2).$$

In this equation a denotes the scale of the universe, $\dot{a} = \frac{da}{dt}$ and $\ddot{a} = \frac{d^2a}{dt^2}$ its time derivatives, H is the Hubble parameter known from the Hubble law, ρ denotes the sum of the energy densities (composed out of matter, radiation and dark energy), while $k = 0, 1$ or -1 for a flat, a spherical or a hyperbolic universe respectively. The factor R_0 denotes the current radius of curvature. The factor P in the second equation describes the pressure in the universe.

In order to completely solve the Friedmann equations, one has to know the nature of the energy densities making up the energy content curving the universe. The behavior of energy during the evolution of our universe is encoded in the second Friedmann equation in combination with the equation of state $P = w\rho$. For baryonic and cold dark matter w is well approximated by 0, while for radiation $w = 1/3$. For dark energy the factor w is not well known. It should be smaller then $-1/3$ in order to generate an accelerated expanding universe and greater than -1 in order to satisfy causality. Dark energy is often equivalent to a cosmological constant by which $w = -1$. The equations of state in combination with the second Friedmann equation lead to the conclusion that the matter density in the universe dilutes like a^{-3}, while radiation dilutes like a^{-4}. The dark energy content with equation of state parameter $w = -1$ remains constant during the expansion of space-time. This is the reason that we may suspect that the cosmological constant is a property of space-time it self.

Assuming the presence of a cosmological constant, the Friedmann equations can be rewritten as

$$\frac{H^2}{H_0^2} = \frac{\Omega_{r,0}}{a^4} + \frac{\Omega_{m,0}}{a^3} + \Omega_{\Lambda,0} + \frac{1 - \Omega_0}{a^2},$$

with Hubble parameter H, current Hubble parameter H_0, current radiation density $\Omega_{r,0} = \rho_{r,0}/\rho_{c,0}$, current matter density $\Omega_{m,0} = \rho_{m,0}/\rho_{c,0}$, current dark energy density $\Omega_{\Lambda,0} = \rho_{\Lambda,0}/\rho_{c,0}$ and current energy density $\Omega_0 = \Omega_{r,0} + \Omega_{m,0} + \Omega_{\Lambda,0}$. The current critical density $\rho_{c,0} = \frac{3H_0^2}{8\pi G}$ is the energy density necessary to make our universe flat ($k = 0$). This form of the Friedmann equations is most convenient in large scale structure formation, since it explicitly describes the evolution of the universe in terms of measurable cosmological parameters.

2.3 Cosmological toy models

As described above, the energy content and geometry of the universe determine the large-scale evolution of the universe. Radiation, baryonic matter and dark matter slow the expansion down whereas the dark energy or cosmological constant accelerate the expansion. In this section we study some solutions of the Friedman equations describing the evolution of different models of the universe.

We start with the radiation, matter-dominated (Einstein-de Sitter) and dark-energy dominated (de Sitter) model after which we describe the concordance model which is based on the Planck satellite observations.

2.3.1 Radiation-dominated universe

After the big bang, the universe went through a phase in which all particles moved with velocities close to the speed of light. The particles were relativistic and contributed to the energy content of the universe in the form of radiation. During this epoch the evolution of the universe can be modeled by a flat, radiation-only universe. Under these assumptions the Friedmann equations simplify to

$$\frac{H^2}{H_0^2} = \frac{\dot{a}^2}{H_0^2 a^2} = \frac{1}{a^4}.$$

This differential equation is equivalent to

$$\dot{a} = \frac{H_0}{a},$$

and can be solved by

$$a(t) = \left(\frac{t}{t_0}\right)^{1/2},$$

with t_0 the current age of the universe.

2.3.2   Einstein-de Sitter universe

One of the earliest epochs of our universe can be modeled by a flat radiation-dominated universe. However since the radiation density evolves as a^{-4} whereas the matter density evolves as a^{-3} there exists a time at which the matter density of the universe becomes more important than the radiation density. At this epoch we model the universe by a flat-matter-only model. This model is commonly known as the Einstein-de Sitter universe. In an Einstein-de Sitter universe, the Friedmann equation simplifies to

$$\frac{H^2}{H_0^2} = \frac{\dot{a}^2}{H_0^2 a^2} = \frac{1}{a^3}.$$

This differential equation is equivalent to

$$\dot{a} = \frac{H_0}{a^{1/2}},$$

and can be solved by

$$a(t) = \left(\frac{t}{t_0}\right)^{2/3}.$$

2.3.3   De Sitter universe

A radiation-dominated phase in which $a \propto t^{1/2}$ followed by a matter-dominated phase in which $a \propto t^{2/3}$ was the generally accepted model of cosmology until 1993-1997. However, in 1998 the High-Z Supernova Search Team led by Brian Schmidt and Adam Reiss [58] and the Supernova Cosmological Project led by Perlmutter found evidence for an accelerated expansion [53]. This discovery led to new interest in the cosmological constant or a dark energy component. In the current model of cosmology we think that the matter-dominated phase is followed by a flat dark-energy-dominated phase, first studied by Willem de Sitter and often called the de Sitter universe.

In a flat dark-energy-dominated universe with $w = -1$ (a cosmological constant), the Friedmann equation simplifies to

$$\frac{H^2}{H_0^2} = \frac{\dot{a}^2}{H_0^2 a^2} = 1.$$

This differential equation is equivalent to

$$\dot{a} = H_0 a,$$

and can be solved by

$$a(t) = e^{H_0(t-t_0)}.$$
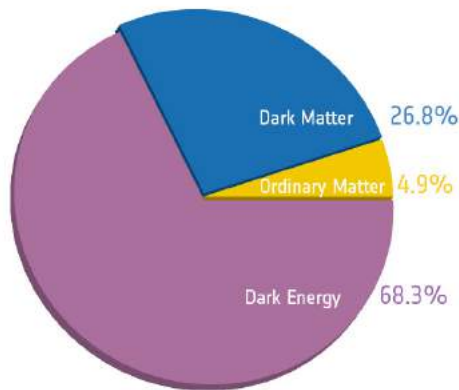
(a) Energy content of the universe estimated by the Planck satellite, credit: ESA/Planck
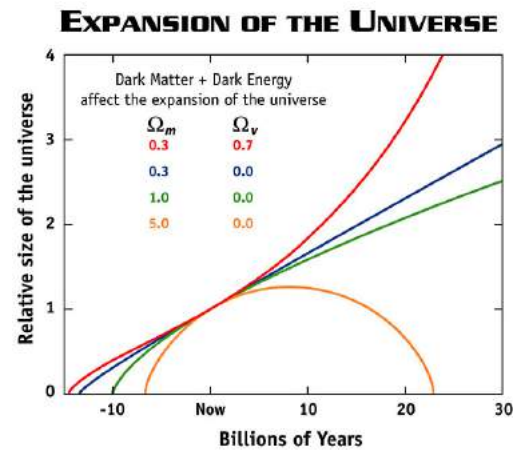
(b) The expansion of the universe, credit: WMAP

2.4 The concordance model

The models above give us insight in the behavior of the Friedmann equations. However, in reality we live in a universe composed of radiation, dark matter, baryonic matter, and dark energy. Observations of the cosmic microwave background with the Planck satellite indicate that our universe is nearly flat and is currently composed for 4.9% out of baryonic matter, for 26.8% dark matter and for 68.3% dark energy (see figure 2.2a). This model is often called the dark energy, cold dark matter model ΛCDM. The universe first went through a radiation-dominated phase in which $a \propto t^{1/2}$, followed by a matter-dominated phase in which $a \propto t^{2/3}$ after which the universe evolved as a de Sitter universe in which $a \propto e^{H_0 t}$. In figure 2.2b we illustrate the expansion history of different cosmological models. The yellow red illustrates the concordance model. The universe was born 13.798 ± 0.037 billion years ago and will forever keep expanding and accelerating.

2.4.1 Open problems in cosmology

In the twentieth century and the start of the twenty-first century we have greatly extended our understanding of the evolution of the universe on the largest scales. The universe was born 13.798 ± 0.037 billion years ago, and expanded to our current universe. However, there are many remaining questions. For example, what is the source and nature of dark matter and dark energy? How does the large-scale cosmology influence the structure in the universe? There are also fine-tuning problems within the ΛCDM model. The extreme flatness of our universe and the homogeneity of the CMB are very special and unlikely circumstances in the concordance model. These problems are well known as the flatness and horizon problems. One of the proposed explanations for these problems is formed by a process called inflation. Inflation theory has however so far not been explained by some fundamental theory.

Chapter 3

Large-Scale Structure Formation

In chapter 2 we described homogeneous and isotropic solutions of the Einstein field equations. These models of the universe are completely specified by the scale factor a which is a function of time. The universe as we observe it today, contains a lot more structure. The solar system is far from homogeneous or isotropic. The cosmological principle is a good approximation only at scales substantially larger than 100 Mpc. On smaller scales several surveys, including the Sloan Digital Sky Survey (SDSS), have detected an intricate weblike structure composed out of galaxies. This structure is commonly called the large-scale structure (LSS) of the universe or the comic web. It originated from small fluctuations which are still observable as small temperature fluctuations in the cosmic microwave background radiation field.

In this chapter we describe the evolution of small density fluctuations upon a homogeneous and isotropic Friedmann universe. In principle this should be done in a general relativistic setting. We will here however only consider the Newtonian limit. We start with the Boltzmann equation and derive the differential equations governing the evolution. We subsequently study Lagrangian approximations. We in particular concentrate on the linear Lagrangian approximation, i.e. Zel'dovich Approximation (ZA) proposed in 1970 by Zel'dovich [72]. In the last part of this thesis, we use these equations to build an effective field theory of large-scale structure formation.

3.1   The Boltzmann equation

The concordance model, described in the previous chapter, consists of radiation, matter (dark and baryonic) and dark energy. The formation of the large-scale structure has taken place in the matter and dark energy dominated eras. For this reason we will neglect the influence of radiation on structure formation. Although the nature of baryonic matter and dark matter differ greatly, i.e. baryonic matter couples to the electro-magnetic field whereas dark matter does not, we will not distinguish between the two in our models. We do not know the precise properties of dark matter. We however do know that there is approximately five times more dark matter than baryonic matter and that both forms of matter couple to gravity. For this reason we will assume

that matter in general is fundamentally described by a collection of identical collisionless classical non-relativistic particles interacting only via gravity.

The evolution of fluctuations in the matter density evolves via the collisionless Boltzmann equation. We follow the analysis of Carrasco et al [16] and Bernardeau et al [10]. For a collisionless system it is not useful to follow the orbits of each individual particle. Instead we can consider the distribution function f which is defined such that $f(\mathbf{x}, \mathbf{p}, t)\mathrm{d}\mathbf{x}\mathrm{d}\mathbf{p}$ is the probability to find chosen particle in the phase-space interval $[\mathbf{x}, \mathbf{x} + \mathrm{d}\mathbf{x}] \times [\mathbf{p}, \mathbf{p} + \mathrm{d}\mathbf{p}]$ at time t. By definition, the distribution function of a system with N particles is normalized such that

$$\int f(\mathbf{x}, \mathbf{p}, t)\mathrm{d}\mathbf{x}\mathrm{d}\mathbf{p} = N \quad \forall t.$$

For a classical point particle,

$$f(\mathbf{x}, \mathbf{p}, t) = \delta^{(d)}(\mathbf{x} - \mathbf{x}_1)\delta^{(d)}(\mathbf{p} - m\mathbf{v}_1),$$

with $\mathbf{v}_1$ velocity and $\mathbf{x}_1$ of particle one and $\delta^{(d)}$ the Dirac delta function in d dimensions. In an N-particle system the total phase space density f is

$$f(\mathbf{x}, \mathbf{p}, t) = \sum_n^N f_n(\mathbf{x}, \mathbf{p}, t) = \sum_n^N \delta^{(d)}(\mathbf{x} - \mathbf{x}_n)\delta^{(d)}(\mathbf{p} - m\mathbf{v}_n),$$

with $\mathbf{x}_n$ and $\mathbf{v}_n$ the position and velocity of the nth particle and $\mathbf{x}$ and $\mathbf{p}$ denoting of the position and momentum of all particles simultaneously.

Any given particle moves through phase-space, by which the probability of finding the particle at any given phase-space location f evolves with time. As f evolves, the probability must be conserved at all times, i.e. we do not allow for the creation or destruction (annihilation) of dark matter particles. This can formally be expressed in terms of the Boltzmann equation. Differentiating the distribution function with respect to time gives the Boltzmann equation

$$\frac{\mathrm{d}f}{\mathrm{d}t} = \frac{\partial f}{\partial t} + \frac{\partial}{\partial \mathbf{x}} \cdot (f\dot{\mathbf{x}}) + \frac{\partial}{\partial \mathbf{p}} \cdot (f\dot{\mathbf{p}}) = \frac{\partial f}{\partial t} + \dot{\mathbf{x}} \cdot \frac{\partial f}{\partial \mathbf{x}} + \dot{\mathbf{p}} \cdot \frac{\partial f}{\partial \mathbf{p}}.$$

For Hamiltonian systems we can use Hamilton's equations to rewrite the Boltzmann equation in the form

$$\frac{\mathrm{d}f}{\mathrm{d}t} = \frac{\partial f}{\partial t} + \frac{\partial f}{\partial \mathbf{x}} \cdot \frac{\partial H}{\partial \mathbf{p}} - \frac{\partial f}{\partial \mathbf{p}} \cdot \frac{\partial H}{\partial \mathbf{x}}.$$

The total derivative on the left hand side describes the collisions between particles. It is for this reason often denoted as

$$\frac{\mathrm{d}f}{\mathrm{d}t} = \frac{\mathrm{d}f}{\mathrm{d}t}\bigg|_{coll}.$$

The partial derivatives on the right hand side describe the evolution of the particles without interactions. When the interactions between the particles do not significantly influence the momenta of the individual particles, we can consider the collisionless limit. The corresponding Boltzmann equation is the collisionless Boltzmann equation

$$0 = \frac{\mathrm{d}f}{\mathrm{d}t}\bigg|_{coll} = \frac{\partial f}{\partial t} + \frac{\partial f}{\partial \mathbf{x}} \cdot \frac{\partial H}{\partial \mathbf{p}} - \frac{\partial f}{\partial \mathbf{p}} \cdot \frac{\partial H}{\partial \mathbf{x}}.$$

In this thesis we will assume collisionless dark matter, described by the collisionless Boltzmann equation. We for this reason always assume

$$\frac{\mathrm{d}f}{\mathrm{d}t}\bigg|_{coll} = 0.$$

There however exist more involved theories of dark matter in which the collisional term should be taken into account.

The distribution function of a single particle f_1 in a gravitational field evolves according to the Boltzmann equation

$$0 = \frac{\partial f_1}{\partial t} + \frac{\mathbf{p}}{m} \cdot \frac{\partial f_1}{\partial \mathbf{x}} - m \sum_{m \neq 1} \frac{\partial \Phi_m}{\partial \mathbf{x}} \cdot \frac{\partial f_1}{\partial \mathbf{p}},$$

where m is the mass of the particle and Φ_n is the single particle Newtonian potential

$$\Phi_n = -\frac{Gm}{|\mathbf{x} - \mathbf{x}_n|}.$$

By assuming that all particles have the same mass and by summing over the N particles in our N-body problem, we obtain the Boltzmann equation for the total phase space density f,

$$0 = \frac{\partial f}{\partial t} + \frac{\mathbf{p}}{m} \cdot \frac{\partial f}{\partial \mathbf{x}} - m \sum_{n,m; m \neq n} \frac{\partial \Phi_m}{\partial \mathbf{x}} \cdot \frac{\partial f_n}{\partial \mathbf{p}}.$$

By solving the Boltzmann equation, we can in principle fully understand the formation of large-scale structure. Physical observables such as the mass density ρ, momentum density π, velocity field $\mathbf{u}$, and kinetic tensor σ can be obtained by taking moments with respect to the phase space density,

$$\rho(\mathbf{x}, t) = m \int f(\mathbf{x}, \mathbf{p}) \mathrm{d}\mathbf{p} = m \sum_n^N \delta^{(d)}(\mathbf{x} - \mathbf{x}_n),$$

$$\pi^i(\mathbf{x}, t) = \rho(\mathbf{x}, t) u^i(\mathbf{x}, t) = \int p^i f(\mathbf{x}, \mathbf{p}) \mathrm{d}\mathbf{p} = m \sum_n^N v_n^i \delta^{(d)}(\mathbf{x} - \mathbf{x}_n),$$

$$\sigma^{ij}(\mathbf{x}, t) = \int p^i p^j f(\mathbf{x}, \mathbf{p}) \mathrm{d}\mathbf{p} = m \sum_n^N v_n^i v_n^j \delta^{(d)}(\mathbf{x} - \mathbf{x}_n).$$

This task is however extremely difficult, since the Boltzmann equation is a $6N$-dimensional non-linear differential equation. We can instead consider lower dimensional approximations. Assume that matter behaves as a so-called dark matter fluid. By integrating the collisionless Boltzmann equation with respect to momentum we obtain the conservation of mass

$$\frac{\partial \rho}{\partial t} + \nabla \cdot (\rho \mathbf{u}) = 0.$$

By multiplying the collisionless Boltzmann equation with p^i and again integrating over all momenta, we obtain the Euler equation

$$\frac{\partial \mathbf{u}}{\partial t} + (\mathbf{u} \cdot \nabla)\mathbf{u} = -\nabla \Phi - \frac{1}{\rho} \nabla \cdot (\rho \sigma^{ij}) = -\nabla \Phi - \frac{1}{\rho} \nabla P.$$

These equations are known as the Jeans equations and will be used in the subsequent chapters. Note that we can also derive the conservation of energy from the collisionless Boltzmann equation, by multiplying with $\frac{p^2}{m}$ and integrating over all momenta. The collection of the conservation of mass, conservation of energy and Euler equation without a gravitational potential are called the fluid equations. This system of equations is closely related to the Navier-Stokes equation which is one of the unsolved millennium problems. The deep connection between the large-scale structure formation and the Navier-Stokes equations underlines the complexity of large-scale structure formation. Large-scale structure formation is just a special application of fluid dynamics.

3.2   Evolution of matter density fluctuations

In the previous section we derived the fluid equations from the collisionless Boltzmann equations. By adding the Poisson equation we close the system of differential equations. The conservation of mass, Euler and Poisson equation in there most familiar form are

$$\frac{\partial \rho}{\partial t} + \nabla_r \cdot \rho \mathbf{u} = 0,$$
$$\frac{\partial \mathbf{u}}{\partial t} + (\mathbf{u} \cdot \nabla_r) \mathbf{u} = -\nabla_r \Phi - \frac{1}{\rho} \nabla_r P,$$
$$\nabla_r^2 \Phi = 4\pi G \rho,$$

with density ρ, velocity $\mathbf{u}$, pressure P, and gravitational potential Φ at some position $\mathbf{r}$ and time t.

The spatial coordinate $\mathbf{r}$ denotes a physical position. This includes the expansion of the homogeneous background universe. We can write the fluid equations above as deviations with respect to the homogeneous expanding universe by introducing comoving coordinates

$$\mathbf{x}(t) = \frac{\mathbf{r}(t)}{a}.$$

Note that in a completely homogeneous universe, the physical position $\mathbf{r}$ evolves whereas the comoving position $\mathbf{x}$ is constant. Analogously, the density ρ can be written in terms of density fluctuations δ with respect to the background (average) density ρ_u by

$$\delta(\mathbf{x}, t) = \frac{\rho(\mathbf{x}, t) - \rho_u(t)}{\rho_u(t)}.$$

The gravitational potential can be written in terms of the potential perturbations, subtracting the potential term describing the homogeneous expansion

$$\phi(\mathbf{x}, t) = \Phi(\mathbf{r}, t) - \frac{1}{2}a\ddot{a}x^2.$$

The velocity $\mathbf{v}$ can be expressed in terms of peculiar velocity defined as the derivative of the comoving coordinate,

$$\mathbf{v} = a\frac{\mathrm{d}x}{\mathrm{d}t} = a\dot{\mathbf{x}} = \mathbf{u} - \dot{a}\mathbf{x}.$$

Substituting the comoving variables, results in the comoving fluid equations

$$\frac{\partial \delta}{\partial t} + \frac{1}{a}\nabla_x \cdot (1 + \delta)\mathbf{v} = 0,$$

$$\frac{\partial \mathbf{v}}{\partial t} + \frac{1}{a}\left(\mathbf{v} \cdot \nabla_x\right)\mathbf{v} + \frac{\dot{a}}{a}\mathbf{v} = -\frac{1}{a}\nabla_x \phi - \frac{1}{a\rho_u(1 + \delta)}\nabla_x P,$$

$$\nabla_x^2 \phi = 4\pi G a^2 \rho_u \delta = \frac{3}{2}\Omega H^2 a^2 \delta.$$

Note that in a medium with vanishing pressure gradient, i.e. $\nabla_x P = 0$, and a gradient field velocity field, with velocity potential $\mathcal{V}$ such that $v = -\frac{\nabla_x \mathcal{V}}{a}$, the Euler equation can be transformed to the Bernoulli equation

$$\frac{\partial \mathcal{V}}{\partial t} - \frac{1}{2a^2}\left(\nabla_x \mathcal{V}\right)^2 = \phi.$$

This allows for an elegant treatment of approximations of the comoving fluid equations.

3.3 Linear Eulerian perturbation theory

The comoving fluid equations described above have two nonlinear terms. The $\nabla_x \cdot (\delta \mathbf{v})$ term in the conservation of mass and the $(\mathbf{v} \cdot \nabla)\mathbf{v}$ term in the Euler equation. Under the assumptions

$$\delta \ll 1$$

and

$$\left(\frac{vt_{exp}}{d}\right)^2 \ll \delta,$$

with d the coherence length for spatial variations of δ, v the characteristic fluid velocity and t_{exp} the expansion time $(G\rho_u)^{-1/2}$, we assume that the terms $\nabla_x \cdot (\delta\mathbf{v})$, $(\mathbf{v} \cdot \nabla_x)\mathbf{v}$ and the pressure gradient are negligible we obtain the linear approximation

$$\dot{\delta} + \frac{1}{a}\nabla \cdot \mathbf{v} = 0$$
$$\dot{\mathbf{v}} + \frac{\dot{a}}{a}\mathbf{v} = -\frac{1}{a}\nabla_x\phi$$
$$\nabla_x^2\phi = 4\pi G\rho_u a^2 \delta.$$

Taking the divergence of the Euler equation, combining it with the Poisson equation and substituting the continuity equation in this equation, we obtain the differential equation

$$\ddot{\delta} + 2\frac{\dot{a}}{a}\dot{\delta} = 4\pi G\rho_u\delta.$$

In a matter-dominated homogeneous Friedmann universe (with $\delta \propto a^{-3}$), the Friedmann equations state that

$$4\pi G\rho_u = \frac{3}{2}\Omega H^2 = \frac{3}{2a^3}\Omega_0 H_0^2.$$

Substituting this equation in the differential equation governing the evolution of δ leads to

$$\ddot{\delta} + 2\frac{\dot{a}}{a}\dot{\delta} = \frac{3}{2a^3}\Omega_0 H_0^2\delta.$$

In general, this equation can be solved in terms of a growing mode D_+ and a decaying mode D_- as

$$\delta(\mathbf{x}, t) = D_+(t)\Delta_+(\mathbf{x}) + D_-(t)\Delta_-(\mathbf{x}),$$

in which D_+ and D_- describe the evolution of δ in time, while Δ_+ and Δ_- describe the behavior of δ in space. If we neglecting the decaying mode D_-, we obtain the approximation

$$\delta(\mathbf{x}, t) = D_+(t)\Delta_+(\mathbf{x}),$$

with the growing mode D_+ explicitly depending on the background cosmology. For universes with matter and dark energy, or a cosmological constant, the growing mode can be solved as

$$D_+(t) = H(t)\int \frac{\mathrm{d}t}{a^2(t)H^2(t)}.$$

In an Einstein-de Sitter universe, the growing mode equals the scale factor, i.e. $D_+(t) = a(t)$. When the dark energy becomes dominant, growing mode tends to become constant.

3.4 Lagrangian perturbation

Among fluid dynamical perturbation theories, we can distinguish Eulerian and La-
grangian approaches. In the previous section we saw the Eulerian approach, in which
we expand in the density. We analyze the flow of mass into and out of a fixed volume
element. In the Lagrangian approach, we expand in the displacement field of volume
elements. We define a Lagrangian volume element which follow the fluid in time. The
mass in such a Lagrangian volume element remains constant, while the shape and vol-
ume of the Lagrangian volume element can change dramatically. The density at some
time can be computed by dividing the mass in the Lagrangian volume element by its
volume at that time.

If no approximations would be made in the process, the Eulerian and Lagrangian
approach would give the same solution. In practice the comoving fluid equations have
the same level of complexity as the Navier-Stokes equations, by which we have to make
approximations and get a branch of Eulerian and Lagrangian approximations. The
Lagrangian approach turns out to form a better approximation of non-linear structure
formation than the Eulerian approach. In this section we study Lagrangian perturbation
theory and show why the Lagrangian approach can be expected to give better results
than the Eulerian approach.

3.4.1 Lagrangian comoving fluid equations

We apply the comoving fluid equations to the Lagrangian approach. A Lagrangian
solution of the fluid equations described above is a map $\mathbb{R}^3 \times \mathbb{R} \to \mathbb{R}^3, (\mathbf{q}, t) \mapsto \mathbf{x}(\mathbf{q}, t)$
mapping an (Lagrangian) initial position $\mathbf{q}$ to an (Eulerian) position $\mathbf{x}(\mathbf{q}, t)$ evolved over
some time t. Let $\mathbf{s}(\mathbf{q}, t) = \mathbf{x}(\mathbf{q}, t) - \mathbf{q}$ be the displacement field, corresponding to this
map.

The conservation of mass has a natural place in the Lagrangian approach. Neglecting
the initial density fluctuations, the density in Lagrangian space $\mathbf{q}$ is equal to the average
cosmic density $\rho_u(t)$ at time t, by which the mass contained in each initial Lagrangian
volume element coincide. At later times, the conservation of mass implies that the mass
in each fluid element remains constant,

$$\rho(\mathbf{x}, t)\mathrm{d}\mathbf{x} = \rho_u(t)\mathrm{d}\mathbf{q}.$$

The transformation of $\mathbf{q}$ to $\mathbf{x}$ can be seen as a coordinate transformation. Using the
Jacobian $\| \ \|$, the density perturbation in the Lagrangian approach can be written as

$$1 + \delta(\mathbf{x}, t) = \frac{\rho(\mathbf{x}, t)}{\rho_u(t)} = \left\| \frac{\partial \mathbf{x}}{\partial \mathbf{q}} \right\|^{-1} = \left\| \frac{\partial(\mathbf{q} + \mathbf{s})}{\partial \mathbf{q}} \right\|^{-1}.$$

In one spatial dimension, the displacement vector consists of one component

$$\mathbf{s} = (s_1).$$

The Jacobian can be expressed in terms of $\partial \mathbf{s}/\partial \mathbf{q}$ as,

$$\left\| \frac{\partial \mathbf{x}}{\partial \mathbf{q}} \right\| = 1 + \frac{\partial s_1}{\partial q_1}.$$

In two spatial dimensions, the displacement field consists of two components

$$\mathbf{s} = \begin{pmatrix} s_1 \\ s_2 \end{pmatrix}.$$

The Jacobian can be written as

$$\left\| \frac{\partial \mathbf{x}}{\partial \mathbf{q}} \right\| = 1 + \left(\frac{\partial s_1}{\partial q_1} + \frac{\partial s_2}{\partial q_2} \right) + \left(\frac{\partial s_1}{\partial q_1} \frac{\partial s_2}{\partial q_2} - \frac{\partial s_1}{\partial q_2} \frac{\partial s_2}{\partial q_1} \right).$$

In three spatial dimensions, the displacement field consists of three components

$$\mathbf{s} = \begin{pmatrix} s_1 \\ s_2 \\ s_3 \end{pmatrix}.$$

The Jacobian can be written as

$$\begin{aligned} \left\| \frac{\partial \mathbf{x}}{\partial \mathbf{q}} \right\| =\, & 1 + \left(\frac{\partial s_1}{\partial q_1} + \frac{\partial s_2}{\partial q_2} + \frac{\partial s_3}{\partial q_3} \right) + \left(\frac{\partial s_1}{\partial q_1} \frac{\partial s_2}{\partial q_2} + \frac{\partial s_1}{\partial q_1} \frac{\partial s_3}{\partial q_3} + \frac{\partial s_2}{\partial q_2} \frac{\partial s_3}{\partial q_3} \right) \\ & - \left(\frac{\partial s_1}{\partial q_2} \frac{\partial s_2}{\partial q_1} + \frac{\partial s_1}{\partial q_3} \frac{\partial s_3}{\partial q_1} + \frac{\partial s_2}{\partial q_3} \frac{\partial s_3}{\partial q_2} \right) \\ & + \left(\frac{\partial s_1}{\partial q_1} \frac{\partial s_2}{\partial q_2} \frac{\partial s_3}{\partial q_3} + \frac{\partial s_1}{\partial q_2} \frac{\partial s_2}{\partial q_3} \frac{\partial s_3}{\partial q_1} + \frac{\partial s_1}{\partial q_3} \frac{\partial s_2}{\partial q_1} \frac{\partial s_3}{\partial q_2} \right) \\ & - \left(\frac{\partial s_1}{\partial q_3} \frac{\partial s_2}{\partial q_2} \frac{\partial s_3}{\partial q_1} + \frac{\partial s_1}{\partial q_1} \frac{\partial s_2}{\partial q_3} \frac{\partial s_3}{\partial q_2} + \frac{\partial s_1}{\partial q_2} \frac{\partial s_2}{\partial q_1} \frac{\partial s_3}{\partial q_3} \right). \end{aligned}$$

Up to linear terms of $\partial \mathbf{s}/\partial \mathbf{q}$, in any number of spatial dimensions, this reduces to

$$\left\| \frac{\partial \mathbf{x}}{\partial \mathbf{q}} \right\| = 1 + \nabla_q \cdot \mathbf{s},$$

with the reciprocal up to linear order

$$1 + \delta = \left\| \frac{\partial \mathbf{x}}{\partial \mathbf{q}} \right\|^{-1} = 1 - \nabla_q \cdot \mathbf{s},$$

since $(1 + \nabla_q \cdot \mathbf{s})(1 - \nabla_q \cdot \mathbf{s}) = 1 - (\nabla_q \cdot \mathbf{s})^2 = 1$. Hence we can approximate the density perturbation δ up to linear order in $\partial \mathbf{s}/\partial \mathbf{q}$ by

$$\delta(\mathbf{x}, t) \approx -\nabla_q \cdot \mathbf{s}.$$

This approximation will be important in the Zel'dovich approximation, since it does not contain products of elements of $\partial\mathbf{s}/\partial\mathbf{q}$ which represent interactions or phase mixing. Substitution of this identity in the comoving Poisson equation results in

$$\nabla^2\phi = -4\pi G a^2 \rho_u \nabla_q \cdot \mathbf{s}.$$

The comoving Euler equation becomes more complex in the Lagrangian approach. Let $\tau : \mathbb{R} \to \mathbb{R}$ be a (strictly increasing) continuous function. This function can be seen as a parametrization of time t. Let $\mathbf{u} = \partial x/\partial\tau$ be the velocity field with respect to τ. Note that by the chain rule we can relate $\mathbf{v}$ to $\mathbf{u}$ via $\mathbf{v} = a\dot\tau\mathbf{u}$. The position $\mathbf{x}$ of a particle originating in $\mathbf{q}$ can be related to the reparametrized velocity $\mathbf{u}$ via

$$\mathbf{x} = \mathbf{q} + \mathbf{s} = \mathbf{q} + \int_0^{\tau(t)} \mathbf{u}\, \mathrm{d}\tau.$$

The Euler equation comes in by taking the Lagrangian derivative of $\mathbf{u}$ with respect to τ,

$$\frac{\mathrm{d}\mathbf{u}}{\mathrm{d}\tau} = \frac{\partial\mathbf{u}}{\partial\tau} + (\mathbf{u}\cdot\nabla_x)\mathbf{u} = \frac{1}{a\dot\tau}\left(B\mathbf{u} - \nabla_x\phi - \frac{1}{(1+\delta)\rho_u}\nabla_x P\right)$$

with $B = -(2a\dot{a}\dot\tau + a^2\ddot\tau) = -\frac{\partial}{\partial t}(a^2\dot\tau)$. The left hand side describes the acceleration of the Lagrangian volume element with respect to τ, while the right hand side describes the force exerted on the Lagrangian volume element.

3.5   Zel'dovich approximation

The fluid equations in the Lagrangian setting enable us to make a first-order Lagrangian approximation of the solutions of the fluid equations. This approximation was derived in 1970 by Zel'dovich [72] and is commonly denoted as the Zel'dovich approximation.

Theorem 1. *For a universe in which the following assumptions are satisfied:*

- *the velocity $\boldsymbol{u}$ with respect to the growing mode $\tau = D_+$ has almost everywhere[1] a nonvanishing divergence, i.e. $\nabla_x \cdot \boldsymbol{u} \neq 0$ almost everywhere,*

- *the density is approximated by the divergence of the displacement vector, i.e. $\delta = -\nabla_q \cdot \boldsymbol{s}$,*

- *the gradient of the pressure is vanishing, i.e. $\nabla_x P = 0$,*

the evolution of the density perturbations is governed by the Zeldovich approximation

$$\boldsymbol{x}(\boldsymbol{q}, t) = \boldsymbol{q} + D_+(t)\boldsymbol{u}.$$

Furthermore $\boldsymbol{u}$ is a constant gradient field. We define the velocity potential Ψ_0 such that $\boldsymbol{u} = -\nabla_q\Psi_0$.

---

[1]The set $\{\mathbf{q} \in \mathbb{R}^3 | \nabla \cdot \mathbf{u}(\mathbf{q}) = 0\}$ has Lebesgue measure zero.

Proof. With a vanishing pressure gradient, the Euler equation in the Lagrangian setting is given by

$$\frac{\mathrm{d}\mathbf{u}}{\mathrm{d}\tau} = \frac{\partial \mathbf{u}}{\partial \tau} + (\mathbf{u} \cdot \nabla_x)\mathbf{u} = \frac{1}{a\dot{\tau}}(B\mathbf{u} - \nabla_x \phi).$$

The existence of a τ such that $\nabla_x \phi = B\mathbf{u}$, would prove that $\mathbf{u}$ is a gradient field. We will show that the growing mode D_+ satisfies this condition. For such a τ, the Euler equation reduces to

$$\frac{\mathrm{d}\mathbf{u}}{\mathrm{d}\tau} = \frac{\partial \mathbf{u}}{\partial \tau} + (\mathbf{u} \cdot \nabla_x)\mathbf{u} = 0$$

by which

$$\mathbf{s} = \int_{\tau(0)}^{\tau(t)} \mathbf{u} \, \mathrm{d}\tau = (\tau(t) - \tau(0))\mathbf{u} = \tau(t)\mathbf{u},$$

if we set $\tau(0) = 0$. Substituting $\nabla \phi = B\mathbf{u}$ in the Poisson equation

$$\nabla_x^2 \phi = -4\pi G a^2 \rho_u \nabla_q \cdot \mathbf{s} \approx -4\pi G a^2 \rho_u \nabla_x \cdot \mathbf{s},$$

results in

$$-B\nabla_x \cdot \mathbf{u} = -4\pi G a^2 \rho_u \tau \nabla_x \cdot \mathbf{u}.$$

Note that according to the chain rule, up to linear terms in $\partial \mathbf{x}/\partial \mathbf{q}$ the gradient $\nabla_x \cdot \mathbf{s} = \nabla_q \cdot \mathbf{s}$. Now since we assume that $\nabla_x \cdot \mathbf{u} \neq 0$ almost everywhere, this equation can be reduced to

$$B = 2a\dot{a}\dot{\tau} + a^2\ddot{\tau} = 4\pi G a^2 \rho_u \tau,$$

leading to the differential equation

$$\ddot{\tau} + 2\frac{\dot{a}}{a}\dot{\tau} = 4\pi G \rho_u \tau.$$

This second order differential equation is identical to the differential equation of the growing and decaying modes $D_{\pm}$ almost everywhere. Neglecting the decaying mode results in the Zel'dovich approximation

$$\mathbf{x} = \mathbf{q} + D_+\mathbf{u} = \mathbf{q} - D_+\nabla_x \Psi$$

with D_+ the growing mode described in the previous section and Ψ the velocity potential of $-\mathbf{u}$. Since in the Zel'dovich approximation the field $\mathbf{u}$ is constant along the flow, we can see that Ψ is constant, i.e. $\Psi = \Psi_0$ for some scalar field Ψ_0.

The Zel'dovich approximation is an extremely simple approximation of gravity in the sense that it only depends on the growing mode D_+ containing the information of the cosmology and a scalar field Ψ_0 containing the information of the initial density fluctuations of the universe. This thesis is largely devoted to understanding the statistics of the geometry of Ψ_0. In the description below, we show that the initial velocity potential Ψ_0 is proportional to the initial gravitational potential. $\qquad\square$

In chapter 18 we will see a more direct prove of this theorem.

This approximation can be related to physical quantities via the peculiar velocity[2]

$$\mathbf{v} = a\frac{\mathrm{d}\mathbf{x}}{\mathrm{d}t} = -a\dot{D}_+\nabla\Psi$$

$$= -aD_+H\frac{a\dot{D}_+}{\dot{a}D_+}\nabla\Psi$$

$$= -aD_+Hf(\Omega)\nabla\Psi,$$

with f the Peebles factor. In a 1980 Peebles found a approximate power law

$$f(\Omega_m) \approx \Omega_m^\gamma$$

with $\gamma = 0.55 + 0.05[1 + w(z = 0)]$, and $w(z = 0)$ the current equation of state of dark energy [51]. In the linear regime furthermore

$$\mathbf{v} = -\frac{2f(\Omega)}{3\Omega H}\frac{\nabla\phi}{a}$$

by which

$$\Psi(\mathbf{q}) = \frac{2}{3D_+a^2H^2\Omega}\phi(\mathbf{x}, t).$$

Combining this with the relation between δ and ϕ we see that in terms of Fourier modes,

$$\hat{u}(\mathbf{k}) = -i\frac{\mathbf{k}}{|\mathbf{k}|^2}\hat{\delta}(\mathbf{k}).$$

The density of the Zel'dovich approximation is given by

$$1 + \delta = \frac{\rho(\mathbf{x}, t)}{\rho_u(t)} = \left\|\frac{\partial\mathbf{x}}{\partial\mathbf{q}}\right\|^{-1}$$

$$= \|\delta_{mn} - D_+(t)\psi_{mn}\|^{-1}$$

$$= \frac{1}{(1 - D_+(t)\lambda_1)(1 - D_+(t)\lambda_2)(1 - D_+(t)\lambda_3)}$$

with $\lambda_1 \geq \lambda_2 \geq \lambda_3$ the ordered eigenvalues of the deformation matrix

$$\psi_{mn} = \frac{D_+}{a}\frac{\partial^2\Psi_0}{\partial q_m\partial q_n} = \frac{2}{3a^3\Omega H^2}\frac{\partial^2\Psi_0}{\partial q_m\partial q_n}.$$

In figure 3.1 the Zel'dovich approximation is depicted. The initial conditions are simulated by a realization of a Gaussian random field with power spectrum $P(k) = Ak^{-1}$ with some constant A. The Zel'dovich approximation describes a linear ballistic motion of fluid elements, which do not interact with each other. The solution is appropriate as long as fluid elements have not crossed. At the time of crossing, infinite densities occur (with zero measure). This phenomenon is called shell crossing and forms the starting point of they story of catastrophe theory in large-scale structure formation.

---

[2]The velocity of stars with respect to the expanding background.
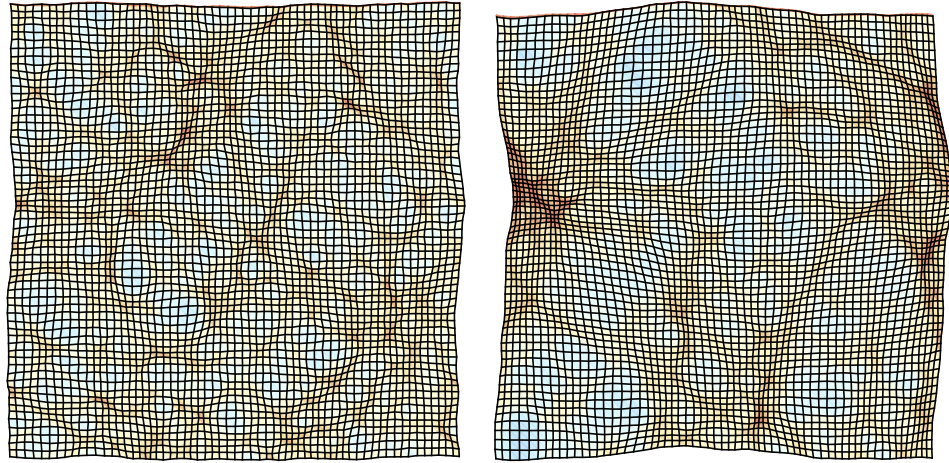
(a) $P = Ak^{-1}$ and $D_+ = 3$

(b) $P = Ak^{-2}$ and $D_+ = 3$
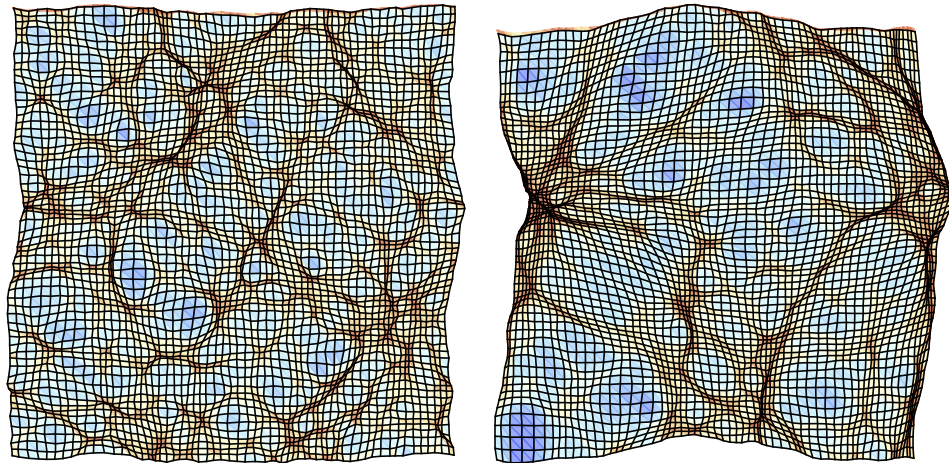
(c) $P = Ak^{-1}$ and $D_+ = 6$

(d) $P = Ak^{-2}$ and $D_+ = 6$
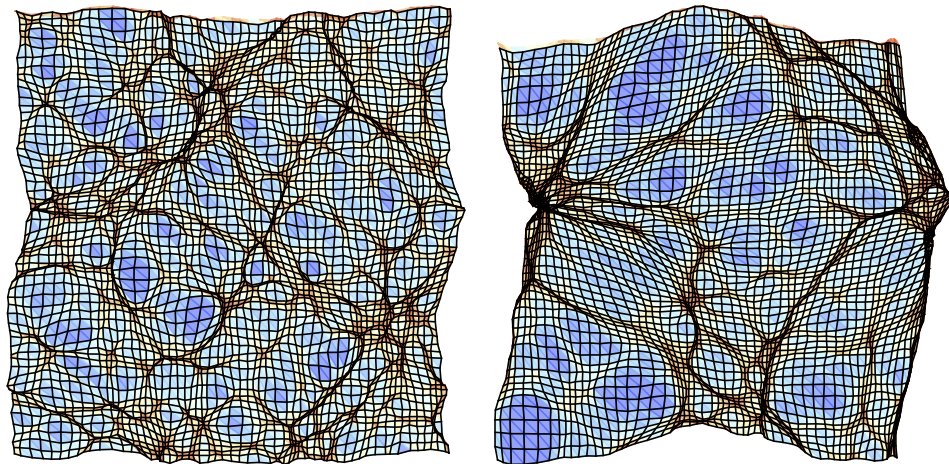
(e) $P = Ak^{-1}$ and $D_+ = 9$

(f) $P = Ak^{-2}$ and $D_+ = 9$

Figure 3.1: The Zeldovich approximation of the smoothened density fluctuations with $\sigma = 1$ corresponding with a power law power spectrum with $n = -1, -2$.

3.5.1 Truncated Zel'dovich approximation

In 1970 [72], Zel'dovich proposed the linear Lagrangian approximation for large-scale structure formation, today well-known as the Zel'dovich approximation. In 1973 [73] Zel'dovich argued that this approximation was only valid for universes in which large-scale wavelength perturbations dominated over small-scale perturbations. Such universes are sometimes denoted as the adiabatic or pancake model. In the 1980s, work indicated that the Zel'dovich might be adequate in a more general setting (see for example Melott et al. [47]). In 1993, Coles et al. [21] performed numerical simulations and compared them with analytical models. They furthermore performed truncations on the initial conditions, by removing the high Fourier modes of the initial conditions. The Zel'dovich approximation with truncation turned out to be the best analytic model of large-scale structure formation they considered. In 1994, Melott et al. [48] found that the Zel'dovich approximation with a truncation can be improved by performing a Gaussian smoothing on the initial conditions. Such a smoothing can be seen as a more subtle truncation since is suppresses certain Fourier modes of the initial conditions instead of removing them. This model is known as the truncated Zel'dovich approximation. In the subsequent chapters we will always denote the truncated Zel'dovich approximation as the Zel'dovich approximation.

N-body simulations of large-scale structure formation show that the evolution of short-wavelength fluctuations is strongly influenced by long-wavelength fluctuations, whereas long-wavelength fluctuations are not significantly influenced by small-wavelength fluctuations, see Little, Weinberg and Park [42]. Now consider a model in which structure formation evolves hierarchically. In such models the first structures to form have a short wavelength. They are gradually followed by structures with longer wavelengths. The Zel'dovich approximation is valid up to the mildly nonlinear stage. In a hierarchically evolving universe, the Zel'dovich approximation will become invalid on short wavelengths before the long-wavelength structures have formed. Since the long-wavelength structures are not significantly influenced by short-wavelength structures, we can still probe the long-wavelength structures in the large-scale structure by removing the short-wavelength fluctuations with a Gaussian smoothing. For different stages of evolution, different scales of structure are formed by which we need a different smoothing scale. This is the truncated Zel'dovich approximation which is used throughout this thesis.

When we consider truncated random fields, we can see the truncation scale as an extra parameter of the field. In the case with two spatial dimensions (with coordinates (x, y)), the truncated random fields can be seen as a three dimensional field (with coordinates (x, y, σ)), with σ the smoothing scale. This truncated space is often denoted as scale-space. Analogously, the truncated Zel'dovich approximation in three spatial dimensions (x, y, z) can be seen as a four dimensional field (x, y, z, σ) in scale-space. All results obtained in the subsequent chapters will be based on the truncated Zel'dovich approximation and are considered in scale-space.

3.5.2 Adhesion model

As discussed in the previous section, the Zel'dovich approximation is a good approxima-
tion of the linear and mildly non-linear regime of structure formation. In the strongly
non-linear regime the approximation becomes invalid, since the particles do not interact
and moves straight through each other. This feature of the Zel'dovich approximation
is due to the assumption that the fluid is pressureless, and that we approximate the
density as $\delta = -\nabla \cdot \mathbf{s}$ in which we ignore gravitational interactions. Many modifications
have been proposed to fix these shortcomings. Matarrese et al. [45] developed a variant
called the 'frozen flow approximation' in which the peculiar velocity field is fixed at its
original value. Brainerd, Scherrer and Villumsen [13] developed an approximation which
assumed a constant gravitational potential. For a more complete discussion see Jones
[38]. The adhesion model modifies the Zel'dovich approximation by adding a artificial
viscosity term to mimic the gravitational interactions occurring after shell crossing. This
results in the a Euler equation in the Lagrangian setting of the form

$$\frac{\mathrm{d}\mathbf{u}}{\partial D_+} = \frac{\partial \mathbf{u}}{\partial D_+} + (\mathbf{u} \cdot \nabla)\mathbf{u} = \nu \nabla^2 \mathbf{u}.$$

We consider solutions of this equation and take the limit $\nu \to 0$, by which the viscosity
term does not affect the Zel'dovich approximation before shell crossing but makes it
sticky at shell crossing. This equation is known as Burgers' equation.

   The Burgers' equation was first introduced in 1940 by the Dutch mathematician
Johannes Marinus Burgers to model turbulence. The equation was introduced in the
context of large-scale structure formation in 1984 by Gurbatov, Saichev and Shandarin
[32] and was discussed extensively by Soviet astrophysicists.

   One of the interesting features of the adhesion model is that it can be solved analyt-
ically. In the limit $\nu \to 0$

$$\mathbf{u}(\mathbf{x}, t) = \sum_\alpha \frac{\mathbf{x} - \mathbf{q}_\alpha}{D_+} j_\alpha \exp\left(-\frac{S_\alpha}{2\nu}\right) \Big/ \sum_\alpha j_\alpha \exp\left(-\frac{S_\alpha}{2\nu}\right)$$

with $\mathbf{q}_\alpha$ the Lagrangian points minimizing the action

$$S_\alpha = \Psi_0(\mathbf{q}_\alpha) + \frac{(\mathbf{x} - \mathbf{q}_\alpha)^2}{2D_+},$$

$$j_\alpha = \left[\det\left(\delta_{ij} + \frac{\partial^2 \Psi_0}{\partial q_i \partial q_j}\right)\right]^{-1/2}\bigg|_{\mathbf{q}=\mathbf{q}_\alpha},$$

as a function of $\mathbf{q}$ for fixed $\mathbf{x}$. The process of minimizing the action results in $\mathbf{q}_\alpha$ such
that

$$\mathbf{x}(\mathbf{q}_\alpha, D_+) = \mathbf{q}_\alpha + D_+ \nabla_q \Psi_0(\mathbf{q}_\alpha)$$
$$S(\mathbf{x}, D_+, \mathbf{q}) \geq S(\mathbf{x}, D_+, \mathbf{q}_\alpha)$$

Zeldovich   Adhesion
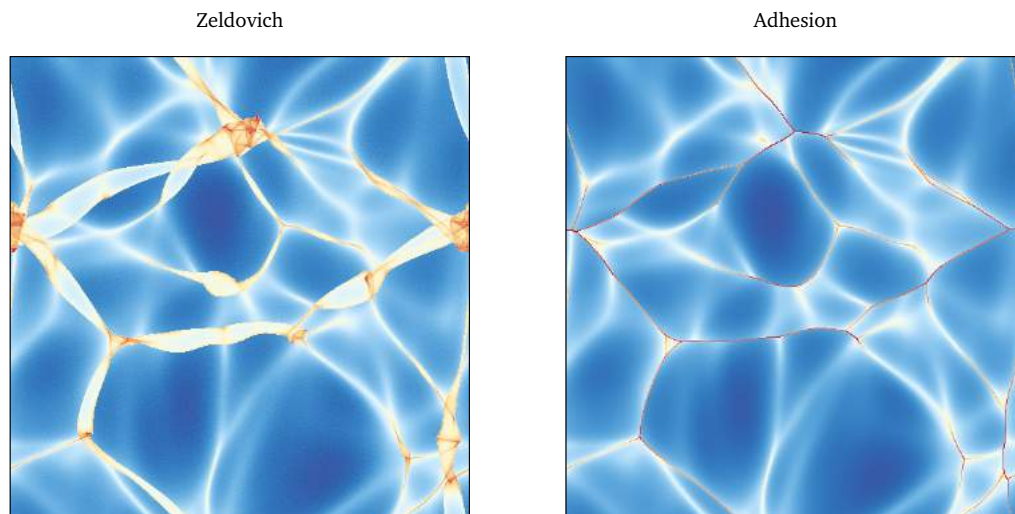
Figure 3.2: The adhesion model and the Zel'dovich approximation by Johan Hidding [34]. The left and right panel depicts the Zel'dovich approximation and adhesion model of an initial density field.

for all **q**. This can be interpreted by saying that the solution of Burgers' equation is equal to the Zel'dovich approximation before shell crossing and sticks to a structure (with zero measure) after shell crossing. In figure 3.2 we can observe the evolution of particles in the adhesion model. The initial conditions were generated form a Gaussian random field with a power-law power spectrum. See the movie by Johan Hidding [35] for an excellent illustration of the adhesion model.

Chapter 4

Caustics in N-Body Simulations

In chapter 3 we studied the equations governing Newtonian large-scale structure formation. We furthermore derived the Zel'dovich approximation. In this approximation regions with infinite density, often called caustics, can be generated in a process called shell crossing. In this chapter we use numerical simulations of one- and two-dimensional models of the universe to investigate the significance of these caustics in the real universe.

4.1   Simulation of dark matter

With the increase of computer power in last decades, numerical simulation of the comoving fluid equations has grown into a extensive field of research. In 2005, the Millennium run simulated a cube with sides of about 2 billion light years containing about 20 million galaxies. In 2010, the Bolshoi simulation and in 2014 the Illustrus simulation performed similar cosmological three-dimensional N-body simulations containing besides the comoving fluid equations, gas dynamics and some star evolution (supernova explosions). In this thesis we restrict our self to small simple one- and two-dimensional N-body simulations. The features appearing in these simple simulations help us understand the more involved three-dimensional simulations. In this section we describe the principles used in the simulation. Appendix A contains the N-body routine used in this chapter.

4.1.1   Leap-Frog integrator

The numerical integration of the comoving fluid equations in this thesis has been performed with the Leap-Frog integrator. The fluid is approximated by a grid of 'particles'. Consider n^d particles labeled by $\mathbf{i} \in (\mathbb{Z}/n\mathbb{Z})^d$ with d the number of spatial dimensions of the simulation. The particles are initially positioned on a cubic grid. The initial positions and momenta are

$$\mathbf{x}_{\mathbf{i},0} = \frac{L}{n}\mathbf{i}, \qquad\qquad \mathbf{p}_{\mathbf{i},0} = 0,$$

with L the length of the sides of the box. The Leap-Frog integrator starts with a displacement according to the Zel'dovich approximation followed by iterations over so-

called drifts and kicks. The positions and momenta of the particles are not evaluated at the same time steps, i.e., the positions are evaluated at times $t = ida$ whereas the momenta are evaluated at times $t = (i + \frac{1}{2})da$ for $i \in \mathbb{N}$. The positions overtake the momentum after which the momenta overtakes the positions in time. This property gives the Leap-Frog integration its name. The integrator is often used since it is reversible in time and enforces conservation of energy on the solutions.

4.1.2 The Zel'dovich approximation

The initial fluctuations in the matter density are modeled with a realization of a Gaussian random field $\delta \in (\mathbb{R}^n)^d$. The initial displacement of the particles is performed according to the Zel'dovich approximation. The velocity potential is computed with discrete Fourier transforms

$$\Phi = \mathcal{F}^{-1}\left(\frac{1}{\mathbf{k}^2}\mathcal{F}(\delta)\right),$$

with $\mathcal{F}$ and $\mathcal{F}^{-1}$ respectively the Fourier and the inverse Fourier transform. The velocity $\mathbf{u}_i$ a computed with a discrete gradient of the potential. We displace the positions by a time step da and the momenta by a time step $\frac{3}{2}da$ resulting in new position and velocity

$$\mathbf{x_{i,1}} = \mathbf{x_{i,0}} + da\mathbf{u_i} \qquad\qquad \mathbf{p_{i,3/2}} = \frac{3}{2}da\mathbf{u_i}.$$

4.1.3 The drift

The drift approximates the differential equation

$$\frac{\partial \mathbf{x}}{\partial t} = \frac{\mathbf{p}}{a^2} \Rightarrow \frac{\partial \mathbf{x}}{\partial a} = \frac{\mathbf{p}}{a^2\dot{a}}$$

and results in the displacement

$$\mathbf{x_{i,t+1}} = \mathbf{x_{i,t}} + \frac{da}{a^2\dot{a}}\mathbf{p_{i,t+1/2}},$$

with $\dot{a}$ given by the Friedmann equations

$$\dot{a} = H_0 a\sqrt{\Omega_\Lambda + \Omega_m a^{-3} + (1 - \Omega_\Lambda - \Omega_m)a^{-2}}.$$

4.1.4 The kick

The kick approximates the differential equation

$$\frac{\partial \mathbf{p}}{\partial t} = -\nabla\phi \Rightarrow \frac{\partial \mathbf{p}}{\partial a} = -\frac{\nabla\phi}{\dot{a}}.$$

We start with a mass deposition of the positions on a regular grid using a Cloud in Cell algorithm CIC, described below. Using the mass deposition, we approximate the gravitational potential

$$\delta = CIC[\mathbf{x}_{i,t}]m - 1$$
$$\phi = \frac{3}{2}\Omega_m H_0^2 \mathcal{F}^{-1}\left(\frac{1}{\mathbf{k}^2}\mathcal{F}(\delta)\right).$$

We subsequently compute a discrete gradient of the potential and interpolate the potential on the positions of the particles $\mathbf{a}_{cc}$. This results in the kick

$$\mathbf{p}_{\mathbf{i},t+3/2} = \mathbf{p}_{\mathbf{i},t+1/2} - \frac{da}{\dot{a}}\mathbf{a}_{cc}.$$

4.1.5 Mass deposition

For the mass deposition we us a Cloud in Cell algorithm. In this algorithm we consider a cubic grid consisting out of $(2n)^d$ points. Each particle $\mathbf{x}_{\mathbf{i},t}$ resembles a cube, the cloud, with side length $\frac{L}{2n}$. The mass deposition distributes the mass of the particles on the cubic grid according to volume of the cube laying in the corresponding grid cell. This algorithm forms an approximation of the density distribution as a function of the position of the particles.

4.2 Caustics in one-dimensional simulations

In figure 4.1 we simulated the evolution of a fluctuation in a one-dimensional universe. We start with a uniform density distribution and a velocity fluctuation of the form

$$v = xe^{-x^2}.$$

This can be seen in the upper phase-space plot. The particles are uniformly distributed in space and have some initial velocity. The particles on the left side move to the right whereas the particles on the right move to left side of the simulation. The curve in phase-space is called the Lagrangian submanifold. In the upper right plot of figure 4.1 we see the density. The boxes are a histogram of the particles with respect to the spatial dimension. This corresponds to the Eulerian density. The black line is the reciprocal of the separation of neighboring points. This corresponds to the Lagrangian density. When time evolves, the particles start to move. In the middle panel, we see that some particles coming from the left collide with particles coming form the right side of the simulation. This is called shell crossing. At this time the Eulerian density becomes large while the Lagrangian density becomes infinite. The particles do not really collide since we simulated a pressurless fluid. In the lower panel of figure 4.1 we see a further stage of evolution. After shell crossing the particles have continued to move, and decelerated due to the density peak in the middle of the simulation. Some particles have even turned

around and generated a second density peak. In the simulation, the Lagrangian sub-manifold will keep winding till the separation of the particles reaches the accuracy of the simulation.

From the simulation described above, we observe points in space corresponding to one unique point on the Lagrangian submanifold. These points form single stream regions. Other points in space correspond to multiple points on the Lagrangian submanifold. These points form the multi stream regions. The different stream regions are separated by points with an infinite Lagrangian density. These points are called caustics. From this simulation we observe the prominent role of the caustics in large-scale structure formation. They correspond to the high density regions and highlight regions with enough mass to form gravitationally bound objects. In more realistic N-body simulations, the dark matter distribution will evolve as depicted in our simulation. The baryonic matter will however experiences pressure and will shock at the time of first shell crossing. The caustic corresponding to this event indicates a collapse which can potentially lead to the formation of stars and galaxies.

4.3   Caustics in two-dimensional simulations

In figures 4.2 we see the evolution of density fluctuations with a power spectrum with index $-\frac{1}{2}$. The time evolution has been performed with the same Leap-Frog integrator as the one-dimensional simulation described above, with a implementation of Johan Hidding [33]. Initially the perturbations are small. In time the over dense regions exert a stronger pull on the surrounding matter than under dense regions. The over densities become clusters and filaments whereas the under dense regions become voids.

In the context of the corresponding four-dimensional phase-space, the evolution can be seen as the stretching and twisting of a two-dimensional Lagrangian submanifold. Initially, there are only single stream regions. Each point in space corresponded to a unique point on the Lagrangian submanifold. As the submanifold however evolved, shell crossing and multi stream regions appeared. This again induces infinite Lagrangian densities and caustics. In filaments and in particular clusters, many shell crossings will have occurred with many flows. We for this reason see that the caustics closely follow the cosmic web. In this thesis, we approximate the density of nodes and length of the line caustics.

The N-body simulation is again a good representation of the evolution of dark matter in a two-dimensional universe. The baryonic matter will again have collapsed during first shell crossing. Since starts are composed out of baryonic matter, we can expect stars and galaxies to form in the nodes and middle of the filaments. This is in good agreement with more involved N-body simulations and the SDSS and 2dF surveys.

4.4   Caustics in three-dimensional simulations

Caustics can also be found in three-dimensional N-body simulations. Since it is more time consuming to perform three-dimensional N-body simulations and more difficult to
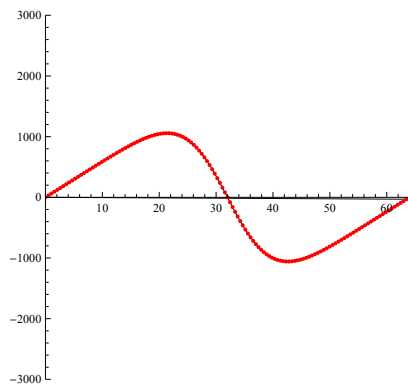
(a) Phase-space distribution at time initial time
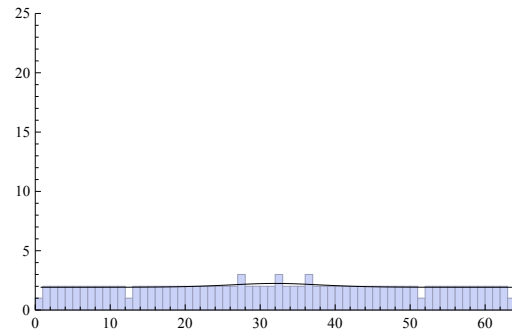
(b) Density at initial time
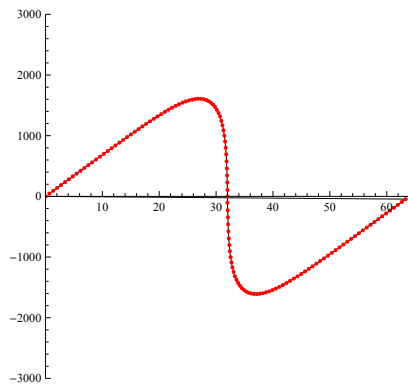
(c) Phase-space distribution at first shell crossing
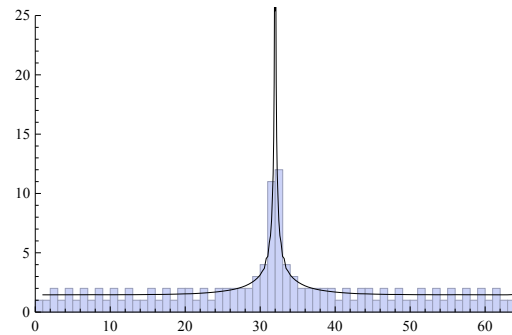
(d) Density at first shell crossing
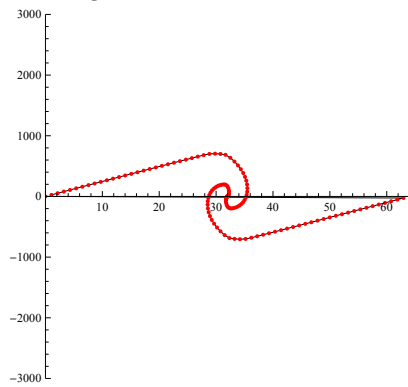
(e) Phase-space distribution after several shell crossings
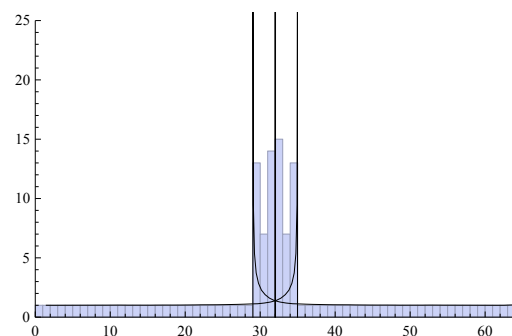
(f) Density after several shell crossings

Figure 4.1: Caustics in a one-dimensional N-body simulation

(a) At $a = 0.1$

(b) At $a = 0.3$

(c) At $a = 0.5$

(d) At $a = 0.7$

(e) At $a = 0.9$

(f) At $a = 1.0$
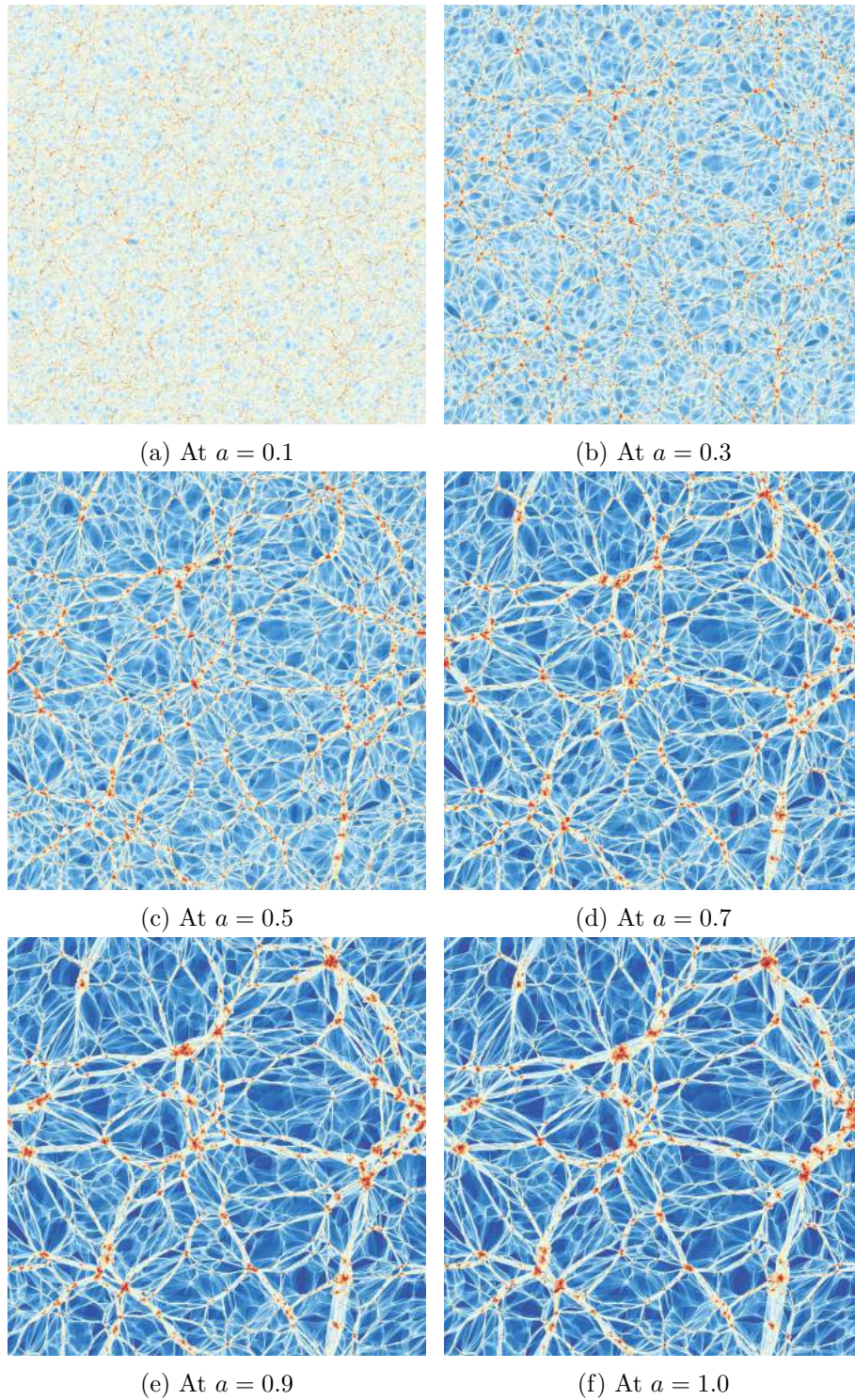
Figure 4.2: Two-dimensional N-Body simulation of Gaussian matter perturbations [33]
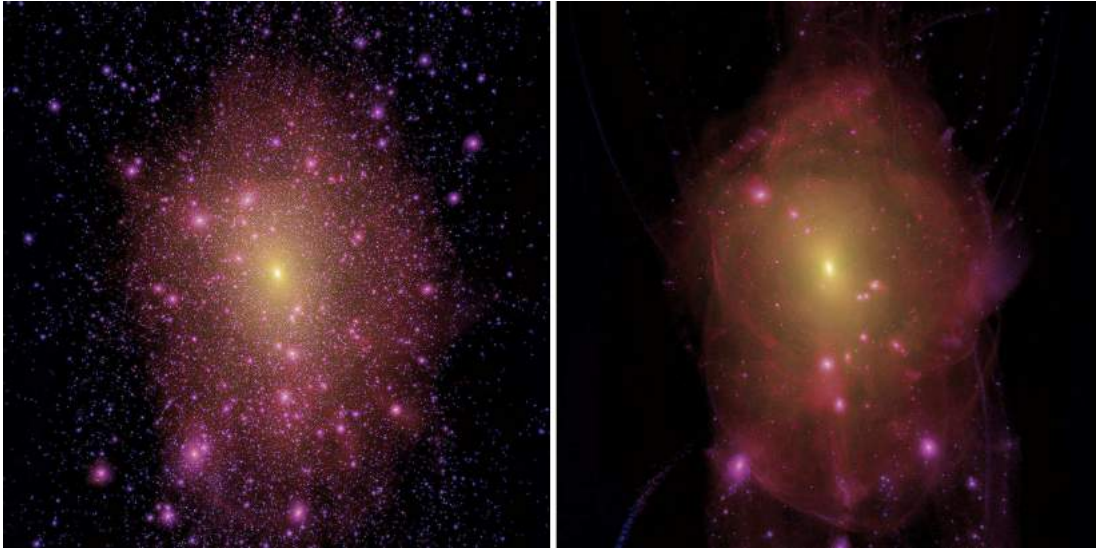
Figure 4.3: Cold dark matter and warm dark matter simulation of a halo.

visualize three-dimensional structures, we use the simulations and illustrations of Lovell et al. [44]. Lovell et al. analyzed whether the 'to big to fail problem' can be resolved by considering a warm dark matter model in stead of the standard ΛCDM model. They have resimulated one of the Aquarius N-body haloes with the power spectrum suppressed at small scales.

The results of the resimulation are illustrated in figure 4.3. The left and right panel contains the cold and warm dark matter simulation respectively. The cold dark matter simulation looks messy with many small satellite halos circling the large central halo. In the warm dark matter simulation, these small structures are suppressed. We instead can see caustics encapsulating the center of the central halo. We see large sheets, thin lines and singular points. A study of caustics in three-dimensions would analyze all these individual features. In this thesis we will however restrict our self to one- and two-dimensional models of the universe.

Chapter 5

Lagrangian Catastrophe Theory

A small push often results in a small movement. A harder push results in a larger movement. This incremental response to incremental stresses is very common in nature. There are however situations in which a small push results in a dramatic response. Consider, for example, the boiling of water, the collapse of a bridge or the capsizing of a boat. Such a response is called a "catastrophe". Although these situations are rare, they are also typical. If we load a bridge with leaves, it is difficult to predict which leave will make the bridge collapse. It is however, certain that the collapse will occur. The study of systems in which catastrophes occur, is called catastrophe theory. This theory can also be used to describe the occurrence of caustics in optical systems or the filaments and clusters in the cosmic web. This branch of catastrophe theory emerges from projections of high-dimensional surfaces to lower-dimensional spaces and is called Lagrangian catastrophe theory.

The term catastrophe theory was introduced in 1972 by René Thom. The subject can however be traced from Huygens, via Cauchy, to Poincaré, Morse, Whitney, Thom, Zeeman to Arnol'd. This list is far from complete. Cayley, Maxwell and later Morse derived a classification of nondegenerate critical points, which is now known as Morse theory. Whitney proposed a classification of degenerate critical points. Thom extended Whitney's theorem. Thom's articles became very popular by articles of Christopher Zeeman on Thom's classification. Arnol'd extended Thom's classification, for more general functions. Moreover, he applied the theory to Lagrangian maps, leading to the branch of Lagrangian catastrophe theory. For a more elaborate description of the history and development of catastrophe theory see 'Catastrophe Theory' by Arnol'd [5]. In this chapter we give an intuitive introduction to Lagrangian catastrophe theory. For a formal discussion of this topic see chapter 7.

5.1 Caustics

Figure 5.1 shows a glass of hot water in which we steep tea. Initially the water is transparent. In the process of steeping tea, a two-dimensional surface in a three-dimensional space appears on the boundary of the colored and transparent water. We however ob-

serve a projection of this surface onto a two-dimensional plane due to the limitations of our eyes. Because of the projection, we observe lines in the projection at places at which the surface is tangential to the line of sight. These lines, generally called caustics, contain differentiable segments and points at which the curve follows a nondifferentiable path. These points are called singular.

Lagrangian catastrophe theory plays a very prominent role in the problem of projecting manifolds onto lower-dimensional spaces. Consider a two-dimensional differentiable manifold M embedded in the three-dimensional space $\mathbb{R}^3$. While the manifold is locally diffeomorphic to $\mathbb{R}^2$ and is smooth at every point, the projection p of the manifold to the two-dimensional plane $\mathbb{R}^2$, defined by $p : (x, y, z) \in M \mapsto (x, y)$, can contain singular features. There can exist points in the plane with an empty preimage $p^{-1}(x, y)$, and points with a finite or even infinite number of points in the preimage. These regions are separated by curves, commonly called caustics.

Lagrangian catastrophe theory classifies these curves and their singular points up to coordinate transformations. Smooth curves are called fold catastrophes also known as A_2-lines. The singular points are cusp catastrophes also known as A_3 points. The fold and cusp catastrophes move over time and evolve, in which they pass through so-called swallowtail and umbilical catastrophes respectively denoted by A_4 and D_4. According to Lagrangian catastrophe theory, the A_2, A_3, A_4, and D_4 catastrophes are the only catastrophes occurring in the projection of a two-dimensional manifold onto a two-dimensional plane (as in the example of steeping tea). In projections of higher-dimensional spaces the A_k, D_k, E_6, E_7, and E_8 catastrophes can additionally occur, with integer $k \geq 5$. In three-dimensional large-scale structure evolution the catastrophes up to $k = 5$ can occur. In the subsequent sections of this chapter we describe several elementary catastrophes pictorially and in dynamical situations. We follow the dynamical examples of Castrigiano et al. [18]. The names of the catastrophes were proposed by Whitney and Thom.

5.2 A_2: The fold catastrophe

For the fold catastrophe, consider a cylinder of unit radius and unit mass on a hill (see figure 5.3). We denote the slope of the hill by α and let the center of mass C of the cylinder be located at an inner circumference with a radius $0 < r < 1$. Point P is the contact point of the cylinder with the hill and Θ is the angle between the horizon and the the line through the center of mass and the center of the cylinder. The potential energy of the system is

$$V(\Theta, \alpha) = \Theta \sin \alpha - r \sin \Theta + c(\alpha)$$

with the gravitation constant g set to 1 and $c : [0, 2\pi) \to \mathbb{R}$. The critical points of this potential can be found by equating

$$F(\Theta, \alpha) = \frac{\partial V}{\partial \Theta} = \sin \alpha - r \cos \Theta$$
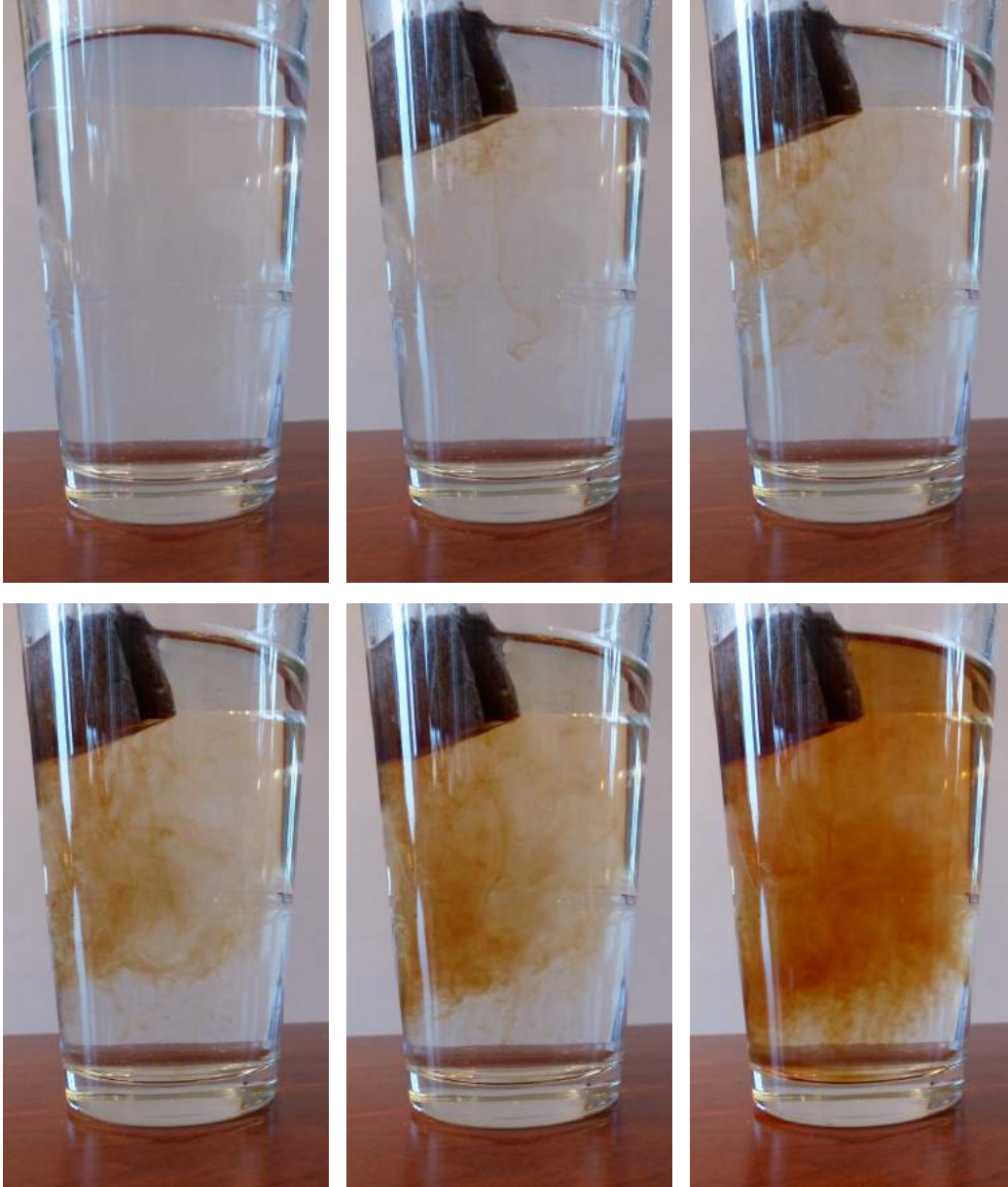
Figure 5.1: The caustics of tea steeping
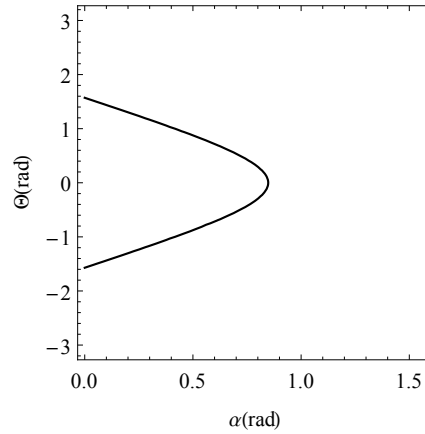
Figure 5.2: The catastrophe surface M_F of a cylinder on the hill

(a) Stable situation   (b) Stable situation   (c) Stable situation   (d) Unstable situation
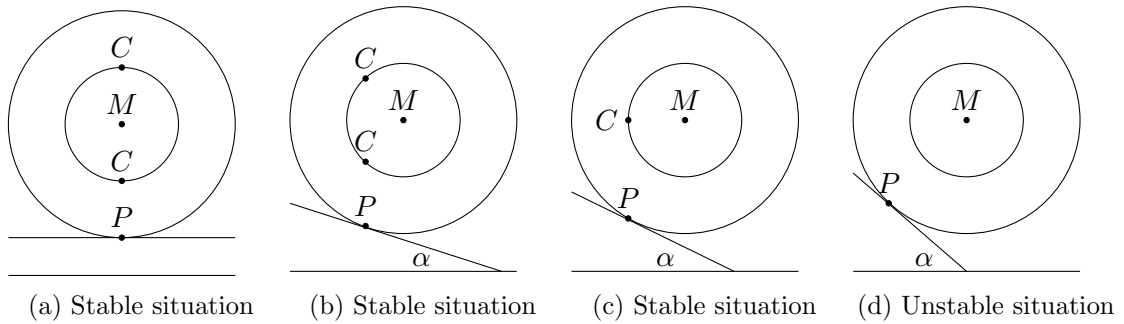
Figure 5.3: Cylinder on hill illustrating the fold catastrophe

with zero. The system is in a equilibrium if and only if

$$(\Theta, \alpha) \in M_F = \left\{ (\Theta, \alpha) \,|\, \cos\Theta = \frac{\sin\alpha}{r} \right\}.$$

The catastrophe surface M_F is illustrated in figure 5.2. For small α, the cylinder has two equilibrium positions in which C is directly above P, one in which C is at the top and one in which C is located bottom of the inner circumference (see figure 5.3a, and 5.3b). If α increases smoothly, the two equilibrium positions will merge into one at $\alpha = \arcsin r$ (see figure 5.3c). For $\alpha > \arcsin r$ no equilibrium position exists. As a consequence the cylinder must rolls off the hill. This catastrophe is called the fold catastrophe. The name fold refers to the shape of the equilibrium surface in configuration space (see figure 5.2).

5.3 A_3: The cusp catastrophe

For the cusp catastrophe we consider the Zeeman catastrophe machine, devised by E. C. Zeeman in 1969 [71]. Consider an elastic string of unit length attached to the origin
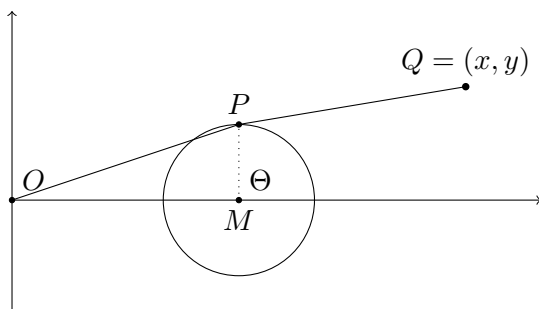
Figure 5.4: Zeeman catastrophe machine

and a fixed point P on the boundary of a unit circle. Let the center of the circle M be horizontally displaced by a distance $a > 1$ from the origin, so $M = (a, 0)$. Attach a second elastic string of unit length with the same elasticity to point P and a point $Q = (x, y)$. The point Q is an external parameter, similar to the angle α in the discussion of the fold. Let Θ be the angle between PM and the horizontal axis. The system is illustrated in figure 5.4. In this figure $\Theta = 90°$.

The potential energy of the Zeeman catastrophe machine as a function of Q and Θ is

$$V(\Theta, x, y) = \left(\sqrt{\frac{17}{4} - 2\cos\Theta} - 1 \right)^2$$
$$+ \left(\sqrt{(x + a)^2 + y^2 + \frac{1}{4} + (x + a)\cos\Theta - y\sin\Theta} - 1 \right)^2.$$

The equilibrium positions of this system are given by the set

$$M_F = \{(\Theta, x, y) \,|\, F(\Theta, x, y) = 0\},$$

plotted in figure 5.5a, with

$$F(\Theta, x, y) = \frac{\partial V(\Theta, x, y)}{\partial \Theta}$$
$$= -\frac{((a + x)\sin\Theta - y\cos\Theta)\left(\sqrt{(a + x)\cos\Theta + (a + x)^2 + y^2 - y\sin\Theta + \frac{1}{4}} - 1\right)}{\sqrt{(a + x)\cos\Theta + (a + x)^2 + y^2 - y\sin\Theta + \frac{1}{4}}}$$
$$+ 2\sin\Theta \left(1 - \frac{2}{\sqrt{17 - 8\cos\Theta}} \right).$$

This set of equilibria turns out to be, up to local coordinate transformations, equivalent to the simpler set

$$\tilde{M}_F = \{(\Theta, x, y) \,|\, 4\Theta^3 - 2x\Theta + y = 0\}.$$

(a) The set of equilibria of the Zeeman catastrophe machine with coordinates (x, y, Θ).

(b) The cusp caustic of the Zeeman catastrophe machine
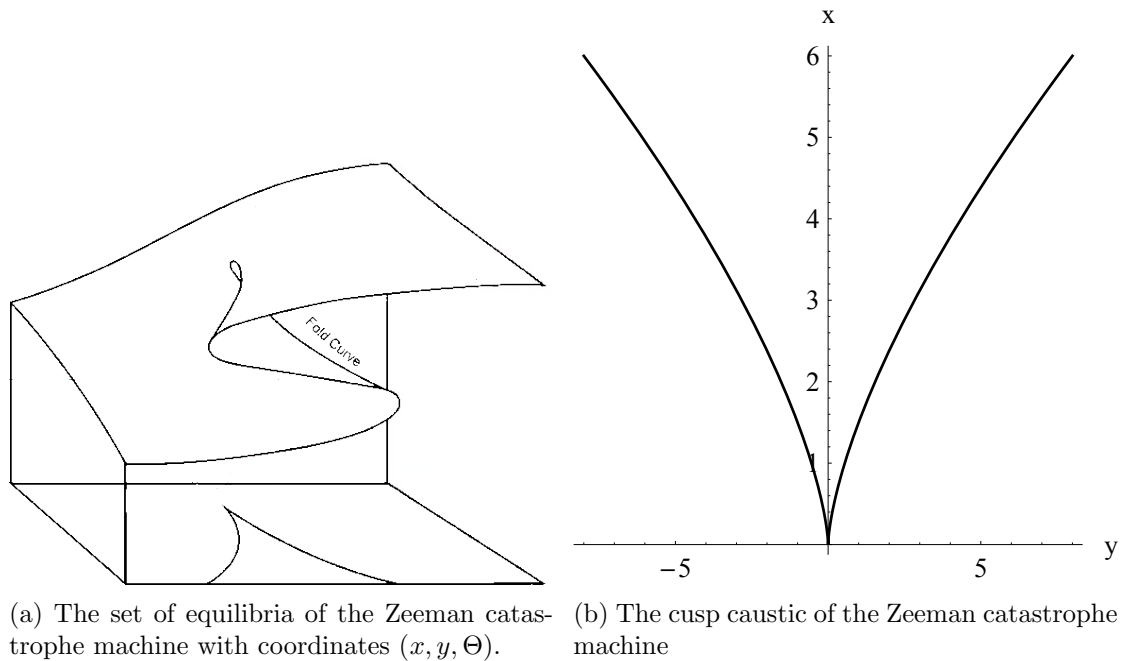
Figure 5.5: Zeeman catastrophe machine

A proof of the equivalence can be found in chapter 7.

From figure 5.5a, we can see the catastrophe behavior by gradually changing the position of $Q = (x, y)$. Starting with a point Q in the upper right quadrant, there is just one equilibrium position of P. This can be seen in figure 5.5a from the fact that there is one point in M_F of the form (Θ, Q). While lowering Q to the x-axis, there comes a moment at which there exist two equilibrium positions, i.e., two points of the form $(\Theta, Q) \in M_F$. However, although there are two equilibria at this moment, the point P will move gradually since we change Q slowly. Moving Q further down the x-axis, there comes a moment the point P will have to jump to the other equilibrium position. For this parameter Q there exists again only one point $(\Theta, Q) \in M_F$. This sudden jump is called a catastrophe. From figure 5.5a we see that these catastrophes occur at points where the tangential plane of the surface is parallel to the Θ-axis. In figure 5.5b we have drawn the set

$$B_F = \{(6\Theta^2, 8\Theta^3) \,|\, \Theta \in \mathbb{R}\},$$

where catastrophes can occur. The regular points of the curve correspond to fold catastrophes denoted by A_2. The point where the curve is singular is called the cusp catastrophe denoted by A_3.

The cusp catastrophe can also be illustrated by projections of a two-dimensional manifold embedded in $\mathbb{R}^3$ to the plane $\mathbb{R}^2$, see figure 5.6. In this thesis the surface will
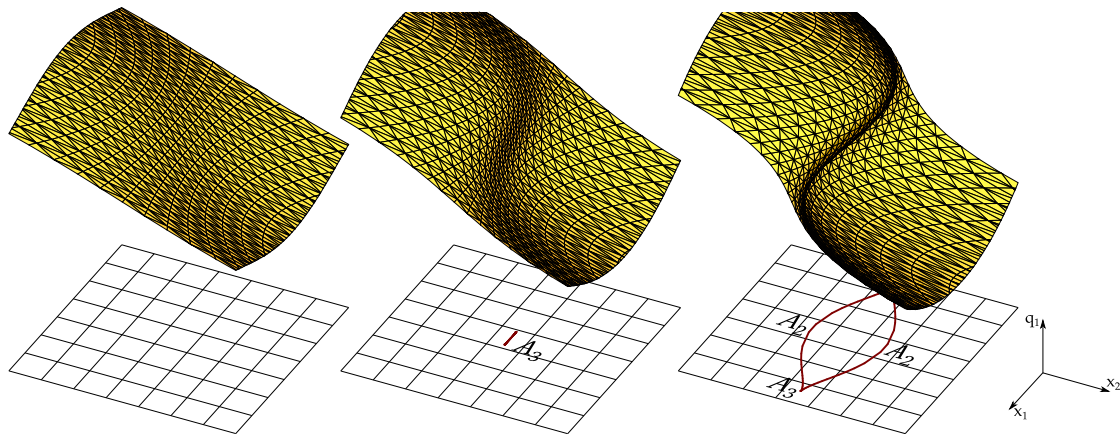
(a) lips bifurcation, in which two cusp catastrophes are created.
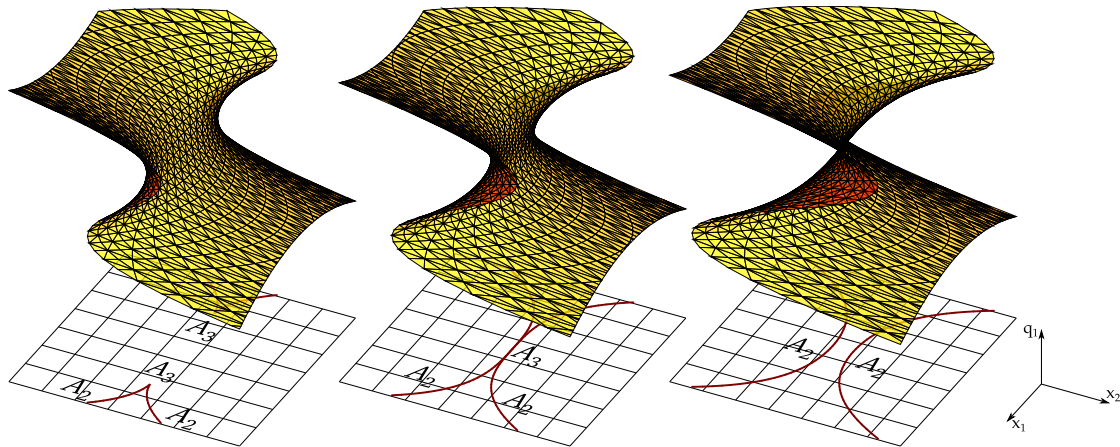
(b) Beak-to-beak bifurcation, in which two cusp catastrophes are annihilated

Figure 5.6: Cusp catastrophe, illustrated by Johan Hidding [33]

always represent a sheet in phase space. First consider the creation of a cusp catastrophe via a so-called lips bifurcation. In the first image the projection is a one to one mapping, allowing no formation of caustics. The manifold subsequently gets twisted till the point, that the origin becomes singular. This is the A_3 catastrophe. In the final plot the surface has twisted further, leading to a second A_3 catastrophe connected by two A_2 catastrophes. This configuration was first identified by Zel'dovich and is called the Zel'dovich pancake.

In the second figure we have a so called beak-beak bifurcation in which two A_3 catastrophes approaching each other. When they meet, they vanish and connect the A_2 singularities. The two A_3 singularities have merged and ceased to exist.
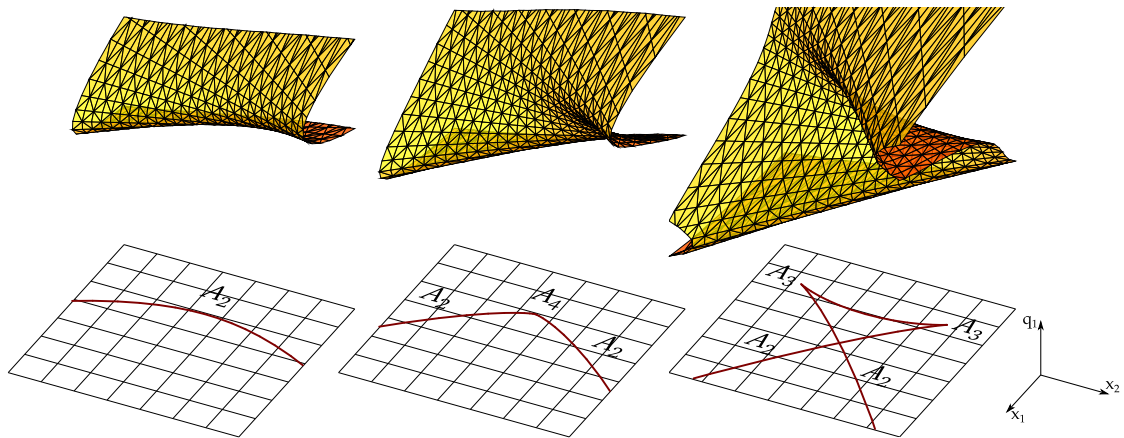
Figure 5.7: Swallowtail catastrophe, illustrated by Johan Hidding [33]

5.4 A_4: The swallowtail catastrophe

Although the swallowtail catastrophe exists in dynamical systems, it is most easily illustrated in a projection example. In the description above we saw that cusp catastrophes can be created and annihilated. There are however more possibilities. In figure 5.7 two cusps are being created by means of a swallowtail catastrophe. Although the swallow tail catastrophe does not occur as often in nature as the cusp, it can easily be observed in evolving systems. In such a system you can observe the process as illustrated in figure 5.7 and identify the moment at which a A_4 catastrophe appears. The A_4 catastrophe will appear in this thesis due to the twisting of the phase space sheet.

5.5 D_4: The umbilic catastrophes

Similar to the swallow tail catastrophe, the elliptic and hyperbolic umbilic catastrophes respectively denoted by, D_4^- and D_4^+, are catastrophes emerging in the evolution of cusp catastrophes. In figure 5.8 and 5.9 we see the elliptic and hyperbolic umbilic catastrophes appear when three cusp catastrophes move through each other.

5.6   Five-dimensional catastrophes

The fold, cups, swallowtail, and elliptic and hyperbolic umbilic, respectively denoted by A_2, A_3, A_4, D_4^-, and D_4^+, are the only stable catastrophes occurring in the projection of a two-dimensional manifold embedded in $\mathbb{R}^3$ onto the two-dimensional plane. In higher-dimensional spaces more catastrophes can occur. However, the number of different catastrophes remains finite. See chapter 7 for a full list. In this thesis we will consider catastrophes occurring in two-dimensional large-scale structure formation. In this setting the above mentioned catastrophes suffice. In three-dimensional large-scale structure
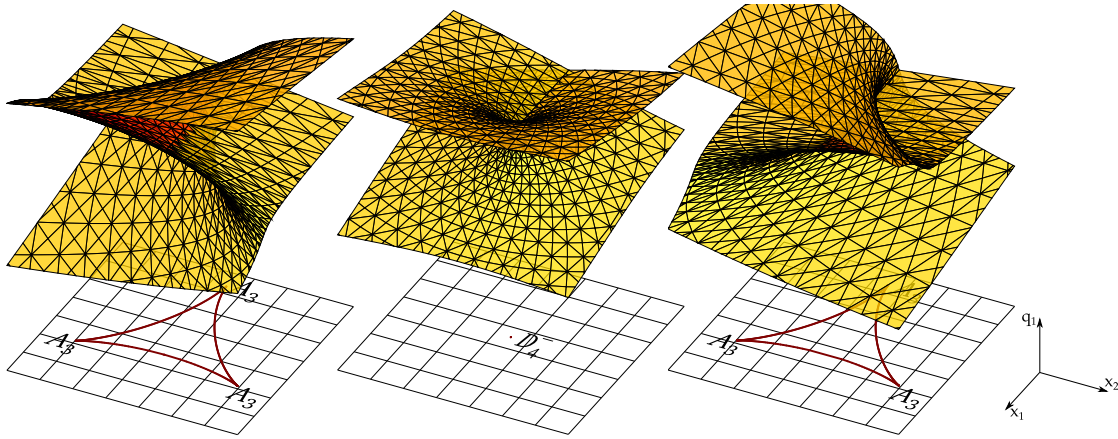
Figure 5.8: Elliptic umbilic catastrophe, illustrated by Johan Hidding [33]
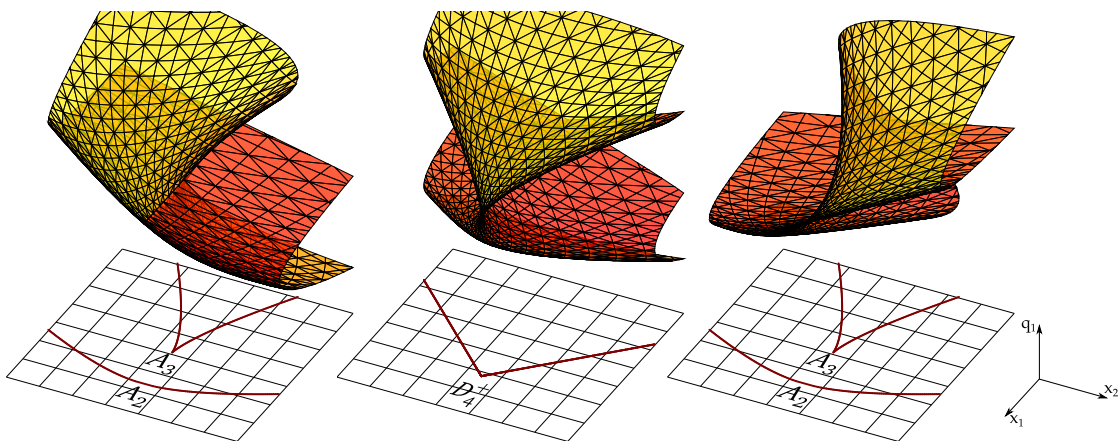
Figure 5.9: Hyperbolic umbilic catastrophe, illustrated by Johan Hidding [33]

formation we must add the butterfly and parabolic umbilic catastrophe, respectively denoted by A_5 and D_5.

Chapter 6

Caustics in the Zel'dovich Approximation

In chapter 3 we studied large-scale structure dynamics and the Zel'dovich approximation as a linear Lagrangian approximation. A general initial density distribution can be seen as a surface (Lagrangian submanifold) in phase space, in which each fluid element is characterized by its initial (Lagrangian) position and evolved (Eulerian) position. Initially, the density fluctuations are small. The projection of the phase space sheet onto position space is one to one. When the density starts to evolve, the phase space sheet will be stretched and twisted. During the evolution of the phase space sheet, the projection onto position space can develop regions in which the projection maps several fluid elements onto the same position, as seen in chapter 4. At the boundaries of these regions are so-called caustics, which are described in catastrophe theory. In this chapter we let the density distribution evolve according to the Zel'dovich approximation, and study the occurrence of catastrophes. The conditions discussed in this chapter for caustics in one- and two-dimensional models of the universes were first derived by Arnol'd, Shandarin and Zel'dovich in 1982 [6].

6.1   Caustics in the Zel'dovich-approximation

The Zel'dovich approximation is given by the equation

$$\mathbf{x}(t) = \mathbf{q} - \nabla \Psi D_+(t).$$

This is a Lagrangian approximation, which means that we study the evolution of fluid elements instead of density distributions. Using the conservation of mass we can obtain the density distribution of the Zel'dovich approximation. In a d-dimensional universe, the density field of the Zel'dovich approximation evolves as

$$1 + \delta = \frac{1}{(1 - D_+(t)\lambda_1)\ldots(1 - D_+(t)\lambda_d)},$$

with $\lambda_1 \geq \cdots \geq \lambda_d$ the ordered eigenvalues of the deformation matrix

$$\psi_{mn} = \frac{2}{3a^3\Omega H^2}\frac{\partial^2 \Psi}{\partial q_m \partial q_n}.$$

For positive eigenvalues, one of the most striking features of the density formula are the poles occurring at the times t satisfying

$$\lambda_i = \frac{1}{D_+(t)}.$$

At these times two sheets move through each other by which the density locally spikes. This feature is a so-called caustic and occurred at the moment of shell crossing. Note that the Zel'dovich approximation is a first-order approximation, which strictly becomes invalid during such an event. In the dark matter distribution nonlinear gravitational interactions will start to be important. In baryonic matter, pressure will prevent these infinite densities form occurring and lead to shock waves. However, even though the Zel'dovich approximation fails to predict the precise evolution of these caustics, we believe that the caustics have a great potential to model the large scale features of the cosmic web. They highlight the most dense regions in which stars and galaxies can start to form.

Since the caustics are produced in the projection of the phase space sheet onto the position space, the nature of the caustics can be described with Lagrangian catastrophe theory. Arnol'd, Zel'dovich and Shandarin generated a complete classification of these caustics in one- and two-dimensional Zel'dovich approximations. In the sections below, we explain the classification.

6.2   Catastrophes in the one-dimensional Zel'dovich approximation

The example used here was introduced by Arnol'd. Consider the initial density perturbation

$$\delta = \cos(\pi q),$$

for a universe ranging from $q \in [-1, 1]$. According the the Poisson equation the velocity potential is

$$\Psi = -\frac{1}{\pi^2} \cos(\pi q),$$

up to physical constants.

According to the Zel'dovich approximation the system evolves as shown in figure 6.1. At $D_+ = 0$ the density is nearly uniform. At $D_+ = 1$ shell-crossing first occurs. At this time, $\frac{\partial x}{\partial q} = 0$ at the point $q = 0$, leading to an infinite density. This feature is a cusp catastrophe (A_3). At time step $D_+ = 3$, the cusp has split into two fold catastrophes (A_2). As time evolves the two fold catastrophes move apart.

First note that the concept of velocity after shell crossing is ill-defined between the fold catastrophes. There are different sheets of matter flowing through each other. We could define it to be the average density. This would however neglect the information in the collapsed region governing the evolution. It would be better to use the phase-space sheet in which the different matter flows remain fully resolved.

In the example above we observe the creation of infinite densities. At $D_+ = 1$ the first A_3 catastrophe appears in the origin. This corresponds with a local maximum of the first eigenvalue of the deformation tensor in the origin. In one dimension the first eigenvalue of the deformation tensor is equal to the second derivative of the velocity potential, which is equal to the density perturbation

$$\lambda = \varphi = \frac{\partial^2 \Psi}{\partial q^2} = \cos(\pi q) = \delta$$

at time $D_+ = \frac{1}{\lambda} = 1$. The A_2 catastrophes correspond to the intersection of the first eigenvalue of the deformation tensor λ with the level $\frac{1}{D_+}$. Since smoothened realizations of Gaussian random fields are almost always Morse functions, any A_3 catastrophe corresponds with a maximum or minimum and any A_2 catastrophe corresponds with a level crossing in one-dimensional universes. The evolution of caustics in the Zel'dovich approximation can, for this reason, be seen as a hierarchical process, in which a line of height $\frac{1}{D_+}$ is lowered. Any maximum hitting the line is a A_3 catastrophe splitting into two A_2 catastrophes. Any minimum hitting this line corresponds with an A_3 catastrophe in which two A_2 catastrophes merge and vanish. The maxima and minima of the first eigenvalue field λ, or in one-dimension the density, form an embryonic skeleton of the structure formation.

It should be noted from the above example that two fold catastrophes were created via a cusp catastrophe. The cusp only exists at one moment of time, whereas the fold catastrophes exist at all times after shell crossing. This is a property of the dimensionality of the model of the universe and the catastrophe under consideration. In the above example we have one spatial and one time dimension. The two-dimensional A_2 catastrophes move in time whereas the three-dimensional A_3 catastrophe only exists at fixed instants. However, even though the A_3 catastrophe does only occur at the creation of A_2 catastrophes, the A_3 catastrophe is stable. If we perturb the density distribution a bit around the A_3 catastrophe, it will move a bit in time and space but will never vanish. In a two-dimensional universe we have two spatial and one time dimension. In these universes A_2 and A_3 catastrophes move through the space whereas the four-dimensional A_4, D_4^- and D_4^+ catastrophes exist only at a point in space-time.

6.3 Catastrophes in the two-dimensional Zel'dovich approximation

For increasing numbers of dimensions of models of the universe, we can find more and more qualitatively different catastrophes. In the two-dimensional case the set of distinct catastrophes is given by A_2, A_3, A_4, D_4, in which A_4 is called the swallowtail and D_4 is the umbilic catastrophe. The discussion of caustics in the two-dimensional Zel'dovich approximation is however very similar to the one-dimensional case.

In two dimensions the velocity potential Ψ is a function from $\mathbb{R}^2$ to $\mathbb{R}$. The deformation tensor is a two-by-two tensor with, assuming Ψ is differentiable, three degrees of freedom. There are two real eigenvalue fields λ_1 and λ_2 on which we impose the ordering

(a) u-x at $D_+ = 0$ (b) q-x at $D_+ = 0$ (c) ρ-x at $D_+ = 0$

(d) u-x at $D_+ = 1$ (e) q-x at $D_+ = 1$ (f) ρ-x at $D_+ = 1$

(g) u-x at $D_+ = 3$ (h) q-x at $D_+ = 3$ (i) ρ-x at $D_+ = 3$
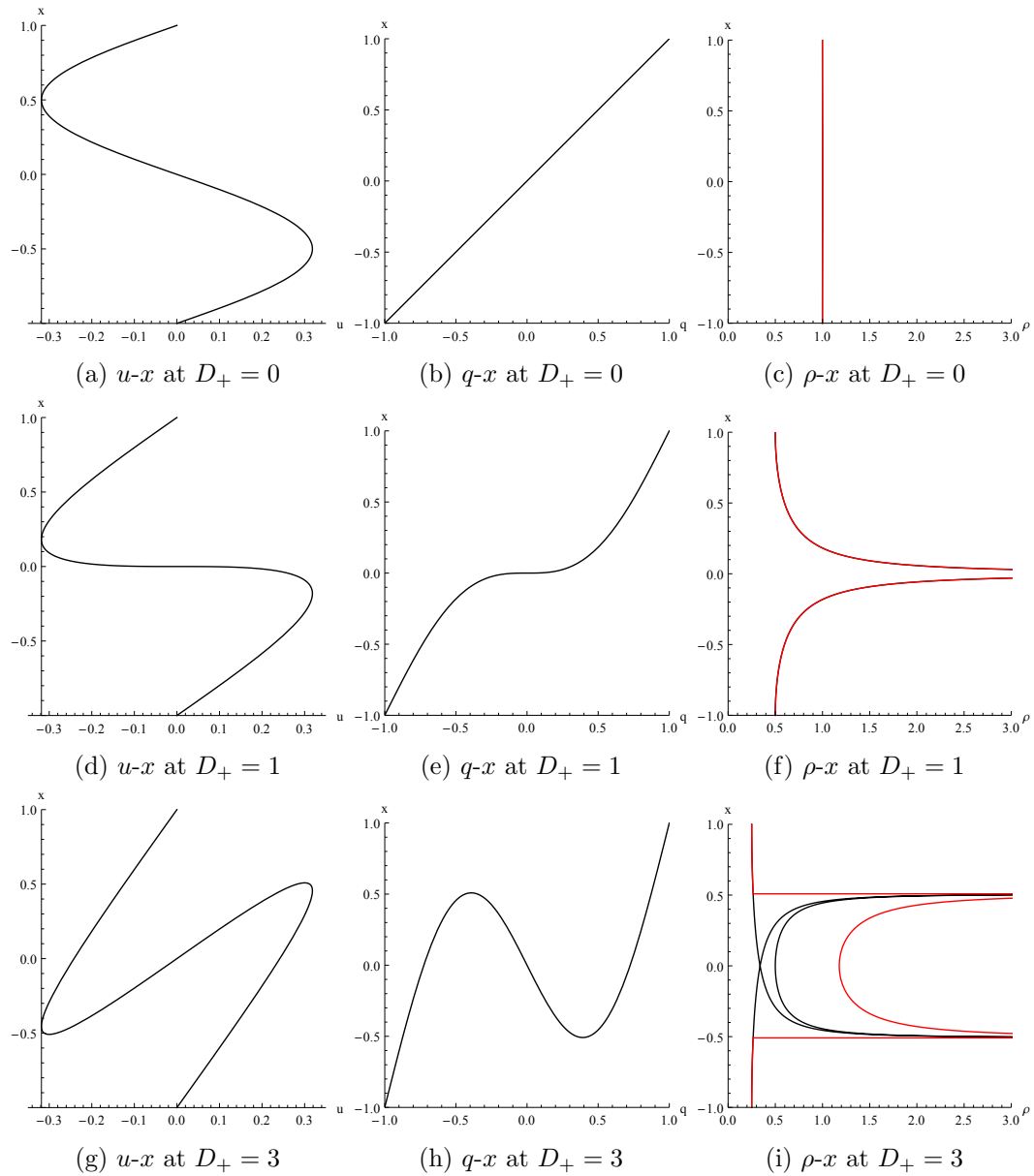
Figure 6.1: Caustics in the one-dimensional Zel'dovich approximation
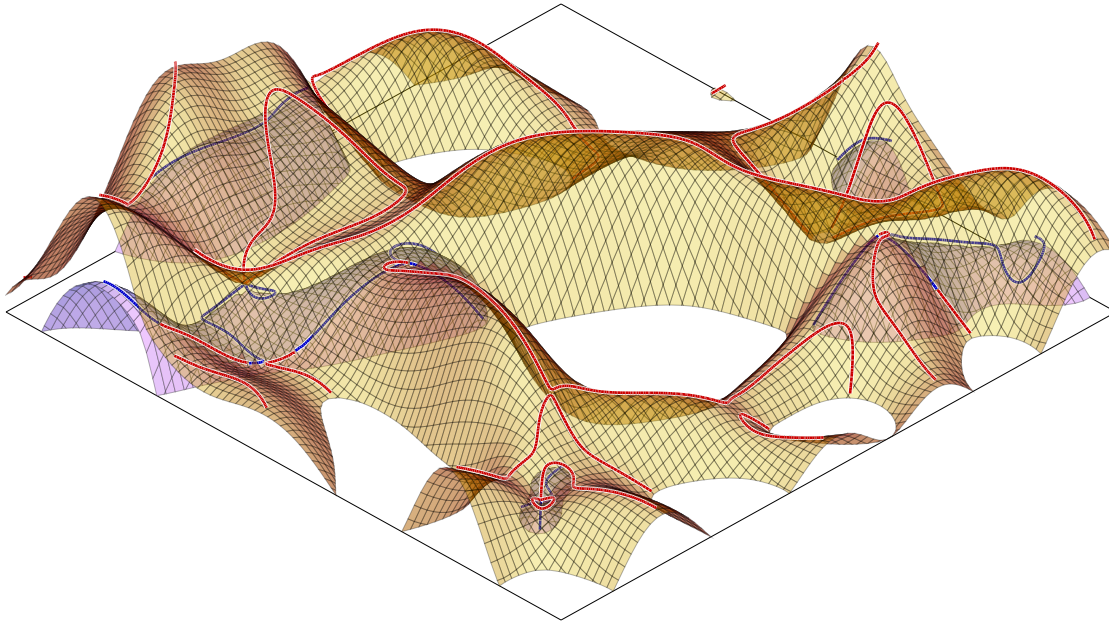
Figure 6.2: The yellow and blue surfaces are the graphs of the first and second eigenvalue fields by Johan Hidding et al. [33]. The points represent the A_4 and D_4 catastrophes whereas the red lines represent the A_3-lines.

condition $\lambda_1 \geq \lambda_2$. The density in the two-dimensional Zel'dovich approximation is

$$1 + \delta = \frac{1}{(1 - D_+\lambda_1)(1 - D_+\lambda_2)},$$

by which first and second shell crossing occur at point $\mathbf{q}$ when $\lambda_1(\mathbf{q}) = \frac{1}{D_+}$ and $\lambda_2(\mathbf{q}) = \frac{1}{D_+}$ occur respectively. Note that not all points undergo shell crossing since $D_+ > L \geq 0$ for some lower bound $L \in \mathbb{R}$ depending on the cosmology, and the eigenvalue can assume any real number.

   Geometrically, the evolution of shell crossing can be viewed in terms of the eigenvalue fields (see figure 6.2. Consider a horizontal plane at hight $1/D_+$. Initially the plane is at infinity, since $D_+(t = 0) = 0$. As time evolves the plane approaches the origin from above. When the plane intersects the eigenvalue field, shell crossing occurs. The points at which shell crossing occur at some time t form the A_2 lines. The points on which the eigenvector fields are parallel to the isocontours of the eigenvalue fields result in the A_3 lines. In figure 6.3, we see a top view of the eigenvalue fields, and catastrophes. In the subsequent sections, we analyze the role of the different catastrophes and connect them via the Zel'dovich approximation to the eigenvalue fields of the deformation tensor.

6.3.1 A_2: The fold catastrophe

The fold singularities A_2 occur at isocontours of the eigenvalue fields λ_1, and λ_2 and form curves. These curves are commonly called A_2-lines and are lines of shell crossing
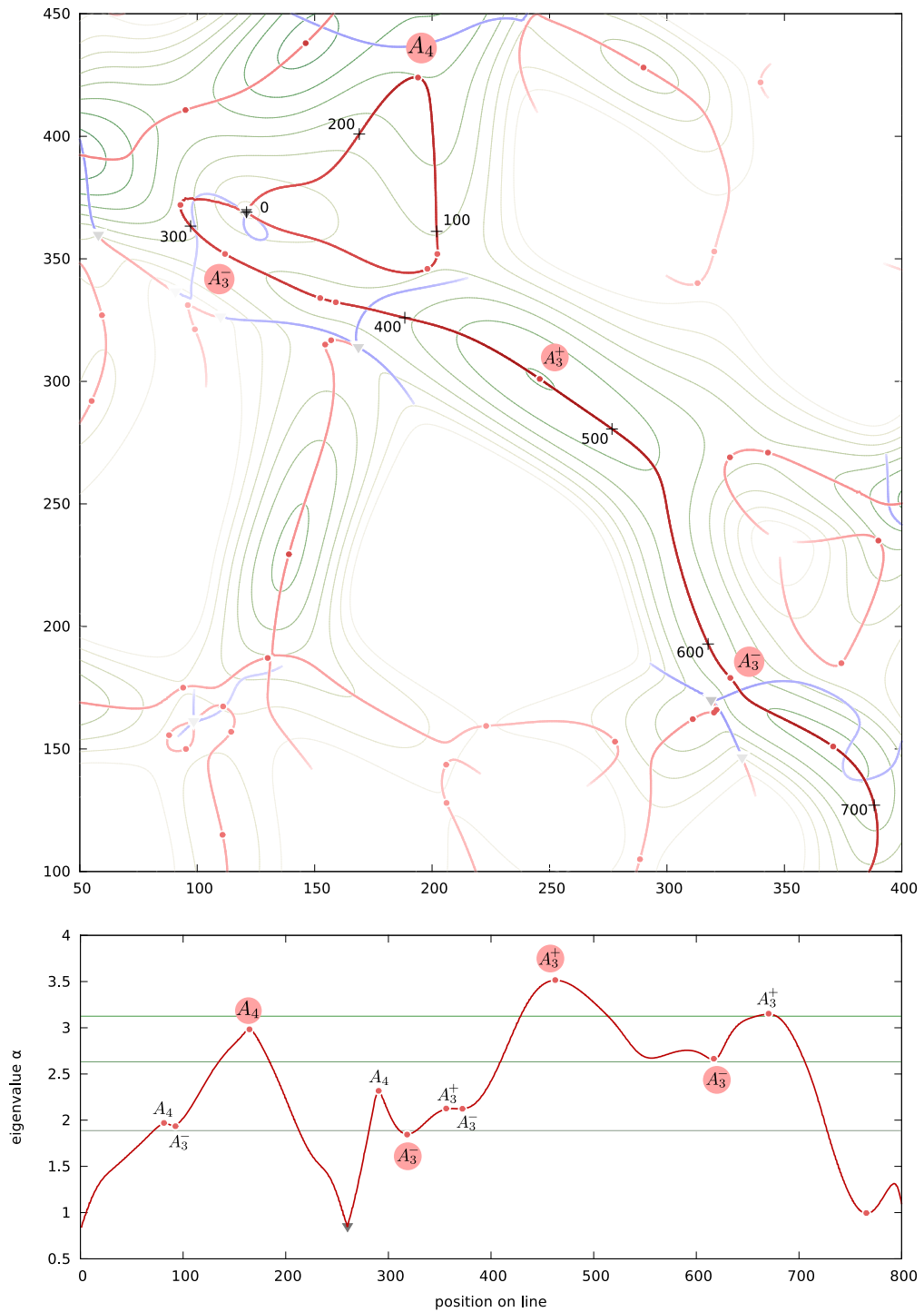
Figure 6.3: A top and side view of the eigenvalue fields and caustics of figure 6.2, by Johan Hidding et al. [33].

(a) First eigenvalue, eigenvector fields with A_3-lines.

(b) Second eigenvalue, eigenvector fields with A_3-lines.

(c) Potential field with A_3-lines.

(d) Time step 1

(e) Time step 2

(f) Time step 3
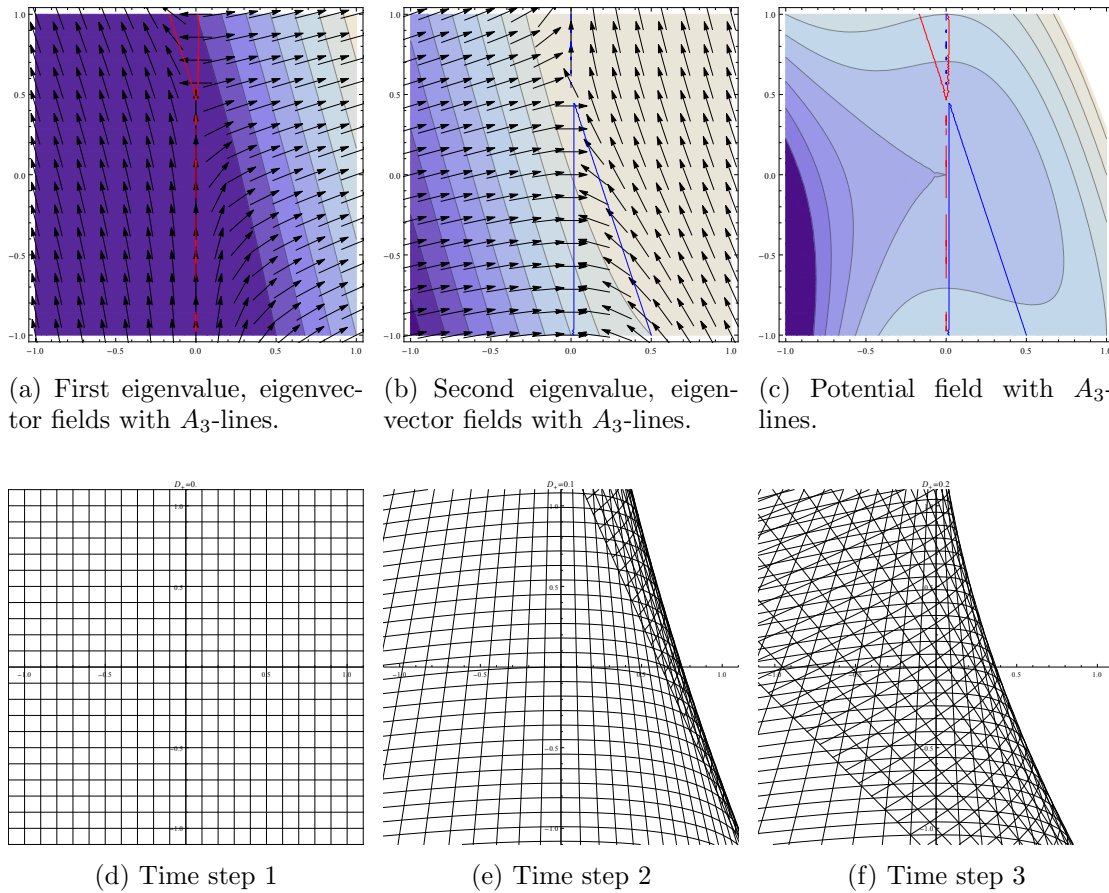
Figure 6.4: Evolution of a fold A_2 catastrophe in two dimensions

and surround collapsed regions of space (see figure 6.4). In nature these A_2-lines are supposed to be related to fronts of shock waves. The folds occurring first in the Zel'dovich approximation correspond to the λ_1 field. Folds appearing in collapsed regions of space correspond with isocontours of the λ_2 field, since $\lambda_1 \geq \lambda_2$.

6.3.2 A_3: The cusp catastrophe

In the Zel'dovich approximation, matter moves in the direction of the eigenvector fields v_1, and v_2 of the deformation tensor, corresponding to the eigenvalues λ_1 and λ_2 respectively. A cusp catastrophe is formed when the isocontour of λ_i for some positive value, is parallel to the eigenvector v_i, for some growing mode D_+ (see figure 6.5). This condition can formally be expressed as

$$v_i(\mathbf{q}) \cdot \nabla \lambda_i(\mathbf{q}) = 0,$$

where $\lambda_i(\mathbf{q}) > 0$. Points $\mathbf{q}$ satisfying this condition form curves called A_3-lines. As D_+ increases, the cusps move through space. The A_3-lines trace the paths of the A_3

(a) First eigenvalue and eigen-vector fields with A_3-lines.

(b) Second eigenvalue, eigen-vector fields with A_3-lines.

(c) Potential field with A_3-lines.

(d) Time step 1

(e) Time step 2

(f) Time step 3
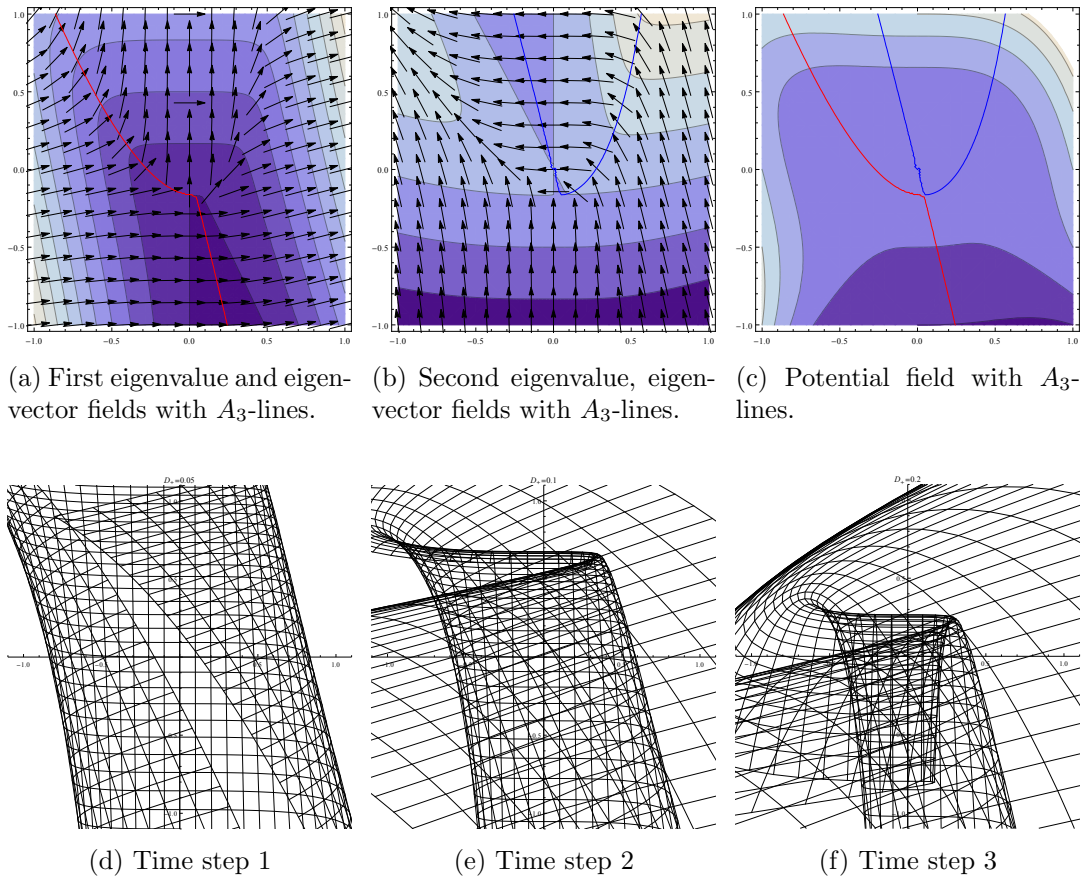
Figure 6.5: Evolution of the cusp A_3 catastrophe in 2 dimensions

catastrophes. The maxima and minima of the λ_i fields form special A_3 singularities. At the maxima shell crossing starts and fold catastrophes are created. At minima two fold singularities annihilate.

6.3.3 A_4: The swallowtail catastrophe

The swallowtail catastrophe occurs at the points in which an A_3-line is parallel to the eigenvector fields v_1 or v_2. The swallowtail catastrophe is the most intricate catastrophe in the A series for 2-dimensional fields. This can be seen in figure 6.6.

6.3.4 D_4: The umbilic catastrophe

The umbilic catastrophes come in two classes: the purse (hyperbolic) catastrophe D_4^+ and the pyramid (elliptic) catastrophe D_4^-. See figure 6.7 for the evolution of the umbilic catastrophes in two dimensions. The umbilics occur when $\lambda_1 = \lambda_2$ in the deformation tensor of Ψ_0. The first and second eigenvalue fields become non differentiable due to the ordering condition ($\lambda_1 \geq \lambda_2$), resulting in the first catastrophes of the D-series. Note
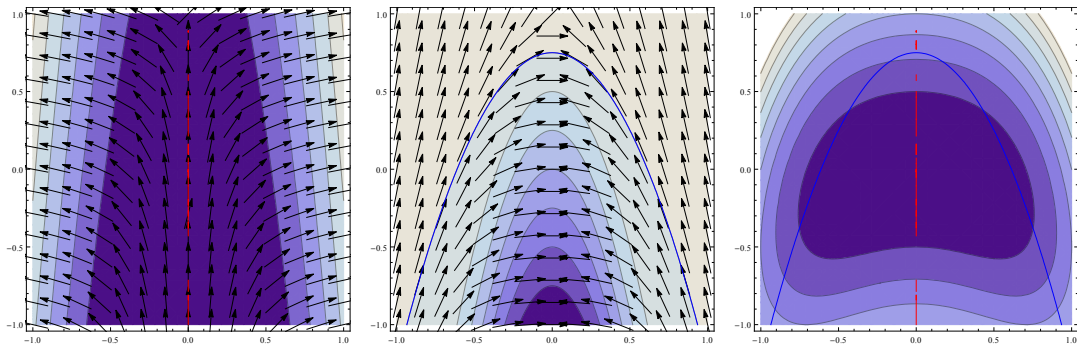
(a) First eigenvalue, eigenvec-
tor fields with A_3-lines.

(b) Second eigenvalue, eigen-
vector fields with A_3-lines.

(c) Potential field with A_3-
lines.
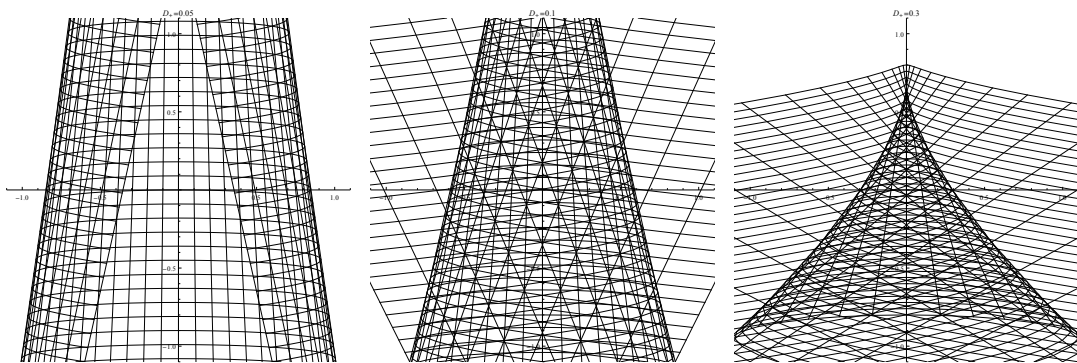
(d) Time step 1

(e) Time step 2

(f) Time step 3

Figure 6.6: Evolution of the swallowtail A_4 catastrophe in two dimensions

(a) First eigenvalue, eigenvector fields with A_3-lines.

(b) Second eigenvalue, eigenvector fields with A_3-lines.

(c) Potential field with A_3-lines.

(d) Time step 1

(e) Time step 2

(f) Time step 3
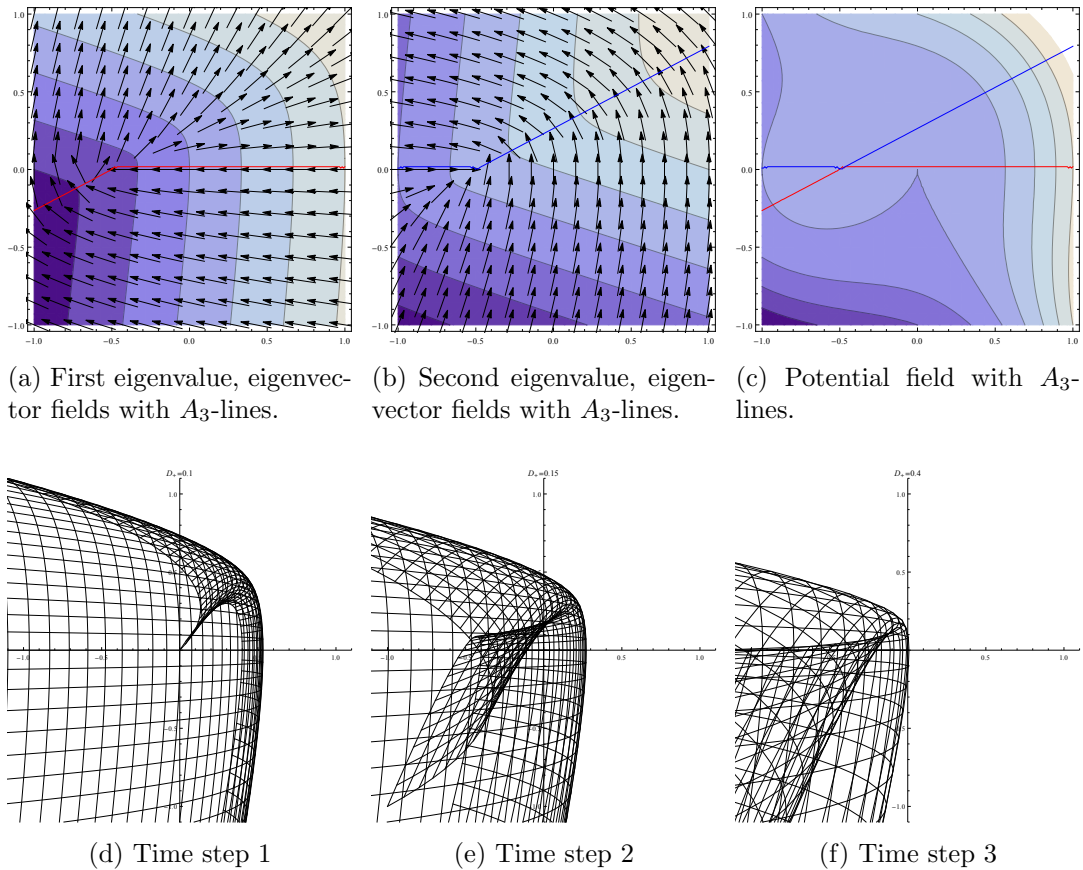
Figure 6.7: Evolution of the hyperbolic umbilic D_4^+ and elliptic umbilic D_4^- catastrophe in two dimensions

that this is the first condition in which two eigenvalues occur. The further classification of the umbilics D_4^+ and D_4^- follows from the eigenvectors v_1, and v_2 at the umbilic. It can be proven that an umbilic singularity always lies on an A_3-line.

6.4   Catastrophe in the Zel'dovich approximation with vorticity

The velocity field in the Zel'dovich approximation is a potential field. By choosing a velocity field instead of a gravitational potential we in general allow for vorticity. In this way more general caustics can appear. See figure 6.8 for a generic velocity field.

Consider the velocity field $\mathbf{u} = \left(\frac{x^2}{2} + xy + 3x, 0 \right)$ leading to figure 6.9. We clearly see shell crossing occur and can observe that the area of the grid cells locally goes to zero. This is the fold catastrophe. Now consider the velocity field $\mathbf{u} = \left(0, -x^2y - \frac{y^3}{3} + 3y \right)$. This leads to the evolution illustrated in figure 6.10. We obtain a so-called Zel'dovich
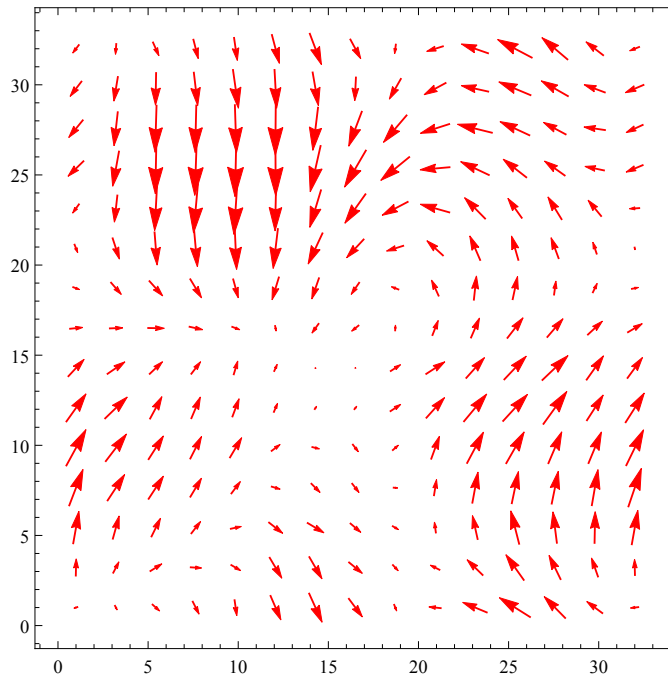
Figure 6.8: A generic velocity field with vorticity

pancake. The pancake consists of two A_2-lines meeting in a singular point. These points form the cusp catastrophe. In time the cusps move through space. The path they trace in Lagrangian space is the A_3-line. This process corresponds to the formation of filaments in the Zel'dovich approximation. The previous velocity fields had only caustics corresponding to the first eigenvalue field. When combining the A_2 and A_3 in the first and second eigenvalue field we can obtain very complex structures. For the velocity field $\mathbf{u} = \left(-\frac{x^3}{3} - xy^2 + 2x, -x^2y - \frac{y^3}{3} + 3y\right)$ we obtain caustics in collapsed regions (see figure 6.11). We furthermore observe many flow regions in which the preimage of the projection goes to more than two points. When the velocity has a large vorticity, the A_2 and A_3 catastrophes can generate patterns which do not occur in the Zel'dovich approximation. For the velocity field $\mathbf{u} = \left(\frac{x^2}{2} + xy + 3x, xy + \frac{y^2}{2} + 2y\right)$, we see A_2 and A_3 catastrophes (see figure 6.12). The conditions described above do not suffice to predict the A_3 catastrophes when the field has vorticity. For the four-dimensional catastrophes we can in principle generate velocity fields. The resulting plots are however not more insightful than the ones already presented in this chapter. For this reason we do not include them here.

(a) First eigenvalue and eigen-vector fields

(b) Second eigenvalue, eigen-vector fields

(c) Eulerian picture of a fold
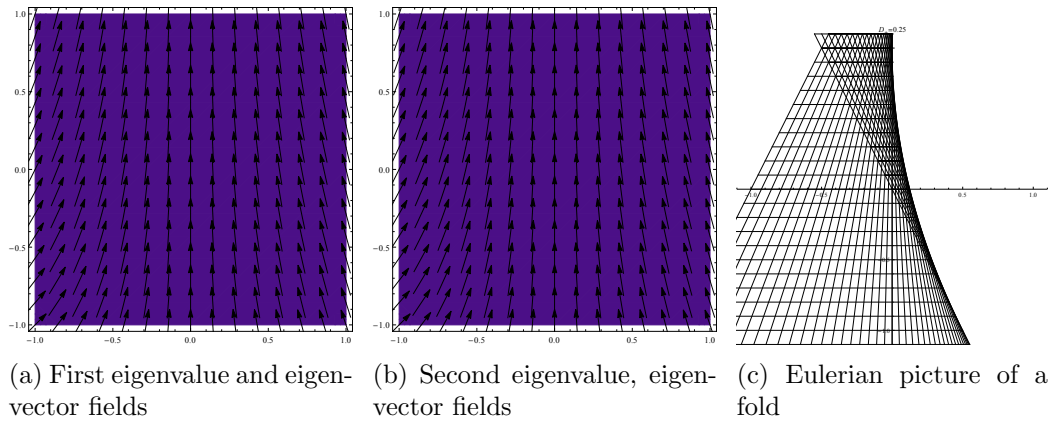
Figure 6.9: Evolution of the fold A_2 catastrophe

(a) First eigenvalue, eigenvec-tor fields with A_3-lines.

(b) Second eigenvalue, eigen-vector fields with A_3-lines.

(c) Eulerian picture time step 1

(d) Eulerian picture time step 2

(e) Eulerian picture time step 3
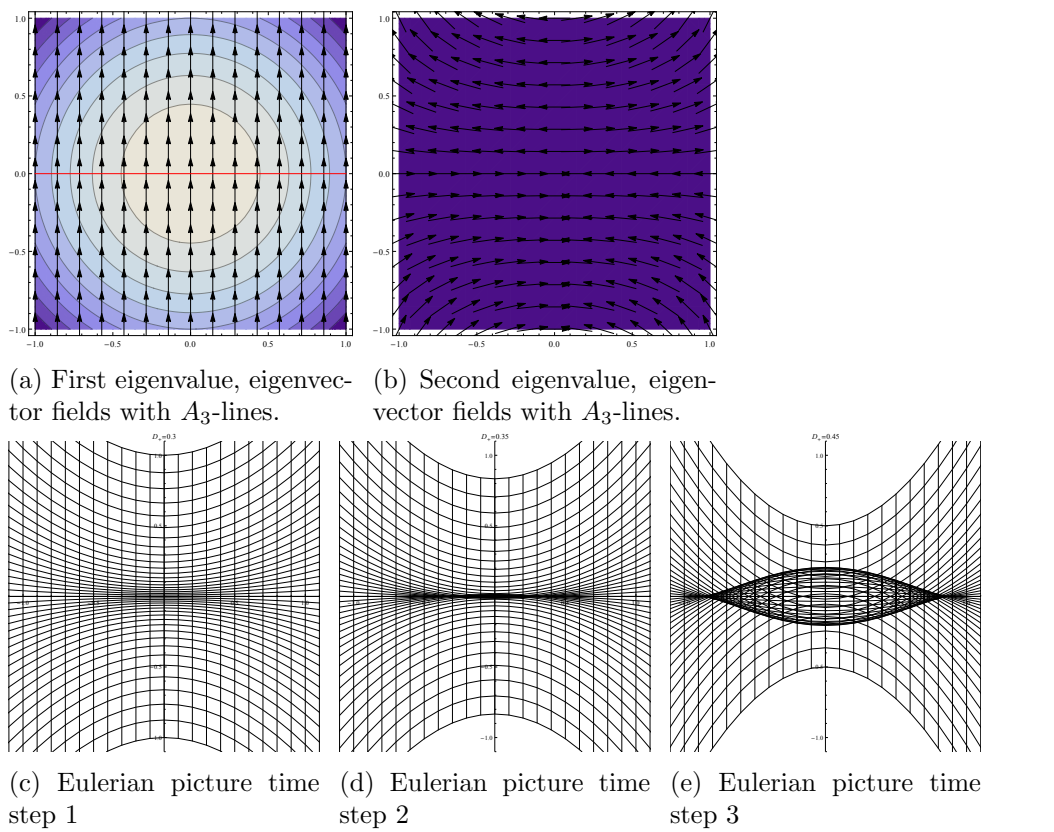
Figure 6.10: Evolution of the cusp A_3 catastrophe in two dimensions

(a) First eigenvalue, eigenvec-
tor fields with A_3-lines.

(b) Second eigenvalue, eigen-
vector fields with A_3-lines.

(c) Eulerian picture time
step 1

(d) Eulerian picture time
step 2

(e) Eulerian picture time
step 3
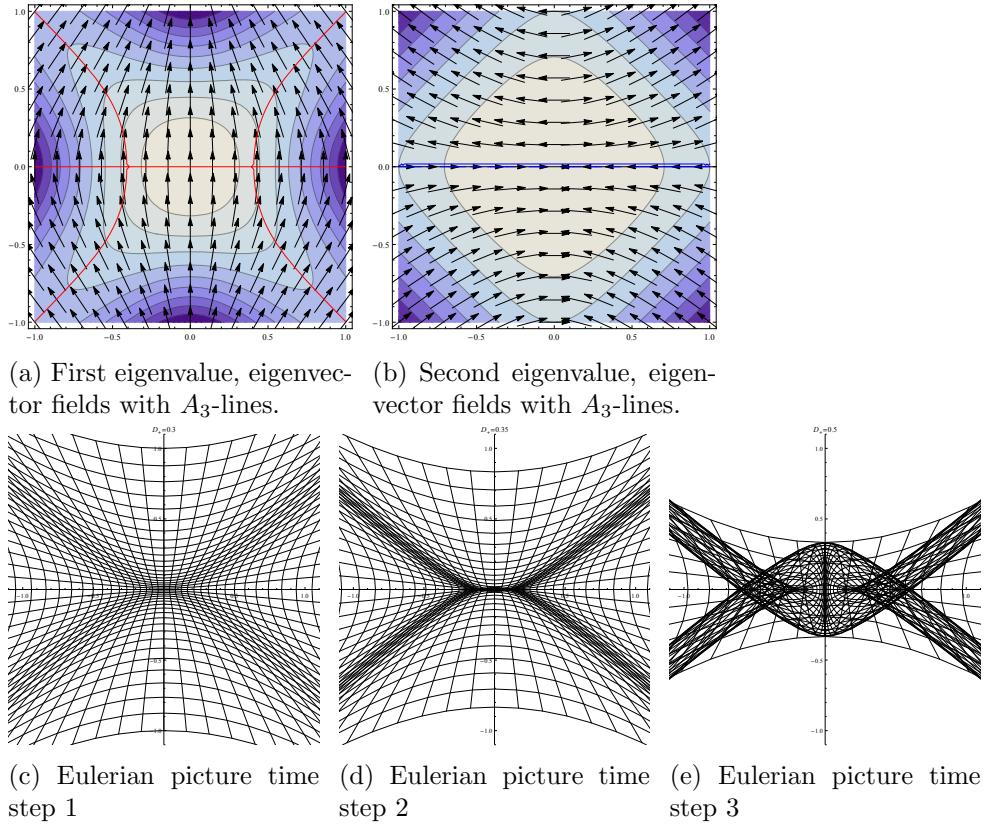
Figure 6.11: Evolution of the double cusp A_3 catastrophe in two dimensions

(a) Eulerian picture time
step 1

(b) Eulerian picture time
step 2

(c) Eulerian picture time
step 3
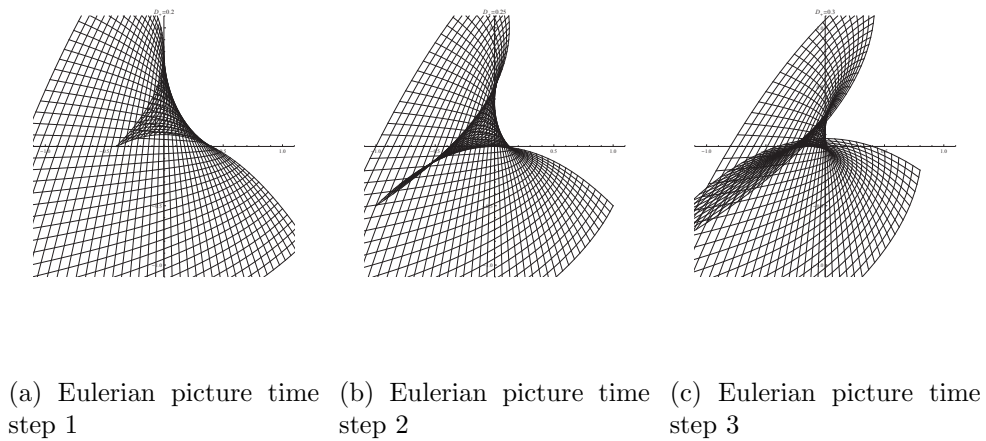
Figure 6.12: Evolution of the fold A_2 and cusp A_3 catastrophe with vorticity

6.5   Embryonic caustic skeleton

The previous sections constructed a list and the physical appearance of catastrophes occurring in large-scale structure formation. We furthermore developed a list of criteria for catastrophes in the Zel'dovich approximation. We observed how the catastrophes are related to the cosmic web and obtained conditions on the eigenvalue field of the deformation tensor for A_3, A_4 and D_4 points and A_2- and A_3-lines of the first eigenvalue field. These points and curves can be seen as a embryonic skeleton of the Lagrangian space. This skeleton gives a qualitative description of the cosmic web formed from fluctuations in Lagrangian space. In chapter 4 we analyzed the relevance of caustics in N-body simulations. In this section we compare the skeleton with the N-body simulation. In chapter 11 we consider a different embryonic skeleton based on Morse-Smale complexes.

In figure 6.13), we overlay the two-dimensional N-body simulation, presented in chapter 4, with the A_3, A_4 and D_4 points and A_3-lines. The N-body simulation is performed on initial density fluctuations generated from a Gaussian random field with a power-law power spectrum $P(k) = k^{-1/2}$ without smoothing. The upper, middle, and lower two frames correspond to an expansion of the universe with a scale factor $a = 0.3$, $a = 0.6$ and $a = 1.0$ respectively. The left frames give the embryonic skeleton in the initial conditions. The density fluctuations are smoothed with a Gaussian at different length scales to remove the small scale structure which which would have collapsed before the time we are considering, i.e. we are using the truncated Zel'dovich approximation. The right frames give the corresponding N-body simulation with Eulerian skeleton which is constructed by evolving the skeleton in Lagrangian space with the Zel'dovich approximation. Note that, since we are considering a power-law power spectrum, time evolution is very similar to zooming in. We could as well consider the different snap shots in time as zoomins of the same N-body simulation. We see that the comparison works good on large scales and starts to deviate on smaller scales.

In the figures we see a great agreement between the cosmic web and the caustics skeleton. In the linear regime, it is difficult to observe the N-body skeleton, due to perfect alignment. In the mildly non-linear regime and non-linear regime small deviations start to occur. Some structures are missed. Another problem is, that the A_3-lines start to wind in the clusters. Although this is what one would expect from the setting, it is problematic for a comparison with observations. We can however introduce a weight depending on the curvature of the A_3-lines to correct for those problems.
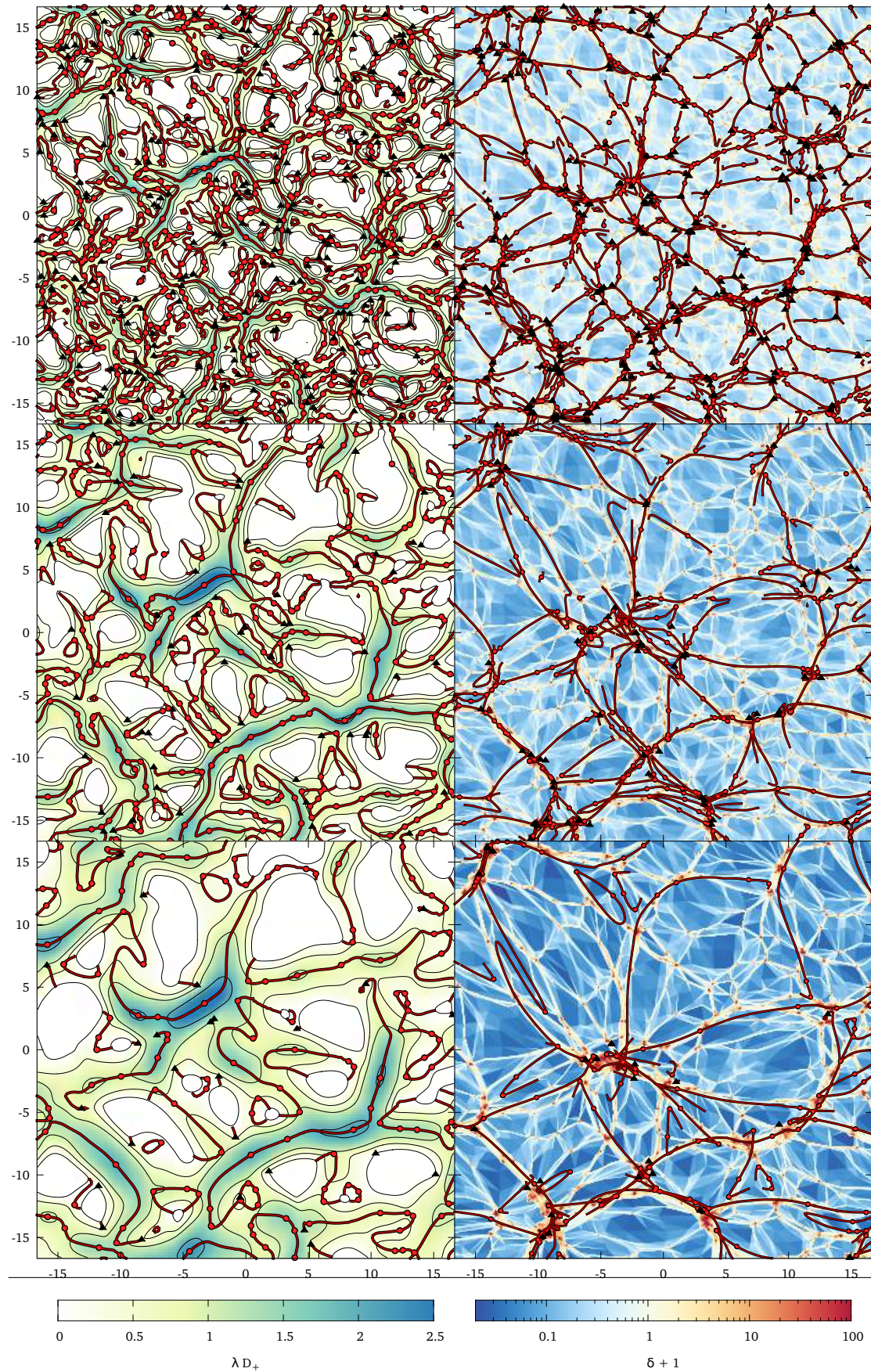
Figure 6.13: Two-dimensional N-Body simulation with A_3^+-lines, and A_3, A_4, and D_4 points. The illustration is made by Johan Hidding [33]

Chapter 7

Catastrophe Theory: Arnol'd's Classification Theorem

In this chapter we will give a more rigorous description of general and Lagrangian catastrophe theory. For a more pictorial description of Lagrangian critical points in low-dimensional functions see chapter 5. The framework of the theory described below is based on 'Catastrophe Theory' of D. Castrigiano and S. Hayes [18], whereas the proofs are based on Arnol'ds article (1972) [4]. In this chapter we illustrate the structure of general and Lagrangian catastrophe theory. The theory is however involved and contains many details. For this reason we prove the most insightful theorems and refer for the more elaborate theorems to standard textbooks. A more complete treatment of catastrophe theory can be found in "Singularities of Differentiable Maps, Volume 1 and 2" by Arnol'd [8],[5]. All functions in this chapter are assumed to be smooth, real-valued, and defined on open subsets U of $\mathbb{R}^n$.

Definition 1. *Let U be an open subset of $\mathbb{R}^n$. A function $f : U \to \mathbb{R}$ is **smooth** if it has derivatives of arbitrary order. Let n be the **dimension** of f.*

A point $x \in U$ has coordinates $x = (x_1, \ldots, x_n)$. The gradient of f in point $p \in U$ is $\nabla f(p) = (\partial_i f(p))_{i=1}^n \in \mathbb{R}^n$ with derivative $\partial_i^k f(p) = \partial^k f(p)/\partial x_i^k$. Catastrophe theory describes the behavior near critical points and classifies critical points of functions up to local coordinate transformations.

Definition 2. *A point $p \in U$ is a **critical point** of f if $\nabla f(p) = 0$.*

According to elementary calculus, the nature of a critical point p of f is determined by the Hessian matrix $Hf(p) = (\partial_i \partial_j f(p))_{i,j=1}^n \in \mathbb{R}^{n \times n}$.

Definition 3. *A critical point $p \in U$ of function f is called **nondegenerate** if the Hessian matrix $Hf(p)$ is invertible. The point p is called **degenerate** if $Hf(p)$ is singular. Let the **rank** of p be defined as the rank of the Hessian matrix rank $Hf(p)$, and let the **corank** of p defined as $n - $ rank $Hf(p)$.*

In the subsequent sections of this chapter, 'simple' critical points are further classified by means of normal forms. The behavior of functions near simple critical points is described using unfoldings and the critical points are restricted to Lagrangian critcal points. The classification of Lagrangian critical points plays an important role in the subsequent chapters of this thesis.

7.1   Classification of nondegenerate critical points

A nondegenerate critical point p of f is a maximum, minimum or saddle point. Functions with only nondegenerate critical points are commonly denoted as a Morse functions. The local behavior of a function f near a nondegenerate critical points is well described by the Morse Lemma. Given a nondegenerate critical point p, Morse's lemma states the existence of a local coordinate transformation (diffeomorphism) which transforms f at p locally to one of $n + 1$ standard functions.

Lemma 1. (Morse's lemma) *Let f vanish at $0 \in U$. The origin is a nondegenerate critical point of f if and only if a local diffeomorphism φ at 0 exists with $\varphi(0) = 0$ such that*

$$f(\varphi(y)) = -y_1^2 - \cdots - y_s^2 + y_{s+1}^2 + \cdots + y_n^2$$

holds around the origin. The integer s denotes the index of f at 0.

A global coordinate transformation (diffeomorphism) is defined as

Definition 4. *Let U, V be open in $\mathbb{R}^n$. A **diffeomorphism** is a local bijection $\varphi : U \to V$ for which both φ and φ^{-1} are smooth maps.*

A local coordinate transformation (local diffeomorphism) is defined as

Definition 5. *A smooth map $\varphi : U \to \mathbb{R}^n$ is a **local diffeomorphism at point** p in U if an open neighborhood of V of p in U exists such that $\varphi(V)$ is open in $\mathbb{R}^n$ and $V \to \varphi(V), x \mapsto \varphi(x)$, is a diffeomorphism.*

Proof. Assume that there exists a local diffeomorphism φ such that

$$f(\varphi(y)) = -y_1^2 - \cdots - y_s^2 + y_{s+1}^2 + \cdots + y_n^2$$

holds around the origin. Then the function f has a nondegenerate critical point at the origin since

$$D_y f(\varphi(0)) = D_y f(0) D_y \varphi(0) = 0$$

by which $Df(0) = 0$ and

$$D^2 f(\varphi(0)) = (D\varphi(0))^t D^2 f(0) D\varphi(0)$$

by which f is nondegenerate and has index s. We observe that the index is invariant under local diffeomorphisms.

Conversely, let f be a function with a nondegenerate critical point in the origin with vanishing function value. Choose local coordinates $(x_1, \ldots, x_n)$ around the origin. From Taylor's theorem we know that since $f(0) = 0$ there exist smooth function $g_1, \ldots, g_n$ such that

$$f(x_1, \ldots, x_n) = \sum_{k=1}^{n} x_i g(x_1, \ldots, x_n)$$

and

$$\frac{\partial f(0)}{\partial x_i} = g_i(0).$$

Since the origin is a critical point of f we see that $g_i(0) = 0$ for all $i = 1, \ldots, n$. Using Taylor's theorem on g_k we know the existence of functions h_{ki} such that

$$g_k(x_1, \ldots, x_n) = \sum_{i=1}^{n} x_i h_{ki}(x_1, \ldots, x_n).$$

Hence we can express f as

$$f(x_1, \ldots, x_n) = \sum_{k,i=1}^{n} x_i x_k h_{ki}(x_1, \ldots, x_n).$$

or in symmetrized form

$$f(x_1, \ldots, x_n) = \sum_{k,i=1}^{n} x_i x_k H_{ki}(x_1, \ldots, x_n)$$

with $H_{ki} = \frac{h_{ki} + h_{ik}}{2}$. However note that the function H_{ki} gives half the k, i component of the Hessian matrix since,

$$\frac{\partial^2 f(0)}{\partial x_k \partial x_i} = 2 H_{ki}.$$

Since the origin is a nondegenerate critical point of f, the matrix $(h_{ki})_{k,i}$ is non-singular.

Suppose inductively there exist local coordinates $u_1, \ldots, u_n$ in a neighborhood U_1 of 0 such that

$$f = \pm u_1 \pm \cdots \pm u_{r-1}^2 + \sum_{i,j \geq r} u_i u_j H_{ij}(u_1, \ldots, u_n).$$

By a linear change of the final r coordinates we can assume that $H_{rr} \neq 0$, since otherwise the matrix $(H_{ij})_{i,j}$ would be singular. Let $g(u_1, \ldots, u_n) = \sqrt{H_{rr}(u_1, \ldots, u_n)}$. By the

| (a) Maximum | (b) Saddle point | (c) Minimum |
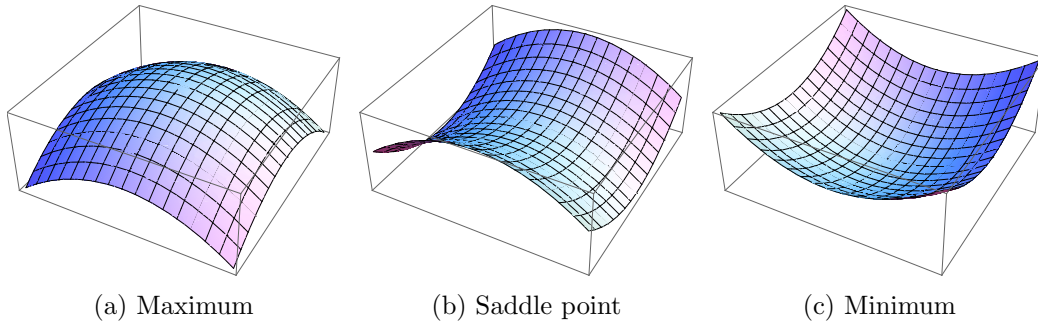
Figure 7.1: Morse normal forms of nondegenerate critical points in two dimensions

Inverse Function Theorem this g is smooth in an neighborhood U_2 of 0 contained in U_1. Now making the coordinate transformation to $(v_1, \ldots, v_n)$ defined by

$$v_i = u_i \text{ for } i \neq r$$

$$v_r = g(u_1, \ldots, u_n) \left(u_r + \sum_{i>r} \frac{u_i H_{ir}(u_1, \ldots, u_n)}{H_{rr}(u_1, \ldots, u_n)} \right)$$

which is a local diffeomorphism by the Inverse Function Theorem, we have in new coordinates

$$f = \pm v_1 \pm \cdots \pm v_r^2 + \sum_{i,j \geq r+1} v_i v_j H_{ij}(v_1, \ldots, v_n).$$

Hence by induction we obtain the morphism φ of Morse's lemma. $\square$

Note that the index of a critical point s is equal to the number of negative eigenvalues of the Hessian $Hf(p)$. The corank of a nondegenerate critical point is 0 whereas the rank of a degenerate critical point is less then n.

Example 1. *For $n = 2$, Morse's lemma gives the normal forms $-x_1^2 - x_2^2$, $-x_1^2 + x_2^2$ and $x_1^2 + x^2$ representing the maximum, saddle point and minimum respectively (see figure 7.1).*

7.2   Classification of simple degenerate critical points

Morse's lemma classifies the nondegenerate critical points up to local diffeomorphism. In a similar spirit, Arnol'd's classification theorem classifies simple degenerate critical points. Note that Arnol'd's theorem is an extension of Thom's classification theorem of nondegenerate critical points of codimension at most 4.[1] The notions of simple and codimension will be formally defined in the proof.

---

[1] Critical points of codimension at most 5 are simple.

The proof of Arnol'd's classification theorem is divided into four parts. In the first part we prove the reduction lemma, which reduces the classification of nondegenerate critical points of rank r to the classfication of nondegenerate critical points of rank 0. In the second part we prove the determinacy lemma which states to which order a Taylor expansion around a critical point contains the qualitative behavior of a function around that point. In the third part the notion of codimension is introduced, central to Thom's classification theorem. Finally in the fourth part Arnol'ds classification theorem is proven.

7.2.1 The reduction lemma

Let $p \in U$ be a critical point of f with rank r and corank $n - r$. If p is nondegenerate, the rank is n and corank vanishes. If p is degenerate, the rank is less than n and the corank does not vanish. According to the **reduction lemma** the study of degenerate critical points with rank r can be reduced to the study of **totally degenerate** critical points with vanishing rank.

Definition 6. *Let r be an integer with $0 \leq r < n$, and let V be open in $\mathbb{R}^{n-r}$ with $0 \in V$. Then f is **reducible** at the origin to a smooth function $g : V \to \mathbb{R}$ if a local diffeomorphism ψ at $0 \in \mathbb{R}^n$ with $\psi(0) = 0$ exists as well as a normal quadratic form q_{sr} on $\mathbb{R}^r$ defined by $q_{sr}(x_1, \ldots, x_r) = -x_1^2 - \cdots - x_s^2 + x_{s+1}^2 + \cdots + x_r^2$ such that $\psi(y) \in U$ and*

$$f(\psi(y)) = q_{sr}(y_1, \ldots, y_r) + g(y_{r+1}, \ldots, y_n)$$

hold for all $y \in W \times V$, where W is open in $\mathbb{R}^r$ with $0 \in W$.

Lemma 2. *(Reduction Lemma)* *If the origin is a degenerate critical point of f, then f is reducible to a smooth function g with vanishing rank at the origin, such that the origin is also a critical point of g. Note that r in the definition is equal to the rank of f.*

Proof. For the proof of the reduction lemma we refer to chapter 3, theorem 2 of 'Catastrophe theory' by Castrigiano and Hayes [18]. The proof follows from Morse's Lemma and the Implicit Function Theorem. The lemma was originally proven by D. Gromoll and W. Meyer in 1969 for a more general setting [30].   □

Example 2. *The function $f(x_1, x_2) = x_1^3 + x_2^2$ is reducible to $g(x_1) = x_1^3$ with vanishing rank and a critical point at 0.*

7.2.2 Determinacy

The proof of Arnol'd's and Thom's classification is based on Taylor expansions. In order to use these expansions we first determine whether the qualitative behavior of a function near a critical point is **determined** by the Taylor expansion around this point. We analyze whether all smooth functions f with a coinciding Taylor polynomial are equivalent under a smooth change of coordinates, near the critical point. Before we can formally

define and find conditions for determinacy, we first have to define some differential and algebraic geometric objects.

In study of critical points of a function f, we are only interested in f near the critical points. In this context we consider the notion of a germ of a map.

Definition 7. *Let $m, n \in \mathbb{N}$. On the set*

$$\{F : U \to \mathbb{R}^m : U \text{ open in } \mathbb{R}^n \text{ with } 0 \in U \text{ and } F \text{ smooth}\}$$

*consider the following equivalence relation: If $F_i : U_i \to \mathbb{R}^m$ for $i = 1, 2$ are in this set, then $F_1 \sim F_2$ means that on an open subset of $U_1 \cap U_2$ containing 0, the maps F_1, F_2 coincide. The equivalence class $[F]$ of an element F is called the **germ of** F **at** 0. Let $\mathcal{E}_{n,m}$ be the set of all such germs at the origin. If $m = 1$ we write $\mathcal{E}$.*

Example 3. *The functions $f_1 : (-1/2, 1) \to \mathbb{R}, f_1(x) = x^2$ and $f_2 : (-1, 1/2) \to \mathbb{R}, f_2(x) = x^2$ are equivalent and are elements of the germ $[x^2] \in \mathcal{E}$. On the subset $(-1/2, 1/2) = (-1/2, 1) \cap (-1, 1/2)$, the functions $f_1 = f_2 = x^2$.*

The set of all germs at the origin $\mathcal{E}$ is a commutative and associative algebra over $\mathbb{R}$ under a natural set of operations. For open sets U_1, U_2 of $\mathbb{R}^n$ and functions $f_i : U_i \to \mathbb{R}$ for $i = 1, 2$ and $\alpha \in \mathbb{R}$ let

- $[f_1] + \alpha[f_2] = [f_1|V + \alpha f_2|V]$

- $[f_1][f_2] = [(f_1|V)(f_2|V)],$

with $f_i|V$ the restriction of f_i to $V = U_1 \cap U_2$. Note that $\mathcal{E}$ has an identity element generated by the unit function $[1]$ and that for $[f]$ there exists an inverse $[f]^{-1}$ if and only if $f(0) \neq 0$.

In the remaining sections of this chapter a multi-index notation is used. For multi-index $\nu = (\nu_1, \ldots, \nu_n) \in \mathbb{N}_0^n$, let $|\nu| = \nu_1 + \cdots + \nu_n$, and $\nu! = \nu_1! \ldots \nu_n!$. For $x = (x_1, \ldots, x_n) \in \mathbb{R}^n$ let $x^\nu = x_1^{\nu_1} \ldots x_n^{\nu_n}$ and $\partial^\nu = \partial^{\nu_1} \ldots \partial^{\nu_n}$. The Taylor polynomial of order k of f at $p \in U$ in multi-index notation is

$$T_{f,p}^k(x) = \sum_{0 \leq |\nu| \leq k} \frac{\partial^\nu f(p)}{\nu!}(x - p)^\nu.$$

Using the multi-index notation we define the space of functions with coinciding Taylor expansions, called the **jet space** J^k.

Definition 8. *Let k be a nonnegative integer. Two germs $[f]$ and $[g]$ in $\mathcal{E}$ are k-**equivalent** if $\partial^\nu f(0) = \partial^\nu g(0)$ for all $\nu \in \mathbb{N}_0^n$ with $|\nu| \leq k$. The class of all germs k-equivalent to $[f]$ is called the k-**jet** of f and is denoted by $j^k[f]$. The set of all k-jets of germs in $\mathcal{E}$ is denoted by J_n^k or J^k.*

Like the space of germs at the origin $\mathcal{E}$, the jet space J^k carries a product operation $j^k[f] \cdot j^k[g] = j^k[f \cdot g]$, omitting the open sets. We furthermore define the a composition of the jet space J^k with the **group of germs of local diffeomorphisms leaving the origin invariant**, to formalize the notion of a local coordinate transformation on a jet.

Definition 9. *For a local diffeomorphism φ of $\mathbb{R}^n$ at the origin with $\varphi(0) = 0$ let $[\varphi]$ be the corresponding germ. The collection of all these germs forms the **group $\mathcal{G}_n$ or $\mathcal{G}$ of local diffeomorphisms of $\mathbb{R}^n$ leaving the origin invariant**.*

Note that the composition of two elements $[\varphi], [\psi] \in \mathcal{G}$ is defined by the composition $[\varphi][\psi] = [\varphi \cdot \psi]$, the group $\mathcal{G}$ has a neutral element generated by the identity $[id]$ and by the properties of local diffeomorphisms each element $[\varphi] \in \mathcal{G}$ has an inverse $[\varphi^{-1}] \in \mathcal{G}$.

The group $\mathcal{G}$ acts on the germs $\mathcal{E}$ via the action

$$\mathcal{E} \times \mathcal{G} \to \mathcal{E}, ([f], [\varphi]) \mapsto [f][\varphi] = [f \circ \varphi].$$

Note that for $\varphi, \psi \in \mathcal{G}$ we have $([f][\varphi])[\psi] = [f]([\varphi][\psi])$ and $[f][id] = [f]$. This leads to an equivalence of germs.

Definition 10. *Two germs $[f], [g] \in \mathcal{E}$ are **equivalent**, denoted by $[f] \sim [g]$, if there exists a $[\varphi] \in \mathcal{G}$ such that $[g] = [f][\varphi]$. The orbit of $[f]$ under $\mathcal{G}$ is defined by*

$$[f]\mathcal{G} = \{[f][\varphi] : [\varphi] \in \mathcal{G}\}$$

of all germs in $\mathcal{E}$ equivalent to $[f]$.

Example 4. *The Morse lemma states that all germs of functions near nondegenerate critical points lie in one of the orbits $[q_{s,n}]\mathcal{G}$, with $0 \leq s \leq n$.*

This enables us to define the determinacy of a germ in $\mathcal{E}$.

Definition 11. *Let k be a positive integer. A germ $[f] \in \mathcal{E}$ is called k-**determined** if every germ that is k-equivalent to $[f]$ is equivalent to $[f]$. A germ is **finitely determined** if k is finite. If $[f]$ is finitely determined, the smallest k for which $[f]$ is k-determined is the **determinacy** of $[f]$ denoted by $det[f]$.*

In the one-dimensional case the property has a simple interpretation

Lemma 3. *A simple germ $[f] \in m_1$ has determinacy k if and only if k is the smallest positive integer satisfying $\partial_1^k f(0) \neq 0$.*

Proof. Let the germ $[f]$ have determinacy k. Since $T_f^k \neq 0$, a small integer $l \leq k$ exists such that $f^{(l)}(0) \neq 0$. Let ϵ be the sign of $f^{(l)}(0)$. Now $[f] \sim [\epsilon^{l-1}x^l]$ since its lth derivative is nonzero and $det[\epsilon^{l-1}x^l] = l$. The determinacy of f is equal to the determinacy of $[\epsilon^{l-1}x^l]$ since this property is invariant under local diffeomorphisms, i.e. $k = l$. Conversely let k be the smallest integer satisfying $f^{(k)}(0) \neq 0$. Now $[f]$ is k-determined since $T_f^{k-1} = 0$. $\qquad\square$
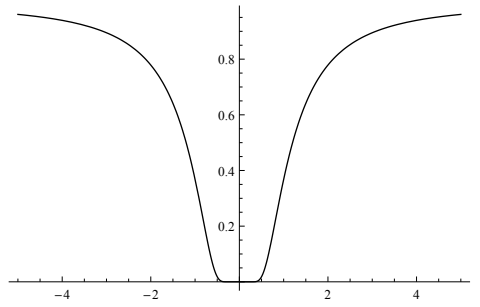
Figure 7.2: The function f_2 has a flat point in the origin

Constant functions and flat points are not finitely determined.

Example 5. *All derivatives of the functions $f_1(x) = 0$ and $f_2(x) = \exp\left(-\frac{1}{x^2}\right)$ vanish in the origin. This is called a flat point (see figure 7.2). No Taylor expansion at 0 can distinguish f_1 and f_2.*

The remaining part of this subsection is devoted to determining the determinacy of $[f]$. For the formulation of a sufficient condition we define the ideals[2] consisting of germs with kth order zeroes at the origin.

$$m_n^k = m^k = \{[f] \in \mathcal{E}_n | \partial^\nu f(0) = 0 \text{ for all } |\nu| < k\}.$$

Note that m^k is an ideal since $m^k \mathcal{E} \subset m^k$. The ideal m is the only maximal ideal of $\mathcal{E}$ since it consists of the set of all non-invertible elements of $\mathcal{E}$. These ideals have a hierarchical structure $\mathcal{E} \supset m \supset m^2 \supset m^3 \supset \ldots$ but $m^k \neq m^{k+1}$ for all positive k. The homogeneous polynomials of order k generate the ideal[3] m^k, i.e.,

$$m^k = \langle x^\nu | |\nu| = k \rangle_\mathcal{E}.$$

Finally we define the **Jacobi ideal** $\mathcal{J}[f]$.

Definition 12. *The **Jacobi ideal** $\mathcal{J}[f]$ of a germ $[f] \in \mathcal{E}$ is the ideal of $\mathcal{E}$ generated by the germs of the partial derivatives $\partial_i f$ for $i = 1, \ldots, n$, i.e.,*

$$\mathcal{J}[f] = \langle \partial_1 f, \ldots, \partial_n f \rangle_\mathcal{E}.$$

This leads to the theorem

Theorem 2. *A germ $[f] \in \mathcal{E}$ is k-determined if $m^{k+1} \subset \langle m^2 \mathcal{J}[f] \rangle$.*

Proof. For the proof we refer to 'Catastrophe Theory' by Castrigiano and Hayes [18]. □

---

[2]An ideal I of $\mathcal{E}$ is a additive subgroup of $\mathcal{E}$ such that for all $i \in I, e \in \mathcal{E}$ the product $i \cdot e \in I$.
[3]The germs $[f_i]$ generate an ideal $I \subset \mathcal{E}$ if $I = \langle f_i | \text{ for all } i \rangle_\mathcal{E} = [f_1]\mathcal{E} + [f_2]\mathcal{E} + \ldots$.

Formally the condition is also necessary, by which $[f]$ is k-determined if and only if $m^{k+1} \subset \langle m^2 \mathcal{J}[f] \rangle$. In the following example the k-determinacy of all polynomials needed in the rest of this chapter is proven.

Example 6. *The following polynomials are k-determined at 0*

polynomial	determinacy	dimension n
$\pm x^k$	k	1
$0, x^2 y, x^3$	∞	2
$x^2 y \pm y^3$	3	2
$x^2 y \pm y^s$	s	2

Proof. Since the origin of the forms $0, x^3$ and $x^2 y$ is a not isolated critical point, we see that they are not finitely determined. The forms $x^2 y \pm y^3$ are 3-determined. Transform the cubic forms by a coordinate transformation to $f = x^2 y \pm \frac{1}{3} y^3$. Now since $\partial_x f = 2xy$, $\partial_y f = x^2 \pm y^2$ and

$$y^4 = (x^2 \pm y^2)(\pm y^2) \mp 2xy(xy/2) \qquad\qquad y^3 x = 2xy(y^2/2)$$
$$x^2 y^2 = 2xy(xy/2) \qquad\qquad\qquad\qquad yx^3 = 2xy(x^2/2)$$
$$x^4 = (x^2 \pm y^2)x^2 \mp 2xy(xy/2)$$

and $m^4 = \langle x^\nu || \nu | = 4 \rangle_\mathcal{E} = \langle y^4, y^3 x, y^2 x^2, yx^3, x^4 \rangle_\mathcal{E}$ we see that $m^4 \subset \langle m^2 \mathcal{J}[f] \rangle$. This concludes the proof. $\square$

7.2.3 Simple critical points and codimension

The main difference between Thom's and Arnol'd's classification theorems comes from the use of the property **simple** and **codimension**. Thom used the notion codimension.

Definition 13. *Let $[f]$ be a germ in m^2. Then the codimension of $[f]$ is $\mathrm{cod}[f] = \dim m/\mathcal{J}[f]$.*

Colloquially the codimension counts the minimal number of parameters to perturb f and get all qualitative different behaviors of f. This concept is formalized in the section about unfoldings. Note that for a nondegenerate germ $[f] \in \mathcal{E}$, we have $m = \mathcal{J}[f]$ by which $\mathrm{cod}[f] = 0$. Conversely we can prove that $\mathrm{cod}[f] = 0$ implies that f has a nondegenerate critical point at 0. A germ $[f]$ with nonzero codimension is degenerate. Thom used the fact[4] that all degenerate germs in $\mathcal{E}$ with codimension at most 5 have rank 1 or 2.

Arnol'd used the slightly more general[5] notion **simple**.

Definition 14. *An orbit V of the action $\mathcal{G}$ on $\mathcal{E}$ is **simple** if a sufficiently small neighborhood of any point $v \in V$ contains only a finite number of orbits.*

---

[4]Thom originally used codimension at most 4.

[5]It can be proven that all critical points of codimension at most 5 are simple.

Example 7. *A germ $[f]$ of a flat point (for example $f = \exp\left(-\frac{1}{x^2}\right)$) is not simple since all orbits $[x^\nu]\mathcal{G}$ lie arbitrarily close to $[f]\mathcal{G}$. Such a point has nonzero moduli.*

Analogously to the codimension, Arnol'd proved that the property simple restricts the corank of germs in $\mathcal{E}$.

Lemma 4. *The corank of a simple germ does not exceed two.*

Proof. This is the property proven by Arnol'd to extend Thom's classification theory. For the proof we refer to Arnol'd 1972 lemma 4.2 [4]. □

7.2.4 Arnol'd's and Thom's classification theorem of critical points of codimension at most 4

The previous statements allow us to prove the classification theorem. The necessary determinacy of polynomials has been proven in example 6. In the upcoming lemmas and theorem, we state that the normal forms A_k, D_k and E_k are simple and give their codimension. The property simple will be proven in the section about unfoldings. The codimension of the normal forms can directly be calculated and is denoted for completeness. In this subsection we first consider germs with corank 1 after which germs with corank 2 follow.

For simple germs of corank 1 we obtain the A (linear) series.

Lemma 5. *A simple germ with a critical point of corank 1 can be reduced to one of the normal forms of type $A_k^\pm$ for some $k \geq 2$, given by*

$$\pm x_1^{k+1} + q_{s,n-1}(x_2, \ldots, x_n),$$

with codimension $k - 1$.

Proof. Let $[f] \in \mathcal{E}$ be a simple germ with corank 1. By the reduction lemma, choose coordinates x such that

$$f = g(x_1) + q_{s,n-1}(x_2, \ldots, x_n),$$

for some $g \in m^3$. The function g cannot have a flat point at the origin (in which all derivatives vanish), since otherwise the germ of f is not simple since all orbits of the form $[x_1^l + q_{s,n-1}(x_2, \ldots, x_n)]\mathcal{G}$ lie arbitrarily close to $[f]\mathcal{G}$. Let $k \geq 2$ be the smallest integer for which $\partial_1^{k+1} g(0) \neq 0$, by which $[g] \sim [\pm x^{k+1}]$ since the Taylor expansion of g consists of a term proportional to x^{k+1} and the germs $[\pm x^{k+1}]$ are $(k+1)$-determined. Hence

$$[f] \sim [g + q_{s,n-1}] = [g] + [q_{s,n-1}] \sim [\pm x^{k+1}] + [q_{s,n-1}] = [\pm x^{k+1} + q_{s,n-1}],$$

by which

$$\pm x_1^{k+1} + q_{s,n-1}(x_2, \ldots, x_n),$$

is a normal form of f. □

For the classification of simple germs with corank 2 we first classify cubic forms of the form $ax^3 + bx^2y + cxy^2 + dy^3 \in \mathbb{R}[x, y]$.

Lemma 6. *Let p be a cubic form on $\mathbb{R}^2$. There is a linear coordinate transformation τ on $\mathbb{R}^2$ such that $p \circ \tau$ is equal to exactly one of the forms*

$$x^2y \pm y^3, x^2y, x^3, 0$$

The cubic forms $x^3 \pm xy^2$ are 3-determined whereas $0, x^3, x^2y$ are not finitely determined.

Proof. The five forms are unique, i.e., no two forms can be transformed into each other by a linear coordinate transformation $\tau : \mathbb{R}^2 \to \mathbb{R}^2, \tau(x, y) = (\alpha x + \beta y, \gamma x + \delta y)$, with $\alpha\delta - \beta\gamma \neq 0$. First note that the null form is invariant under τ and therefore linearly inequivalent to the other four forms. Now consider the zero set of the four remaining forms:

form	zero set	set of critical points
$x^2y + y^3$	$\{y = 0\}$	$\{0\}$
$x^2y - y^3$	$\{y = 0\} \cup \{x = y\} \cup \{x = -y\}$	$\{0\}$
x^2y	$\{x = 0\} \cup \{y = 0\}$	$\{x = 0\}$
x^3	$\{x = 0\}$	$\{x = 0\}$

Only the zero sets of $x^2y + y^3$ and x^3 can be transformed into each other by τ. However the set of critical points of $x^2y + y^3$ and x^3 cannot be transformed into each other. Hence the five cubic forms are pairwise linearly inequivalent.

Now we show that every cubic form p on $\mathbb{R}^2$ is linearly equivalent to exactly one of the 5 standard forms. Let $p = ax^3 + bx^2y + cxy^2 + dy^3$ and $p' = a'x^3 + b'x^2y + c'xy^2 + d'y^3$ with $p' = p \circ \tau$, which is equivalent to

$$\begin{aligned}
a' &= a\alpha^3 + b\alpha^2\gamma + c\alpha\gamma^2 + d\gamma^3 \\
b' &= 3a\alpha^2\beta + b(2\alpha\beta\gamma + \alpha^2\delta) + c(2\alpha\gamma\delta + \beta\gamma^2) + 3d\gamma^3\delta \\
c' &= 3a\alpha\beta^2 + b(2\alpha\beta\delta + \beta^2\gamma) + c(2\beta\gamma\delta + \alpha\delta^2) + 3d\gamma\delta^2 \\
d' &= a\beta^3 + b\beta^2\delta + c\beta\delta^2 + d\delta^3
\end{aligned}$$

Choose τ such that $d' = 0$. If $a = 0$, we get $\alpha = \delta = 0$ and $\beta = \gamma = 1$. If $a \neq 0$, then $\alpha = \delta = 1, \gamma = 0$, and let β be a real zero of the cubic equation $a\beta^3 + b\beta^2 + c\beta + d = 0$. Consequently, we may start with a cubic form $p(x, y) = ax^3 + bx^2y + cxy^2$.

Now choose τ such that $b' = d' = 0$. If $c \neq 0$, then such a τ is found by setting $\alpha = \delta = 1, \beta = 0$ and $\gamma = -b/2c$. When $c = 0, b \neq 0$, let $\alpha = 0, \beta = \gamma = 1, \delta = -a/b$, and for $c = b = 0$ set $\beta = 0$. Thus it is no restriction to assume that both b and d vanish, i.e., $p(x, y) = ax^3 + cxy^2$.

By scaling x and y we see that every cubic form p can be transformed to exactly one of the 5 cubic forms.

$\square$

Lemma 7. *The germs of the normal cubic forms on $\mathbb{R}^2$ are mutually inequivalent*

Proof. Let p and q be two different normal cubic forms on $\mathbb{R}^2$. For any $[\varphi] \in \mathcal{G}_2$, the homogeneous part of degree 3 of $[p][\phi]$ is given by $[p][\tau]$, where τ is the linear part of ϕ. So, if $[p]$ and $[q]$ would be equivalent they would also be linearly equivalent. This is in contradiction with the previous lemma. $\qquad \square$

For simple germs of corank 2 we obtain the D (orthogonal) series and the special series E_6, E_7 and E_8.

Lemma 8. *A simple germ with a critical point of corank 2 with cubic form $x_1^2 x_2$ or $x^2 y \pm y^3$ (for some coordinate sytem) can be reduced to one of the normal forms of the type $D_k^{\pm}$ for some $k \geq 4$, given by*

$$x_1^2 x_2 \pm x_2^{k-1} + q_{s,n-2}(x_3, \ldots, x_n),$$

with codimension $k - 1$.

Proof. Let $[f]$ be a simple germ with a critical point of corank 2 and cubic form equivalent to $x_1^2 x_2$ at the origin. By the reduction lemma, we can choose coordinates such that $f = g(x_1, x_2) + q_{s,n-2}(x_3, \ldots, x_n)$, with $g \in m^3$. The 4-jet of g is of the form $g(x, y) = x^2 y + \varphi_4(x, y)$ with

$$\begin{aligned}
\varphi_4(x, y) &= ay^4 + 2bxy^3 + cx^2y^2 + dx^3y + ex^4 \\
&= ay^4 + 2bxy^3 + x^2 \psi, \\
\psi &= ex^2 + dxy + cy^2.
\end{aligned}$$

A local diffeomorphic transformation $(x, y) \mapsto (x - by^2, y - \psi)$ reduces g to the form $g = x^2 y + ay^4 \mod m^5$. For this form, we distinguish the situation $a = 0$ and $a \neq 0$. If $a \neq 0$, then $[g] \sim [x^2 y + ay^4]$ which is 4-determined. In the case $a = 0$, the 4-jet of g can be reduced to the form $x^2 y$ and the 5-jet has the form $x^2 y + \varphi_5(x, y)$ with φ_5 homogeneous of degree 5 in x and y.

Now assume that the s-jet of g is of the form $g(x, y) = x^2 y + \varphi_s(x, y)$ and φ_s homogeneous of degree s of the form

$$\varphi_s(x, y) = ay^s + 2bxy^{s-1} + x^2 \psi(x, y),$$

for some $\psi \in m^{s-2}$. Performing a local diffeomorphic transformation $(x, y) \mapsto (x - by^{s-2}, y - \psi)$ reduces g to the form $g = x^2 y + ay^s \mod m^{s+1}$. For this form we distinguish the situation $a = 0$ and $a \neq 0$. If $a \neq 0$, then $[g] \sim [x^2 y + ay^s]$ which is s-determined. In the case $a = 0$, the s-jet of g can be reduced to the form $x^2 y$, by which the $(s + 1)$-jet of g is of the form $g = x^2 y + \varphi_{s+1}(x, y)$.

Starting with $s = 4$ and repeating the procedure for $s \to s + 1$ if $a = 0$, this protocol has to terminate for some finite s. If the process would continue indefinitely, the orbit $[f]\mathcal{G}$ lies arbitrarily close to all orbits of the form $[x^2 y + x^k]\mathcal{G}$. This forms a contradiction with the assumption that $[f]$ is simple.

Hence there exists a $s \geq 5$ such that $[g] \sim [x^2 y \pm y^{s-1}]$ by which $[f] \sim [x_1^2 y \pm y^{s-1}]$. $\quad \square$

Lemma 9. *A simple germ with a critical point of corank* 2 *with cubic form* x_1^3 *can be reduced to one of the normal forms of type* E_k *for some* $k = 6, 7, 8$, *given by*

$$E_6 : x_1^3 \pm x_2^4 + q_{s,n-2}(x_3, \ldots, x_n)$$
$$E_7 : x_1^3 + x_1 x_2^3 + q_{s,n-2}(x_3, \ldots, x_n)$$
$$E_8 : x_1^3 + x_2^5 + q_{s,n-2}(x_3, \ldots, x_n)$$

with codimension k.

Proof. For a proof we refer to Arnol'd 1972 lemma 6.1 [4]. The proof goes similar to the previous two proofs. $\qquad\square$

Theorem 3. *A simple germ of a critical point can be reduced to one following normal forms. For nondegenerate critical points,*

$$q_{sn}(x_1, \ldots, x_n), \qquad\qquad 0 \le s \le n \quad cod\,[q_{sn}] = 0.$$

For degenerate critical points

$$A_k : \pm x_1^{k+1} + q_{s,n-1}(x_2, \ldots, x_n) \qquad\qquad k \ge 1 \quad cod\,A_k = k - 1$$
$$D_k : x_1^2 x_2 \pm x_2^{k-1} + q_{s,n-2}(x_3, \ldots, x_n) \qquad k \ge 4 \quad cod\,D_k = k - 1$$
$$E_6 : x_1^3 \pm x_2^4 + q_{s,n-2}(x_3, \ldots, x_n) \qquad\qquad cod\,E_6 = 6$$
$$E_7 : x_1^3 + x_1 x_2^3 + q_{s,n-2}(x_3, \ldots, x_n) \qquad\qquad cod\,E_7 = 7$$
$$E_8 : x_1^3 + x_2^5 + q_{s,n-2}(x_3, \ldots, x_n) \qquad\qquad cod\,E_8 = 8$$

Proof. This proof follows from Morse's lemma and lemmas 3,4 and 5. $\qquad\square$

7.2.5 Unfoldings

Degenerate critical points are unstable, in the sense that a perturbation of the function near the critical point removes it or lets if fall apart into other critical points, ultimately resulting in nondegenerate critical points. In the previous chapter we introduced the fold (A_2) and cusp (A_3) catastrophe by means of physical examples. In these examples, the catastrophes existed at a point in configuration space and could only be found by considering the function near the critical point. In the system with the cylinder on the hill and the Zeeman catastrophe machine, the angle Θ is the state space describing the dynamics whereas the angle α and the point Q are external parameters perturbing the system. This classification of the parameters is of course a bit artificial. In this section we will discuss these deformations of the system systematically for all simple normal forms discussed in the previous section. A deformation will be denoted by an unfolding. The proofs of the statements given in this section can be found in Arnol'd and Castrigiano.

Definition 15. *Let* $[f] \in \mathcal{E}$. *A germ* $F \in \mathcal{E}_{n+r}$ *is an* r-parameter ***unfolding*** *of* $[f]$, *if* $F(x, 0) = f(x)$ *for all* x *in a neighborhood of the origin of* $\mathbb{R}^n$. *The space* $\mathbb{R}^n$ *of the first arguments of* F *is called the state space. The space* $\mathbb{R}^r$ *of the second argument s of* F *is called the space of external parameters.*

For a given germ in $\mathcal{E}$ a vast amount of unfoldings are possible. In order to determine the 'quality' of an unfolding, we introduce the notion that an unfolding G can be induced by another unfolding F.

Definition 16. *Let $[F] \in \mathcal{E}_{n+r}$ be an unfolding of $[f] \in \mathcal{E}$. The unfolding $[G] \in \mathcal{E}_{n+s}$ is **induced** by $[F]$ if there exist germs $[\varphi] \in m_{n+s,n}, [\psi] \in m_{s,r}$ and $[\gamma] \in m_s$ such that*

- $\varphi(y, 0) = y$

- $G(y, v) = F(\varphi(y, v), \psi(v)) + \gamma(v)$

for all (y, v) in an open neighborhood of the origin in $\mathbb{R}^{n+s}$.

By the definition of induced unfoldings, an unfolding G induced by an unfolding F is diffeomorphic to G near the critical point then F does. Using this notion we can consider the most efficient unfolding of a germ $[f] \in \mathcal{E}$.

Definition 17. *An unfolding of a germ in $\mathcal{E}$ is **versal**[6] if it induces all unfoldings of the germ. If the number of external parameters of a versal unfolding is minimal, we call the unfolding **universal**. Arnol'd denotes universal unfoldings by miniversal unfoldings.*

The existence of a universal unfolding is described by the **Fundamental Theorem on Universal Unfoldings** not proven here, but available in Castrigiano. The Fundamental Theorem on universal unfoldings states that a universal unfolding of a germ $[f]$ exists if and only if $[f]$ has finite determinacy or equivalently codimension. If the universal unfolding of $[f]$ exists, it can be explicitly generated by calculating the quotient space $m/\mathcal{J}[f]$ and picking representatives $[g_1], \ldots, [g_r]$ of the cosets. The germ of the resulting function

$$F(x, u) = f(x) + u_1 g_1(x) + \cdots + u_r g_r(x)$$

can be proven to be a universal unfolding of the germ $[f]$. Note that the codimension of $[f]$ equals the number of external parameters in the universal unfolding.

Arnol'd calculated versal unfoldings of the standard catastrophes A_k, D_k and E_k.

Theorem 4. *For the versal deformation for the germs of functions A_k, D_k and E_k one can take the following k-parameter deformations.*

$A_k : \pm x_1^{k+1} + q_{s,n-1}(x_2, \ldots, x_n) + u_{k-1}x_1^{k-1} + u_{k-2}x_1^{k-2} + \cdots + u_0$

$D_k : x_1^2 x_2 \pm x_2^{k-1}(x_3, \ldots, x_n) + q_{s,n-2} + u_{k-1}x_1 + u_{k-2}x_2^{k-2} + \cdots + u_1 x_2 + u_0$

$E_6 : x_1^3 \pm x_2^4 + q_{s,n-2}(x_3, \ldots, x_n) + u_5 x_1 x_2^2 + u_4 x_1 x_2 + u_3 x_2^2 + u_2 x_2 + u_1 x_1 + u_0$

$E_7 : x_1^3 + x_1 x_2^3 + q_{s,n-2}(x_3, \ldots, x_n) + u_6 x_1 x_2 + u_5 x_2^4 + u_4 x_2^3 + u_3 x_2^2 + u_2 x_2 + u_1 x_1 + u_0$

$E_8 : x_1^3 + x_2^5 + q_{s,n-2}(x_3, \ldots, x_n) + u_7 x_1 x_2^3 + u_6 x_1 x_2^2 + u_5 x_1 x_2 + u_4 x_2^3$

$\qquad + u_3 x_2^2 + u_2 x_2 + u_1 x_1 + u_0$

---

[6]The term versal comes form the intersection of the terms universal and transversal.

Proof. For the proof we refer to Arnol'd 1972 [4].   □

One can calculate how the simple catastrophes decompose into other catastrophes under the influence of unfoldings. Arnol'd has found specific one-parameter families of perturbations that let the E_k catastrophe decompose into $E_{k-1}, A_{k-1}, A_{k-2}$ catastrophes, the D_k catastrophe decompose into D_{k-1}, A_{k-1} catastrophes and the A_k catastrophe decompose into the A_{k-1} catastrophe. This forms a proof of a structure of catastrophes depicted in the figure below [4].

$$A_1 \leftarrow A_2 \leftarrow A_3 \leftarrow A_4 \leftarrow A_5 \leftarrow A_6 \leftarrow A_7 \leftarrow A_8 \leftarrow A_9 \leftarrow \cdots$$

$$D_4 \leftarrow D_5 \leftarrow D_6 \leftarrow D_7 \leftarrow D_8 \leftarrow A_9 \leftarrow \cdots$$

$$E_6 \leftarrow E_7 \leftarrow E_8$$

7.3 Lagrangian catastrophe theory

Lagrangian catastrophe theory can be developed alongside general catastrophe theory. General catastrophe theory considers critical points of functions in C^∞ up to local diffeomorphisms. Lagrangian catastrophe theory considers critical points in Lagrangian maps, up to Lagrangian equivalences. This branch of catastrophe theory was initiated by Arnol'd, who proved the first classification theorem.

Lagrangian maps have applications in many optical and dynamical systems. The corresponding catastrophe theory can be applied to the formation of caustics in optical systems, deformations of images in gravitational lenses and structure formation. In this thesis we concentrate on the last application. In this section we describe symplectic geometry, Lagrangian submanifolds, Lagrangian maps and the classification of Lagrangian maps.

Let V be a finite-dimensional real vector space. A bilinear form b on V is a bilinear map

$$b : V \times V \to \mathbb{R},$$

in the sense that the map $u \mapsto b(u,v)$ for fixed v and $v \mapsto b(u,v)$ for fixed u are both linear maps. The bilinear form b is called nondegenerate if the condition $b(u,v) = 0$ for all v implies $u = 0$. Furthermore the bilinear form is called symplectic if it is antisymmetric, i.e. $b(u,v) = -b(v,u)$ for all $u,v \in V$. A nondegenerate bilinear symplectic form on V will be denoted by ω.

For a manifold M, the tangent space $T_x M$ is spanned by the derivative at $t = 0$ of all curves $\gamma : U \subset \mathbb{R} \to M$ through $x \in M$ with $0 \in U$ and $\gamma(0) = x$. The tangent space $T_x M$ is a vector space. Let $\Omega^2(M)$ denote the space of smooth 2-forms on M. A 2-form $\alpha \in \Omega^2(M)$ assigns to each point $x \in M$ an antisymmetric 2-form α_x of degree p on the tangent space $T_x M$ varying smoothly with x. The 2-form α is nondegenerate if α_x is

nondegenerate on $T_x M$ for all $x \in M$. The 2-form is called closed if $d\alpha = 0$, with d the exterior derivative. For a smooth map $\phi : M \to N$ of smooth manifolds M, N we define the pullback of the smooth p-form α on N under ϕ as the smooth p-form $\phi^* \alpha$ by

$$(\phi^* \alpha)_x (v_{1x}, \dots, v_{px}) = \alpha_{\phi(x)}((T_x \phi) v_{1x}, \dots, (T_x \phi) v_{px}),$$

with $T_x \phi : T_x M \to T_{\phi(x)} N$ the tangent map of ϕ at x and $v_{1x}, \dots, v_{px} \in T_x M$. For a more elaborate explanation of symplectic geometry an above definitions see Arnol'd et al. [8].

Using these notions we now define the symplectic manifold.

Definition 18. *A symplectic manifold is a pair (M, ω), with a smooth even-dimensional manifold M, and a nondegenerate closed symplectic 2-form $\omega \in \Omega^2(M)$.*

In this thesis, the symplectic manifold is composed out of the Lagrangian (initial) and Eulerian position (after some time t). In n dimensions we therefore have $M = \mathbb{R}^n \times \mathbb{R}^n$, with $(\mathbf{q}, \mathbf{x}) \in M$ representing the initial position $\mathbf{q}$ and final position $\mathbf{x}$ after some time t. According to the theorem of Darboux, all symplectic structures on a manifold M with fixed dimension are locally equivalent. In the context of this paper, the standard symplectic structure $\omega = d\mathbf{q} \wedge d\mathbf{x}$ is used.

A Lagrangian submanifold L of (M, ω) is a maximal-dimensional submanifold on which the symplectic structure ω vanishes.

Definition 19. *A Lagrangian manifold $L \subset M$ is a subset with half the dimension of the symplectic manifold (M, ω) on which the 2-form induced by the inclusion $i : L \to M$ vanishes, i.e., $i^* \omega = 0$.*

This manifold M can be seen as a Lagrangian fibration (a fibration with Lagrangian fibers), with projection map $\pi : M \to B = \mathbb{R}^n, (\mathbf{q}, \mathbf{x}) \mapsto \mathbf{x}$, mapping phase space M to Eulerian space B. This leads to the notion of Lagrangian maps.

Definition 20. *Given a symplectic manifold (M, ω) with projection $\pi, M \to B$, a Lagrangian submanifold $L \subset M$ has a corresponding Lagrangian map defined as $\pi \circ i : L \to (M, \omega) \to B$, with $i : L \to (M, \omega)$ the inclusion map. The Lagrangian map of a Lagrangian manifold L is a projection onto the base B.*

As in general catastrophe theory, we can consider the germs of Lagrangian maps. These germs are commonly denoted by Lagrangian map germs $[\pi \circ i]$. In general catastrophe theory, the germs are related by local diffeomorphism. In Lagrangian catastrophe theory, Lagrangian map germs are related by Lagrangian equivalence.

Definition 21. *Two Lagrangian maps $(\pi_1 \circ i_1) : L_1 \to M_1 \to B_1$ and $(\pi_2 \circ i_2) : L_2 \to M_2 \to B_2$ are Lagrangian equivalent if diffeomorphisms σ, τ and ν exist such that $\tau \circ i_1 = i_2 \circ \sigma, \nu \circ \pi_1 = \pi_2 \circ \tau$ and $\tau^* \omega_2 = \omega_1$. The maps $\pi_1 \circ i_1$ and $\pi_2 \circ i_2$ are equivalent if the diagram below commutes.*

$$L_1 \overset{i_1}{\hookrightarrow} (M_1, \omega_1) \overset{\pi_1}{\twoheadrightarrow} B_1$$
$$\sigma \downarrow \qquad \tau \downarrow \qquad \nu \downarrow$$
$$L_2 \overset{i_2}{\hookrightarrow} (M_2, \omega_2) \overset{\pi_2}{\twoheadrightarrow} B_2$$

Every Lagrangian map germ can be described by a generating function. This function relates Lagrangian catastrophe theory to general catastrophe theory.

Theorem 5. *Every Lagrangian map-germ can be generated by a generating family* $F(x, \lambda)$ *by the points*

$$\left\{ \lambda, \kappa | \exists x \ such \ that \ \frac{\partial F}{\partial x_i} = 0, \kappa = \frac{\partial F}{\partial \lambda} \right\}.$$

Proof. For the proof we refer to the book 'Singularities of differential maps I.' by Arnol'd et al. [8]. $\qquad \square$

Given a symplectic manifold (M, ω) and Lagrangian submanifold L, the orbit of the Lagrangian map germ $i \circ \pi$ is given by all Lagrangian map germs Lagrangian equivalent to $i \circ \pi$. If this orbit is open, the Lagrangian map germ is called stable since every element in the orbit has a open environment contained in the orbit. If the orbit is not open, the Lagrangian map germ is not stable.

This notion of stability can be related to the versality of the generating family.

Theorem 6. *A Lagrangian map is stable if, the Lagrangian map germ given by a generating family of functions* $F(x, \lambda)$ *with parameters* λ, *is Lagrangian stable. This condition is satisfied if and only if the deformation* F *of the function* $f = F(\cdot, 0)$ *is* R^+-*versal. The* R^+ *equivalence implies: two functions* F_1 *and* F_2 *are* R^+ *equivalent if there exists diffeomorphisms* $h : \mathrm{R}^n \times \mathbb{R}^l \to \mathbb{R}^n \times \mathbb{R}^l, \varphi : \mathbb{R}^n \to \mathbb{R}^n$ *and a smooth function* Ψ *such that*

$$F_1(x, \lambda) = F_2(h(x, \lambda), \varphi(\lambda)) + \Psi(\lambda).$$

Proof. For the proof we refer to the book 'Singularities of differential maps I.' by Arnol'd et al. [8]. $\qquad \square$

One can apply and verify this condition for the unfoldings of the normal forms of the catastrophes in general catastrophe theory. This results in the classification of Lagrangian catastrophes in $n \leq 5$ dimensions. These results have been extended to $n \leq 11$ dimensions by Zukalyukin in 1976 [74]. In the context of this thesis, Arnol'd's theorem will suffice.

Theorem 7. *At every point, the germs of generic Lagrangian maps of manifolds of dimension* $n \leq 5$ *are equivalent to germs of projetions* $(p, q) \mapsto q$ *of Lagrangian manifolds*

$p_I = \partial S / \partial q_I, q_J = -\partial S / \partial p_J$, *where*

$$
\begin{aligned}
&\textit{for } n \geq 1 & A_1 &: S = p_1^2 \\
& & A_2 &: S = p_1^3 \\
&\textit{for } n \geq 2 \textit{ also} & A_3 &: S = \pm p_1^4 + q_2 p_1^2 \\
&\textit{for } n \geq 3 \textit{ also} & A_4 &: S = p_1^5 + q_2 p_1^3 + q_3 p_1^2 \\
& & D_4 &: S = p_1^3 \pm p_1 p_2^2 + q_3 p_1^2 \\
&\textit{for } n \geq 4 \textit{ also} & A_5 &: S = \pm p_1^6 + q_2 p_1^4 + q_3 p_1^3 + q_4 p_1^2 \\
& & D_5 &: S = p_1 p_2^2 \pm p_1^4 + q_3 p_1^3 + q_4 p_1^2 \\
&\textit{for } n \geq 5 \textit{ also} & A_6 &: S = p_1^7 + q_2 p_1^5 + q_3 p_1^4 + q_4 p_1^3 + q_5 p_1^2 \\
& & D_6 &: S = p_1 p_2^2 \pm p_1^5 + q_3 p_1^4 + q_4 p_1^3 + q_5 p_1^2 \\
& & E_6 &: S = p_1^3 \pm p_2^4 + q_3 p_1^2 p_2 + q_4 p_1 p_2 + q_5 p_1^2.
\end{aligned}
$$

Proof. For the proof we refer to the book 'Singularities of differential maps I.' by Arnol'd et al. [8]. $\qquad\qquad\qquad\qquad\qquad\qquad\qquad\qquad\qquad\qquad\qquad\qquad\qquad\qquad$ $\square$

In this thesis we will be interested in Lagrangian maps with $n = 3$ and $n = 4$. For the case $n = 3$ we have the stable catastrophes A_1, A_2, A_3, A_4, and D_4. For the case $n = 4$ we add the stable catastrophes A_5 and D_5 to this list.

Chapter 8

Gaussian Random Field Theory

Random field theory is a branch of mathematics with many applications, ranging from finance, medical imaging, and quantum physics to cosmology. In essence, we attach a random variable to each point in space. If the space is $\mathbb{Z}$ or $\mathbb{R}$ we call the random field a random process. Brownian motion or the Wiener process are common examples of random processes. We can however also consider more general spaces like $\mathbb{Z}^d, \mathbb{R}^d$ or various manifolds. In this chapter we introduce random fields and in particular Gaussian random fields. Examples of Gaussian random fields can be found in non-interacting Euclidean quantum field theories, studied by Guerra, Rosen and Simon [31] or Gllmm, Jaffe, and Wilczek [29], some situations in statistical mechanics and the density fluctuations in the early universe. We here discuss properties of Gaussian random fields and show how to generate draws, hereafter called realizations. All concepts and formulas presented in this chapter can be found in Random Fields and Geometry by Adler and Taylor [1] and Bardeen et al. [37].

Stephen O. Rice was in 1944 one of the first to study geometric properties of stationary random processes, discussing the nature of electrical noise in communication devices [57]. In his paper, Rice calculates the average number of times a stationary random process crosses a fixed level. This calculation, now called Rice's formula, forms the foundation for the statistical analysis performed in this thesis. The formula is derived in chapter 10. Longuet-Higgins in 1957 [43] expanded upon Rice's analysis by considering 2-dimensional Gaussian random fields, analyzing ocean waves [43]. Doroshkevich in 1970 was one of the first to apply Gaussian random fields to cosmological problems [23]. Today Gaussian random field theory has become an important concept in cosmology. According to models of the early universe, quantum mechanical fluctuations grew during inflation and formed the seeds for all structure formation in the universe. Observations of these early density distribution in the Cosmic Microwave Background (CMB) indicate that these initial fluctuations were approximately Gaussian distributed. For this reason cosmological N-body simulations often start with a Gaussian random field initial condition and all statistical properties of our current universe can in principle be calculated from the statistics of these fields.

In order to develop some intuition for random fields, consider the following examples.

(a) A roll of a die can be seen as a single draw from a probability distribution.

(b) A roll of multiple dice is a simultaneous draw of multiple statistics from a probability distribution. In this figure the dice are not correlated in any way, every die is rolled independently of every other dice.

(c) A roll of multiple dice which are correlated can be seen as a random field. Compared to figure 8.1b these dice show a clear correlation. The distribution of these dice is clearly smoother than that of the dice in figure 8.1b.

Figure 8.1: Draws of dice

A fair die maps the point set $\{p\}$ to the set $\{1, 2, 3, 4, 5, 6\}$ with uniform probability $1/6$. When we for example throw a 6 with a die, we obtain a realization $p \mapsto 6$ (see figure 8.1a). If we extend this example to several independent dice, we obtain a map from several points to the set $\{1, 2, 3, 4, 5, 6\}$. The illustration in figure 8.1b corresponds to the realization

$$\begin{pmatrix} 1 & 4 & 3 & 6 \\ 6 & 2 & 5 & 1 \\ 2 & 3 & 6 & 2 \\ 4 & 1 & 3 & 1 \end{pmatrix}.$$

For random fields the draws of the dice however do not have to be independent. There can be correlations between several points defining a field as in figure 8.1c. The field furthermore does not have to be restricted to a finite base or range. In figure 8.2 we see for example a realization of a 2-dimensional real-valued Gaussian random field which could represent the 2-dimensional projection of the initial density fluctuations in the early universe.

8.1   Gaussian random fields

In the introduction of this chapter we saw a intuitive example of a random field. For completeness we now formally define a random field, although the abovementioned intuition will prove to be more useful throughout this thesis.

Definition 22 (Random Fields)**.** *Let $(\Omega, \mathcal{F}, \mathbb{P})$ be a complete probability space and T a topological space. A measurable map $f : \Omega \to \mathbb{C}^T = \{g : T \to \mathbb{C}\}$ is a complex-valued random field.*

In this thesis it is often enough to consider real-valued random fields. However since we will analyze random fields in Fourier space we need the complex-valued definition random fields. In this definition $\mathbb{C}^T$ has some topology induced by the topological space T. Measurable implies that the preimage f^{-1}, of any set in the topology of $\mathbb{C}^T$, is in the σ-algebra $\mathcal{F}$. With abuse of notation, a realization of such a random field can be seen as a map

$$f : \Omega \times T \to \mathbb{C},$$

with a randomness and an index argument respectively Ω and T.

Gaussian random fields are a subclass of random fields and are defined by specifying the probability density.

Definition 23 (Gaussian Random Fields (GRF)). *A random field is a Gaussian random field with zero mean if and only if $\langle f(t) \rangle = 0$ for all $t \in T$ and for all $t_1, t_2, \ldots, t_n \in T$ the vector $(f(t_1), f(t_2), \ldots, f(t_n))$ is a multivariate Gaussian random variable, i.e.*

$$P((f(t_1), \ldots, f(t_n))) = \frac{\exp[-\frac{1}{2} \sum_{i,j} f(t_i)(M^{-1})_{ij} f(t_j)]}{[(2\pi)^n \det M]^{1/2}} \mathrm{d}f(t_1) \ldots \mathrm{d}f(t_n),$$

is the probability $(f(t_1), \ldots, f(t_n)) \in [f(t_1), f(t_1) + \mathrm{d}f(t_1)] \times \cdots \times [f(t_n), f(t_n) + \mathrm{d}f(t_n)]$ where the covariance matrix M is defined by $M_{ij} = \langle f(t_i) f^*(t_j) \rangle$, where $\langle \ldots \rangle$ denotes the average over the field. In this equation * denotes complex conjugation.

From these definitions we observe that the statistical properties of Gaussian random field are completely determined by the covariance matrix M with elements given by the two-point correlation function

$$M_{i,j} = \xi(t_i, t_j) = \langle f(t_i) f^*(t_j) \rangle.$$

In this thesis we will be interested in stationary Gaussian random fields for which the two-point correlation function satisfies

$$\xi(t_1, t_2) = \tilde{\xi}(d(t_1, t_2)).$$

for some function $\tilde{\xi} : T \to \mathbb{R}$, assuming some metric d on T. In this thesis we, with abuse of notation, omit the tilde and identify the function by the number of arguments.

8.2 Gaussian random fields on Euclidean spaces

In this thesis we are interested in stationary Gaussian random fields on $\mathbb{R}^d$ with the standard topology. As specified in the previous section, all information of such a field is contained in the two-point correlation function

$$\xi(r) = \xi(\mathbf{r}) = \xi(\mathbf{x}, \mathbf{x} + \mathbf{r}) = \langle f(\mathbf{x}) f^*(\mathbf{x} + \mathbf{r}) \rangle,$$
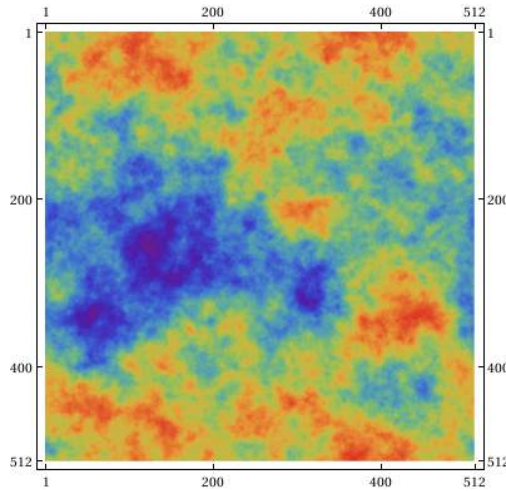
(a) A density plot of a realization of a Gaussian random field
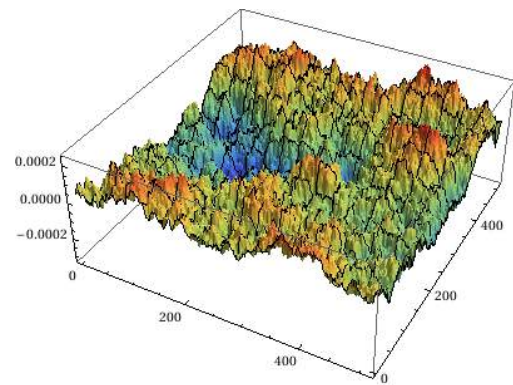
(b) A 3-dimensional plot of a realization of a Gaussian random field
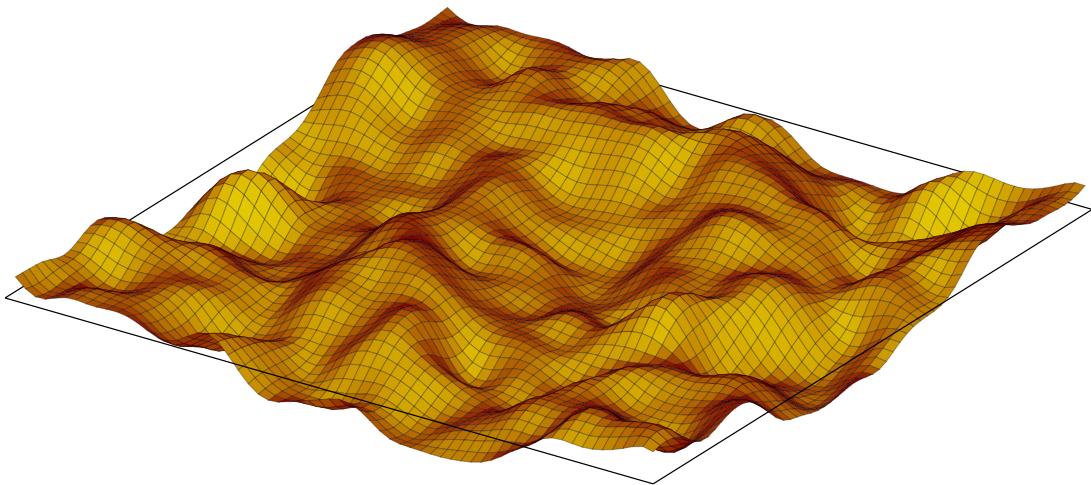
(c) A 3-dimensional plot of a realization of a Gaussian random field [33]. The hight of the surface corresponds to the function value of the realization

Figure 8.2

for all $\mathbf{r}$ and $\mathbf{x}$ in $\mathbb{R}^d$ and $r = |\mathbf{r}|$. The definition of Gaussian random fields on Euclidean spaces is equivalent to special relations in Fourier space. Throughout this thesis, we will use the Fourier convention

$$\hat{f}(\mathbf{k}) = \int f(\mathbf{x})e^{i\mathbf{k}\cdot\mathbf{x}}\mathrm{d}\mathbf{x},$$

with inverse Fourier transform

$$f(\mathbf{x}) = \int \hat{f}(\mathbf{k})e^{-i\mathbf{k}\cdot\mathbf{x}}\frac{\mathrm{d}\mathbf{k}}{(2\pi)^d},$$

where $\hat{f}$ is a complex-valued function. The function f is always real-valued by which

$$\hat{f}(\mathbf{k}) = \hat{f}^*(-\mathbf{k}),$$

for all $\mathbf{k} \in \mathbb{R}^d$. The Fourier transform of the two-point correlation function is the so-called power spectrum P,

$$\begin{aligned}
\langle \hat{f}(\mathbf{k}_1)\hat{f}^*(\mathbf{k}_2)\rangle &= \iint \langle f(\mathbf{x}_1)f(\mathbf{x}_2)\rangle e^{-i\mathbf{k}_1\cdot\mathbf{x}_1 + i\mathbf{k}_2\cdot\mathbf{x}_2}\mathrm{d}\mathbf{x}_1\mathrm{d}\mathbf{x}_2 \\
&= \iint \xi(r)e^{-i(\mathbf{k}_1-\mathbf{k}_2)\cdot\mathbf{x} + i\mathbf{k}_2\cdot\mathbf{r}}\mathrm{d}\mathbf{x}\mathrm{d}\mathbf{r} \\
&= (2\pi)^d\delta^{(d)}(\mathbf{k}_1 - \mathbf{k}_2)\int \xi(r)e^{i\mathbf{k}_1\cdot\mathbf{r}}\mathrm{d}\mathbf{r} \\
&= (2\pi)^d\delta^{(d)}(\mathbf{k}_1 - \mathbf{k}_2)P(k_1),
\end{aligned}$$

where $k_1 = |\mathbf{k}_1|$ and $P(k) = \int \xi(r)e^{i\mathbf{k}\cdot\mathbf{x}}\mathrm{d}\mathbf{x}$. Conversely we can express the two-point correlation function ξ in terms of the power spectrum P with the inverse Fourier transform

$$\xi(x) = \int P(k)e^{-i\mathbf{k}\cdot\mathbf{x}}\frac{\mathrm{d}\mathbf{k}}{(2\pi)^d}.$$

We furthermore observe that the Fourier modes are independently distributed. We now compute the distribution of each mode.

From the definition of Gaussian random fields, it follows that the probability density is given by

$$P_n = \frac{\exp[-\frac{1}{2}\sum_{i,j} f(\mathbf{x}_i)(M^{-1})_{ij}f(\mathbf{x}_j)]}{[(2\pi)^n\mathrm{det}M]^{1/2}},$$

for any points $\mathbf{x}_1, \ldots, \mathbf{x}_n \in \mathbb{R}^d$. If we choose the points $\mathbf{x}_i$ on a cubic grid with grid size h and let the grid approach the continuum, i.e. $h \to 0$, we obtain the probability distribution

$$P[f] = Ae^{-S[f]} = Ae^{-\frac{1}{2}\int \mathrm{d}\mathbf{x}_1 \int \mathrm{d}\mathbf{x}_2 f(\mathbf{x}_1)K(\mathbf{x}_1-\mathbf{x}_2)f(\mathbf{x}_2)},$$

with action $S[f]$, similar to the path integral formulation of quantum field theory. For a more extended treatment of the action formulation of Gaussian random field theory see Van de Weygaert and Bertschinger [67]. See chapter 15 for a comparison. In this equation A is a normalization constant, S the action and K the inverse of the two-point correlation function ξ defined by

$$\int K(\mathbf{x}_1 - \mathbf{x})\xi(\mathbf{x} - \mathbf{x}_2)\mathrm{d}\mathbf{x} = \delta^{(d)}(\mathbf{x}_1 - \mathbf{x}_2).$$

According to the convolution theorem, the definition of the inverse K is equivalent to

$$\int \hat{K}(\mathbf{k})P(k)e^{-i\mathbf{k}\cdot(\mathbf{x}_1-\mathbf{x}_2)}\frac{\mathrm{d}\mathbf{k}}{(2\pi)^d} = \delta^{(d)}(\mathbf{x}_1 - \mathbf{x}_2),$$

with $\hat{K}$ the Fourier transform of K. Using the definition of the Dirac delta distribution

$$\delta^{(d)}(\mathbf{x}) = \int e^{-i\mathbf{x}\cdot\mathbf{k}}\frac{\mathrm{d}\mathbf{k}}{(2\pi)^d},$$

we see that $\hat{K}(\mathbf{k}) = 1/P(|\mathbf{k}|)$, by which

$$K(\mathbf{x}) = \int \frac{e^{i\mathbf{k}\cdot\mathbf{x}}}{P(k)}\frac{\mathrm{d}\mathbf{k}}{(2\pi)^d}.$$

Note that the inverse of the two-point correlation function is the inverse Fourier transform of the reciprocal of the power spectrum. Applying $\hat{K}(\mathbf{k}) = 1/P(|\mathbf{k}|)$ to the double convolution of $S[f]$ gives

$$S[f] = \frac{1}{2}\int \hat{f}^*(\mathbf{k})\hat{K}(\mathbf{k})\hat{f}(\mathbf{k})\frac{\mathrm{d}\mathbf{k}}{(2\pi)^d} = \int \frac{|\hat{f}(\mathbf{k})|^2}{2P(|\mathbf{k}|)}\frac{\mathrm{d}\mathbf{k}}{(2\pi)^d},$$

by which the probability distribution $P[\hat{f}]$ can be written as

$$P[f] = P[\hat{f}] = \tilde{A}\exp\left[-\int \frac{|\hat{f}(\mathbf{k})|^2}{2P(k)}\frac{\mathrm{d}\mathbf{k}}{(2\pi)^d}\right].$$

From this equation we observe that each Fourier mode $\hat{f}(\mathbf{k})$ is an independently normally distributed complex number with standard deviation $\sqrt{P(\mathbf{k})}$, i.e.

$$P[\hat{f}(\mathbf{k})] = \frac{1}{\sqrt{2\pi P(k)}}e^{-\frac{|\hat{f}(\mathbf{k})|^2}{2P(k)}}.$$

Writing the Fourier component in the form $\hat{f}(\mathbf{k}) = |\hat{f}(\mathbf{k})|e^{i\theta(\mathbf{k})}$, we observe that

$$P[|\hat{f}(\mathbf{k})|, \theta(\mathbf{k})]\mathrm{d}|\hat{f}(\mathbf{k})|\mathrm{d}\theta(\mathbf{k}) = e^{-\frac{|\hat{f}(\mathbf{k})|^2}{2P(k)}}\frac{|f_k|}{2\pi P(k)}\mathrm{d}|\hat{f}(\mathbf{k})|\mathrm{d}\theta(\mathbf{k}).$$

Hence the Fourier modes are independently distributed, with random phase and Rayleigh distributed norm. From this statement, it follows that the real and imaginary components of $\hat{f}(\mathbf{k})$ are independently normal distributed. For Gaussian random fields on a sphere, similar relations hold when one uses spherical harmonics instead of Fourier transforms.

8.3   Smoothing realizations of random fields

A realization of a random field does not generically have to be continuous or differentiable. For this reason, we convolve realizations with a smoothing kernel W, i.e.

$$f_s(\mathbf{x}) = \int W(\mathbf{y}) f(\mathbf{x} + \mathbf{y}).$$

By the convolution theorem,

$$\hat{f}_s(\mathbf{k}) = \hat{W}(\mathbf{k}) \hat{f}(\mathbf{k}),$$

for all $\mathbf{k} \in \mathbb{R}^d$ and $\hat{W}$ the Fourier transform of the smoothing kernel. Commonly top hat and Gaussian filters W are used. In this thesis we will always use the Gaussian kernel

$$W(\mathbf{x}) = \frac{1}{\sigma\sqrt{2\pi}} e^{-\frac{x^2}{2\sigma^2}},$$

with Fourier transform

$$\hat{W}(\mathbf{k}) = e^{-\frac{\sigma^2 k^2}{2}},$$

as a function of the smoothing scale σ. The effect of the convolution can be seen in figure 8.3 for different smoothing scales. Realizations of random fields convolved with a Gaussian filter on scales $\sigma \neq 0$ become continuous and differentiable. See Adler et al. [1] for a formal proof and conditions for smoothness and differentiability.

Smoothing is a natural operation in the context of initial conditions in cosmology. We often model the cosmic microwave background field by a Gaussian random field. This field is continuous and differentiable due to for example the diffusion of photons in a plasma, which is called Silk damping. Within the framework of the truncated Zel'dovich approximation the smoothing takes another meaning. We can probe the evolution of specific scales in the Zel'dovich approximation by smoothing the initial conditions on that scale. In this thesis we consider Gaussian random fields in scale space, in which the scale is an extra dimension to the field.

8.4   Generating realizations of Gaussian random fields

We can use the statistical properties of Gaussian random fields in Fourier space to generate Gaussian random fields. In order for the reality condition

$$\hat{f}^*(\mathbf{k}) = -\hat{f}(-\mathbf{k})$$

to be satisfied, we start with d-dimensional discrete white noise. This can be generated by building a d-dimensional matrix δ_w with independent normally distributed elements
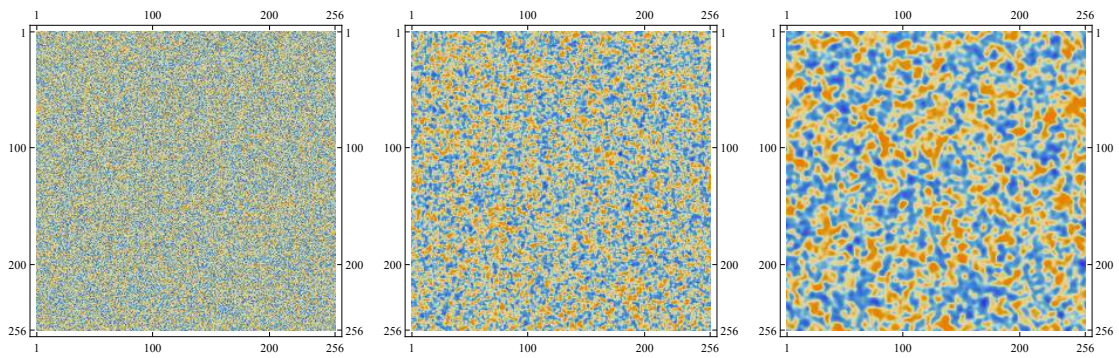
(a) A realization of a Gaussian random field without smoothing

(b) A realization of a Gaussian random field smoothing scale $\sigma = 1$

(c) A realization of a Gaussian random field smoothing scale $\sigma = 2$
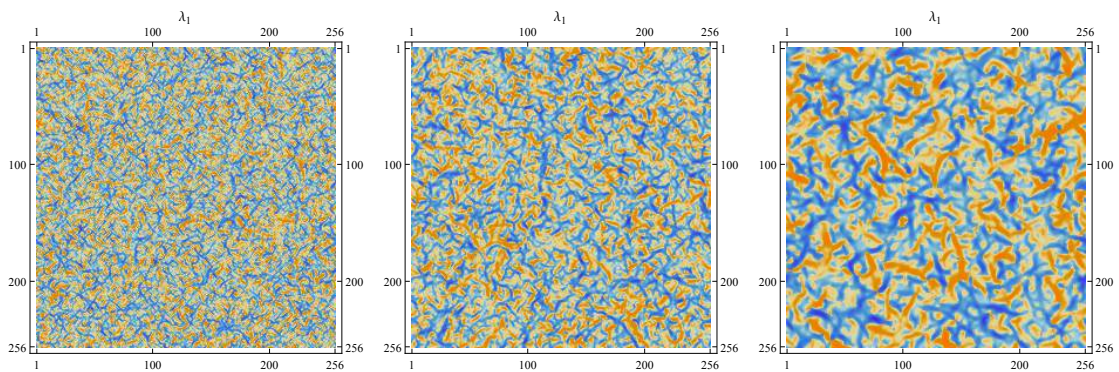
(d) The first eigenvalue of the deformation tensor of the potential corresponding to the realization illustrated above

(e) The first eigenvalue of the deformation tensor of the potential corresponding to the realization illustrated above

(f) The first eigenvalue of the deformation tensor of the potential corresponding to the realization illustrated above
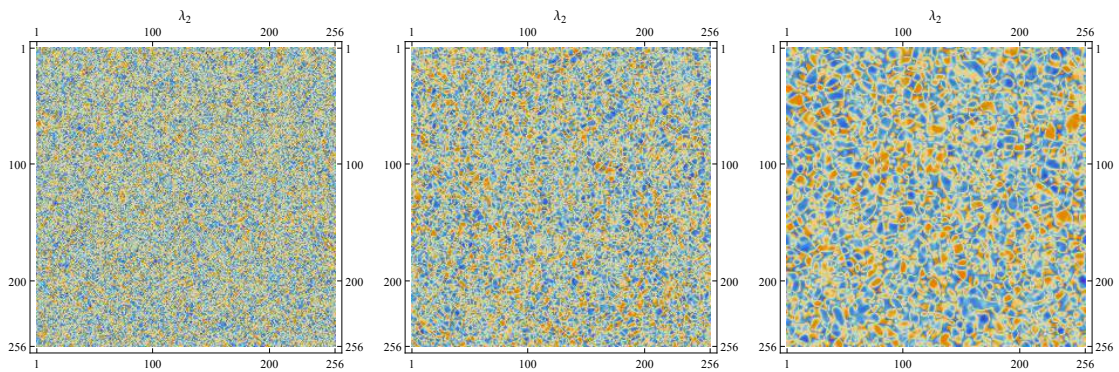
(g) The second eigenvalue of the deformation tensor of the potential corresponding to the realization illustrated above

(h) The second eigenvalue of the deformation tensor of the potential corresponding to the realization illustrated above

(i) The second eigenvalue of the deformation tensor of the potential corresponding to the realization illustrated above

Figure 8.3: Realizations and eigenvalue field of a white noise Gaussian random field, smoothed with a Gaussian kernel on different smoothing scales

with mean 0 and standard deviation 1. We Fourier transform the distribution and multiply each element with $\sqrt{P(k)}$ and $\hat{W}(\mathbf{k})$, with $\mathbf{k}$ the frequency corresponding to the matrix element, i.e.

$$\mathcal{F}(\delta_w)(\mathbf{k})\sqrt{P(k)}\hat{W}(k),$$

with $\mathcal{F}$ the Fourier transform. After performing an inverse Fourier transform $\mathcal{F}^{-1}$, we obtain a real Gaussian random field δ with power spectrum P smoothed on scale σ. Note that the realization δ does not have the power spectrum P due to the smoothing procedure. We can either say that the field with power spectrum P is smoothed with a Gaussian distribution on scale σ or say that δ is a field with effective power spectrum

$$P_{eff}(k) = \hat{W}^2(k)P(k).$$

It can be proven that the effective power spectrum induces smooth realizations.

8.5   Correlations of Gaussian random fields

As described in the above sections, all statistical information of Gaussian random fields is contained in the 2-point correlation function or equivalently the power spectrum. Due to the special properties of Gaussian random fields in Fourier space, we will work with the power spectrum. The power spectrum enters the probability function via the covariance matrix. In this section we calculate the elements of the covariance matrix for field statistics up to the fourth derivative in one and two dimensions. These will be used in further chapters.

All statistics in this thesis are expressed in the matter power spectrum P_δ. The formation of large-scale structure is however governed by the potential. From the Poisson equation

$$\nabla^2\Psi = 4\pi G\rho_0\delta \Rightarrow \hat{\Psi}(\mathbf{k}) = -4\pi G\rho_0\frac{\hat{\delta}(\mathbf{k})}{k^2}$$

it follows that the power spectrum of the potential field P_Φ is related to the matter power spectrum via

$$P_\Psi(k) = 16\pi^2 G^2\rho_0^2\frac{P_\delta(k)}{k^4} \propto \frac{P_\delta(k)}{k^4}.$$

The numerical factor $16\pi^2 G^2\rho_0^2$ is not of great importance in this thesis, since we do not yet apply the theory to observations. We often replace this factor by 1.

Throughout this thesis we will use the notation

$$T(r) = \Psi(r) \quad T_i(r) = \partial_i\Psi(r) \quad T_{ij}(r) = \partial_i\partial_j\Psi(r) \quad \partial_i\partial_j\partial_k\Psi(r) \quad T_{ijkl}(r) = \partial_i\partial_j\partial_k\partial_l\Psi(r),$$

with ∂_i the spatial derivative and $i = 1,\ldots,d$.

8.5.1   Correlations in one dimension

The correlation between the T's can be calculated by expanding T in Fourier space

$$T(r) = \int \hat{T}(k)e^{-ikr}\frac{\mathrm{d}k}{2\pi},$$

and using the definition of the power spectrum

$$\langle \hat{T}(k)\hat{T}^*(k')\rangle = 2\pi\delta^{(1)}(k - k')\hat{W}^2(k)P_\Phi(k) = 2\pi\delta^{(1)}(k - k')k^{-4}\hat{W}^2(k)P_\delta(k).$$

In general we reduce the correlation function to a one-dimensional integral

$$\langle T(x)T(y)\rangle = \left\langle \iint \hat{T}(k_1)\hat{T}^*(k_2)e^{-ik_1x}e^{ik_2y}\frac{\mathrm{d}k_1\mathrm{d}k_2}{(2\pi)^2} \right\rangle$$

$$= \iint \left\langle \hat{T}(k_1)\hat{T}^*(k_2) \right\rangle e^{-ik_1x}e^{ik_2y}\frac{\mathrm{d}k_1\mathrm{d}k_2}{(2\pi)^2}$$

$$= \int P_\Phi(k)\hat{W}^2(k)e^{-ik(x-y)}\frac{\mathrm{d}k}{2\pi}.$$

In the case $x = y$ the resulting correlations can be written as a correlation matrix with the correlation of an odd number of derivatives with an even number of derivatives being equal to zero,

$$
\begin{array}{c}
\begin{array}{ccccc} T & T_1 & T_{11} & T_{111} & T_{1111} \end{array} \\
\begin{array}{c} T \\ T_1 \\ T_{11} \\ T_{111} \\ T_{1111} \end{array}
\left(
\begin{array}{ccccc}
\sigma_0^2 & 0 & -\sigma_2^2 & 0 & \sigma_4^2 \\
0 & \sigma_2^2 & 0 & -\sigma_4^2 & 0 \\
-\sigma_2^2 & 0 & \sigma_4^2 & 0 & -\sigma_6^2 \\
0 & -\sigma_4^2 & 0 & \sigma_6^2 & 0 \\
\sigma_4^2 & 0 & -\sigma_6^2 & 0 & \sigma_8^2
\end{array}
\right),
\end{array}
$$

with

$$\sigma_j(r)^2 = \int_{-\infty}^{\infty} P_\delta(|k|)W^2(k)k^{j-4}\frac{\mathrm{d}k}{2\pi}.$$

When x does not coincide with y, we can write the correlation matrix as

$$
\begin{array}{c}
\begin{array}{ccccc} T(r) & T_1(r) & T_{11}(r) & T_{111}(r) & T_{1111}(r) \end{array} \\
\begin{array}{c} T(0) \\ T_1(0) \\ T_{11}(0) \\ T_{111}(0) \\ T_{1111}(0) \end{array}
\left(
\begin{array}{ccccc}
\sigma_0(r)^2 & i\sigma_1(r)^2 & -\sigma_2(r)^2 & -i\sigma_3(r)^2 & \sigma_4(r)^2 \\
-i\sigma_1(r)^2 & \sigma_2(r)^2 & i\sigma_3(r)^2 & -\sigma_4(r)^2 & -i\sigma_5(r)^2 \\
-\sigma_2(r)^2 & -i\sigma_3(r)^2 & \sigma_4(r)^2 & i\sigma_5(r)^2 & -\sigma_6(r)^2 \\
i\sigma_3(r)^2 & -\sigma_4(r)^2 & -i\sigma_5(r)^2 & \sigma_6(r)^2 & i\sigma_7(r)^2 \\
\sigma_4(r)^2 & i\sigma_5(r)^2 & -\sigma_6(r)^2 & -i\sigma_7(r)^2 & \sigma_8(r)^2
\end{array}
\right)
\end{array}
$$

with $r = |x - y|$ and

$$\sigma_j(r)^2 = \int_{-\infty}^{\infty} P_\delta(k) W^2(k) k^{j-4} e^{ikr} \frac{\mathrm{d}k}{2\pi}.$$

Point statistics of stationary Gaussian processes only contain the correlation at $r = 0$. For those calculations we use $\sigma_i(0) = \sigma_i$. In figure 8.4 we illustrate the correlation functions of a field with power spectrum $P(k) = 1$ and smoothing scale $\sigma = 1$. Note that σ_i for i even has a real square, is symmetric and does not vanish at the origin whereas σ_i for i odd, has a imaginary and antisymmetric square and vanishes at the origin. For this reason we do not consider the odd-i sigmas in local statistics. The odd-i sigmas do appear in calculations of two-point correlation functions.

8.5.2 Correlations in two dimensions

In two dimensions, the correlation between the T's can be calculated by expanding T again in Fourier space,

$$\langle T(\mathbf{x}) T(\mathbf{y}) \rangle = \int P_\Phi(k) \hat{W}^2(k) e^{-i\mathbf{k} \cdot (\mathbf{x} - \mathbf{y})} \frac{\mathrm{d}\mathbf{k}}{2\pi}.$$

In this thesis we are only interested in point statistics in two dimensions, i.e. $\mathbf{x} = \mathbf{y}$. We can further simplify the expression by going to polar coordinates (r, φ) with

$$\mathbf{k} = \begin{pmatrix} r \cos \varphi \\ r \sin \varphi \end{pmatrix},$$

by which

$$\langle T(\mathbf{x}) T(\mathbf{y}) \rangle = \int_0^{2\pi} \int_0^{\infty} P_\Phi(r) \hat{W}^2(r) r \frac{\mathrm{d}r \mathrm{d}\varphi}{2\pi} = \int_0^{\infty} P_\Phi(r) \hat{W}^2(r) r \mathrm{d}r.$$

In this thesis we are interested in the statistics of partial derivatives up to fourth order

$$Y_T = (T_{11}, T_{22}, T_{12}; T_{111}, T_{122}, T_{222}, T_{112}; T_{1111}, T_{2222}, T_{1122}, T_{1112}, T_{1222}).$$

The corresponding correlation matrix can be computed in this way

$$\begin{pmatrix}
\frac{3}{8}\sigma_5^2 & \frac{1}{8}\sigma_5^2 & 0 & 0 & 0 & 0 & 0 & -\frac{5}{16}\sigma_7^2 & -\frac{1}{16}\sigma_7^2 & -\frac{1}{16}\sigma_7^2 & 0 & 0 \\
\frac{1}{8}\sigma_5^2 & \frac{3}{8}\sigma_5^2 & 0 & 0 & 0 & 0 & 0 & -\frac{1}{16}\sigma_7^2 & -\frac{5}{16}\sigma_7^2 & -\frac{1}{16}\sigma_7^2 & 0 & 0 \\
0 & 0 & \frac{1}{8}\sigma_5^2 & 0 & 0 & 0 & 0 & 0 & 0 & 0 & -\frac{1}{16}\sigma_7^2 & -\frac{1}{16}\sigma_7^2 \\
0 & 0 & 0 & \frac{5}{16}\sigma_7^2 & \frac{1}{16}\sigma_7^2 & 0 & 0 & 0 & 0 & 0 & 0 & 0 \\
0 & 0 & 0 & \frac{1}{16}\sigma_7^2 & \frac{1}{16}\sigma_7^2 & 0 & 0 & 0 & 0 & 0 & 0 & 0 \\
0 & 0 & 0 & 0 & 0 & \frac{5}{16}\sigma_7^2 & \frac{1}{16}\sigma_7^2 & 0 & 0 & 0 & 0 & 0 \\
0 & 0 & 0 & 0 & 0 & \frac{1}{16}\sigma_7^2 & \frac{1}{16}\sigma_7^2 & 0 & 0 & 0 & 0 & 0 \\
-\frac{5}{16}\sigma_7^2 & -\frac{1}{16}\sigma_7^2 & 0 & 0 & 0 & 0 & 0 & \frac{35}{128}\sigma_9^2 & \frac{3}{128}\sigma_9^2 & \frac{5}{128}\sigma_9^2 & 0 & 0 \\
-\frac{1}{16}\sigma_7^2 & -\frac{5}{16}\sigma_7^2 & 0 & 0 & 0 & 0 & 0 & \frac{3}{128}\sigma_9^2 & \frac{35}{128}\sigma_9^2 & \frac{5}{128}\sigma_9^2 & 0 & 0 \\
-\frac{1}{16}\sigma_7^2 & -\frac{1}{16}\sigma_7^2 & 0 & 0 & 0 & 0 & 0 & \frac{5}{128}\sigma_9^2 & \frac{5}{128}\sigma_9^2 & \frac{3}{128}\sigma_9^2 & 0 & 0 \\
0 & 0 & -\frac{1}{16}\sigma_7^2 & 0 & 0 & 0 & 0 & 0 & 0 & 0 & \frac{5}{128}\sigma_9^2 & \frac{3}{128}\sigma_9^2 \\
0 & 0 & -\frac{1}{16}\sigma_7^2 & 0 & 0 & 0 & 0 & 0 & 0 & 0 & \frac{3}{128}\sigma_9^2 & \frac{3}{128}\sigma_9^2
\end{pmatrix},$$

(a) The dependence of σ_4 on distance r

(b) The dependence of σ_5 on distance r

(c) The dependence of σ_6 on distance r

(d) The dependence of σ_7 on distance r

(e) The dependence of σ_8 on distance r
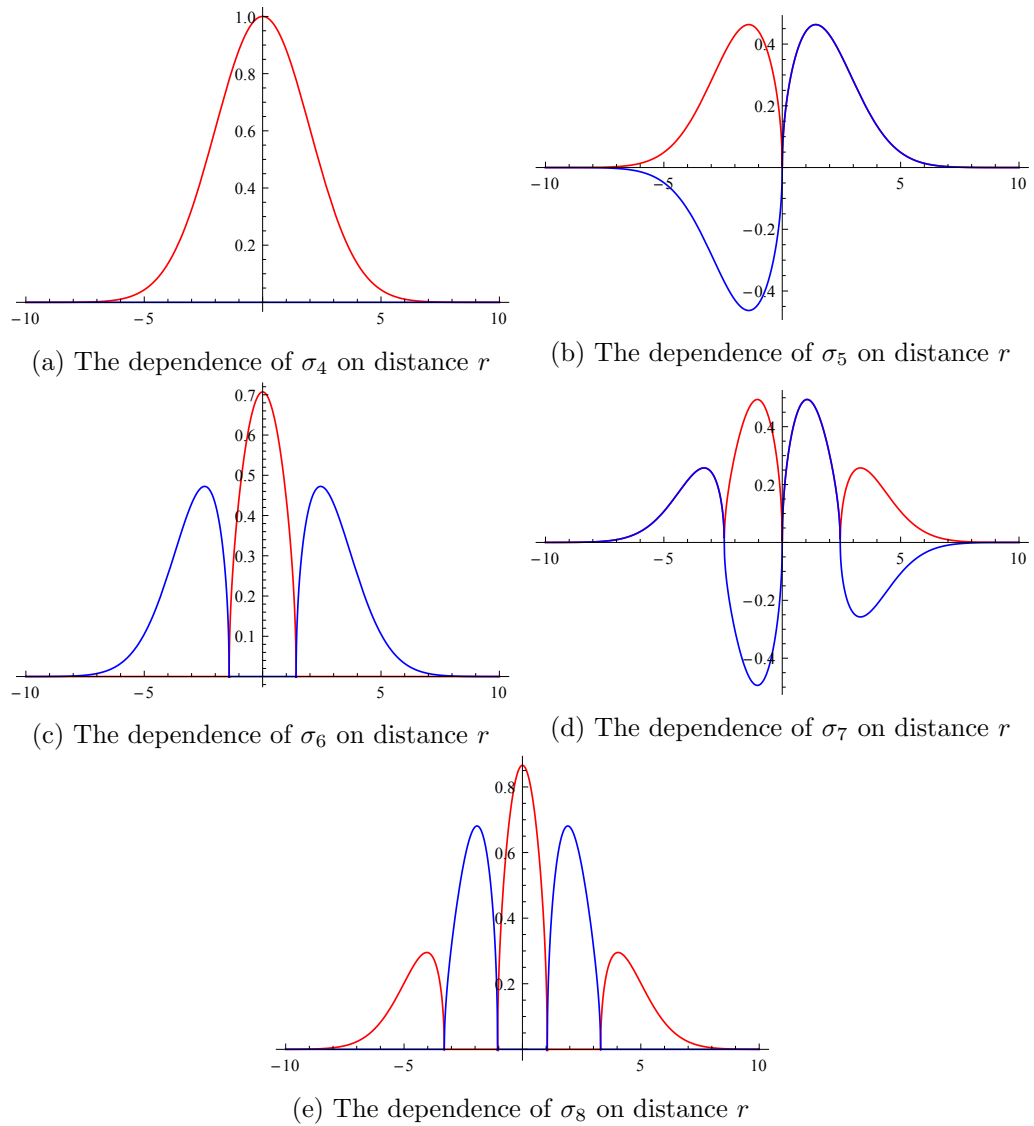
Figure 8.4: The distance-dependence of correlation functions in one dimension with power spectrum $P(k) = 1$ and unit smoothing scale. The red line is the real part and blue line is the imaginary part of σ_i.

with the moments σ_5^2, σ_7^2 and σ_9^2, defined by

$$\sigma_j^2 = \frac{1}{2\pi} \int_0^\infty P_\delta(k) W^2(k) k^{j+4} \mathrm{d}k.$$

The correlation matrices described above contain all the statistical information of Gaussian random fields used in further chapters. In one dimension, the density of point catastrophes and length of the A_2 and A_3 lines only contain the moments σ_4, σ_6, and σ_8. Two-point correlation functions of point catastrophes depend on the set of functions $\{\sigma_4(r), \sigma_5(r), \sigma_6(r), \sigma_7(r), \sigma_8(r))$. In two dimensions the caustics can only depend on the moments σ_5, σ_7, and σ_9. If the analysis developed in this thesis would be developed to a stage in which it can be compared to observations, we would be able to infer these statistics. In the subsequent chapters we will show how to perform the calculations.

Chapter 9

Gaussian Random Fields in Cosmology

Realizations of Gaussian random field are often seen as initial conditions in the study of large-scale structure formation. This can most directly be justified by the observation that the temperature fluctuations in the cosmic microwave background radiation field (CMB) are closely modeled by realizations of Gaussian random fields. These temperature fluctuations indicate small Gaussian fluctuations in the density field at the epoch of last scattering.

There exist more fundamental reasons to expect that the density distribution at the epoch of last scattering is well modeled by a realization of a Gaussian random field. Within the inflation paradigm, the fluctuations observed in the cosmic microwave background originated from quantum fluctuations of the inflaton field. During the expansion at the epoch of inflation, the quantum fluctuations got stretched to super-horizon scales and became classical. At times after inflation, these fluctuations reentered the observable universe as density fluctuations and induced the fluctuations observed in the CMB. According to quantum field theory arguments, these fluctuations would be approximately realizations of Gaussian random fields for the most simple slow-roll single-field inflation models. Although the analysis of Gaussian random field fluctuations from inflation, presented in this chapter, is widely accepted in cosmology, the process heavily depends on our understanding of quantum mechanics and other explanations are still being proposed.

Another justification follows from a probabilistic considerations. It can be shown that the superposition of uncorrelated pulses, in the limit of many small pulses, gives rise to realizations of Gaussian random fields. This is in line with the central limit theorem. Gaussian random fields form, in this respect, a natural assumption for the initial density perturbations. Note that the superposition property is crucial, since a product of independent pulses results in a lognormal distribution instead of a normal distribution.

In this chapter we will start with a discussion of the generation of temperature fluctuations in the CMB from quantum fluctuations at inflation. We subsequently show why realizations or Gaussian random fields arise naturally from linear stochastic systems. In the last section we discuss the statistical properties of the cosmic microwave background as measured by the Planck satellite.

9.1   The cosmic microwave background from inflation

Although the ΛCDM model is in good agreement with measurements, there still exist fine-tuning problems which we mentioned in chapter 2. These problems are well known as the flatness, and horizon problem. Both problems do not contradict the ΛCDM model. They merely state that the enormously flat geometry of our current universe, and enormous isotropy of the temperature in the CMB are unnatural situations in the ΛCDM model. We either had very special initial conditions after the big bang, or a mechanism to flattens the geometry of space and thermalize the photon plasma before the moment of last scattering. Inflation theory developed by Alan Guth and Andrei Linde in the 1980s is at the moment one of the most popular proposed mechanisms. One of the elegant features of inflation theory is that it simultaneously explains the enormous isotropy observed in the CMB and predicts the small anisotropies. The generation of these small anisotropies was primarily investigated by Claus Kiefer, David Polarski and Alexei Starobinsky [40]. We here sketch the overview presented by Kiefer and Polarski in 2008 [39].

Inflation theory proposes an epoch of great expansion. In a fraction of a second, the universe expanded to enormous proportions and in the process smoothed the geometry of space. This would furthermore explain the isotropy in the CMB, since points currently opposite on the sky would have been in causal contact before inflation and would have the possibility to get in thermal equilibrium. As derived in chapter 2, the evolution of a homogeneous universe is governed by the Friedmann equations

$$\left(\frac{\dot{a}}{a}\right)^2 = \sum_i \frac{8\pi G}{3}\rho_i - \frac{k}{a^2},$$
$$\frac{\ddot{a}}{a} = -\frac{4\pi G}{3}\sum_i(\rho_i + 3p_i).$$

In order to facilitate such a great expansion, we must find a energy source i satisfying

$$\rho_i + 3p_i < 0.$$

A space independent scalar field $\phi(t)$ satisfying the perfect fluid equations

$$\rho_\phi = \frac{1}{2}\dot{\phi}^2 + V(\phi),$$
$$p_\phi = \frac{1}{2}\dot{\phi}^2 - V(\phi),$$

with V the so-called inflaton potential, is an interesting candidate. To see this, observe that

$$w_\phi = \frac{\frac{1}{2}\dot{\phi}^2 - V(\phi)}{\frac{1}{2}\dot{\phi}^2 + V(\phi)},$$

approaches -1 when

$$\dot{\phi}^2 \ll V(\phi).$$

The scalar field ϕ driving inflation is called the inflaton. There exist many different inflation models, with several choices for V and sometimes several inflaton fields. We here restrict our self to the most simple single field inflation models. The inflaton field ϕ evolves in time according to the Klein-Gordon equation in comoving coordinates

$$\ddot{\phi} + 3H\dot{\phi} + \frac{\mathrm{d}V}{\mathrm{d}\phi} = 0.$$

The second term is the familiar Hubble drag. In most inflationary models, we can take the slow-roll condition $\ddot{\phi} \ll 3H\dot{\phi}$, which is equivalent to the conditions

$$\dot{H} \ll 3H^2, \quad \frac{\mathrm{d}^2V}{\mathrm{d}\phi^2} \ll 9H^2.$$

The equation of motion can in this context be approximated by

$$3H\dot{\phi} \approx -\frac{\mathrm{d}V}{\mathrm{d}\phi}.$$

We see from this formula that the predictions of single field slow-roll inflation theory heavily depend on the inflaton potential V. From a particle physics perspective, the inflaton field would a field corresponding to some scalar particle described in the fundamental theory of particle physics. A candidate in the standard model setting is formed the only yet observed scalar particle, the Higgs boson. Inflation based on the Higgs potential is called Higgs-inflation. However, Higgs-inflation does not straightforwardly explain current observations. It furthermore remains controversial, whether the standard model can be applied at the energy scale of inflation. Other candidates would be scalar fields predicted by string theory such as axion monodromy inflation or other physical models beyond the standard model. The physical community has not yet found a final fundamental model of the inflaton potential. For this reasons, people often use effective models. One can for example use chaotic inflation proposed by Andrei Linde.

The generic picture is however, that the inflaton potential is qualitative like figure 9.1. On the horizontal part of the potential, the inflaton field slowly moves down. During this process, the universe dramatically expands. When the inflaton reaches the part of the potential with a greater slope it accelerates and rolls down. While the inflaton rolls down, the slow-roll conditions are violated and the expansion rate decreases. When the inflaton reaches the minimum of the potential, the inflaton starts to perform a damped oscillation, while generating particles in the process. This epoch is called reheating.

The discussion above suffices to give a qualitatively picture of the evolution of fluctuations during inflation. The Hubble radius $R_H = H^{-1} = \frac{a}{\dot{a}}$, which is roughly the radius of an observable universe, is an important cosmological length scale. The distance between two points λ, hereafter called the physical length scale is a second characteristic
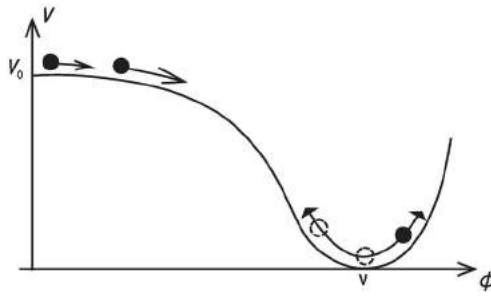
Figure 9.1: The generic form of the inflaton potential

scale in cosmology. The physical length scale evolves roughly proportional to a. For an expansion $a \propto t^{\alpha}$, we see that the Hubble radius and physical distances evolve as $R_H \propto t$ and $\lambda \propto t^{\alpha}$. We observe that for a decelerated expansion with $\alpha < 1$, the Hubble radius R_H grows faster than the physical length scale λ by which fluctuations from outside the horizon enter the observable universe. In a accelerated universe with $\alpha > 1$, the physical length scale λ grows faster then the Hubble radius R_H by which fluctuations get stretched outside the Horizon.

In most inflationary single-field, slow-roll models the Hubble parameter is approximately constant and the universe expands as a de Sitter universe with $a \propto e^{Ht}$. Since this is an accelerated phase of the universe, all fluctuations get stretched. The largest sub-horizon fluctuations get stretched to super-horizon scales. On super-horizon scales, the fluctuations do not evolve significantly, since different parts of the fluctuations are no longer in causal contact with each other. These super-horizon fluctuations are often called 'frozen in'. When the universe enters the radiation dominated epoch, the expansion becomes decelerated and super-horizon scale fluctuations start to reenter the universe. Note that the fluctuations stretched to super-horizon scales at the end of inflation, will reenter the universe the earliest (first in, last out). Based on the observations of the Planck satellite, it is generally thought that the fluctuations observed in the CMB became super-horizon approximately 65 e-folds before the end of inflation, i.e. $a_e = e^{65} a_k$ with a_e the scale parameter at the end of inflation and a_k the scale factor when the fluctuations of the CMB where stretched to scales larger than the Hubble radius.

9.1.1 The evolution of quantum fluctuations in the Heisenberg picture

The discussion above is a standard description of inflation theory. The universe expanded dramatically, solving the flatness and horizon problem, and fluctuations present at the epoch of inflation get stretched to super-horizon scales and reenter our observable universe at a later epoch. This however is not full satisfactory, since it does not describe how the initial sub-horizon fluctuations were generated and what the nature of the fluctuations is after the second horizon crossing.

According to current observations, inflation is supposed to take place at energy scales

of about $10^{15} GeV$. This is still well below the Planck scale of $10^{19} GeV$. At this scale space-time is still supposed to be described by classical curved space-time. Quantum fluctuations in the inflaton field $\delta\phi(\mathbf{x}, t)$, which do depend on space in contrary to the classical inflaton field, are modeled as massless a massless scalar field. This is a good approximation for slow-roll inflation and is exact for primordial gravitational waves []. In the rest of this section, we rescale the fluctuations by the scale factor $y(\mathbf{x}, t) = a(t)\delta\phi(\mathbf{x}, t)$ and work with conformal time $\eta = \int \frac{\mathrm{d}t}{a(t)}$. The classical Hamiltonian of a massless scalar field is

$$
\begin{aligned}
H &= \int \mathrm{d}\mathbf{x}\mathcal{H}(y, p, \partial_i y, \eta) \\
&= \frac{1}{2}\int \left[p(\mathbf{k})p^*(\mathbf{k}) + k^2 y(\mathbf{k})y^*(\mathbf{k}) + \frac{a'}{a}(y(\mathbf{k})p^*(\mathbf{k}) + p(\mathbf{k})y^*(\mathbf{k})) \right],
\end{aligned}
$$

with the prime indicating the derivative with respect to conformal time and p the conjugate momentum to y given as

$$
p = \frac{\partial\mathcal{L}(y, y')}{\partial y'} = y' - \frac{a'}{a}y.
$$

The equation of motion of the massless scalar field is

$$
y''(\mathbf{k}, \eta) + \left(k^2 - \frac{a''}{a} \right) y(\mathbf{k}, \eta) = 0.
$$

We can quantize the system by transforming y and p to operators and imposing the canonical commutation relations

$$
\begin{aligned}
[y(\mathbf{k}, \eta), p^\dagger(\mathbf{k}, \eta)] &= i\delta^{(3)}(\mathbf{k} - \mathbf{k}'), \\
[y(\mathbf{k}, \eta), y(\mathbf{k}', \eta)] &= [p(\mathbf{k}, \eta), p(\mathbf{k}', \eta)] = 0,
\end{aligned}
$$

with units such that $\hbar = 1$. As in the quantum mechanical harmonic oscillator, we can write the quantum Hamiltonian in terms of creation and annihilation operators,

$$
\begin{aligned}
a(\mathbf{k}, \eta) &= \frac{1}{\sqrt{2}}\left(\sqrt{k}y(\mathbf{k}, \eta) + \frac{i}{\sqrt{k}}p(\mathbf{k}, \eta) \right), \\
a^\dagger(\mathbf{k}, \eta) &= \frac{1}{\sqrt{2}}\left(\sqrt{k}y(\mathbf{k}, \eta) - \frac{i}{\sqrt{k}}p(\mathbf{k}, \eta) \right).
\end{aligned}
$$

In terms of these operators, the y and p operators can be written as,

$$
\begin{aligned}
y(\mathbf{k}, \eta) &= \frac{a(\mathbf{k}, \eta) + a^\dagger(-\mathbf{k}, \eta)}{\sqrt{2k}}, \\
p(\mathbf{k}, \eta) &= -i\sqrt{\frac{k}{2}}(a(\mathbf{k}, \eta) - a^\dagger(-\mathbf{k}, \eta)).
\end{aligned}
$$

The commutation relation and Hamiltonian in terms of the creation and annihilation operators are

$$[a(\mathbf{k},\eta), a^\dagger(\mathbf{k}',\eta)] = \delta^{(3)}(\mathbf{k}-\mathbf{k}'),$$
$$[a(\mathbf{k},\eta), a(\mathbf{k}',\eta)] = [a^\dagger(\mathbf{k},\eta), a^\dagger(\mathbf{k}',\eta)] = 0,$$

and

$$H = \int \frac{d\mathbf{k}}{2}\bigg[k(a(\mathbf{k},\eta)a^\dagger(\mathbf{k},\eta) + a^\dagger(-\mathbf{k},\eta)a(-\mathbf{k},\eta))$$
$$+ i\frac{a'}{a}(a^\dagger(\mathbf{k},\eta)a^\dagger(-\mathbf{k},\eta) - a(\mathbf{k},\eta)a(-\mathbf{k},\eta))\bigg].$$

In the Heisenberg picture[1], the creation and annihilation operators satisfy the differential equations

$$\begin{pmatrix} a'(\mathbf{k},\eta) \\ (a^\dagger(\mathbf{k},\eta))' \end{pmatrix} = k \begin{pmatrix} -i & \frac{aH}{k} \\ \frac{aH}{k} & i \end{pmatrix} \begin{pmatrix} a(\mathbf{k},\eta) \\ a^\dagger(\mathbf{k},\eta) \end{pmatrix}.$$

If the matrix would have been diagonal, the system of differential equations would have been uncoupled and the creation an annihilation operator would have evolved independently. The off-diagonal terms generate a mixing between the creation and annihilation operators. Note that the off-diagonal term $\frac{aH}{k}$ is large for super-horizon scales and is negligible for sub-horizon scales. This will lead to the quantum-classical transformation of the fluctuations.

By combining the system of differential equations with the expression of $y(\mathbf{k},\eta)$ in terms of the creation and annihilation operators we can show that

$$y(\mathbf{k},\eta) = f_k(\eta)a_\mathbf{k} + f_k^*(\eta)a^\dagger_{-\mathbf{k}}$$

with $a_\mathbf{k} = a(\mathbf{k},\eta_0)$ at some initial time η_0 and f_k satisfying the classical equation of motion with the initial condition $f_k(\eta_0) = \frac{1}{\sqrt{2k}}$. We can write this equation without direct reference to the creation and annihilation operators as

$$y(\mathbf{k},\eta) = \sqrt{2k}f_{k1}(\eta)y_\mathbf{k} - \sqrt{\frac{2}{k}}f_{k2}(\eta)p_\mathbf{k}$$

with $y_\mathbf{k} = y(\mathbf{k},\eta_0), p_\mathbf{k} = p(\mathbf{k},\eta_0), f_{k1} = Re[f_k]$, and $f_{k2} = Im[f_k]$. Analogously, the evolution of the momentum operator can be written as

$$p(\mathbf{k},\eta) = \sqrt{\frac{2}{k}}g_{k1}(\eta)p_\mathbf{k} - \sqrt{2k}g_{k2}(\eta)y_\mathbf{k},$$

with g_k satisfying the equation of motion with initial condition $g_k(\eta_0) = \sqrt{\frac{k}{2}}$ and $g_{k1} = Re[g_k], g_{k2} = Im[g_k]$.

---

[1]A quantum mechanical framework in which the wave functions are static and the operators evolve in time.

For single field slow-roll inflation models, the discussion above completely describes the evolution of quantum fluctuations, without the collapse of the wave function. In most inflation models, space-time evolves as a de Sitter space with the expansion $a \propto e^{Ht}$, with a constant Hubble parameter H. In this approximation, we can solve f_k and g_k exactly,

$$f_k = \frac{-i}{\sqrt{2k}} e^{-ik\eta} \left(1 - \frac{i}{k\eta} \right),$$

$$g_k = -i\sqrt{\frac{k}{2}} e^{-ik\eta},$$

$$\eta = -\frac{1}{aH} < 0.$$

For a more general discussion see Kiefer et al. [39]. For modes outside the horizon, we are in the limit $k\eta \ll 1$. In this limit f_{k2} and g_{k1} vanish, while f_{k1} and g_{k2} do not vanish. In this limit we have approximately

$$y(\mathbf{k}, \eta) = \sqrt{2k} f_{k1}(\eta) y_{\mathbf{k}},$$

$$p(\mathbf{k}, \eta) = -\sqrt{2k} g_{k2}(\eta) y_{\mathbf{k}},$$

satisfying the commutation relation

$$[y(\mathbf{k}, \eta), p(\mathbf{k}, \eta)] = 0.$$

Hence we see that the quantum fluctuations outside the horizon, act as classical fluctuations. Note that this is independent of the initial wave function.

9.1.2   The evolution of quantum fluctuations in the Schrödinger picture

In the Schrödinger picture[2], we can do an analogous calculation. Assume that the initial state of the perturbations is the vacuum state $|0, \eta_0\rangle$ satisfying

$$a_{\mathbf{k}}|0, \eta_0\rangle = 0,$$

for all $\mathbf{k}$. The time-dependent Schrödinger equation

$$i\hbar \frac{\partial}{\partial t} \Phi = H\Phi$$

can be directly solved using the Heisenberg computation and results in the wave function

$$\Phi = \frac{1}{\sqrt[4]{\pi|f_k|^2}} \exp\left(-\frac{|y_{\mathbf{k}}|^2}{2|f_k|^2} (1 - 2i(f_{k1}g_{k2} - f_{k2}g_{k1})) \right).$$

---

[2]A quantum mechanical framework in which the operators are static and the wave function evolves in time.

It can be shown that the wave function in the limit of fluctuations on super-horizon scales, get so-called squeezed when the quantity $(f_{k1}g_{k2} - f_{k2}g_{k1})$ becomes large. The probability distribution of the fluctuations is unaffected by the this property since the modulus of Φ is independent of the phase. The probability distribution is

$$p(y_{\mathbf{k}}) = \frac{1}{\sqrt{\pi|f_k|^2}} e^{-\frac{|y_{\mathbf{k}}|^2}{|f_k|^2}},$$

which coincides with the probability distribution of Fourier modes a of Gaussian random field with power spectrum

$$P(k) = \frac{1}{2}|f_k|^2.$$

The power spectrum turns out to be proportional to k^{-1} in the limit $k\eta \ll 1$. Hence the power spectrum of the potential in the super-horizon limit is approximately a k^{-1} power law. The corresponding density power spectrum is linear in k. This observation is in agreement with measurements of the cosmic microwave background and is known as the Harrison-Zel'dovich power spectrum.

9.1.3   Collapse of the wave function

The analysis in the Heisenberg picture showed that fluctuations outside the horizon behave as classical fluctuations. The analysis in the Schrödinger picture showed that the fluctuations outside the horizon are well modeled by Gaussian random fields. Note however that in the analysis above, the fluctuations above remain quantum mechanical in nature. Even though they may look like classical fluctuations, nothing forbids them to become quantum mechanical in nature while reentering the horizon. We furthermore assumed that the Fourier modes evolved isolated and did not experience measurements and wave collapses. This is an unrealistic assumption since evolution of the inflaton is unlikely to be linear and will have to couple to different fields in order for the process of reheating to occur. Here, we shortly describe how the collapse of the wave function, makes the classically behaving quantum fluctuations really classical. For a more elaborate discussion see Kiefer et al. [39].

Small couplings between different Fourier modes can have huge implications. While the interaction my have negligible influence on the fluctuations, the fluctuations can get entangled and lead to a collapse of the wave function at a later time. Studies have shown that highly squeezed quantum states have a higher probability to collapse than non-squeezed states. This is the reason that it is difficult to generate squeezed quantum states in quantum optics. Hence even though the fluctuations outside the horizon do not evolve significantly due to interactions, they do collapse due to the entanglement with other fluctuations probably existing in a part of the universe outside the causal horizon. There are effects of the collapse on the fluctuations. Different couplings can lead to slightly different collapses. These effects are however not measurable with current telescopes due to the fact that the fluctuations are highly squeezed before they collapse.

The collapse of the wave function plays a crucial role in a formal description of the quantum to classical transition of the fluctuations generated by inflation. In order to do it properly, we have to understand the full Hamiltonian of the inflaton field and must have a good understanding of the collapse of the wave function. However since our understanding of the interpretation of the collapse of the wave function is still not fully developed, there are still ongoing discussions about the details of the transition. See for example [64] for an discussion of the sort comings of the discussion presented here. These details however do not significantly influence the predictions presented here. We seem to know enough about quantum mechanics to understand the CMB up to the accuracy with which we can measure it.

9.2 Gaussian random fields from the central limit theorem

In this section we approximate the statistics of functions generated by the superposition of many small uncorrelated pulses. We follow the reasoning of Feynman and Hibbs [26]. Imagine for example the signal of a Geiger-Muller counter, in which the signal is generated by cosmic rays, the distribution of raindrops or the hight in a mountain landscape.

For simplicity we take the Geiger-Muller counter example and assume that every cosmic ray generates an identical pulse. We furthermore assume that the signal of Geiger-Muller counter $f : [0, T] \rightarrow \mathbb{R}$ in the interval $[0, T]$ is the superposition of n pulses, i.e.,

$$f(t) = \sum_{j=1}^{n} g(t - t_j),$$

with $t_1, \ldots, t_n \in [0, T]$ the times at which the cosmic rays are detected and the function g defined as the pulse generated by a single cosmic ray observed at time $t = 0$. See figure 9.2 for an example of such a function. If we know the number of detections n and times of detection $t_1, \ldots, t_n$, this would be a reasonable model of the signal f. However, in concrete situations, we do not know beforehand how many signals one detects in a given time interval or at which times a detection is made. We can only reasonable assume that a observation run results in a Poisson distributed number of detections, and that the times of detection are uniformly distributed over the observation time interval, i.e.

$$P(n = k) = \frac{(\mu T)^k}{k!} e^{-\mu T},$$

with μ the rate of detections and

$$P(t_i = t) = \begin{cases} 1/T & \text{if } t \in [0, T], \\ 0 & \text{otherwise}, \end{cases}$$
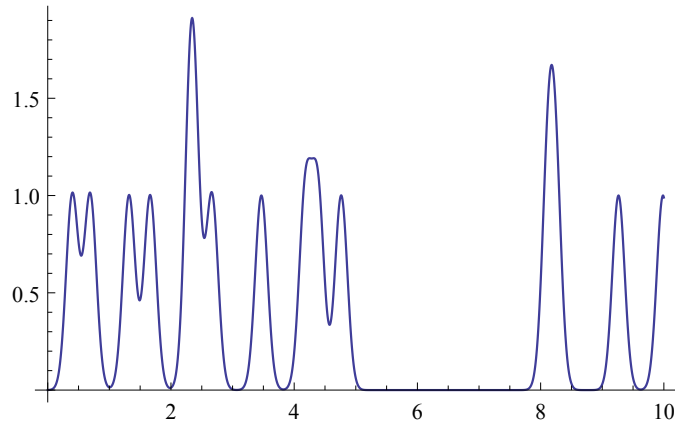
Figure 9.2: A random signal

for $i \in \{1, 2, \ldots, n\}$. It is clear that these assumptions completely determine the probability distribution of f, i.e. we can easily generate realizations, the formulation is very implicit. That is to say, the distribution is not obviously Gaussian and it is difficult to determine the measure for some arbitrary function h. In the subsequent derivation, we make this explicit and show the limit in which the distribution becomes Gaussian.

In order to analyze this problem, we discuss some standard probabilistic machinery and extend it to a functional formulation. Given a probability distribution P with respect to x, the average of x is

$$\langle x \rangle = \frac{\int x P(x) \mathrm{d}x}{\int P(x) \mathrm{d}x},$$

where P is normally normalized such that $\int P(x)\mathrm{d}x = 1$. The so-called characteristic function of P is

$$\phi(k) = \langle e^{ikx} \rangle = \frac{\int e^{ikx} P(x) \mathrm{d}x}{\int P(x) \mathrm{d}x},$$

which is the Fourier transform of P and contains the same information since we can always return to the probability density via

$$P(x) = \int e^{-ikx} \phi(k) \frac{\mathrm{d}k}{2\pi}.$$

The characteristic function has the nice property that

$$\phi(0) = 1, \phi'(0) = i\langle x \rangle, \phi''(0) = -\langle x^2 \rangle, \phi'''(0) = -i\langle x^3 \rangle, \ldots,$$

which can be proven by interchanging the order of integration and differentiation in the definition of the characteristic function.

In functional notation, we have a functional P which is the probability density with respect to functions, i.e. the probability that a function is contained in a subset A of function space is

$$\int_A P[f(t)]\mathcal{D}f(t),$$

where straight brackets indicate functionals and the (t) merely serves to indicate that we integrate over functions. The average in this setting is defined as

$$\langle Q \rangle = \frac{\int Q[f(t)]P[f(t)]\mathcal{D}f(t)}{\int P[f(t)]\mathcal{D}f(t)},$$

where we always explicitly write the normalization factor, since it is often difficult to normalize P properly. The characteristic function in this functional framework is defined as

$$\Phi[k(t)] = \frac{\int e^{i \int k(t)f(t)\mathrm{d}t}P[f(t)]\mathcal{D}f(t)}{\int P[f(t)]\mathcal{D}f(t)},$$

with inverse

$$P[f(t)] = \int e^{-i \int k(t)f(t)\mathrm{d}t}\Phi[k(t)]\mathcal{D}k(t).$$

Note that the integral in the exponent arises from the limit of a product of exponents. The characteristic functional satisfies similar moment equations

$$\Phi[0] = 1, \left.\frac{\delta\Phi}{\delta k(a)}\right|_{k(t)=0} = i\langle f(a)\rangle, \left.\frac{\delta^2\Phi}{\delta k(a)\delta k(b)}\right|_{k(t)=0} = -\langle f(a)f(b)\rangle, \ldots,$$

with $\delta/\delta k(a)$ the functional derivative.

This allows us to determine the explicit probability distribution of the signal of the Geiger-Muller counter. We use the definition of the characteristic functional, and compute it using the given probabilities of the signal f. We subsequently approximate the functional in the above mentioned limit and perform the functional inverse Fourier transform.

First assume that we know the number of detections n in the time interval $[0, T]$. The characteristic functional is

$$\begin{aligned}
\Phi[k(t)] &= \frac{\int e^{i \int k(t)f(t)\mathrm{d}t}P[f(t)]\mathcal{D}f(t)}{\int P[f(t)]\mathcal{D}f(t)} \\
&= \int_0^T \cdots \int_0^T \int_0^T e^{i \sum_{j=1}^n \int k(t)g(t-t_j)\mathrm{d}t}\frac{\mathrm{d}t_1}{T}\frac{\mathrm{d}t_2}{T}\cdots\frac{\mathrm{d}t_n}{T} \\
&= \left(\int_0^T e^{i \int k(t+x)g(t)\mathrm{d}t}\frac{\mathrm{d}s}{T}\right)^n,
\end{aligned}$$

where in the last equation we used a change of variables to remove the t_j dependence. For clarity we will write the last expression as A^n. However, we in reality do not know the number of detections n. We however do know that n is assumed to be Poisson distributed. The functional, including the uncertainty in the number of detections and times of detections is

$$\Phi[k(t)] = \sum_n A^n \frac{(\mu T)^n}{n!} e^{-\mu T} = e^{-(1-A)\mu T} = \exp\left[-\mu \int_0^T \left(1 - e^{i\int k(t+s)g(t)\mathrm{d}t}\right)\mathrm{d}s\right],$$

where we used the Taylor expansion of e^x in x around $x = 0$. So far everything has been exact. We in principle would like to perform the functional inverse Fourier transform on this characteristic functional. This however results in a path integral which we are unable to solve (yet). Instead we consider the limit in which the detection rate μ becomes very large while the pulse g becomes very small. In this limit, we can expand $e^{i\int k(t+s)g(t)\mathrm{d}t}$ in a Taylor series. If we expand up to quadratic order, we obtain the characteristic functional

$$\Phi[k(t)] = e^{i\mu \int_0^T \int_0^T k(t+s)g(t)\mathrm{d}t\mathrm{d}s} e^{-\frac{\mu}{2}\int_0^T \int_0^T k(t)g(t+s)\mathrm{d}t \int_0^T k(t')g(t'+s)\mathrm{d}t'\mathrm{d}s}.$$

Since we assume that g is small, g will not significantly couple to k in the integral of the first exponent. In the limit of large μ and small g, we can make a further approximation

$$\int_0^T \int_0^T k(t+s)g(t)\mathrm{d}t\mathrm{d}s = G \int_0^T k(t)\mathrm{d}t,$$

with $G = \int_0^T g(t)\mathrm{d}t$. We can write the integral in the second exponent more clearly by defining the so-called two point correlation function

$$\lambda(\tau) = \int g(t)g(t+\tau)\mathrm{d}t.$$

We will show in a minute, that this is indeed the two point correlation function as used in the previous chapter. These two equations simplify the characteristic functional considerably

$$\Phi[k(t)] = e^{i\mu G \int k(t)\mathrm{d}t} e^{-\mu/2 \iint k(t)k(t')\lambda(t-t')\mathrm{d}t\mathrm{d}t'}.$$

By taking functional differentials of the characteristic functional we obtain the moments in this approximation. The first derivative gives the expectation value of f

$$\left.\frac{\delta\Phi[k(t)]}{\delta k(a)}\right|_{k(t)=0} = i\langle f(a)\rangle = i\mu G - \left[\mu\int k(t)\lambda(t-a)\mathrm{d}t\right]\Phi[k(t)]\bigg|_{k(t)=0} = i\mu G,$$

which is expected since in a unit time interval there are μ copies of g, and since the problem is symmetric in time. Since we are in general not interested in the general

signal, but rather the fluctuations with respect to the average, we rescale f to obtain the characteristic functional

$$\Phi[k(t)] = e^{-\mu/2 \iint k(t)k(t')\lambda(t-t')\mathrm{d}t\mathrm{d}t'}.$$

The second functional differential gives

$$
\begin{aligned}
\frac{\delta^2 \Phi}{\delta k(a)\delta k(b)}\bigg|_{k(t)=0} = & - \langle f(a)f(b) \rangle = -\bigg[\mu\lambda(a-b)\Phi[k(t)] \\
& - \bigg[\int k(t)\lambda(t-a)\mathrm{d}t\bigg]\bigg[\int k(t')\lambda(t'-a)\mathrm{d}t'\bigg]\Phi[k(t)]\bigg]\bigg|_{k(t)=0} \\
= & -\lambda(a-b).
\end{aligned}
$$

Hence λ is indeed the two point correlation function. We directly observe that higher order correlation functions are expressed in terms of the two point correlation function. This turns out to go according to the Wick contractions. This in principle proofs that f is a realization of a Gaussian random field in this approximation.

We can compute the probability functional of the Geiger-Muller counter signal f explicitly in this approximation by performing the inverse functional Fourier transform. For Gaussian functionals we can perform this path integral. The resulting probability functional is

$$P[f(t)] = e^{-\frac{1}{2\mu} \iint f(t)K(t-t')f(t')\mathrm{d}t\mathrm{d}t'},$$

with K the inverse of λ defined as

$$\int \lambda(t-\tau)K(\tau-s)\mathrm{d}\tau = \delta^{(1)}(t-s),$$

with $\delta^{(1)}$ the Dirac delta function. This is exactly the same as the continues limit of the definition of Gaussian random fields discussed in the previous chapter.

Firstly, note that this derivation did not use the fact the domain of f is one-dimensional. The proof can trivially be extended to higher dimensional spaces. Secondly, note that the derivation was a bit artificial. When we would include third order approximations of the exponent, we would preserve more information of g and generate deviations from the Gaussian case, often called non-Gaussianities. The main problem with this approach is that we so far are unable to perform the path integral in the inverse Fourier transform for quadratic terms. In the literature, people circumvent this problem by perturbing the definition of Gaussian random fields directly with so-called Edschward expansions in terms of so-called cummulants. Although possible to implement, we will not consider non-Gaussian statistics in this thesis and always assume the initial density fluctuations to be purely Gaussian distributed.

9.3   The cosmic microwave background

The most detailed observations of the cosmic microwave background anisotropies are currently obtained with the Planck satellite. The temperature map of this survey is

plotted in figure 9.3a. The power spectrum (in spherical harmonic modes, which we here will interpret as Fourier modes) of this map is depicted in figure 9.3b. Note that this is the reduced power spectrum with respect to the Harrison-Zel'dovich power spectrum. In the literature, this is however always denoted as the power spectrum. The oscillations in the power spectrum are small deviations form the Harrison-Zel'dovich approximation. They are an imprint of the acoustic oscillations, and are well modeled by the concordance ΛCDM model described in chapter 2. In fact, the peaks are able to constrain cosmological parameters as the geometry and energy content of our universe.

The power spectrum is the Fourier transform of the two-point correlation function. The Planck consortium, has also tried to constrain higher order correlation functions (see figure 9.3b). So far, measurements of the Planck map have not led to a detection of deviations from the Gaussian random field assumption. Hence if present, non-Gaussianties are small. This forms one of the strongest proofs in favor of Gaussian statistics of the initial density perturbations.
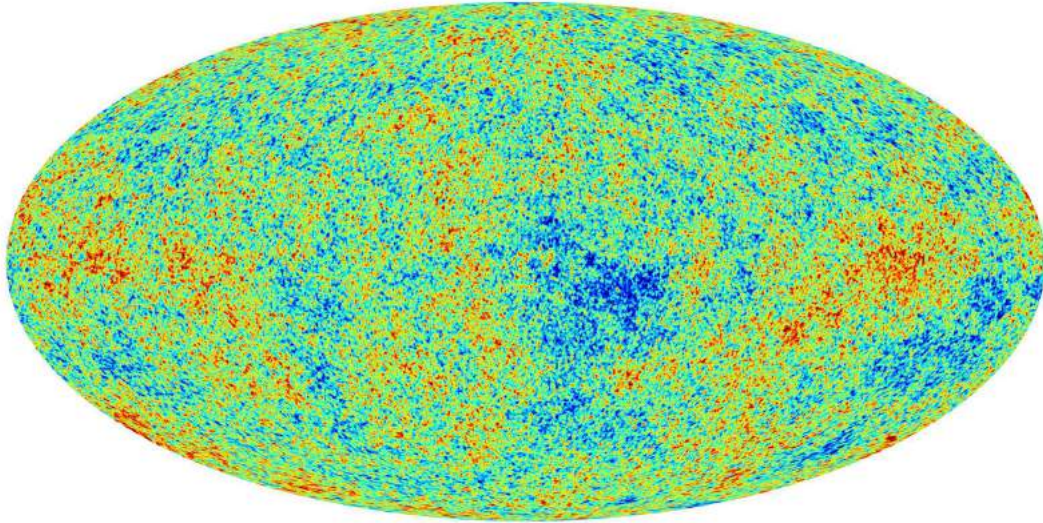
(a) The cosmic microwave background observed with the Planck satellite
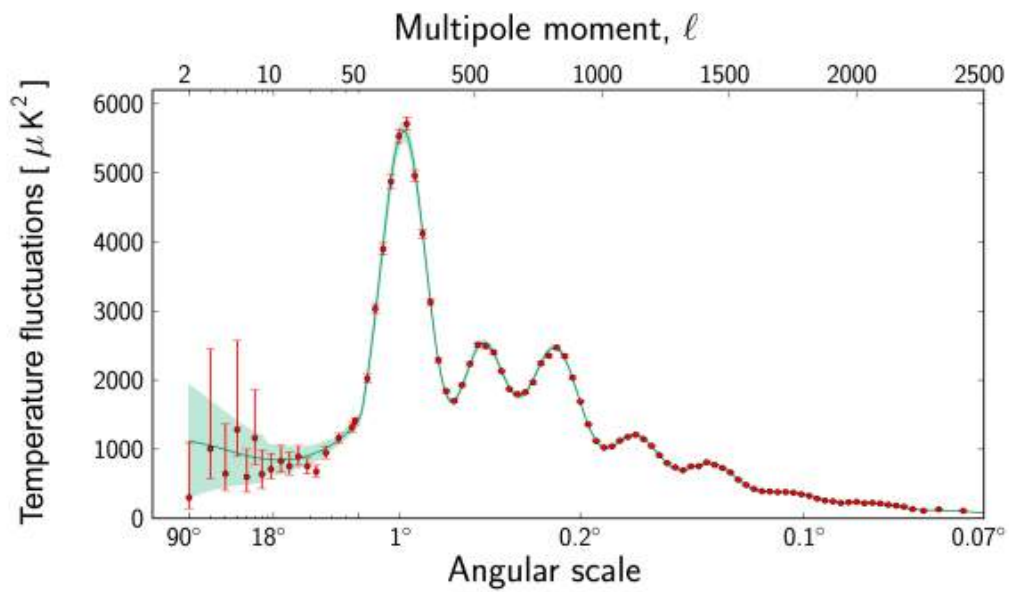
(b) The power spectrum of the cosmic microwave background observed with the Planck satellite

Figure 9.3: Measurements made with the Planck satellite

Chapter 10

Geometric Statistics of Random Fields

In chapter 8 we introduced random fields. In this chapter we study geometric statistics of stationary random fields. We start with Rice's formula which estimates the number of level crossings, for smooth stochastic processes in continuous time. In this thesis we look at continuous space (or continuous manifolds). Besides the statistics of points characterized by certain conditions, we also study curves, i.e. level sets in two dimensions. These curves are studied for stationary Gaussian random fields which have continuous realisations obtained by convolving realizations with a Gaussian distribution.

The proofs presented in this chapter are restrictive in the sense that they assume continuity and differentiability of the realizations. These assumptions make the proofs elementary and comprehensible. They are justified by the fact that the initial density fluctuations are smooth. We follow the analysis of Longuet-Higgins [43] and Bardeen et al. [37]. The theorems however hold in a less restrictive setting. Proofs can be found in "Random Fields and Geometry" by Adler and Taylor [1].

10.1   Point statistics of random fields

Geometric statistics studies the expectation values and probability distributions of geometrical features occurring in random fields. For point features we consider the average number of and correlation of level crossings in one-dimension and the average number and correlation of critical points in d-dimensions. The formulas presented in this section are nowadays basic tools and can be proven in a more general setting.

10.1.1   Rice's formula

In 1936 Stephen Rice studied one-dimensional random fields at Bell-Labs and calculated the average number of level crossings of realizations of random fields. Rice's formula was conjectured, while the theory was in its infancy. It was rigorously proven in later years. Although fundamental, the formula is commonly used in geometric statistics.

Theorem 8 (Rice's formula)**.** *Consider a stationary random field with probability density*

$p(f, f')$ *with function value* f *and spatial derivative* f'. *Let*

$$D_\lambda = \{number\ of\ x\ per\ unit\ distance\ :\ f(x) = \lambda\},$$

then Rice's formula states that the average number of level crossings is

$$\mathcal{N}(\lambda) = \mathbb{E}(D_\lambda) = \int |f'| p(f = \lambda, f') \mathrm{d}f',$$

assuming that level crossings are isolated point features.

Proof. Given a continuous, differentiable realization f of the random field, consider the generalized function

$$n(x) = \sum_{x_\lambda \in f^{-1}(\lambda)} \delta^{(1)}(x - x_\lambda),$$

with $\delta^{(1)}$ the one-dimensional Dirac delta function. By construction, the number of level crossings of f is given by

$$\int n(x) \mathrm{d}x = \int \sum_{x_\lambda \in f^{-1}(\lambda)} \delta^{(1)}(x - x_\lambda) \mathrm{d}x.$$

The average number of level crossings of such a realization is

$$\mathcal{N}(\lambda) = \langle n(x) \rangle = \int \sum_{x_\lambda \in f^{-1}(\lambda)} \delta^{(1)}(x - x_\lambda) p(f) \mathrm{d}x.$$

All level crossings are assumed to be isolated. For each $x_\lambda \in f^{-1}(\lambda)$ let U_{x_λ} be an open environment containing only level crossing x_λ. Since $\delta^{(1)}(x - x_\lambda)$ is zero outside U_{x_λ},

$$\mathcal{N}(\lambda) = \langle n(x) \rangle = \sum_{x_\lambda \in f^{-1}(\lambda)} \int_{U_{xy}} \delta^{(1)}(x - x_\lambda) p(f) \mathrm{d}x.$$

Now using a change of variables

$$\int_{U_{x_\lambda}} \delta^{(1)}(x - x_\lambda) \mathrm{d}x = \int_{U_{x_\lambda}} \delta^{(1)}(f(x) - \lambda) |f'(x)| \mathrm{d}x,$$

and by the fact that $\delta^{(1)}(f(x) - \lambda)$ is nonzero if and only if $\delta^{(1)}(x - x_\lambda)$ is nonzero, we observe that

$$\mathcal{N}(\lambda) = \int |f'(x)| \delta^{(1)}(f(x) - \lambda) p(f(x), f'(x)) \mathrm{d}x = \int |f'(x)| p(f = \lambda, f'(x)) \mathrm{d}x$$

$$= \langle |f'(x)| \delta^{(1)}(f(x) - \lambda) \rangle.$$

This proves Rice's formula. □

In the Gaussian case, Rice's formula reduces to the Gaussian

$$\mathcal{N}(\lambda) = \int |f'| p(f = \lambda, f') \mathrm{d}f' = \frac{1}{2\pi\sigma_0\sigma_2} e^{-\frac{f^2}{2\sigma_0^2}} \int f' e^{-\frac{f'^2}{2\sigma_2^2}} \mathrm{d}f' = \frac{\sigma_2}{\pi\sigma_0} e^{-\frac{f^2}{2\sigma_0^2}},$$

with $\sigma_0^2 = \langle f^2 \rangle$ and $\sigma_2^2 = \langle f'^2 \rangle$. Note that the power spectrum completely determines the correlation functions and the level crossing density.

10.1.2 d-dimensional one-point correlation

Rice's formula can be extended to point features in higher-dimensional stationary random fields.

Theorem 9 (one-point correlation). *Consider d continuous and differentiable realizations of (possibly different) d-dimensional random fields $f_i : \mathbb{R}^d \to \mathbb{R}$ with $i = 1, \ldots, d$. If the points in $\Lambda(y_1, \ldots, y_d) = \{\boldsymbol{x} \in \mathbb{R}^d | f_i(\boldsymbol{x}) = \lambda_i\}$ are isolated, the average number of points in $\Lambda(y_1, \ldots, y_d)$ per unit volume is*

$$\mathcal{N}(\lambda) = \langle | \det \partial_i f_j | \delta^{(d)}(f(\boldsymbol{x}) - \lambda) \rangle.$$

with $f = (f_1, \ldots, f_d)$ and $\lambda = (\lambda_1, \ldots, \lambda_d)$.

Proof. The proof is identical to the proof of Rice's formula, where we use

$$\delta^{(d)}(f(\mathbf{x}) - \lambda) | \det \partial_i f_j | = \delta^{(d)}(\mathbf{x} - \mathbf{x}_\lambda)$$

on regions with only one solution of $f(\mathbf{x}) = \lambda$. $\square$

We can for example consider critical point densities. This analysis is analogous to Bardeen et al. [37]. A realization $f : \mathbb{R}^d \to \mathbb{R}$ in a critical point $\mathbf{x}_y$ satisfies $\partial_i f(\mathbf{x}_y) = f_i = 0$ for $i = 1, 2, \ldots, d$. The number density of critical points with function value f is

$$\mathcal{N}_{crit}(f) = \langle | \det f_{ij} | \delta^1(f_1) \ldots \delta^1(f_d) \rangle = \int | \det f_{ij} | p(f, f_i = 0, f_{ij}) \prod \mathrm{d} f_{ij}.$$

where we $f_{ij} = \partial_i \partial_j f(\mathbf{x}_y)$ and we integrate over all independent variables (we can chose $i \geq j$). By integrating over regions of the parameter space $\{f_{ij}\}$ we can calculate the average number of critical points with a given index, i.e. maxima, minima or saddle points.

10.1.3   Two-point correlation functions

Above we described the density of point features in random fields. We calculated the so called one-point correlation function. The clustering of point distributions is traced by the higher correlation functions. In this thesis we restrict ourself to the two-point correlation function. The calculations can however be easily extended to higher-point correlation functions.

Given the probability $P_2(r)$ that two points are separated by distance r, the two-point correlation function ξ_2 is defined as

$$P_2(r) = \mathcal{N}^2(1 + \xi_2(r)),$$

where $\mathcal{N}$ is the mean number of points per unit volume (the one-point correlation function). The two-point correlation function measures the excess probability of clustering with respect to the unclustered Poisson distributions.

In the above section we calculated the one-point correlation function. We now calculate P_2 for a stationary field.

Theorem 10 (two-point probability). *Consider $2d$ continuous and differentiable realizations of (possibly different) d-dimensional random fields $f_i, g_i : \mathbb{R}^d \to \mathbb{R}$ with $i = 1, \ldots, d$. If the points in $\Lambda(y_1, \ldots, y_d, \mu_1, \ldots, \mu_d) = \{\boldsymbol{x} \in \mathbb{R}^d | f_i(\boldsymbol{x}) = \lambda_i \text{ and } g_i(\boldsymbol{x}) = \mu_i\}$ are isolated, the average number of points in $\Lambda(y_1, \ldots, y_d, \mu_1, \ldots, \mu_d)$ per unit volume is*

$$\mathcal{N}(\lambda) = \langle |\det \partial_i f_j| |\det \partial_i g_j| \delta^{(d)}(f(\boldsymbol{x}) - \lambda) \delta^{(d)}(g(\boldsymbol{x}) - \mu) \rangle.$$

with $f = (f_1, \ldots, f_d), g = (g_1, \ldots, g_d)$ and $\lambda = (\lambda_1, \ldots, \lambda_d), \mu = (\mu_1, \ldots, \mu_d)$.

Proof. By subsequently performing the proof of the d-dimensional one-point correlation function on the two points one obtains this relation. $\qquad \square$

Peter Coles has used this computation in 1989 [20] to compute the two-point correlation function of peaks in a one-dimensional Gaussian random field. In 1993 Coles et al. [21] performed a analogous calculation on the three-point correlation function. For a stationary GRF one can compute this by identifying $f_1 = f'(0), g_1 = g'(r)$, using $\lambda = \mu = 0$ and integrating over negative $f''(0), f''(r)$.

10.2   Line statistics of random fields

Above we considered correlation functions of point features in stationary random fields. For one-dimensional features in stationary random fields, i.e. curves, we calculate the flux. This is the density of curves crossings with a line element, or the average line length per unit volume. In principle this can be extended to higher-dimensional features, i.e. volumes. In this thesis we will however restrict ourself to two-dimensional random fields and consider the statistics of point and curves features. The average length of the curve has been calculated by Longuet-Higgins in 1957 [43] and Dmitri Novikov et al. in 2006 [50].

Theorem 11 (Flux of lines in 2-dimensions). *Given a continuous, differentiable realization $f : \mathbb{R}^2 \to \mathbb{R}$, consider the level set $f^{-1}(\lambda) = \{\boldsymbol{x} \in \mathbb{R}^2 | f(\boldsymbol{x}) = \lambda\}$. The average length per unit area is*

$$\mathcal{L}(\lambda) = \int \sqrt{f_1^2 + f_2^2} \, p(f = \lambda, f_1, f_2) \mathrm{d}f_1 \mathrm{d}f_2.$$

Proof. Consider a line in the x_1 direction. According to Rice's formula, f intersects the level set $f^{-1}(\lambda)$ in an interval $[r_1 - \mathrm{d}r_1/2, r_1 + \mathrm{d}r_1/2]$ along with probability

$$\mathrm{d}r_1 \int |f_1| p(f = \lambda, f_1, f_2) \mathrm{d}f_1 \mathrm{d}f_2.$$

The length of the level set $f^{-1}(\lambda)$ in the square $[r_1 - \mathrm{d}r_1/2, r_1 + \mathrm{d}r_1/2; r_1 - \mathrm{d}r_1/2, r_1 + \mathrm{d}r_1/2]$ is $\frac{\mathrm{d}r_2}{\cos \alpha}$ with α the angle of the level set with respect to the direction r_2. We can express α in terms of f_1 and f_2 as

$$\cos \alpha = \frac{|f_1|}{\sqrt{f_1^2 + f_2^2}},$$

by which the statistical length is

$$\mathcal{L}(\lambda)\mathrm{d}r_1\mathrm{d}r_2 = \mathrm{d}r_1\mathrm{d}r_2 \int \frac{1}{\cos\alpha}|f_1|p(f=\lambda, f_1, f_2)\mathrm{d}f_1\mathrm{d}f_2$$
$$= \int \sqrt{f_1^2 + f_2^2}\, p(f=\lambda, f_1, f_2)\mathrm{d}f_1\mathrm{d}f_2\mathrm{d}r_1\mathrm{d}r_2.$$

This proves the statement.   □

In this thesis we compute the statistics of caustics in one- and two-dimensional models of the universe. Since our universe has three spatial dimensions, the statistics of zero- and one-dimensional objects will not be sufficient when we compare predictions to observations. In an analysis of caustics in three-dimensional models of the universe we have to extend the analysis to the statistics of surfaces. We then have to consider the average area of a surface per volume element. The geometric statistical analysis has been developed and is completely analogous to computation of the average line length per unit area. However since the expression is significantly more complex and since we will only consider caustics in one- and two-dimensional models of the universe, we will not study that expression here.

Chapter 11

Critical Line Statistics

In this thesis we use caustics, appearing in the Zel'dovich approximation, to guide us to a skeleton of the initial density perturbations. Such a skeleton is often denoted as an embryonic skeleton and is used to determine the regions in Lagrangian space which grow to become filaments, walls, clusters and voids. Generally, the peaks will be related to clusters, dips to voids and saddle points to filaments. In this thesis we furthermore used the Zel'dovich approximation to estimate the evolution of the skeleton during structure formation. Dmitri Novikov et al. have in 2006 [50] proposed a different two-dimensional embryonic skeleton. This skeleton is guided by the Morse-Smale complex of the initial density perturbations, a tessellation of the density field using the critical points and critical lines. This approach has been extended to the three-dimensional case by Pogosyan et al. [55]. In this thesis we discuss the analysis of Novikov et al. and compare it to the skeleton based on caustics.

11.1 Morse-Smale complex

The Morse-Smale complex is a tessellation of the domain of a smooth Morse function[1]. The vertices of the tessellation correspond to the critical points of the function, while the curves correspond to critical lines. We here sketch the tessellation and indicate its importance. For a formal definition on a compact manifold $M \subset \mathbb{R}^2$, let $f : M \to \mathbb{R}$ be a Morse function. The integral lines of this function are the curves $p : \mathbb{R} \to M$ satisfying

$$\frac{\mathrm{d}}{\mathrm{d}s} p(s) = \nabla h(p(s)),$$

for all $s \in \mathbb{R}$. The path p originates in the origin org $p = \lim_{s \to -\infty} p(s)$ and ends in the so-called destination dest $p = \lim_{s \to \infty} p(s)$. The compactness of M can be used to proof the existence of the two limits. We do not prove this here. Using the definition of the origin and destination we can define the stable and unstable manifolds. The stable

---

[1] Morse function contain only nondegenerate critical points.
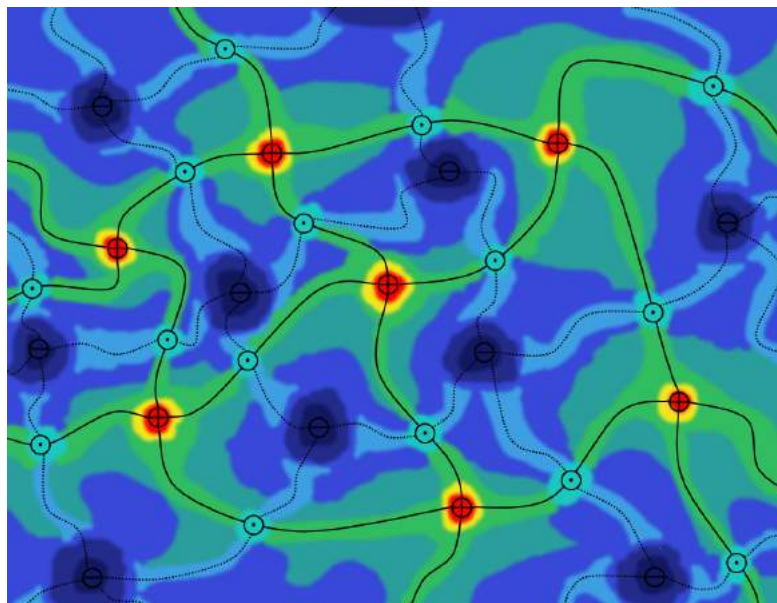
Figure 11.1: The Morse-Smale complex of a function

manifold of the critical point e is defined as

$$S(e) = \{p \mid \text{dest } p = e\} \cup \{e\}.$$

The unstable manifold of the critical point e is defined as

$$U(e) = \{p \mid \text{org } p\} \cup \{e\}.$$

In terms of the stable and unstable manifold, we define the Morse-Smale complex. The Morse-Smale cells are the connected components of the set

$$S(e_1) \cap U(e_2)$$

for all critical points $e_1, e_2 \in M$. The resulting Morse-Smale complex is the collection of all Morse-Smale cells of h. For an illustration of a Morse-Smale complex see figure 11.1. The boundaries of the complex give a skeleton. If we assume that δ is a Morse function and perform this protocol on the initial density field δ, we obtain a skeleton of the initial conditions. The maxima of the perturbations are assumed to absorb matter from their surroundings and become clusters. The curves connecting the maxima via a saddle point are assumed to represent embryonic filaments. The enclosed areas are under dense and are assumed to form voids in the cosmic web.

11.2   Skeleton based on Morse-Smale complex

In the article by Dmitri Novikov et al. [50], the critical lines of the Morse-Smale complex are approximated. Instead of solving the differential equation of integral lines

$$\frac{\mathrm{d}p}{\mathrm{d}t} = \nabla\delta,$$

they state that near maxima and saddle points, to leading order, the gradient $\nabla\delta$ is the eigenvector of the Hessian $\mathcal{H}$ of the density perturbations δ corresponding to the largest eigenvalue. That is,

$$\lambda_2 < 0,$$
$$\mathcal{H}\nabla\delta = \mu_1\nabla\delta,$$

with $\mu_1 \geq \mu_2$ the ordered eigenvalues of the Hessian $\mathcal{H}$ of the density perturbation δ.

For Morse functions this condition results in a set of curves. These curves are an approximation of the integral lines discussed above and are called the stiff approximation of the integral lines. They deviate a bit, away from the critical points, while they are close to integral lines near maxima and sadle points. This condition is linear and is easier to handle, in Gaussian random field theory, than the condition for integral lines.

The condition of the stiff approximation is equivalent to stating that the lines of the stiff approximation are the zero set of the function

$$\mathcal{S} = \det\left(\mathcal{H}\nabla\delta, \nabla\delta\right).$$

Using this formulation, Novikov et al. [50] prove that the length of the stiff approximation skeleton, above the threshold δ_{th} is

$$\mathcal{L}_s(\delta_{th}) = \int_{\delta>\delta_{th}} \sqrt{\mathcal{S}_1^2 + \mathcal{S}_2^2}P(\delta, \mathcal{S}=0, \mathcal{S}_1, \mathcal{S}_2)\mathrm{d}\delta\mathrm{d}\mathcal{S}_1\mathrm{d}\mathcal{S}_2,$$

with $\mathcal{S}_i = \frac{\partial\mathcal{S}}{\partial x_i}$ the partial derivative of $\mathcal{S}$ in the spatial directions. Novikov et al. furthermore numerically estimated the evolution of the line length in the Zel'dovich approximation.

Pogosyan et al. [55] extended the work of Novkov et al. by defining a primary skeleton, and anti-skeleton and secondary skeleton. The components of the skeleton are defined by the conditions

Primary skeleton	$\mathcal{H} \cdot \nabla\delta = \mu_1\nabla\delta,$	$\mu_1 + \mu_2 \geq 0,$
Primary anti-skeleton	$\mathcal{H} \cdot \nabla\delta = \mu_2\nabla\delta,$	$\mu_1 + \mu_2 > 0,$
Secondary	$\mathcal{H} \cdot \nabla\delta = \mu_2\nabla\delta,$	$\mu_1 + \mu_2 \leq 0,$
Secondary	$\mathcal{H} \cdot \nabla\delta = \mu_1\nabla\delta,$	$\mu_1 + \mu_2 > 0.$

The primary skeleton corresponds with the points in which $\nabla\delta$ is aligned with the direction in which the field δ is the least curved, i.e. where the eigenvalue is smallest in

magnitude. The secondary skeleton corresponds with the points in which $\nabla\delta$ is aligned with the direction in which the field δ is most curved. For the primary skeleton we distinguish to types. The primary skeleton is formed by the points at which $\nabla\delta$ is the eigenvector corresponding to the highest eigenvalue of the Hessian. This corresponds to the filamentary ridges spreading from the maxima in the direction of the slowest descent. The primary anti-skeleton is formed by the points at which $\nabla\delta$ is aligned with the second eigenvalue of the Hessian. These lines correspond to the filamentary valleys spreading from the minima in the direction of the slowest ascent. The anti-skeleton can be seen as the skeleton of the $-\delta$ field. They furthermore computed the statistics of the average line length of the individual components of the skeleton.

11.3 Morse-Smale skeleton versus caustics skeleton

There is one main difference between the skeleton based on the Morse-Smale complex and the skeleton based on the Caustics of the Zel'dovich approximation. The Morse-Smale approach is based on the density field whereas the caustics approach is based on the corresponding gravitational potential field. The two are related via the Poisson equation, by which the two fields contain the same information. However the resulting skeletons do differ on some points. In order to see the differences we compare the conditions and show the differences numerically in realizations.

In the caustics approach, we have the gravitational potential Φ, with the corresponding Hessian $\mathcal{H}_\Phi$, the ordered eigenvalues $\lambda_1 \geq \lambda_2$ and the corresponding orthogonal eigenvectors $\mathbf{v}_1, \mathbf{v}_2$. The A_3 lines corresponding to the λ_1 and λ_2 eigenvalue fields satisfy

$$0 = \lambda_{11} = \nabla\lambda_1 \cdot \mathbf{v}_1 \text{ and}$$
$$0 = \lambda_{22} = \nabla\lambda_2 \cdot \mathbf{v}_2,$$

respectively.

In the Morse-Smale approach, we start with the density perturbation δ, compute the Hessian $\mathcal{H}_\delta$, the ordered the eigenvalues $\mu_1 \geq \mu_2$ and the corresponding orthogonal eigenvectors $\mathbf{w}_1$, and $\mathbf{w}_2$. The primary skeleton and primary anti-skeleton are defined as

$$\mathcal{H} \cdot \nabla\delta = \mu_1 \nabla\delta, \qquad\qquad \mu_1 + \mu_2 \geq 0, \text{ and}$$
$$\mathcal{H} \cdot \nabla\delta = \mu_2 \nabla\delta, \qquad\qquad \mu_1 + \mu_2 > 0.$$

This is equivalent to $\nabla\delta \propto \mathbf{w}_1$ and $\nabla\delta \propto \mathbf{w}_2$ under the conditions of the trace of the Hessian. Since $\mathbf{w}_1$ and $\mathbf{w}_2$ are orthogonal, the primary skeleton and primary anti-skeleton can equivalently be defined as

$$0 = \nabla\delta \cdot \mathbf{w}_2, \qquad\qquad \mu_1 + \mu_2 \geq 0, \text{ and}$$
$$0 = \nabla\delta \cdot \mathbf{w}_1, \qquad\qquad \mu_1 + \mu_2 > 0,$$

respectively.

The main difference between the equations is the role of the density perturbations and gravitational potential in these equations. From the Poisson equation we know that $\delta = \lambda_1 + \lambda_2$. In regions in which $\lambda_1 \geq \lambda_2 \geq 0$, we can approximate λ_1 with δ. In this case the A_3 line condition corresponding to the λ_1 field approaches the primary anti-skeleton condition. In the converse case $0 \leq \lambda_1 \ll \lambda_2$ the A_3-line condition corresponding to the λ_2 eigenvalue field approaches the definition of the primary skeleton.

Generally we expect that the Morse-Smale and caustics skeleton behave similarly in the regions indicated above. In intermediate regions, the skeletons will deviate since the gravitational field is generally more smooth and large scale then the density field. A formal treatment of the differences would amount constraint Gaussian random fields, containing both the statistics of the density perturbation and the eigenvalues of the Hessian of the gravitational potential. Such Gaussian random field statistics have been analyzed by Rossi [59]. However, in this thesis we will not delve further in such an analytic comparison.

11.3.1   Dynamics of caustics skeleton

One of the main advantages of the caustics-oriented skeleton over the Morse-Smale-oriented skeleton is the role of dynamics. In the Morse-Smale-oriented skeleton we use the intuition that peaks lead to clusters, saddle points to filaments and minima to voids. The caustics-oriented skeleton is based on the gravitational field and the truncated Zel'dovich approximation which describes the dynamics and contains more information about the surrounding of a peak, saddle point or minimum. The fact that the caustics-oriented skeleton is more directly related to the evolution of the perturbations makes it possible to transform statistical calculations from the initial (Lagrangian) skeleton to the present day (Eulerian) skeleton. Potentially, the caustics-oriented skeleton can approximate the correlation functions of vertices's of the skeleton and average curve lengths of the Eulerian skeleton. In practice this may allow us to analytically predict the length of filaments and correlations between clusters. In the Morse-Smale-oriented skeleton, such calculations will be less straightforward to perform.

Chapter 12

Analytic Statistics of Caustics in one Dimension

In this chapter we compute the statistics of caustics in the one-dimensional Zel'dovich approximation performed on Gaussian random fields. In one dimension the Zel'dovich approximation is exact up to shell crossing. The one-dimensional analysis is not only valid in one-dimensional toy universes, but also in situations in higher-dimensional universes in which collapse occurs in only one direction.

Given the density perturbation in Fourier space $\hat{\delta}$, we can use the Poisson equation to express the Fourier transform of the gravitational potential as $\hat{\Phi}(k) = -4\pi G \rho_0 \frac{1}{k^2} \hat{\delta}$. The deformation tensor is the second spatial derivative of the potential $T_{11} = \partial^2 \Phi$. We will denote this with the eigenvalue notation λ_1 , for consistency. The A_3 catastrophes occur at local maxima and minima of T_{11}, and the A_2 catastrophes occur at level sets of T_{11} with nonnegative function value.

12.1   Eigenvalue distribution

The eigenvalue distribution of one-dimensional Gaussian random fields can be calculated by considering the statistic $Y = (T_{11})$. The corresponding covariance matrix is $M = \langle T_{11} T_{11} \rangle = \sigma_4^2$, with probability distribution

$$P(\lambda_1) = \frac{1}{\sigma_4 \sqrt{2\pi}} e^{-\frac{\lambda_1^2}{2\sigma_4^2}}.$$

This result is a normal distribution with the variance given by

$$\sigma_4^2 = \int_{-\infty}^{\infty} P_\delta(k) W^2(k) \frac{\mathrm{d}k}{2\pi}.$$

In this chapter we normalize the power spectrum such that the density fluctuations have zero mean and unit variance. Since in one dimension the density coincides with the eigenvalue, we have $\sigma_4 = 1$.

12.2 A_2 point density

In a 1-dimensional universe, a fold catastrophe occurs at the points where the eigenvalue λ_1 coincides with $1/D_+$. The distribution of A_2 singularities is given by

$$\mathcal{N}_{A_2}(\lambda) = \langle |\lambda_{11}| \delta^{(1)}(\lambda_1 - \lambda)\rangle = \langle |T_{111}| \delta^{(1)}(T_{11} - \lambda)\rangle$$
$$= \int_{-\infty}^{\infty} |T_{111}| p(T_{11} = \lambda, T_{111}) dT_{111}.$$

The distribution p can be computed by considering the statistic $Y = (\lambda_1, \lambda_{11}) = (T_{11}, T_{111})$ with covariance matrix and its inverse

$$V = \langle Y^T Y\rangle = \begin{pmatrix} \sigma_4^2 & 0 \\ 0 & \sigma_6^2 \end{pmatrix}, \qquad\qquad C = V^{-1} = \begin{pmatrix} \frac{1}{\sigma_4^2} & 0 \\ 0 & \frac{1}{\sigma_6^2} \end{pmatrix}.$$

The corresponding probability distribution is

$$p(\lambda_1, \lambda_{11}) = \frac{1}{4\pi\sigma_4\sigma_6} e^{-\frac{\lambda_1^2}{2\sigma_4^2} - \frac{\lambda_{11}^2}{2\sigma_6^2}}.$$

The number density of A_2 singularities can be analytically evaluated

$$\mathcal{N}_{A_2}(\lambda) = \int_{-\infty}^{\infty} |T_{111}| p(T_{11} = \lambda, T_{111}) dT_{111} = \frac{\sigma_6}{\pi\sigma_4} e^{-\frac{\lambda^2}{2\sigma_4^2}}.$$

This distribution is very similar to the distribution of the eigenvalue. The number of level crossings is proportional to the distribution of the eigenvalue with proportionality constant

$$\sqrt{\frac{2}{\pi}}\sigma_6.$$

This is what one would intuitively expect. For fields in which the density has unit variance, the density of A_2 catastrophes is given by

$$\mathcal{N}_{A_2}(\lambda) = \frac{\sigma_6}{\pi} e^{-\frac{1}{2}\lambda^2}.$$

This distribution is illustrated in figure 12.1 for different power-law power spectra and Gaussian smoothing kernels.

12.3 A_2 two-point correlation functions

The 2-point correlation of A_2 singularities is

$$\xi_{A_2\text{-}A_2}(r, \lambda) = \frac{\mathcal{N}_{A_2\text{-}A_2}(r, \lambda)}{\mathcal{N}_{A_2}(\lambda)^2} - 1,$$

for two A_2 singularities at eigenvalues λ and μ separated by a spatial distance r. The number density of two A_2 singularities is

$$
\begin{aligned}
\mathcal{N}_{A_2\text{-}A_2}(r,\lambda,\mu) =& \langle|\lambda_{11}(0)||\lambda_{11}(r)|\delta^{(1)}(\lambda_1(0)-\lambda)\delta^{(1)}(\lambda_1(r)-\lambda)\rangle \\
=& \langle|T_{111}(0)||T_{111}(r)|\delta^{(1)}(T_{11}(0)-\lambda)\delta^{(1)}(T_{11}(r)-\lambda)\rangle \\
=& \iint |T_{111}(0)||T_{111}(r)|p(T_{11}(0)=\lambda, T_{111}(0), T_{11}(r)=\lambda, T_{111}(r)) \\
& \times \mathrm{d}T_{111}(0)\mathrm{d}T_{111}(r).
\end{aligned}
$$

The probability distribution $p(\lambda_1(0),\lambda_{11}(0),\lambda_1(r),\lambda_{11}(r))$ can be computed using the linear statistic $Y=(\lambda_1(0),\lambda_1(r),\lambda_{11}(0),\lambda_{11}(r))=(T_{11}(0),T_{11}(r),T_{111}(0),T_{111}(r))$ with the covariance matrix

$$
V = \begin{pmatrix}
\sigma_4(0)^2 & \sigma_4(r)^2 & 0 & i\sigma_5(r)^2 \\
\sigma_4(r)^2 & \sigma_4(0)^2 & -i\sigma_5(r)^2 & 0 \\
0 & i\sigma_5(r)^2 & \sigma_6(0)^2 & \sigma_6(r)^2 \\
-i\sigma_5(r)^2 & 0 & \sigma_6(r)^2 & \sigma_6(0)^2
\end{pmatrix}.
$$

Unfortunately Mathematica is unable to analytically evaluate this integral within several days. We can however evaluate one of the double integrals. The integral of interest is of the form

$$
\iint |x||y|e^{-ax^2-bxy-cy^2-dx-ey-f}\mathrm{d}x\mathrm{d}y,
$$

with a,b,c,d,e,f real constants with $a,b\geq 0$. Analytically integrated over x we obtain

$$
\begin{aligned}
& \iint |x||y|e^{-ax^2-bxy-cy^2-dx-ey-f}\mathrm{d}x\mathrm{d}y \\
& = \int_{-\infty}^{\infty} \frac{1}{2}a^{-3/2}e^{-y(cy+e)-f}\left(\sqrt{\pi}(by+d)e^{\frac{(by+d)^2}{4a}}\mathrm{erf}\left(\frac{by+d}{2\sqrt{a}}\right)+2\sqrt{a}\right)\mathrm{d}y.
\end{aligned}
$$

In the joint density of two A_2 points, we have

$$x = T_{111}(0)$$
$$y = T_{111}(r)$$
$$a = -M_{33}^{-1} = \frac{\sigma_4^4 \left(-\sigma_6^2\right) + \sigma_4^2 \tau_5^4 + \sigma_6^2 \tau_4^4}{\sigma_4^4 \left(\sigma_6^4 - \tau_6^4\right) - 2\sigma_4^2 \sigma_6^2 \tau_5^4 - \sigma_6^4 \tau_4^4 + \left(\tau_4^2 \tau_6^2 + \tau_5^4\right)^2}$$
$$b = -2M_{34}^{-1} = -\frac{2\left(\tau_6^2 \left(\tau_4^4 - \sigma_4^4\right) + \tau_4^2 \tau_5^4\right)}{\sigma_4^4 \left(\sigma_6^4 - \tau_6^4\right) - 2\sigma_4^2 \sigma_6^2 \tau_5^4 - \sigma_6^4 \tau_4^4 + \left(\tau_4^2 \tau_6^2 + \tau_5^4\right)^2}$$
$$c = -M_{44}^{-1} = \frac{\sigma_4^4 \left(-\sigma_6^2\right) + \sigma_4^2 \tau_5^4 + \sigma_6^2 \tau_4^4}{\sigma_4^4 \left(\sigma_6^4 - \tau_6^4\right) - 2\sigma_4^2 \sigma_6^2 \tau_5^4 - \sigma_6^4 \tau_4^4 + \left(\tau_4^2 \tau_6^2 + \tau_5^4\right)^2}$$
$$d = -2M_{13}^{-1}\lambda - 2M_{23}^{-1}\mu = \frac{2i\tau_5^2 \left(\lambda(\sigma_4\tau_6 + \sigma_6\tau_4)(\sigma_6\tau_4 - \sigma_4\tau_6) + \mu\left(-\sigma_4^2\sigma_6^2 + \tau_4^2\tau_6^2 + \tau_5^4\right)\right)}{\sigma_4^4 \left(\sigma_6^4 - \tau_6^4\right) - 2\sigma_4^2 \sigma_6^2 \tau_5^4 - \sigma_6^4 \tau_4^4 + \left(\tau_4^2 \tau_6^2 + \tau_5^4\right)^2}$$
$$e = -2M_{14}^{-1}\lambda - 2M_{24}^{-1}\mu = -\frac{2i\tau_5^2 \left(\lambda\left(-\sigma_4^2\sigma_6^2 + \tau_4^2\tau_6^2 + \tau_5^4\right) + \mu(\sigma_4\tau_6 + \sigma_6\tau_4)(\sigma_6\tau_4 - \sigma_4\tau_6)\right)}{\sigma_4^4 \left(\sigma_6^4 - \tau_6^4\right) - 2\sigma_4^2 \sigma_6^2 \tau_5^4 - \sigma_6^4 \tau_4^4 + \left(\tau_4^2 \tau_6^2 + \tau_5^4\right)^2}$$
$$f = -M_{11}^{-1}\lambda^2 - 2M_{12}^{-1}\lambda\mu - M_{22}^{-1}\mu^2$$
$$= \frac{\sigma_6^4 \left(2\lambda\mu\tau_4^2 - \sigma_4^2 \left(\lambda^2 + \mu^2\right)\right) + \tau_6^4 \left(\sigma_4^2 \left(\lambda^2 + \mu^2\right) - 2\lambda\mu\tau_4^2\right) + \sigma_6^2\tau_5^4 \left(\lambda^2 + \mu^2\right) - 2\lambda\mu\tau_5^4\tau_6^2}{\sigma_4^4 \left(\sigma_6^4 - \tau_6^4\right) - 2\sigma_4^2 \sigma_6^2 \tau_5^4 - \sigma_6^4 \tau_4^4 + \left(\tau_4^2 \tau_6^2 + \tau_5^4\right)^2},$$

with $\sigma_i = \sigma_i(0)$ and $\tau_i = \sigma_i(r)$. This allows us to evaluate the A_2-A_2-correlation function.

12.4 A_3 point density

In a 1-dimensional universe, the A_3 singularities correspond to the maxima and minima of the second derivative of the potential field. The number density of points with second derivative $\lambda_1 = \lambda$, vanishing third derivative λ_{11} and fourth derivative $T_{1111} = \lambda_{111}$ is

$$\mathcal{N}_{A_3^+}(\lambda) = \mathcal{N}_{max}(\lambda) = \langle |\lambda_{111}| \delta^{(1)}(\lambda_1 - \lambda)\delta^{(1)}(\lambda_{11})1_{(-\infty,0]}(\lambda_{111})\rangle$$
$$= \langle |T_{1111}| \delta^{(1)}(T_{11} - \lambda)\delta^{(1)}(T_{111})1_{(-\infty,0]}(T_{1111})\rangle$$
$$= \int_{-\infty}^0 |T_{1111}| p(T_{11} = \lambda, T_{111} = 0, T_{1111}) \mathrm{d}T_{1111}$$

The probability distribution $p(\lambda_1, \lambda_{11}, \lambda_{111})$ can be computed using the linear statistic $Y = (T_{11}, T_{111}, T_{1111}) = (\lambda_1, \lambda_{11}, \lambda_{111})$ with the covariance matrix and inverse

$$V = \begin{pmatrix} \sigma_4^2 & 0 & -\sigma_6^2 \\ 0 & \sigma_6^2 & 0 \\ -\sigma_6^2 & 0 & \sigma_8^2 \end{pmatrix}, \qquad C = V^{-1} = \begin{pmatrix} \frac{\sigma_8^2}{\sigma_4^2\sigma_8^2 - 2\sigma_6^3} & 0 & \frac{\sigma_6}{\sigma_4^2\sigma_8^2 - 2\sigma_6^3} \\ 0 & \frac{1}{\sigma_6^2} & 0 \\ \frac{\sigma_6^2}{\sigma_4^2\sigma_8^2 - 2\sigma_6^3} & 0 & \frac{\sigma_4^2}{\sigma_4^2\sigma_8^2 - 2\sigma_6^3} \end{pmatrix}.$$

with $\sigma_j^2 = \int_{-\infty}^{\infty} P(k)W^2(k)k^{j+4}\mathrm{d}k$. This leads to the distribution

$$p(\lambda_1, \lambda_{11}, \lambda_{111}) = \frac{1}{2\pi^{3/2}\sqrt{2\sigma_4^2\sigma_6^2\sigma_8^2 - 2\sigma_6^5}} e^{\frac{\sigma_8^2(\lambda_1^2\sigma_6^2 + \lambda_{11}^2\sigma_4^2) + \sigma_6^2(\lambda_1\lambda_{11}\sigma_6(\sigma_6 + 1) - \lambda_{11}^2\sigma_6 + \lambda_{111}^2\sigma_4^2)}{2\sigma_6^2(\sigma_6^3 - \sigma_4^2\sigma_8^2)}}$$

and a number density of A_3 singularities

$$\mathcal{N}_{A_3^+}(\lambda) = \frac{e^{\frac{\lambda^2\sigma_8^2}{2\sigma_6^3 - 2\sigma_4^2\sigma_8^2}}}{8\pi^{3/2}\sigma_4^3\sigma_6} \left(\sqrt{\pi}\lambda(\sigma_6 + 1)\sigma_6 e^{\frac{\lambda^2\sigma_6^2(\sigma_6+1)^2}{8\sigma_4^4\sigma_8^2 - 8\sigma_4^2\sigma_6^3}} \left(\frac{\mathrm{erf}(\lambda\sigma_6(\sigma_6 + 1))}{2\sigma_4\sqrt{2\sigma_4^2\sigma_8^2 - 2\sigma_6^3}} + 1 \right) \right.$$
$$\left. + 2\sigma_4\sqrt{2\sigma_4^2\sigma_8^2 - 2\sigma_6^3} \right).$$

The number density of A_3^-, or minima in the second derivative of the potential field can be computed analogously,

$$\mathcal{N}_{A_3^-} = \mathcal{N}_{min}(\lambda) = \langle |\lambda_{111}|\delta^{(1)}(\lambda_1 - \lambda)\delta^{(1)}(\lambda_{11})1_{[0,\infty)}(\lambda_{111})\rangle$$
$$= \langle |T_{1111}|\delta^{(1)}(T_{11} - \lambda)\delta^{(1)}(T_{111})1_{[0,\infty)}(T_{1111})\rangle$$
$$= \int_0^{\infty} |T_{1111}|p(T_{11} = \lambda, T_{111} = 0, T_{1111})\mathrm{d}T_{1111}$$
$$= \frac{e^{\frac{\lambda^2\sigma_8^2}{2\sigma_6^3 - 2\sigma_4^2\sigma_8^2}}}{8\pi^{3/2}\sigma_4^2\sigma_6} \left(2\sqrt{2\sigma_4^2\sigma_8^2 - 2\sigma_6^3} - \frac{\sqrt{\pi}\lambda\sigma_6(\sigma_6 + 1)(\mathrm{erfc}(\lambda\sigma_6(\sigma_6 + 1)))e^{\frac{\lambda^2\sigma_6^2(\sigma_6+1)^2}{8\sigma_4^4\sigma_8^2 - 8\sigma_4^2\sigma_6^3}}}{2\sigma_4^2\sqrt{2\sigma_4^2\sigma_8^2 - 2\sigma_6^3}} \right).$$

The total density of A_3 catastrophes or critical points is

$$\mathcal{N}_{A_3}(\lambda) = \int_{-\infty}^{\infty} |T_{1111}|p(T_{11} = \lambda, T_{111} = 0, T_{1111})\mathrm{d}T_{1111}$$
$$= \frac{e^{\frac{\lambda^2\sigma_8^2}{2\sigma_6^3 - 2\sigma_4^2\sigma_8^2}}}{4\pi^{3/2}\sigma_4^2\sigma_6} \left(\frac{\sqrt{\pi}\lambda(\sigma_6 + 1)\sigma_6(\mathrm{erf}(\lambda\sigma_6(\sigma_6 + 1)))e^{\frac{\lambda^2\sigma_6^2(\sigma_6+1)^2}{8\sigma_4^4\sigma_8^2 - 8\sigma_4^2\sigma_6^3}}}{2\sigma_4^2\sqrt{2\sigma_4^2\sigma_8^2 - 2\sigma_6^3}} + 2\sqrt{2\sigma_4^2\sigma_8^2 - 2\sigma_6^3} \right).$$

The distributions derived above are illustrated in figure 12.2 for several power spectra and smoothing scales. Note that this is a scale space analysis of the problem, in which different stages of evolution correspond with different scales σ.

12.5 A_3 two-point correlation function

The 2-point correlation of A_3 singularities is

$$\xi_{A_3\text{-}A_3}(r, \lambda, \mu) = \frac{\mathcal{N}_{A_3\text{-}A_3}(r, \lambda, \mu)}{\mathcal{N}_{A_3}(\lambda)\mathcal{N}_{A_3}(\mu)} - 1,$$

for two A_3 singularities at eigenvalues λ and μ separated by a spatial distance r, and the number density of the A_3 singularities

$$
\begin{aligned}
\mathcal{N}_{A_3\text{-}A_3}(r, \lambda, \mu) =& \langle |\lambda_{111}||\mu_{111}|\delta^{(1)}(\lambda_1 - \lambda)\delta^{(1)}(\lambda_{11})1_{(-\infty,0]}(\lambda_{111})\delta^{(1)}(\mu_1 - \mu) \\
& \times \delta^{(1)}(\mu_{11})1_{(-\infty,0]}(\mu_{111})\rangle \\
=& \langle |T_{1111}(0)||T_{1111}(r)|\delta^{(1)}(T_{11}(0) - \lambda)\delta^{(1)}(T_{111}(0)) \\
& \times 1_{(-\infty,0]}(T_{1111}(0))\delta^{(1)}(T_{11}(r) - \mu)\delta^{(1)}(T_{111}(r))1_{(-\infty,0]}(T_{1111}(r))\rangle \\
=& \iint |T_{1111}(0)||T_{1111}(r)|p(T_{11}(0) = \lambda, T_{111}(0) = 0, T_{1111}(0), T_{11}(r) = \mu \\
& , T_{111}(r) = 0, T_{1111}(r))\mathrm{d}T_{1111}(0)\mathrm{d}T_{1111}(r).
\end{aligned}
$$

The probability distribution $p(\lambda_1, \lambda_{11}, \lambda_{111}, \mu_1, \mu_{11}, \mu_{111})$ can be computed using the linear statistic $Y = (\lambda_1, \mu_1, \lambda_{111}, \mu_{111}, \lambda_{11}, \mu_{11}) = (T_{11}(0), T_{11}(r), T_{1111}(0), T_{1111}(r), T_{111}(0), T_{111}(r))$ with the covariance matrix

$$
V = \begin{pmatrix}
\sigma_4(0)^2 & \sigma_4(r)^2 & -\sigma_6(0)^2 & -\sigma_6(r)^2 & i\sigma_5(r)^2 & 0 \\
\sigma_4(r)^2 & \sigma_4(0)^2 & -\sigma_6(r)^2 & -\sigma_6(0)^2 & 0 & -i\sigma_5(r)^2 \\
-\sigma_6(0)^2 & -\sigma_6(r)^2 & \sigma_8(0)^2 & \sigma_8(r)^2 & -i\sigma_7(r)^2 & 0 \\
-\sigma_6(r)^2 & -\sigma_6(0)^2 & \sigma_8(r)^2 & \sigma_8(0)^2 & 0 & i\sigma_7(r)^2 \\
i\sigma_5(r)^2 & 0 & -i\sigma_7(r)^2 & 0 & -\sigma_6(0)^2 & -\sigma_6(r)^2 \\
0 & -i\sigma_5(r)^2 & 0 & i\sigma_7(r)^2 & -\sigma_6(r)^2 & -\sigma_6(0)^2
\end{pmatrix}.
$$

In principle this is all we need to evaluate the two-point correlation function of A_3 points. However due to the same problems as in the A_2 two-point correlation function we cannot analytically evaluate this integral. Numerical evaluation turn out to be difficult, but should be possible with current integration routines.

12.6   Correlation function in Zel'dovich approximation

We can compute the 2-point correlation function of catastrophes in Eulerian space by adding the $T_1(0) - T_1(r)$ term in the linear statistic and using the Zel'dovich approximation. Assume that initially the singularities A and B are separated by a spatial distance x. Assume without loss of generality that A is initially in the origin and B is positioned at x. After some time t, the point A and B have moved to $D_+(t)u(0) = -D_+(t)T_1(0)$, and $x + D_+(t)u(x) = x - D_+(t)T_1(x)$ respectively. The separation at time t is

$$
r = |x + D_+(t)(T_1(0) - T_1(x))|.
$$

The 2-point correlation function of A and B singularities is given by

$$
\xi_{A\text{-}B}(r, D_+, \lambda, \mu) = \frac{\mathcal{N}_{A\text{-}B}(r, D_+, \lambda, \mu)}{\mathcal{N}_A(\lambda)\mathcal{N}_B(\mu)} - 1
$$

with

$$\mathcal{N}_{A\text{-}B}(r, D_+, \lambda, \mu) = \int_{-x/D_+}^{\infty} \mathcal{N}_{A\text{-}B}(r - D_+U, \lambda, \mu, U)\mathrm{d}U$$
$$+ \int_{-\infty}^{-x/D_+} \mathcal{N}_{A\text{-}B}(-r - D_+U, \lambda, \mu, U)\mathrm{d}U.$$

(a) $r = -1/2$, and $\sigma = 1, 2, 3$ from top to bottom

(b) $r = 0$, and $\sigma = 1, 2, 3$ from top to bottom

(c) $r = 1/2$, and $\sigma = 1, 2, 3$ from top to bottom

(d) $r = 1$, and $\sigma = 1, 2, 3$ from top to bottom
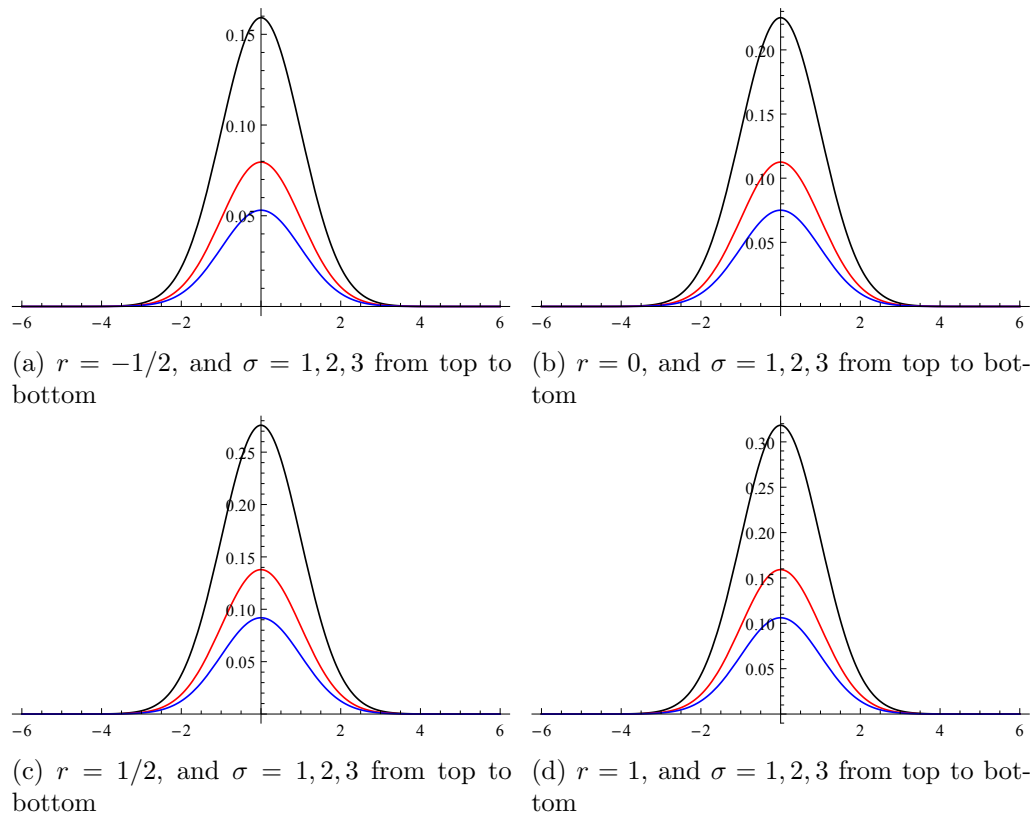
Figure 12.1: The density of A_2 folds as function of the eigenvalue for power-law power spectrum $P(k) = k^r$ and Gaussian smoothing.

(a) $r = -1/2$ and $\sigma = 1$

(b) $r = 0$ and $\sigma = 1$

(c) $r = 1/2$ and $\sigma = 1$

(d) $r = 1$ and $\sigma = 1$
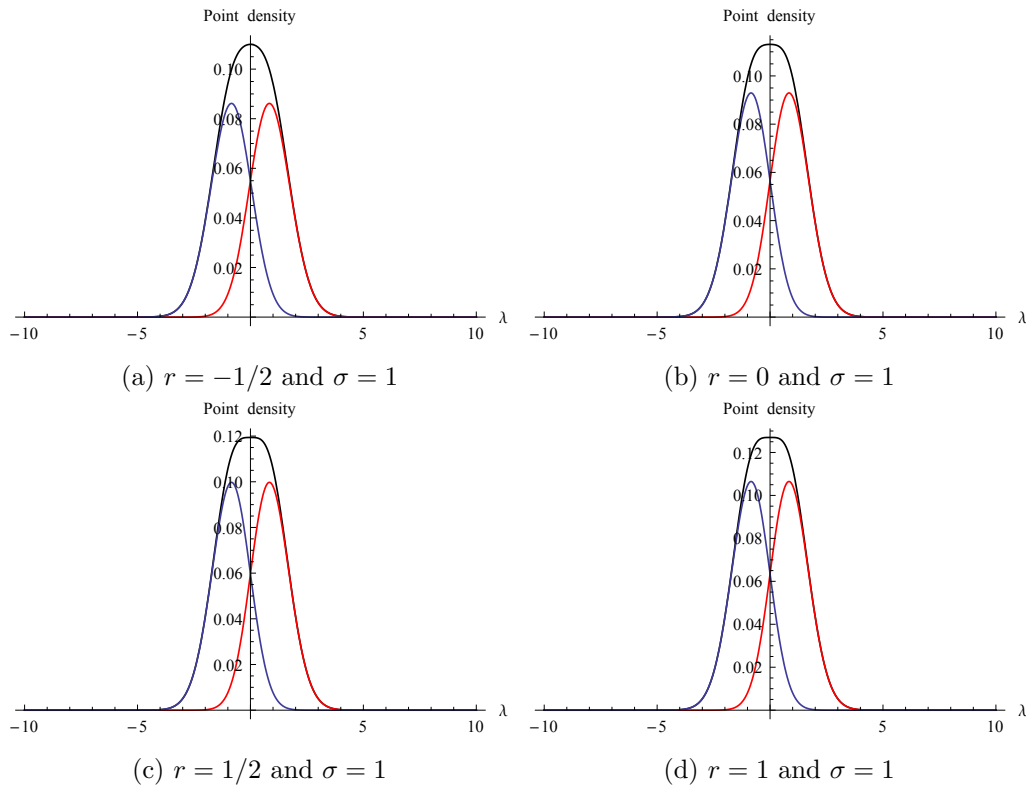
Figure 12.2: Density of A_3^+, A_3^- and the total A_3 points with smoothing $\sigma = 1$ depicted in red, blue and black respectively
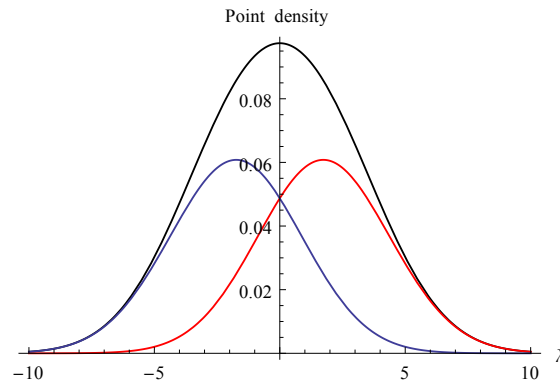
Figure 12.3: Density of critical points in the eigenvalue field of the 1-dimensional deformation tensor, with $\sigma_4 = 2, \sigma_6 = 1, \sigma_8 = 1$. The blue line depicts the minima density. The red line depticts the maxima density of A_3 singularities. The black illustrates the density of critical points.

Chapter 13

Analytic Statistics of Caustics in two Dimensions

In the previous chapter we derived analytic statistics of caustics in the one-dimensional Zel'dovich approximation. In this chapter we extend these results to the two-dimensional Zel'dovich approximation. We determine the expected densities of A_4 and D_4 catastrophes and determine the average length or flux of A_2- and A_3-lines. In one dimension, the second derivative of the potential field, denoted by the eigenvalue λ_1, coincides with the initial density perturbation. In two dimensions this is no longer true since we have two eigenvalues. In the first section of this chapter we derive the properties of the eigenvalues in two dimensions. In the subsequent chapters we derive the density of point catastrophes and flux of line catastrophes.

13.1   Properties of eigenvalues

Let Ψ be a smoothed realization of a Gaussian random field, representing the potential field. Entries of the Hessian matrix or deformation matrix of Ψ are denoted by the second partial derivatives

$$T_{ij} = \frac{\partial^2 \Psi}{\partial q_i \partial q_j}.$$

According to Young's theorem or the Schwarz integrability condition, the deformation tensor of smooth functions is a real symmetric 2×2 matrix with three degrees of freedom T_{11}, T_{22}, T_{12}. For symmetric real-valued 2×2 matrices the eigenvalues λ_1, λ_2 are real. We will always assume the ordering $\lambda_1 \geq \lambda_2$. The corresponding eigenvectors v_1, v_2 are orthogonal and can be assumed to be unit vectors in $\mathbb{R}^2$ with the Euclidean norm. In the Hessian frame, i.e in the frame with eigenvector basis (v_1, v_2), the deformation tensor is diagonal

$$\begin{pmatrix} T_{11} & T_{12} \\ T_{12} & T_{22} \end{pmatrix} = \begin{pmatrix} \lambda_1 & 0 \\ 0 & \lambda_2 \end{pmatrix}.$$

Denote the third and fourth derivatives of Ψ in the Hessian frame by

$$T_{ijk} = \frac{\partial^3 \Psi}{\partial q_i \partial q_j \partial q_k}, \text{ and } T_{ijkl} = \frac{\partial^4 \Psi}{\partial q_i \partial q_j \partial q_k \partial q_l},$$

with according to Schwarz's theorem respectively four $(T_{111}, T_{112}, T_{122}, T_{222})$ and five $(T_{1111}, T_{1112}, T_{1122}, T_{1222}, T_{2222})$ degrees of freedom. We describe the second, third, and fourth derivatives of Ψ by means of the statistic

$$Y_T = (T_{11}, T_{22}, T_{12}; T_{111}, T_{122}, T_{222}, T_{112}; T_{1111}, T_{2222}, T_{1122}, T_{1112}, T_{1222}),$$

consisting of 12 linear terms in Ψ.

The statistic Y_T can be written in terms of the eigenvalues and derivatives of the eigenvalues in the direction of the eigenvectors, i.e. we can write Y_T in terms of

$$Y_\lambda = (\lambda_1, \lambda_2; \lambda_{11}, \lambda_{12}, \lambda_{21}, \lambda_{22}; \lambda_{111}, \lambda_{112}, \lambda_{122}, \lambda_{211}, \lambda_{212}, \lambda_{222}),$$

with $\lambda_{ij} = \nabla \lambda_i \cdot v_j$ and $\lambda_{ijk} = \nabla(\nabla \lambda_i \cdot v_j) \cdot v_k$. The eigenvalue statistic Y_λ is nonlinear with respect to Ψ. It is however a more natural choice of parameters than the Y_T statistic since it is composed of the inner product of vector fields, which make Y_λ invariant under all isometries including rotations.

Starting with the general expression of the λ_i parameters in terms of T_{ij} we can rotate to the Hessian frame and obtain the expression

$$T_{11} = \lambda_1, \qquad\qquad T_{22} = \lambda_2, \qquad\qquad T_{12} = 0.$$

In the Hessian frame this substitution in combination with the condition $T_{11} \geq T_{22}$ simplifies the expressions of λ_{ij} and λ_{ijk} in terms of T_{ij}, T_{ijk}, and T_{ijkl} to

$$T_{111} = \lambda_{21}, \qquad\qquad\qquad T_{112} = \lambda_{22},$$
$$T_{122} = \lambda_{11}, \qquad\qquad\qquad T_{222} = \lambda_{12},$$
$$T_{1111} = \lambda_{211} - \frac{2\lambda_{22}^2}{\lambda_1 - \lambda_2}, \qquad\qquad T_{1112} = \lambda_{212} - \frac{2\lambda_{11}\lambda_{22}}{\lambda_1 - \lambda_2},$$
$$T_{1122} = \lambda_{111} + \frac{2\lambda_{22}^2}{\lambda_1 - \lambda_2}, \qquad\qquad T_{1122} = \lambda_{222} - \frac{2\lambda_{11}^2}{\lambda_1 - \lambda_2},$$
$$T_{1222} = \lambda_{112} + \frac{2\lambda_{11}\lambda_{22}}{\lambda_1 - \lambda_2}, \qquad\qquad T_{2222} = \lambda_{122} + \frac{2\lambda_{11}^2}{\lambda_1 - \lambda_2}.$$

We can in principle go to higher derivatives. This however makes the expressions more complicated. In this thesis we restrict ourself to statistics containing only derivatives of fourth order. Note that Y_λ consists of 13 terms whereas Y_T consists out of 12 terms. The statistics Y_λ are not independent. This however does not lead to practical problems as long as we construct our calculations in a consistent way.

In going from the derivatives of the potential to the eigenvalues of the deformation matrix, we perform a nonlinear coordinate transformation. We rotate from the parameter space (T_{11}, T_{22}, T_{12}) to the eigenvectors $\mathbf{v}_1, \mathbf{v}_2$. Originally the probabilities are computed by integrating over the parameter space of interest with measure $dT_{11} \wedge dT_{22} \wedge dT_{12}$.

After the coordinate transformation we have to express this measure in terms of the measure $d\lambda_1 \wedge d\lambda_2$. The analysis presented here is analogous to Bardeen et al. 1986, appendix B [37].

We can express the deformation tensor T in terms of its eigenvalues λ_1, λ_2 and corresponding eigenvectors $v_1 = (\cos\omega, \sin\omega)^T$, $v_2 = (-\sin\omega, \cos\omega)^T$ parametrized by $\omega \in [0, \pi)$ via eigenvalue decomposition. The angle ω is an element of the interval $[0, \pi)$ due to the ordering of eigenvalues. For

$$\lambda = \begin{pmatrix} \lambda_1 & 0 \\ 0 & \lambda_2 \end{pmatrix},$$

$$R = (v_1, v_2) = \begin{pmatrix} \cos\omega & -\sin\omega \\ \sin\omega & \cos\omega \end{pmatrix},$$

the eigenvalue decomposition states that the deformation tensor T is given by

$$T = R^T \lambda R = \begin{pmatrix} T_{11} & T_{12} \\ T_{12} & T_{22} \end{pmatrix} = \begin{pmatrix} \lambda_1 \cos^2\theta + \lambda_2 \sin^2\theta & (\lambda_2 - \lambda_1)\cos\theta\sin\theta \\ (\lambda_2 - \lambda_1)\cos\theta\sin\theta & \lambda_1 \sin^2\theta + \lambda_2 \cos^2\theta \end{pmatrix}.$$

The Jacobian matrix of the corresponding map

$$(\lambda_1, \lambda_2, \omega) \mapsto (T_{11}, T_{22}, T_{12}) = (\lambda_1 \cos^2\omega + \lambda_2 \sin^2\omega, \lambda_1 \sin^2\omega + \lambda_2 \cos^2\omega,$$
$$(\lambda_2 - \lambda_1)\cos\omega\sin\omega)$$

is given by

$$\begin{pmatrix} \cos^2\omega & \sin^2\omega & (\lambda_2 - \lambda_1)\sin(2\omega) \\ \sin^2\omega & \cos^2\omega & (\lambda_1 - \lambda_2)\sin(2\omega) \\ -\cos\omega\sin\omega & \cos\omega\sin\omega & (\lambda_2 - \lambda_1)\cos(2\omega) \end{pmatrix}.$$

The absolute value of the determinant of the Jacobian matrix is $|\lambda_1 - \lambda_2|$. Hence we obtain the equality

$$dT_{11} \wedge dT_{22} \wedge dT_{12} = (\lambda_1 - \lambda_2)d\lambda_1 \wedge d\lambda_2 \wedge d\omega.$$

which we use when going from integrals over Y_T to Y_λ. In three dimensions the Jacobian is equal to $(\lambda_1 - \lambda_2)(\lambda_1 - \lambda_3)(\lambda_2 - \lambda_3)$ which is well known form Doroshkevich's formula of the distribution of eigenvalues in three dimensions.

For the remaining variables, the transformation from $\lambda_1, \lambda_2, \lambda_{11}, \lambda_{12}, \lambda_{21}, \lambda_{22}, \lambda_{111},$ $\lambda_{112}, \lambda_{122}, \lambda_{211}, \lambda_{212}, \lambda_{222}$ to $T_{1111}, T_{1112}, T_{1122}, T_{1222}, T_{2222}$ turns out to have unit Jacobian. For this reason we can always switch between λ and T_{ijk}, T_{ijkl} variables without inserting a Jacobian factor.

13.1.1 Doroshkevich formula in two-dimensions

The distribution of eigenvalues in three dimensions is denoted by the Doroshkevich formula proposed in 1970 [24]

$$P(\lambda_1, \lambda_2, \lambda_3) = \frac{15^3}{16\sqrt{5}\pi^3} e^{-\frac{3\sigma_0}{2}(2k_1^2 - 5k_2)}(\lambda_1 - \lambda_2)(\lambda_1 - \lambda_3)(\lambda_2 - \lambda_3),$$

with

$$k_1 = \lambda_1 + \lambda_2 + \lambda_3,$$
$$k_2 = \lambda_1\lambda_2 + \lambda_1\lambda_3 + \lambda_2\lambda_3,$$
$$\sigma_0^2 = \frac{1}{2\pi^2}\int_0^\infty k^2 P(k)W^2(k)\mathrm{d}k.$$

In two dimensions we derive a similar result. Consider the statistic $Y = (T_{11}, T_{22}, T_{12})$. The corresponding covariance matrix is

$$V = \langle Y^T Y\rangle = \begin{pmatrix} \frac{3}{8}\sigma_5^2 & \frac{1}{8}\sigma_5^2 & 0 \\ \frac{1}{8}\sigma_5^2 & \frac{3}{8}\sigma_5^2 & 0 \\ 0 & 0 & \frac{1}{8}\sigma_5^2 \end{pmatrix},$$

with determinant $\left(\frac{\sigma_5}{2}\right)^6$ and the inverse of the covariance matrix

$$C = V^{-1} = \sigma_5^{-2}\begin{pmatrix} 3 & -1 & 0 \\ -1 & 3 & 0 \\ 0 & 0 & 8 \end{pmatrix}.$$

The distribution of the elements of the deformation tensor is

$$p(T_{11}, T_{22}, T_{12}) = \frac{2\sqrt{2}}{\pi^{3/2}\sigma_5^3}e^{-\frac{3k_1^2 - 8k_2}{2\sigma_5^2}}$$
$$k_1 = T_{11} + T_{22}$$
$$k_2 = T_{11}T_{22} - T_{12}^2.$$

The distribution is independent of the choice of basis. For the symmetric matrix T, the characteristic polynomial is

$$\det(T - \lambda I) = \lambda^2 - (T_{11} + T_{22})\lambda + (T_{11}T_{22} - T_{12}^2)\lambda = \lambda^2 - k_1\lambda + k_2.$$

The coefficients are invariant under coordinate transformations. Note that k_1 is the trace and k_2 is the determinant of T. In terms of the ordered eigenvalues λ_1, λ_2 of the deformation tensor,

$$k_1 = \lambda_1 + \lambda_2,$$
$$k_2 = \lambda_1\lambda_2.$$

By performing the change of variables on the measure $\mathrm{d}T_{11}\wedge\mathrm{d}T_{22}\wedge\mathrm{d}T_{12}$, and integrating out the angular dependence of $\mathrm{d}\lambda_1\wedge\mathrm{d}\lambda_2\wedge\mathrm{d}\omega$ we obtain the eigenvalue distribution,

$$p(\lambda_1, \lambda_2) = \frac{2\sqrt{2}}{\pi^{1/2}\sigma_5^3}e^{-\frac{3(\lambda_1+\lambda_2)^2 - 8\lambda_1\lambda_2}{2\sigma_5^2}}(\lambda_1 - \lambda_2).$$
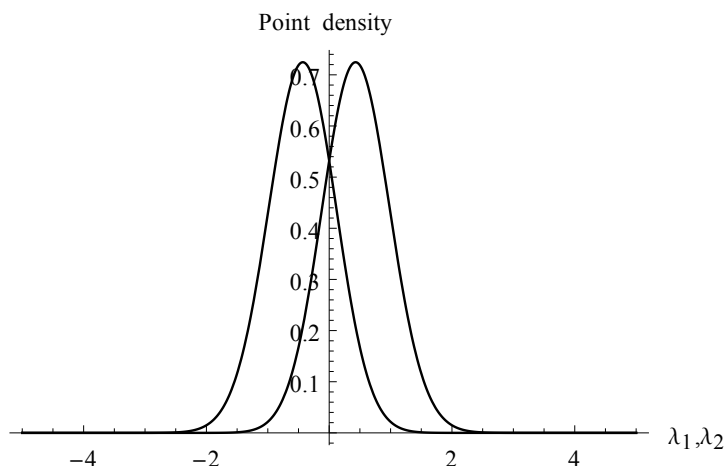
Figure 13.1: Individual eigenvalue distributions. The right line is the distribution of λ_1, the left line is the distribution for λ_2 for $\sigma_5 = 1$

13.1.2   Unconditional distribution of eigenvalues

The unconditional eigenvalue distributions can be obtained by integrating out the dependence on one eigenvalue, i.e.

$$p(\lambda_1) = \int_{-\infty}^{\lambda_1} p(\lambda_1, \lambda_2) \mathrm{d}\lambda_2 = \frac{1}{9}\sigma_5^{-2} e^{-\frac{2\lambda_1^2}{\sigma_5^2}} \left(4\sqrt{3}\lambda_1 e^{\frac{2\lambda_1^2}{3\sigma_5^2}} \left(\frac{\mathrm{erf}\left(\sqrt{\frac{2}{3}}\lambda_1\right)}{\sigma_5} + 1 \right) + 6\sqrt{\frac{2}{\pi}}\sigma_5 \right),$$

$$p(\lambda_2) = \int_{\lambda_2}^{\infty} p(\lambda_1, \lambda_2) \mathrm{d}\lambda_1 = \frac{1}{9}\sigma_5^{-2} e^{-\frac{2\lambda_2^2}{\sigma_5^2}} \left(6\sqrt{\frac{2}{\pi}}\sigma_5 - \frac{4\sqrt{3}\lambda_2 \left(\mathrm{erfc}\left(\sqrt{\frac{2}{3}}\lambda_2\right)\right) e^{\frac{2\lambda_2^2}{3\sigma_5^2}}}{\sigma_5} \right).$$

These individual eigenvalue distributions are illustrated in figure 13.1. The distribution of the eigenvalues is not identical due to the ordering condition $\lambda_1 \geq \lambda_2$. The symmetry around the vertical axis is due to the statistical symmetry under the operation $\Psi \to -\Psi$ of Gaussian random fields.

13.1.3   The distribution of eigenvalues constrained with derivatives

By including the third order derivatives in the statistics, the probability distribution of the eigenvalues and their derivatives can be computed. Consider the linear statistic

$$Y = (T_{11}, T_{22}, T_{12}; T_{111}, T_{122}, T_{222}, T_{122})$$

with covariance matrix

$$
V = \langle Y^T Y \rangle =
\begin{pmatrix}
\frac{3\sigma_5^2}{8} & \frac{\sigma_5^2}{8} & 0 & 0 & 0 & 0 & 0 \\
\frac{\sigma_5^2}{8} & \frac{3\sigma_5^2}{8} & 0 & 0 & 0 & 0 & 0 \\
0 & 0 & \frac{\sigma_5^2}{8} & 0 & 0 & 0 & 0 \\
0 & 0 & 0 & \frac{5\sigma_7^2}{16} & \frac{\sigma_7^2}{16} & 0 & 0 \\
0 & 0 & 0 & \frac{\sigma_7^2}{16} & \frac{\sigma_7^2}{16} & 0 & 0 \\
0 & 0 & 0 & 0 & 0 & \frac{5\sigma_7^2}{16} & \frac{\sigma_7^2}{16} \\
0 & 0 & 0 & 0 & 0 & \frac{\sigma_7^2}{16} & \frac{\sigma_7^2}{16}
\end{pmatrix},
$$

and inverse

$$
C = V^{-1} =
\begin{pmatrix}
\frac{3}{\sigma_5^2} & -\frac{1}{\sigma_5^2} & 0 & 0 & 0 & 0 & 0 \\
-\frac{1}{\sigma_5^2} & \frac{3}{\sigma_5^2} & 0 & 0 & 0 & 0 & 0 \\
0 & 0 & \frac{8}{\sigma_5^2} & 0 & 0 & 0 & 0 \\
0 & 0 & 0 & \frac{4}{\sigma_7^2} & -\frac{4}{\sigma_7^2} & 0 & 0 \\
0 & 0 & 0 & -\frac{4}{\sigma_7^2} & \frac{20}{\sigma_7^2} & 0 & 0 \\
0 & 0 & 0 & 0 & 0 & \frac{4}{\sigma_7^2} & -\frac{4}{\sigma_7^2} \\
0 & 0 & 0 & 0 & 0 & -\frac{4}{\sigma_7^2} & \frac{20}{\sigma_7^2}
\end{pmatrix}.
$$

This leads to the probability distribution

$$
p(T_{11}, T_{22}, T_{12}, T_{111}, T_{112}, T_{122}, T_{222}) = \frac{2^7\sqrt{2}}{\pi^{3/2}\sigma_5^3\sigma_7^4} e^{-\frac{3k_1^2 - 8k_2}{2\sigma_5^2}}
$$

$$
\times e^{-\frac{10(T_{112}^2 + T_{122}^2) - 4(T_{111}T_{122} + T_{112}T_{222}) + 2(T_{111}^2 + T_{222}^2)}{\sigma_7^2}}
$$

$$
k_1 = T_{11} + T_{22}
$$

$$
k_2 = T_{11}T_{22} - T_{12}^2.
$$

In terms of the eigenvalues and derivatives of the eigenvalues, this probability distribution reads

$$
p(\lambda_1, \lambda_2, \lambda_{11}, \lambda_{12}, \lambda_{21}, \lambda_{22}) = \frac{2^5\sqrt{2}}{\pi^{7/2}\sigma_5^3\sigma_7^4} e^{-\frac{3(\lambda_1 + \lambda_2)^2 - 8\lambda_1\lambda_2}{2\sigma_5^2}}
$$

$$
\times e^{-\frac{10(\lambda_{11} + \lambda_{22}) - 4(\lambda_{11}\lambda_{21} + \lambda_{12}\lambda_{22}) + \lambda_{12}^2 + \lambda_{21}^2}{\sigma_7^2}}.
$$

Upon integrating over the eigenvalues λ_1 and λ_2 we have to multiply with the Jacobian $(\lambda_1 - \lambda_2)$.

13.1.4   Density of points with specific eigenvalue configurations

The point density of points having eigenvalue $\lambda_1 = \mu$, $\lambda_2 = \nu$ can be expressed as

$$
\begin{aligned}
\mathcal{N}_\lambda(\mu, \nu) &= \langle |\lambda_{11}\lambda_{22} - \lambda_{12}\lambda_{21}| \delta^{(1)}(\lambda_1 - \mu)\delta^{(1)}(\lambda_1 - \nu)\rangle \\
&= \int p(\lambda_1 = \mu, \lambda_2 = \nu, \lambda_{11}, \lambda_{12}, \lambda_{21}, \lambda_{22})|\lambda_{11}\lambda_{22} - \lambda_{12}\lambda_{21}|\mathrm{d}\lambda_{11}\mathrm{d}\lambda_{12}\mathrm{d}\lambda_{21}\mathrm{d}\lambda_{22}.
\end{aligned}
$$

The probability distribution can be computed using the linear statistic

$$
Y = (T_{11}, T_{22}, T_{12}; T_{111}, T_{122}, T_{222}, T_{112}),
$$

with covariance matrix

$$
V = \langle Y^T Y \rangle =
\begin{pmatrix}
\frac{3\sigma_5^2}{8} & \frac{\sigma_5^2}{8} & 0 & 0 & 0 & 0 & 0 \\
\frac{\sigma_5^2}{8} & \frac{3\sigma_5^2}{8} & 0 & 0 & 0 & 0 & 0 \\
0 & 0 & \frac{\sigma_5^2}{8} & 0 & 0 & 0 & 0 \\
0 & 0 & 0 & \frac{5\sigma_7^2}{16} & \frac{\sigma_7^2}{16} & 0 & 0 \\
0 & 0 & 0 & \frac{\sigma_7^2}{16} & \frac{\sigma_7^2}{16} & 0 & 0 \\
0 & 0 & 0 & 0 & 0 & \frac{5\sigma_7^2}{16} & \frac{\sigma_7^2}{16} \\
0 & 0 & 0 & 0 & 0 & \frac{\sigma_7^2}{16} & \frac{\sigma_7^2}{16}
\end{pmatrix},
$$

and inverse covariance matrix

$$
C = V^{-1} =
\begin{pmatrix}
\frac{3}{\sigma_5^2} & -\frac{1}{\sigma_5^2} & 0 & 0 & 0 & 0 & 0 \\
-\frac{1}{\sigma_5^2} & \frac{3}{\sigma_5^2} & 0 & 0 & 0 & 0 & 0 \\
0 & 0 & \frac{8}{\sigma_5^2} & 0 & 0 & 0 & 0 \\
0 & 0 & 0 & \frac{4}{\sigma_7^2} & -\frac{4}{\sigma_7^2} & 0 & 0 \\
0 & 0 & 0 & -\frac{4}{\sigma_7^2} & \frac{20}{\sigma_7^2} & 0 & 0 \\
0 & 0 & 0 & 0 & 0 & \frac{4}{\sigma_7^2} & -\frac{4}{\sigma_7^2} \\
0 & 0 & 0 & 0 & 0 & -\frac{4}{\sigma_7^2} & \frac{20}{\sigma_7^2}
\end{pmatrix}.
$$

Rotating to the eigenvector system, and writing in eigenvalue coordinates, the corresponding probability distribution can be written as

$$
p(\lambda_1, \lambda_2, \lambda_{11}, \lambda_{12}, \lambda_{21}, \lambda_{22}) = \frac{2^5\sqrt{2}}{\pi^{7/2}\sigma_5^3\sigma_7^4} e^{-\frac{3(\lambda_1^2 + \lambda_2^2) - 2\lambda_1\lambda_2}{2\sigma_5^2}}
$$

$$
\times\, e^{-\frac{10(\lambda_{11} + \lambda_{22})^2 - 4(\lambda_{11}\lambda_{21} + \lambda_{12}\lambda_{22}) + \lambda_{12}^2 + \lambda_{21}^2}{\sigma_7^2}}.
$$

This leads to the number density of points with $\lambda_1 = \mu, \lambda_2 = \nu$,

$$\mathcal{N}_\lambda(\mu,\nu) = \frac{2^5\sqrt{2}}{\pi^{5/2}\sigma_5^3\sigma_7^4}e^{-\frac{3(\mu^2+\nu^2)-2\mu\nu}{2\sigma_5^2}}$$

$$\times \int e^{-\frac{10(\lambda_{11}+\lambda_{22})^2-4(\lambda_{11}\lambda_{21}+\lambda_{12}\lambda_{22})+\lambda_{12}^2+\lambda_{21}^2}{\sigma_7^2}}\,\mathrm{d}\lambda_{11}\mathrm{d}\lambda_{12}\mathrm{d}\lambda_{21}\mathrm{d}\lambda_{22}$$

$$\propto e^{-\frac{3(\mu^2+\nu^2)-2\mu\nu}{2\sigma_5^2}}$$

Note that the result is a two-dimensional Gaussian distribution (see figure 13.3).

13.2 A_3 point distribution

The A_3 points correspond with the maxima and minima of the λ_1 and λ_2 fields. We first consider a maximum of the λ_1 field. A maximum with field value $\lambda_1 = \lambda$ satisfies the conditions

$$\lambda_1 = \lambda,$$
$$\lambda_{11} = \lambda_{12} = 0.$$

The number density of maxima in the λ_1 field or A_3^+ catastrophes corresponding to the first eigenvalue in the Zel'dovich approximation is

$$\mathcal{N}_{A_3^+} = \left\langle \left| \begin{matrix} \lambda_{111} & \lambda_{112} \\ \lambda_{112} & \lambda_{122} \end{matrix} \right| \delta^{(1)}(\lambda_1 - \lambda)\delta^{(1)}(\lambda_{11})\delta^{(1)}(\lambda_{12}) \right\rangle$$

$$= \int |\lambda_{111}\lambda_{122} - \lambda_{112}^2| p(\lambda_1 = \lambda, \lambda_2, \lambda_{11} = 0, \lambda_{12} = 0, \lambda_{111}, \lambda_{112}, \lambda_{122})(\lambda_1 - \lambda_2)$$

$$\times \mathrm{d}\lambda_{111}\mathrm{d}\lambda_{112}\mathrm{d}\lambda_{122}\mathrm{d}\lambda_2,$$

integrated over the domain

$$(\lambda_2, \lambda_{111}, \lambda_{112}, \lambda_{122}) \in (-\infty, \lambda] \times (0, \infty) \times \mathbb{R} \times \left(\frac{\lambda_{112}^2}{\lambda_{111}}, \infty \right).$$

The Hessian matrix of λ_1 in this domain is positive definite. For the A_3^- catastrophes of the first eigenvalue field we integrate over the domain

$$(\lambda_2, \lambda_{111}, \lambda_{112}, \lambda_{122}) \in (-\infty, \lambda] \times (-\infty, 0) \times \mathbb{R} \times \left(-\infty, \frac{\lambda_{112}^2}{\lambda_{111}} \right).$$

The Hessian matrix of λ_1 in this domain is negative definite. For saddle points of the field λ_1 we integrate over the remaining parameter domain.

For A_3 points occurring due to critical points in the λ_2 field we can derive similar formulas by interchanging λ_1 by λ_2 and λ_{1ij} by λ_{2ij}.

13.3 A_4 point distribution

In this thesis we consider statistics dependent on the first and second derivatives of the eigenvalues λ_1, and λ_2. The conditions of swallowtail catastrophes however contain the fifth derivative which is more difficult to handle in terms of derivatives of the field Ψ. For this reason we keep the calculation of the swallowtail catastrophe for future research, although the computation is very similar to the computation for the A_3 catastrophes.

13.4 D_4 distribution

The D_4 points in the initial distribution are given by the points in which the two eigenvalues coincide. In therms of the eigenvalue statistics, the D_4 points satisfy

$$\lambda_1 = \lambda_2 = \lambda,$$

for some λ. The number density of D_4 points in a Gaussian initial density field is

$$
\begin{aligned}
\mathcal{N}_{D_4}(\lambda) =& \mathcal{N}_\lambda(\lambda, \lambda) = \langle |\lambda_{11}\lambda_{22} - \lambda_{12}\lambda_{21}| \delta^{(1)}(\lambda_1 - \lambda)\delta^{(1)}(\lambda_2 - \lambda)\rangle \\
=& \frac{2^5\sqrt{2}}{\pi^{5/2}\sigma_5^3\sigma_7^4} e^{-\frac{2\lambda^2}{\sigma_5^2}} \\
& \times \int e^{-\frac{10(\lambda_{11}+\lambda_{22})-4(\lambda_{11}\lambda_{21}+\lambda_{12}\lambda_{22})+\lambda_{12}^2+\lambda_{21}^2}{\sigma_7^2}} \, \mathrm{d}\lambda_{11}\mathrm{d}\lambda_{12}\mathrm{d}\lambda_{21}\mathrm{d}\lambda_{22}
\end{aligned}
$$

which is again a Gaussian. We evaluated the integral for several power spectra and smoothing scales in figure 13.2. We observe that the amplitude of the density decreases with increasing smoothing scale. This is what we expect since a larger smoothing suppresses the number of fluctuations and peaks in the field per area. We furthermore observe that the variance increases for power-law power spectra with higher index. The density is always maximal at zero, reflecting the statistical symmetry $\Psi \to -\Psi$ of Gaussian random fields.

13.5 A_2 line length

The A_2-lines of an initial density field are given by the level set of the two eigenvalue fields of the deformation tensor

$$\lambda_1 = \lambda \text{ or } \lambda_2 = \lambda.$$

The A_2^1-line of the λ_1 field corresponds to first shell crossing whereas the A_2^2-line of the λ_2 field corresponds to shell crossing in collapsed regions. The differential lengths of the two A_2-lines in the two-dimensional Zel'dovich approximation are given by

$$
\mathcal{L}_{A_2^1}(\lambda_1) = \pi \int p(\lambda_1, \lambda_2, \lambda_{11}, \lambda_{12})\sqrt{\lambda_{11}^2 + \lambda_{12}^2}(\lambda_1 - \lambda_2)\mathrm{d}\lambda_{11}\mathrm{d}\lambda_{12}\mathrm{d}\lambda_2,
$$

$$
\mathcal{L}_{A_2^2}(\lambda_2) = \pi \int p(\lambda_1, \lambda_2, \lambda_{21}, \lambda_{22})\sqrt{\lambda_{21}^2 + \lambda_{22}^2}(\lambda_1 - \lambda_2)\mathrm{d}\lambda_{21}\mathrm{d}\lambda_{22}\mathrm{d}\lambda_1.
$$

(a) $r = -1$ and $\sigma = 1, 2, 3$ from top to bottom

(b) $r = 0$ and $\sigma = 1, 2, 3$ from top to bottom

(c) $r = 1$ and $\sigma = 1, 2, 3$ from top to bottom

(d) $r = 2$ and $\sigma = 1, 2, 3$ from top to bottom
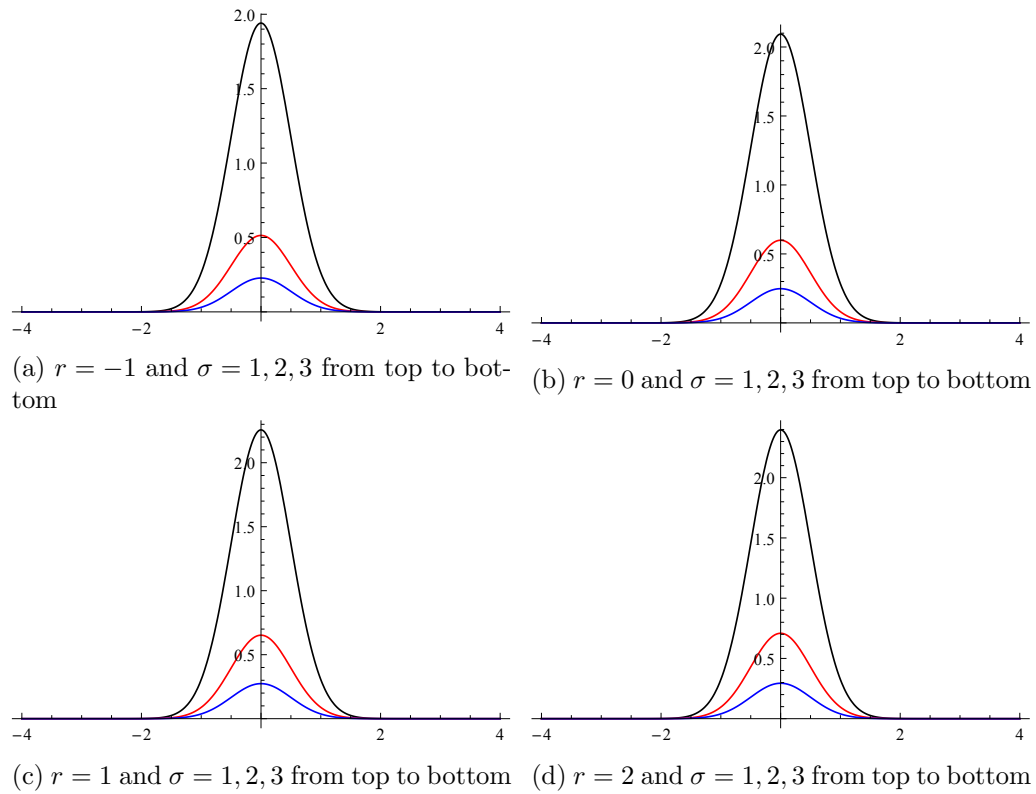
Figure 13.2: Density of D_4 points

(a) 3-dimensional plot

(b) Contour plot
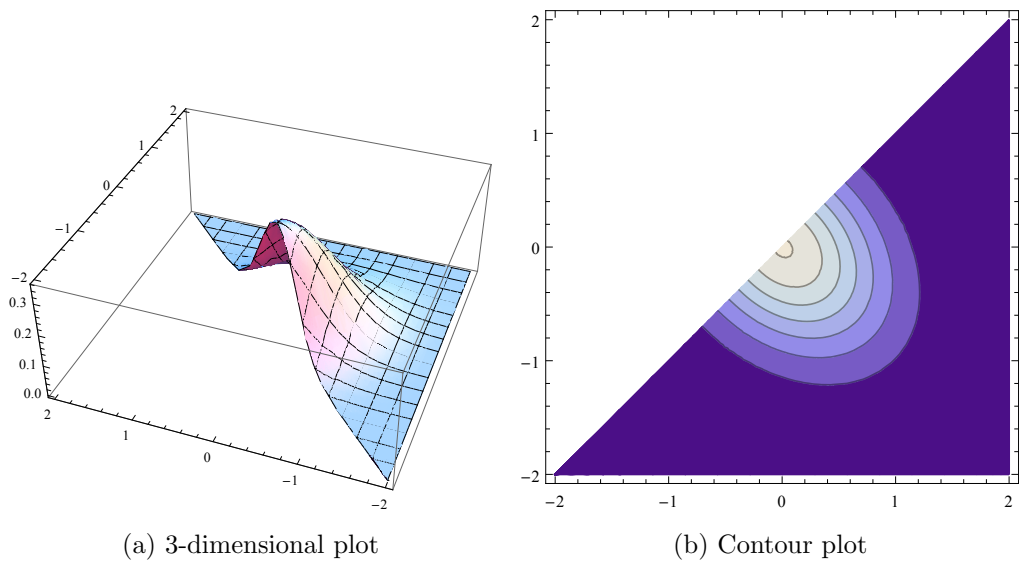
Figure 13.3: Distribution of eigenvalues

In oder to compute this distribution, consider the linear statistic $Y = (T_{11}, T_{22}, T_{12}; T_{222}, T_{122})$ with the covariance matrix

$$V = \langle Y^T Y \rangle = \begin{pmatrix} \frac{3\sigma_5^2}{8} & \frac{\sigma_5^2}{8} & 0 & 0 & 0 \\ \frac{\sigma_5^2}{8} & \frac{3\sigma_5^2}{8} & 0 & 0 & 0 \\ 0 & 0 & \frac{\sigma_5^2}{8} & 0 & 0 \\ 0 & 0 & 0 & \frac{5\sigma_7^2}{16} & 0 \\ 0 & 0 & 0 & 0 & \frac{\sigma_7^2}{16} \end{pmatrix},$$

and inverse covariance matrix

$$C = V^{-1} = \begin{pmatrix} \frac{3}{\sigma_5^2} & -\frac{1}{\sigma_5^2} & 0 & 0 & 0 \\ -\frac{1}{\sigma_5^2} & \frac{3}{\sigma_5^2} & 0 & 0 & 0 \\ 0 & 0 & \frac{8}{\sigma_5^2} & 0 & 0 \\ 0 & 0 & 0 & \frac{16}{\sigma_7^2} & 0 \\ 0 & 0 & 0 & 0 & \frac{16}{5\sigma_7^2} \end{pmatrix}.$$

The distribution in eigenvalue coordinates is

$$p(\lambda, \lambda_2, \lambda_{11}, \lambda_{12}) = \frac{8\sqrt{2}}{\pi^{3/2}\sigma_5^3\sigma_7^2} e^{-\frac{3(\lambda_1^2+\lambda_2^2)-2\lambda_1\lambda_2}{2\sigma_5^2}} e^{-\frac{10\lambda_{11}^2-4\lambda_{11}\lambda_{12}+2\lambda_{12}^2}{\sigma_7^2}},$$

by which

$$\mathcal{L}_{A_2^1}(\lambda) = \frac{8\sqrt{2}}{\pi^{3/2}\sigma_5^3\sigma_7^4} e^{-\frac{3(\lambda_1^2+\lambda_2^2)-2\lambda_1\lambda_2}{2\sigma_5^2}} \int e^{-\frac{10\lambda_{11}^2-4\lambda_{11}\lambda_{12}+2\lambda_{12}^2}{\sigma_7^2}} \sqrt{\lambda_{11}^2 + \lambda_{12}^2} \, \mathrm{d}\lambda_2 \mathrm{d}\lambda_{11}\mathrm{d}\lambda_{12}$$

$$= \frac{\sqrt{5}\sigma_7 E(\frac{4}{5}) e^{-\frac{2\lambda^2}{\sigma_5^2}} \left(\sqrt{6\pi}\lambda e^{\frac{2\lambda^2}{3\sigma_5^2}} \left(\frac{\mathrm{erf}\left(\sqrt{\frac{2}{3}}\lambda\right)}{\sigma_5} + 1 \right) + 3\sigma_5 \right)}{9\pi\sigma_5^2}$$

with E the complete elliptic integral of the first kind. The differential A_2-line length is computed for several power-law power spectra and smoothing scales in figure 13.4. We observe that the mean of the differential A_2^1-line length is independent of the smoothing scale or index of power-law power spectrum. The line length is suppressed by the smoothing which is expected since a smoothed field will have fewer wiggles in the A_2^1-lines. The line length increases as a function of the index of the power-law power spectrum.

We can evaluate the differential A_2^2-line length in a similar fashion. We can however also use the statistical symmetry of Gaussian random fields and use

$$\mathcal{L}_{A_2^2}(\lambda) = \mathcal{L}_{A_2^1}(-\lambda).$$

(a) $r = -1$ and $\sigma = 1, 2, 3$ from top to bottom

(b) $r = 0$ and $\sigma = 1, 2, 3$ from top to bottom

(c) $r = 1$ and $\sigma = 1, 2, 3$ from top to bottom

(d) $r = 2$ and $\sigma = 1, 2, 3$ from top to bottom
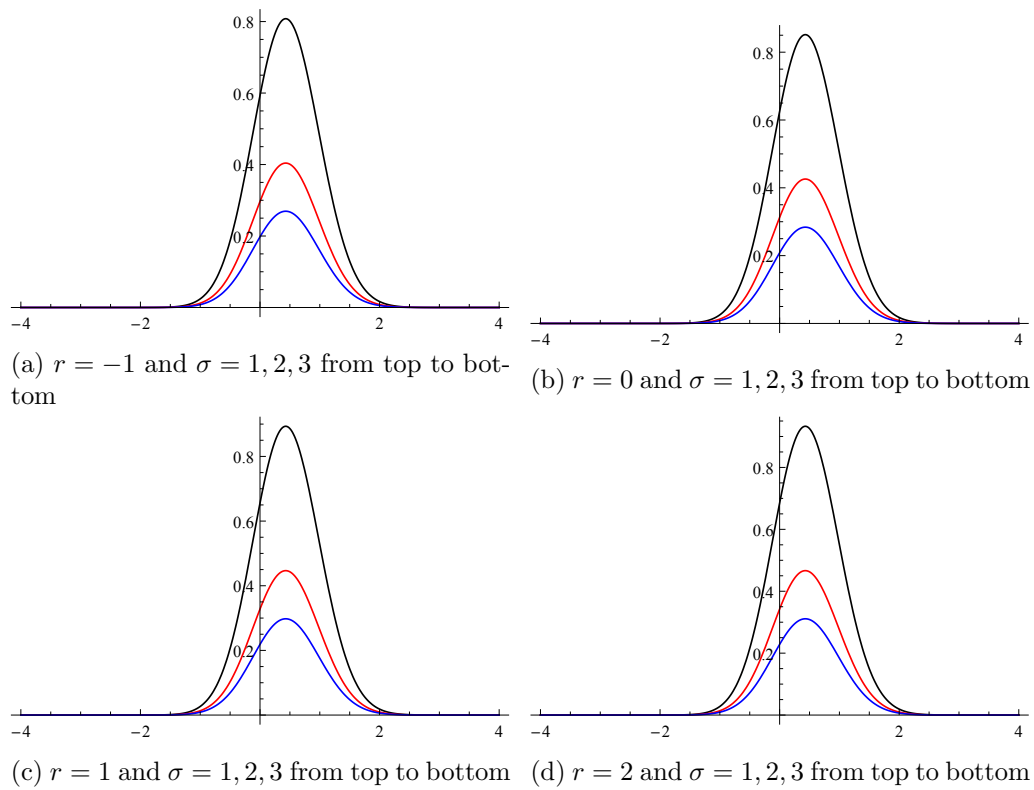
Figure 13.4: Length of A_2-lines

(a) $r = -1$ and $\sigma = 1$

(b) $r = 0$ and $\sigma = 1$

(c) $r = 1$ and $\sigma = 1$
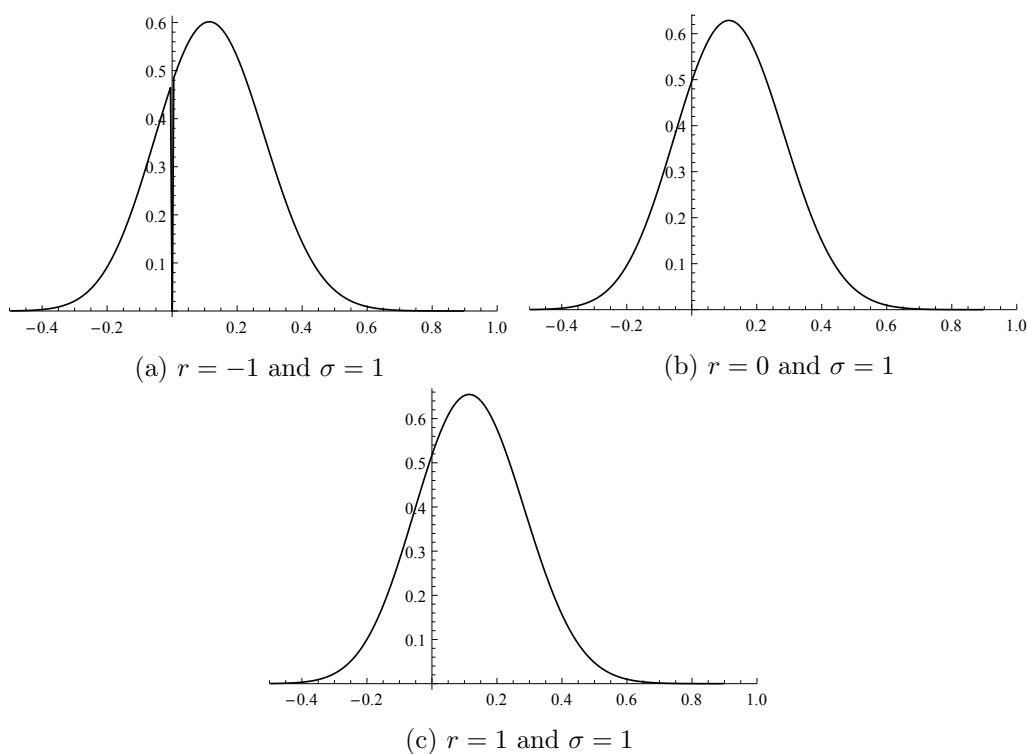
Figure 13.5: Length of A_3-lines

13.6 A_3 line length

The length density of A_3-lines with respect to the eigenvalue fields λ_1, λ_2 can be computed in a similar fashion. Points on the A_3^1- and A_3^2-lines satisfy the condition

$$\lambda_{11} = 0, \lambda_{22} = 0,$$

respectively. The differential line length of the A_3^1- and A_3^2-lines is given by

$$\mathcal{L}_{A_3^1}(\lambda_1) = \pi \int \sqrt{\lambda_{111}^2 + \lambda_{112}^2} \, p(\lambda_1, \lambda_2, \lambda_{11} = 0, \lambda_{111}, \lambda_{112})(\lambda_1 - \lambda_2) \mathrm{d}\lambda_{111} \mathrm{d}\lambda_{112} \mathrm{d}\lambda_2,$$

$$\mathcal{L}_{A_3^2}(\lambda_2) = \pi \int \sqrt{\lambda_{221}^2 + \lambda_{222}^2} \, p(\lambda_1, \lambda_2, \lambda_{22} = 0, \lambda_{221}, \lambda_{222})(\lambda_1 - \lambda_2) \mathrm{d}\lambda_{221} \mathrm{d}\lambda_{222} \mathrm{d}\lambda_1.$$

We are unable to analytically evaluate this integral with Mathematica. For this reason we evaluated the integral numerically for several power-law power spectra (see figure 13.5).

Note that all these results are considered in scale space. We should take the truncated Zel'dovich approximation on different scales during at different stages of the evolution. When small scales collapse we should consider a small σ, while when larger scales collapse we should consider a larger σ.

Chapter 14

Numerical Statistics of Caustics

In the previous chapters we studied the Zel'dovich approximation and caustics described by catastrophe theory. Caustics play a prominent role in the evolution of large-scale structure. In this chapter we numerically calculate the density of caustics in the one-dimensional Zel'dovich approximation. For an explanation of the random fields used in this chapter see chapter 8.

14.1   One-dimensional caustics

One-dimensional caustics are points with infinite density in one-dimensional matter distributions. They occur not only in one-dimensional models of the universe but also in two- or three-dimensional universes in configurations in which the collapse occurs in one direction, i.e. in regions in which shell crossing occurs in one direction while expanding according to the Hubble law in the orthogonal directions.

In one dimension stable caustics can be classified as fold A_2 and cusp A_3 catastrophes. Catastrophes are introduced in the one-dimensional Zel'dovich approximation by an A_3 catastrophe which corresponds to maximum in the density field. The A_3 catastrophe exists at a point in space-time. A moment after its appearance the A_3 catastrophe splits in two A_2 catastrophes. The A_2 catastrophes correspond with level crossings of the density field. In principle two A_2 catastrophes can subsequently annihilate via a A_3 catastrophe corresponding with a minimum of the density field.

In this section we numerically determine the density of A_3 and A_2 catastrophes for several power-law power spectra. We start by generating a realization of a one-dimensional Gaussian random field $v = (v_1, v_2, \ldots, v_n) \in \mathbb{R}^n$ on a regular discrete lattice with a given power spectrum. The algorithm used for the generation of the Gaussian random field is described in chapter 8. We subsequently determine the difference of the sign of the difference of v, i.e.

$$w = \mathrm{dif} \circ \mathrm{sign} \circ \mathrm{dif}\ v$$

with $\mathrm{dif}\, v = (v_2 - v_1, v_3 - v_2, \ldots, v_n - v_{n-1})$ and $\mathrm{sign}\, v = (\mathrm{sign}\, v_1, \ldots, \mathrm{sign}\, v_n)$ defining $\mathrm{sign}(\alpha) = 1$ for $\alpha > 0$, $\mathrm{sign}(\alpha) = 0$ for $\alpha = 0$ and $\mathrm{sign}(\alpha) = -1$ for $\alpha < 0$. The maxima

(a) Power spectrum $P = k^1$, smoothing $\sigma = 1$

(b) Power spectrum $P = 1$, smoothing $\sigma = 1$

(c) Power spectrum $P = k^{-1}$, smoothing $\sigma = 1$
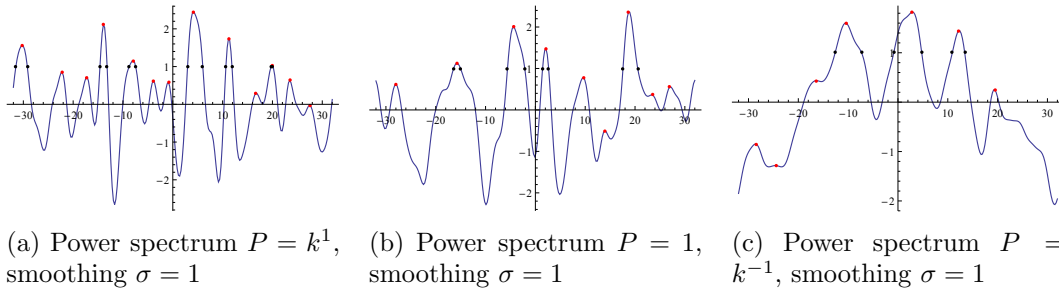
Figure 14.1: Realization of one-dimensional Gaussian random fields with maxima and level crossings

and minima of the realization v correspond with the positions in w in which w assumes -2 and 2 respectively. The level crossings at the level $\lambda \in \mathbb{R}$ are determined by the positions in

$$w = |\operatorname{dif} \circ \operatorname{sign}(v - \lambda)|$$

in which w assumes 2. We increase the accuracy of the positions of the level crossings by performing a linear interpolation with the two neighboring points identified in the previous step and determining the place of intersection with the interpolated function. A realization with the corresponding linear interpolation, maxima, and level crossings is illustrated in figure 14.1.

In figure 14.2 the density of maxima, minima and level crossings at different field values are plotted by the points. The lines are the predicted distributions, described in chapter 10. The shape of the distributions is sensitive to the power spectrum while the amplitude is sensitive to the smoothing scale.

14.2   Two-dimensional caustics in Lagrangian space

Two-dimensional caustics are points with infinite density in two-dimensional matter distributions. They occur not only in two-dimensional models of the universe but also in three-dimensional universes in configurations in which the collapse occurs in two direction, i.e. in regions in which shell crossing occurs in two direction while expanding according to the Hubble law in the orthogonal direction. In two dimensions the caustics are described by cusps A_3, swallow tail A_4, umbilical points D_4, and A_2- and A_3-lines. In this section we numerically determine statistics of these catastrophes. The program used for these computations is design by Johan Hidding [33].

Starting with a power-law power spectrum, we generate a two-dimensional realization representing the density field. We subsequently determine the corresponding potential field, the deformation tensor and the two corresponding eigenvalue fields. Finally the catastrophes are identified. The density and eigenvalue fields for a specific realization are plotted in figure 14.3.

(a) Power spectrum $P = k^1$, smoothing $\sigma = 1$

(b) Power spectrum $P = k^1$, smoothing $\sigma = 2$

(c) Power spectrum $P = k^1$, smoothing $\sigma = 3$

(d) Power spectrum $P = 1$, smoothing $\sigma = 1$

(e) Power spectrum $P = 1$, smoothing $\sigma = 2$

(f) Power spectrum $P = 1$, smoothing $\sigma = 3$

(g) Power spectrum $P = k^{-1}$, smoothing $\sigma = 1$

(h) Power spectrum $P = k^{-1}$, smoothing $\sigma = 2$

(i) Power spectrum $P = k^{-1}$, smoothing $\sigma = 3$
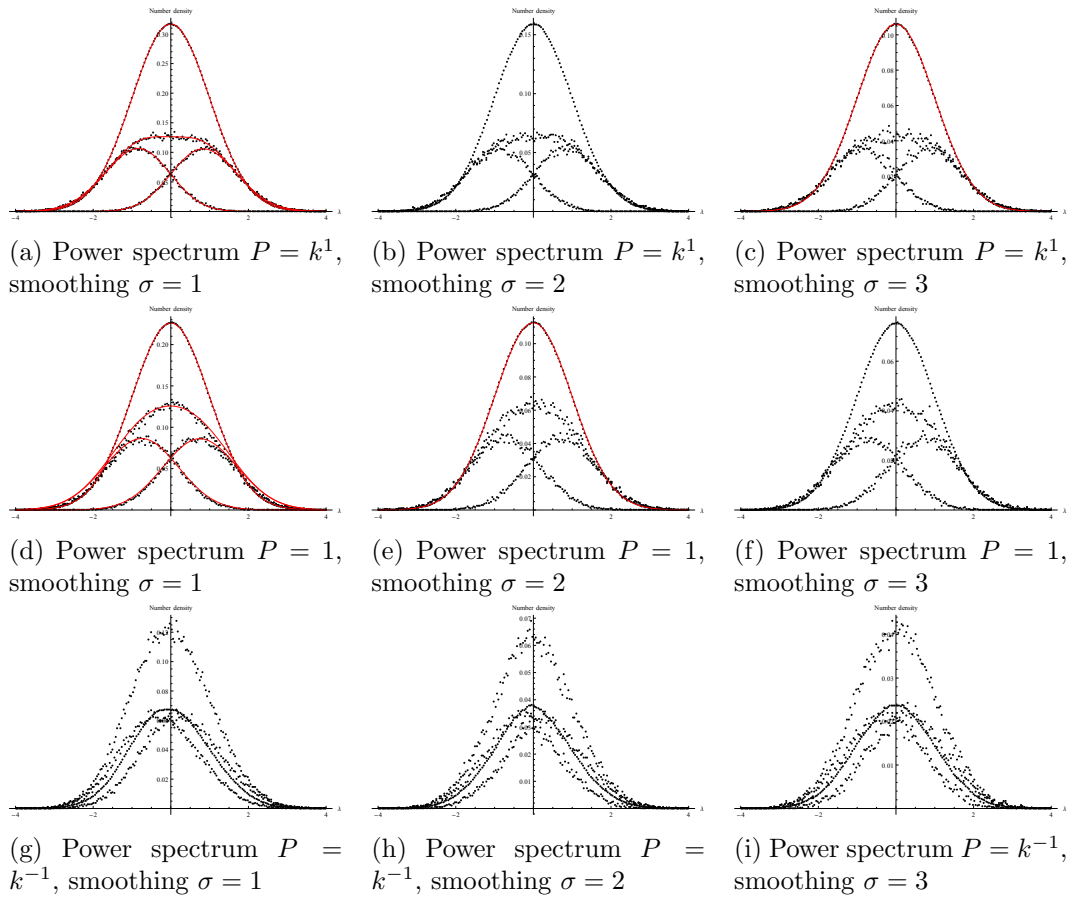
Figure 14.2: Density of maxima, minima and level crossings.
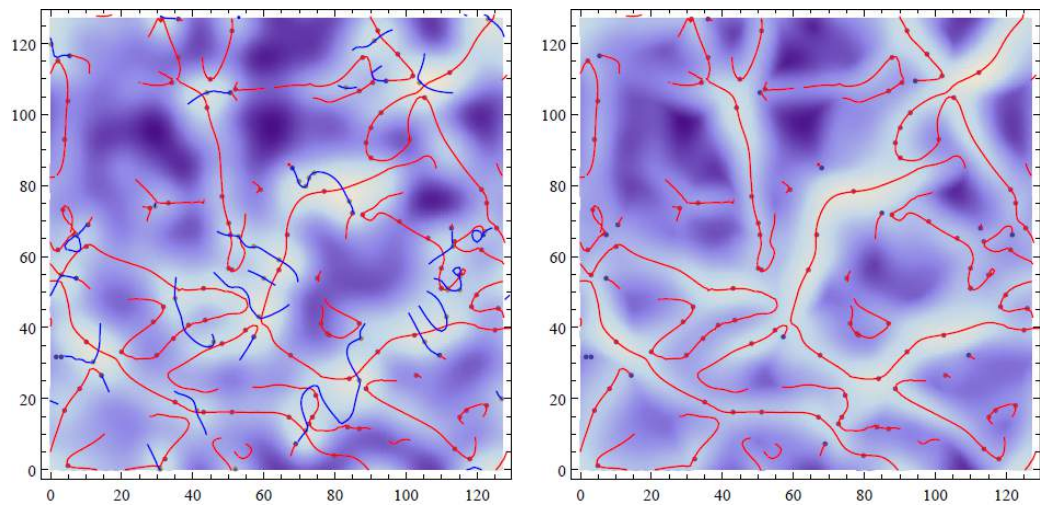
(a) The density field with A_3-lines and A_3, A_4 and D_4 catastrophes

(b) The first eigenvalue field, with the A_3^α-lines, A_3^α, A_4^α and D_4 points.
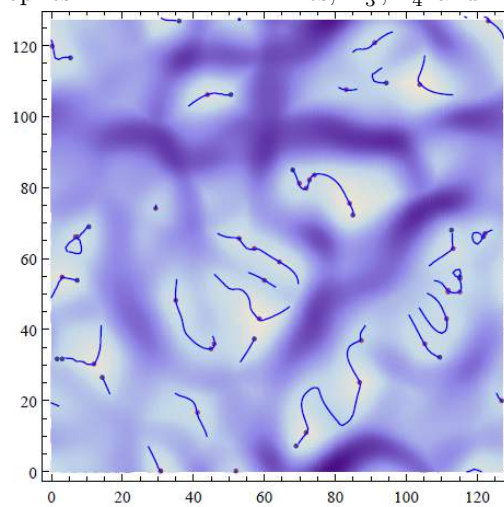
(c) The second eigenvalue field, with the A_3^β-lines, A_3^β, A_4^β and D_4 points.

Figure 14.3: Realization of two-dimensional Gaussian random fields with catastrophes and A_3-lines

(a) Power spectrum $P = k^1$, smoothing $\sigma = 1$

(b) Power spectrum $P = k^1$, smoothing $\sigma = 1$

(c) Power spectrum $P = k^1$, smoothing $\sigma = 1$
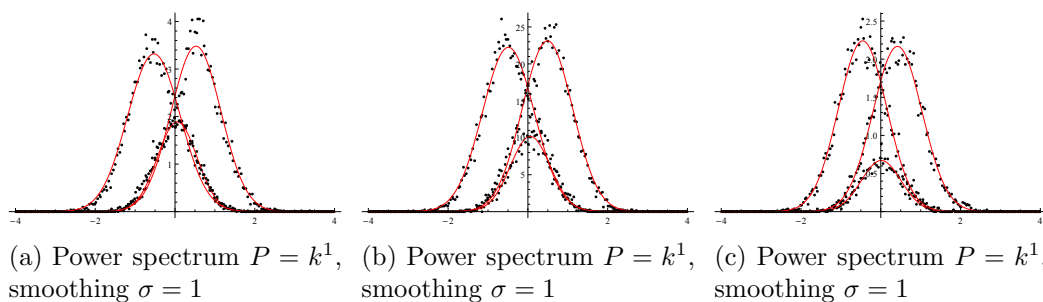
Figure 14.4: The density of D_4 density and combined A_3^α, A_4^α, and A_3^β, A_4^β point densities.

(a) Power spectrum $P = k^1$, smoothing $\sigma = 1$

(b) Power spectrum $P = k^1$, smoothing $\sigma = 1$

(c) Power spectrum $P = k^1$, smoothing $\sigma = 1$
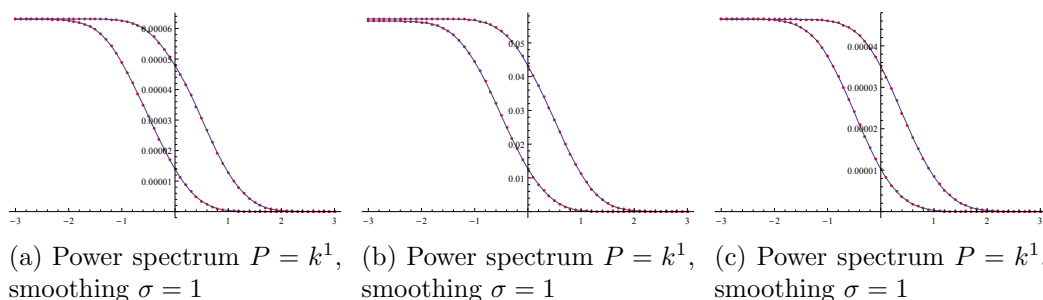
Figure 14.5: The cumulative length of A_3-lines of the first and second eigenvalue fields.

Using the caustics of the realization, we determine the statistical behavior of the different catastrophes. The density of the three and four dimensional catastrophes is illustrated by the points in figure 14.4. The red lines are fits with Gaussian distributions.

For the initial conditions we can determine the A_3^1- and A_3^2-line length as a function of the threshold of the eigenvalue field (see figure 14.5). The derivative of the A_3^1- and A_3^2-line length with respect to the threshold is the differential length calculated in chapter 13.

14.3   Two-dimensional caustics in Eulerian space

Using the Zel'dovich approximation we can also estimate the behavior of the statistic of the caustic skeleton in Eulerian space. The densities of point catastrophes, described in the previous section, do not change. The two-point correlation function does, but this lays outside the scope of this thesis. The A_3-lines can stretch and contract during structure formation. The A_2-lines are introduced when considering the evolution in the Zel'dovich approximation. In this section we study there evolution.

For different power-law power spectra, the A_2-length at different eigenvalues in Eulerian and Lagrangian space is illustrated in figure 14.6. We see that the A_2-line length corresponding to the first eigenvalue and second eigenvalue increases during the evolution. Note that the A_2-line length of the first eigenvalue increases faster than the A_2-line length of the second eigenvalue. This can be explained by the fact that the displace-

(a) Lagrangian A_2-line lengths with power spectrum $P = k^{-1}$, smoothing $\sigma = 4$

(b) Lagrangian A_2-line lengths with power spectrum $P = k^0$, smoothing $\sigma = 4$

(c) Lagrangian A_2-line lengths with power spectrum $P = k^1$, smoothing $\sigma = 4$

(d) Eulerian A_2-line lengths with power spectrum $P = k^{-1}$, smoothing $\sigma = 4$

(e) Eulerian A_2-line lengths with power spectrum $P = k^0$, smoothing $\sigma = 4$

(f) Eulerian A_2-line lengths with power spectrum $P = k^1$, smoothing $\sigma = 4$

Figure 14.6: The A_2-line lengths as a function of growing mode. The higher plot gives the A_2-line length of the first eigenvalue whereas the lower line gives the A_2-line length of the second eigenvalue.

ment of the matter field will be dominated by the eigenvector of the deformation tensor corresponding to the first eigenvalue.

In figure 14.7 we show the Eulerian A_3-line lengths for different power-law power spectra at different stages of evolution as function of the threshold. We see that before the first shell crossing occurs the total A_3-line length corresponding to the first eigenvalue increases while the total A_3-line length corresponding to the second eigenvalue decreases. After the first shell crossing has occurred, both total lengths increase.

(a) The Eulerian A_3-line lengths with power spectrum $P = k^{-1}$, smoothing $\sigma = 4$

(b) The Eulerian A_3-line lengths with power spectrum $P = k^{-1}$, smoothing $\sigma = 4$

(c) The Eulerian A_3-line lengths with power spectrum $P = k^{-1}$, smoothing $\sigma = 4$

(d) The Eulerian A_3-line lengths with power spectrum $P = k^{0}$, smoothing $\sigma = 4$

(e) The Eulerian A_3-line lengths with power spectrum $P = k^{0}$, smoothing $\sigma = 4$

(f) The Eulerian A_3-line lengths with power spectrum $P = k^{0}$, smoothing $\sigma = 4$

(g) The Eulerian A_3-line lengths with power spectrum $P = k^{1}$, smoothing $\sigma = 4$

(h) The Eulerian A_3-line lengths with power spectrum $P = k^{1}$, smoothing $\sigma = 4$

(i) The Eulerian A_3-line lengths with power spectrum $P = k^{1}$, smoothing $\sigma = 4$

Figure 14.7: The A_3-line lengths as a function the threshold of the eigenvalue field. The higher plot gives the A_3-line length corresponding to the first eigenvalue field whereas the lower line gives the A_3-line length corresponding to the second eigenvalue field.

Chapter 15

Quantum Field Theory and Feynman Diagrams

In this thesis, we so far studied Gaussian random field theory. In the subsequent chapters we will apply effective field theory to large-scale structure formation. Both approaches are closely related to quantum field theory. In this chapter we give a short introduction to Lagrangian and Hamiltonian mechanics. We furthermore discuss quantum field theory and indicate the relations to Gaussian random field theory and effective field theory. The statements in this chapter will not be proven. All proofs can be found in any standard textbook about classical mechanics and quantum field theory. For classical mechanics you can for example consult 'Classical dynamics of particles and systems' by Thornton and Marion [66] or 'Mathematical methods of classical mechanics' by Arnol'd [7]. For quantum field theory see for example 'Quantum field theory in a nutshell' by Zee [70] or 'An introduction to quantum field theory' by Peskin and Schroeder [54].

15.1   Classical mechanics

Classical mechanics concerns the movement of objects as we experience in daily life. It for example accurately describes spring systems, the flight of a bullets, the tides, the orbit of the moon around the earth, the solar system, and the rotation of galaxies. It is common practice to consider classical mechanics from the Newtonian, Lagrangian and Hamiltonian perspective.

15.1.1   Newtonian mechanics

As taught in high school, classical mechanics can be formulated in terms of forces obeying Newton's laws of motion. These laws were first formulated in the Principia Mathematica 1687 by Newton.

1. An object either remains at rest or continues to move at constant velocity, unless

acted upon by an external force [1],

2. The sum of the forces on an object $\sum \mathbf{F}$ is equal to the mass m times the acceleration $\mathbf{a}$, i.e. $\sum \mathbf{F} = m\mathbf{a}$,

3. When one object exerts a force on a second object, the second object simultaneously exerts a force equal in magnitude and opposite in direction on the first object.

In making predictions of the trajectories of objects we systematically determine the forces acting on a body, apply Newton's second law $\sum \mathbf{F} = m\mathbf{a}$ and solve the resulting differential equation. This procedure can in principle be applied to any problem in classical mechanics. There exist however more efficient and elegant formulations.

15.1.2   Lagrangian mechanics

The first notable re-formulation of Newtonian classical mechanics was performed in 1788 by Joseph Louis Lagrange. In Lagrangian mechanics we work in the framework of energy, completely dual to the framework of forces. The energy of an system is a measure of the work performed on an object. When a force $\mathbf{F}$ is applied over an infinitesimal distance $\mathrm{d}\mathbf{s}$ while the object moves with velocity $\mathbf{v}$, the change in the work W is defined as

$$\mathrm{d}W = \mathbf{F} \cdot \mathrm{d}\mathbf{s} = \mathbf{F} \cdot \mathbf{v}\mathrm{d}t,$$

with $\mathrm{d}t$ the time it takes to travel distance $\mathrm{d}\mathbf{s}$ with velocity $\mathbf{v}$. Consider an object with velocity $\mathbf{v}$ exposed to a force $\mathbf{F}(t)$ in the time interval $[t_i, t_f]$. The work performed on the object is defined as

$$W = \int_{t_i}^{t_f} \mathbf{F} \cdot \mathbf{v}\mathrm{d}t.$$

An object with a velocity $\mathbf{v}$ has a kinetic energy, since it takes work to get the object into motion. Let an object be at rest at t_i and let it be accelerated to a velocity $\mathbf{v}_f$ in the interval $[t_i, t_f]$. The work exerted on the object in this time interval is

$$\int_{t_i}^{t_f} \mathbf{F} \cdot \mathbf{v}\mathrm{d}t = \int_{t_i}^{t_f} m\mathbf{a} \cdot \mathbf{v}\mathrm{d}t = \int_{t_i}^{t_f} m\frac{\partial \mathbf{v}}{\partial t} \cdot \mathbf{v}\mathrm{d}t = \int_{t_i}^{t_f} \frac{1}{2}\frac{\partial (m\mathbf{v}^2)}{\partial t}\mathrm{d}t = \frac{1}{2}m\mathbf{v}_f^2,$$

with m the mass of the object. Note that we assume that mass to be constant during the acceleration. It is shown in any classical mechanics textbook that this result is independent of the force $\mathbf{F}$ or the path followed in the interval $[t_i, t_f]$. For this reason we define the kinetic energy as

$$E_{kin} = \frac{1}{2}m\mathbf{v}^2.$$

---

[1]Assuming the observer views the object form an inertial reference system, i.e. the observer does not accelerate.

Forces, in the energy framework, are described by the potential energy U. The potential energy $U(\mathbf{x})$ at a point $\mathbf{x}$ is defined by the work it takes to move the object from some fixed point to $\mathbf{x}$. We define the potential energy to locally satisfy

$$\mathbf{F} = -\nabla U.$$

From the conservation of energy it follows that the potential energy can be globally defined. In Lagrangian mechanics the kinetic and potential energy are combined in the Lagrange function, often called the Lagrangian

$$L(\mathbf{x}, \mathbf{v}, t) = E_{kinetic} - U = \frac{1}{2} m \mathbf{v}^2 - U.$$

In Lagrangian mechanics Newton's laws of motion are replaced by the action principle. The action principle states that the integral of the Lagrangian L over a path $\mathbf{q}(t)$, called the action

$$S[\mathbf{q}(t)] = \int L[\mathbf{q}(t)] \mathrm{d}t = \int \left[\frac{1}{2} m \dot{\mathbf{q}}^2(t) - U[\mathbf{q}(t)] \right] \mathrm{d}t,$$

is an extremum for the motion of classical particles. The extremum condition can be shown to be equivalent to the Euler-Lagrange equation

$$\frac{\mathrm{d}}{\mathrm{d}t} \frac{\partial L}{\partial \mathbf{v}} = \frac{\partial L}{\partial \mathbf{x}}.$$

Substitution of the definition of the Lagrangian in the Euler-Lagrange equation results into Newton's second law of motion. The Lagrangian formulation is more efficient since we only have to take care of the scalar objects E_{kin} and U in stead of the vector objects $\mathbf{F}$ which are in practice often more difficult to determine. It is an amazing property of nature that no matter how complicated the motion, nature always tries to maximize or minimize a simple functional which we call the action.

15.1.3   Hamiltonian mechanics

Lagrangian mechanics was in 1833 re-formulated by William Rowan Hamilton. In the Hamilton formulation of classical mechanics we perform a so-called Legendre transformation on the Lagrangian to obtain the Hamilton function, often called the Hamiltonian. Defining the conjugate momentum as

$$\mathbf{p} = \frac{\partial L}{\partial \mathbf{v}},$$

the so called Hamiltonian $H(\mathbf{x}, \mathbf{p})$ is defined as the Legendre transformation of the Lagrangian, i.e.

$$H(\mathbf{x}, \mathbf{p}) = \dot{x} p - L.$$

For the Lagrangian described above this amounts to

$$\mathbf{p} = m\mathbf{v}, \text{ and}$$

$$H(\mathbf{x}, \mathbf{p}) = E_{kin} + U = \frac{\mathbf{p}^2}{2m} + U.$$

Note that for the classical one-particle Lagrangian discussed above, the conjugate momentum coincides with the familiar linear momentum known in Newtonian mechanics. The Hamiltonian for such a Lagrangian coincides with the total energy of the system. In the Hamiltonian formalism, the Euler-Lagrange equation transforms to Hamilton's equations

$$\dot{x} = \frac{\partial H}{\partial \mathbf{p}}, \quad \dot{p} = -\frac{\partial H}{\partial \mathbf{x}}.$$

This very symmetric formulation gives great practical ease. The total energy of the system directly leads to the equations of motion. There exist further re-formulations of Newtonian mechanics. For the discussion below the Lagrangian and Hamiltonian formulation however suffice.

15.2 Path integral formulation of quantum physics

Classical mechanics is deterministic. The Newtonian, Lagrangian or Hamiltonian formulation lead to a set of differential equations which one can uniquely solve for some set of initial conditions. Quantum mechanics is not deterministic. The best one can do is to predict probabilities for events to occur. In a measurement, the wave function collapses with some probability to some state. These probabilities are calculated in terms of amplitudes, i.e. the absolute square of the amplitude is the probability. In quantum mechanics, the amplitude to propagate from a point q_I to a point q_F in time T is given by

$$\langle q_F | e^{-iHT} | q_I \rangle,$$

with H the Hamiltonian of the particle, and $|q_I\rangle$ and $\langle q_F|$ the initial and final state in Dirac notation. The probability for the particle to propagate form q_I to q_F is given by

$$|\langle q_F | e^{-iHT} | q_I \rangle|^2.$$

For the path integral formulation of quantum mechanics we divide the time T into N segments each lasting $\delta t = T/N$. We can now write

$$\langle q_F | e^{-iH\delta t} e^{-iH\delta t} \dots e^{-iH\delta t} | q_I \rangle.$$

Let the state of the particle at the ith time segment be q_i. If the states are properly normalized, i.e. $\langle q' | q \rangle = \delta^{(d)}(q' - q)$ and from a complete set of states, i.e. $\int dq |q\rangle\langle q| = 1$,

we can write the amplitude for propagating form q_I to q_F as

$$\langle q_F|e^{-iHT}|q_I\rangle = \left(\prod_{j=1}^{N-1}\int \mathrm{d}q_j\right)\langle q_F|e^{-iH\delta t}|q_{N-1}\rangle\langle q_{N-1}|e^{-iH\delta t}|q_{N-2}\rangle\ldots\langle q_1|e^{-iH\delta t}|q_I\rangle.$$

For the Hamiltonian given in the previous section

$$H = \frac{\hat{p}^2}{2m} + U,$$

with $\hat{p}$ the momentum operator in stead of the momentum variable, each term in this expression can be individually evaluated,

$$\begin{aligned}
\langle q_{j+1}|e^{-i\delta t(\hat{p}^2/(2m)+U)}|q_j\rangle &= \int \frac{\mathrm{d}p}{2\pi}\langle q_{j+1}|e^{-i\delta t(\hat{p}^2/(2m)+U)}|p\rangle\langle p|q_j\rangle\\
&= \int \frac{\mathrm{d}p}{2\pi}e^{-i\delta t(p^2/(2m)-U(q_j))}\langle q_{j+1}|p\rangle\langle p|q_j\rangle\\
&= \int \frac{\mathrm{d}p}{2\pi}e^{-i\delta t(p^2/(2m)-U(q_j))}e^{ip(q_{j+1}-q_j)}\\
&= \left(\frac{-im}{2\pi\delta t}\right)^{1/2}e^{i\delta t(m/2)[(q_{j+1}-q_j)/\delta t]^2-i\delta tU(q_j)},
\end{aligned}$$

where the momentum states $|p\rangle$ are normalized by $\int \frac{\mathrm{d}p}{2\pi}|p\rangle\langle p| = 1$ and $\langle q|p\rangle = e^{ipq}$. The state $|p\rangle$ is an eigenstate of the operator $\hat{p}$ with eigenvalue p, i.e. $\hat{p}|p\rangle = p|p\rangle$. In the last line we used the Gaussian integral. Substituting this term in the amplitude for the propagation from q_I to q_F gives

$$\langle q_F|e^{-iHT}|q_I\rangle = \left(\prod_{j=1}^{N-1}\int \mathrm{d}q_j\right)\left(\frac{-im}{2\pi\delta t}\right)^{N/2}e^{i\delta t(m/2)\sum_{j=0}^{N}[(q_{j+1}-q_j)/\delta t]^2-i\delta t\sum_{j=0}^{N}U(q_j)}.$$

In the setup of the path integral formulation, we divided the propagation time T in N intervals with duration δt. We subsequently evaluated the integral for each step. The number of steps N is however artificial. We remove the dependence on N by dividing the propagation time T in infinitely many intervals of infinitesimal duration such that $N\Delta t = T$. In this limit the amplitude to travel form q_I to q_F in a time T becomes

$$\langle q_F|e^{-iHT}|q_I\rangle = \lim_{N\to\infty}\left(\left(\frac{-im}{2\pi\delta t}\right)^{N/2}\left(\prod_{j=1}^{N-1}\int \mathrm{d}q_j\right)\right)e^{i\int_0^T\left[\frac{1}{2}mv^2-U\right]\mathrm{d}t},$$

which is often written as

$$\langle q_F|e^{-iHT}|q_I\rangle = \int e^{iS[q(t)]}\mathcal{D}q(t).$$

The term $\mathcal{D}q(t)$ represents an integral over all possible paths $q(t)$. This is known as the path integral formalism. It is one of the ways to quantize[2] a dynamical system. The path integral formation was mathematically first invented by Dirac. However Feynman was the first to interpret the path integral as an integral over all possible paths between two points. According to Feynman, fundamental particles are 'free spirits'. They evolve simultaneously in all possible ways, violating classical laws, and are only pinned down in measurements.

15.3   Quantum field theory

The path integral formalism, derived in the previous section, can be used to obtain a quantum field theory. We start by replacing the trajectory $q(t)$ by a field $\varphi(t, x)$ representing a particle (species). From this moment onwards we will suppress the boldface notation for vectors. Such a field assumes values at all points of spacetime. We can write the action in the general form

$$S[\varphi] = \int \mathrm{d}^4 x \mathcal{L}(\varphi),$$

with $\mathcal{L}$ the Lagrangian density, and $\mathrm{d}^4 x = \mathrm{d}t\mathrm{d}x\mathrm{d}y\mathrm{d}z$. The Lagrangian density, often abbreviated by the Lagrangian, contains all the physical input. In principle we can include many field and use the quantum electrodynamics, quantum chromodynamics, or standard model Lagrangian, modeling the electromagnetic force, strong nuclear force or combined forces respectively. In this chapter we only consider the general framework of quantum field theory and only study two single field toy models. The Lagrangian in one field is generally of the form

$$\mathcal{L}(\varphi) = \frac{1}{2}(\partial \varphi)^2 - \frac{1}{2}m^2 \varphi^2 - \frac{g}{3!}\varphi^3 - \frac{\lambda}{4!}\varphi^4 + \dots,$$

with

$$(\partial \varphi)^2 = \partial_\mu \varphi \partial^\mu \varphi = \left(\frac{\partial \varphi}{\partial t}\right)^2 - \left(\frac{\partial \varphi}{\partial x}\right)^2 - \left(\frac{\partial \varphi}{\partial y}\right)^2 - \left(\frac{\partial \varphi}{\partial z}\right)^2$$

often used in relativistic notation. The constants m, g, λ turn out to be parameters representing the mass and interaction strengths of the field φ respectively. We here for simplicity only consider the case in which all interaction terms are zero and the case in which only the interaction term λ is nonzero. The first case is called the free or Gaussian theory. The second case is known as the φ^4 theory. To summarize, quantum field theory can be seen as evaluating path integrals like

$$\int e^{\frac{i}{\hbar} \int \mathrm{d}^4 x \left[\frac{1}{2}(\partial \varphi)^2 - \frac{1}{2}m^2 \varphi^2 - \frac{g}{3!}\varphi^3 - \frac{\lambda}{4!}\varphi^4 - \cdots \right]} \mathcal{D}\varphi.$$

We unfortunately only know how to evaluate very specific integrals of this kind. We however do know how approximate the integral using perturbation theory. In the φ^4-theory, we illustrate the perturbation theory by deriving so-called Feynman diagrams.

---

[2]A procedure to transform classical mechanics to quantum mechanics.

15.3.1 Gaussian quantum field theory

In this section, we start with the free or Gaussian theory containing no interaction terms. The action of the free theory is

$$S[\varphi] = (\partial\varphi)^2 - m^2\varphi^2.$$

For mathematical convenience we will add a source term $J\varphi$ to the Lagrangian, which leads to the path integral

$$Z(J) = \int e^{\frac{i}{\hbar}\int d^4x\left[\frac{1}{2}(\partial\varphi)^2 - \frac{1}{2}m^2\varphi^2 + J\varphi\right]}\mathcal{D}\varphi.$$

This path integral is very similar to the definition of Gaussian random fields in the continuous limit. After a Wick rotation, the theory becomes Euclidean and coincides with the definition of Gaussian random fields. Bary Simon extensively studied such theories in statistical mechanics [63].

Using integrating by parts and assuming that all boundary term vanishes, the amplitude for the propagation from q_I to q_F can be expressed as

$$Z(J) = \int e^{\frac{i}{\hbar}\int d^4x\left[\frac{1}{2}\varphi(\partial^2 + m^2)\varphi + J\varphi\right]}\mathcal{D}\varphi.$$

Using Gaussian integrals, we can evaluate this path integral,

$$Z(J) = Z(J=0)e^{-\frac{i}{2}\iint d^4x d^4y J(x)D(x-y)J(y)} = Z(J=0)e^{iW[J]},$$

with the propagator or Green function D satisfying the condition

$$-(\partial^2 + m^2)D(x-y) = \delta^{(4)}(x-y).$$

Using the Fourier representation of the Dirac delta function

$$\delta^{(4)}(x-y) = \int \frac{d^4k}{(2\pi)^4}e^{ik(x-y)},$$

we can derive an explicit expression for the propagator

$$D(x-y) = \int \frac{d^4k}{(2\pi)^4}\frac{e^{ik(x-y)}}{k^2 - m^2}.$$

The propagator in quantum field theory plays the role of the inverse of the two-point correlation in Gaussian field theory. From a quantum field theory perspective, the propagator completely solves the free theory. Unfortunately this does not directly lead to many physical insights and predictions. The theory does not contain any interactions and for that reason cannot influence other particles. Particles in the theory cannot be measured.

15.3.2 φ^4 theory and Feynman diagrams

In the previous section we solved the free theory. In this section we introduce an interaction term. For simplicity we only consider φ^4 theory with a nonzero λ term. Unfortunately we do not know how to solve the resulting path integral

$$Z(J) = \int e^{\frac{i}{\hbar} \int d^4x \left[\frac{1}{2}(\partial\varphi)^2 - \frac{1}{2}m^2\varphi^2 - \frac{\lambda}{4!}\varphi^4 + J\varphi \right]} \mathcal{D}\varphi.$$

Instead we can develop a perturbation theory in terms of the coupling λ and show how to represent perturbation series in Feynman diagrams. We will peruse the Schwinger way to perturbation theory.

We start by rewriting the path integral as a Taylor series in λ

$$Z(J,\lambda) = \int e^{\frac{i}{\hbar} \int d^4x \left[\frac{1}{2}(\partial\varphi)^2 - \frac{1}{2}m^2\varphi^2 + J\varphi \right]} \sum_{j=1}^{\infty} \frac{\left[-\frac{i\lambda}{4!\hbar} \int d^4x\,\varphi^4 \right]^j}{j!} \mathcal{D}\varphi$$

$$= \sum_{j=1}^{\infty} \frac{\left[-\frac{i\lambda}{4!\hbar} \right]^j}{j!} \int e^{\frac{i}{\hbar} \int d^4x \left[\frac{1}{2}(\partial\varphi)^2 - \frac{1}{2}m^2\varphi^2 + J\varphi \right]} \left[\int d^4x\,\varphi^4 \right]^j \mathcal{D}\varphi$$

$$= \sum_{j=1}^{\infty} \frac{\left[-\frac{i\lambda}{4!\hbar} \int d^4w \frac{\delta}{\delta J(w)} \right]^j}{j!} \int e^{\frac{i}{\hbar} \int d^4x \left[\frac{1}{2}(\partial\varphi)^2 - \frac{1}{2}m^2\varphi^2 + J\varphi \right]} \mathcal{D}\varphi$$

$$= e^{-(i/4!)\lambda \int d^4w [\delta/\delta J(w)]^4} \int e^{\frac{i}{\hbar} \int d^4x \left[\frac{1}{2}(\partial\varphi)^2 - \frac{1}{2}m^2\varphi^2 + J\varphi \right]} \mathcal{D}\varphi$$

$$= Z(J=0,\lambda=0) e^{-\frac{i}{4!}\lambda \int d^4w [\frac{\delta}{\delta J(w)}]^4} e^{-\frac{i}{2} \iint d^4x d^4y\, J(x) D(x-y) J(y)}$$

$$= Z(J=0,\lambda=0) e^{-\frac{i}{4!}\lambda \int d^4w [\frac{\delta}{\delta J(w)}]^4} e^{iW[J]},$$

where we used the functional derivative $\frac{\delta}{\delta J(w)}$ to pull down φ terms down from the exponent and we used the free theory path integral. So far we have not approximated anything. In practice we do not know how to systematically calculate all the derivatives of $e^{iW[J]}$ and sum them. We can only compute the terms in the sum of the third line for increasing power in λ. This perturbation is trustworthy for small interaction strengths, i.e. with $\lambda \ll 1$. For strong coupled interactions we can not use this technique.

For the terms linear in λ we start by replacing $e^{-\frac{i}{4!}\lambda \int d^4w [\frac{\delta}{\delta J(w)}]^4}$ by $-\frac{i}{4!}\lambda \int d^4w [\frac{\delta}{\delta J(w)}]^4$ and $e^{iW[J]}$ by $\frac{i^4}{4!2^4} \left[\iint d^4x d^4y\, J(x) D(x-y) J(y) \right]^4$, resulting in the expression

$$-\frac{i}{4!}\lambda \int d^4w [\frac{\delta}{\delta J(w)}]^4 \frac{i^4}{4!2^4} \left[\iint d^4x d^4y\, J(x) D(x-y) J(y) \right]^4$$

$$= -i\lambda \int D(x_a - w) D(x_b - w) D(x_c - w) D(x_d - w)$$

$$\times J(x_a) J(x_b) J(x_c) J(x_d) d^4x_a d^4x_b d^4x_c d^4x_d d^4w.$$

We have to take all possible contractions of the positions x_a, x_b, x_c and x_d with the point w. The term

$$-i\lambda \int D(x_a - w)D(x_b - w)D(x_c - w)D(x_d - w)\mathrm{d}^4 w$$

should be interpreted as the amplitude for two identical particles initially positioned at x_a and x_b to travel to w and scatter to the final positions x_c and x_d. Note that every path, i.e. the paths $x_a, x_b \to w$ and $w \to x_c, x_d$ correspond to a propagator. Feynman had this insight and used this to draw Feynman diagrams and compute cross sections. The Feynman diagram of the term calculated above is represented by the diagram in figure 15.1a. The lines correspond with the propagator, the vertex with a factor $i\lambda$ and the integral over all possible positions of w. In 1949, Freeman Dyson derived the diagrams from the formal work of Julian Schwinger and Shin-Itiro Tomonaga. The Feynman rules for φ^4 theory are

1. Draw a connected Feynman diagram and attach to every line a momentum such that conservation of momentum is satisfied in very vertex.

2. Every vertex corresponds to a coupling $-i\lambda$.

3. Each line corresponds with a propagator with some momentum k. Multiply the propagators.

4. Integrate over the momenta which are not fixed by conservation of momentum. This is often called, integrating over loops.

5. Multiply by some symmetry factor.

The Feynman rules of the φ^4 theory are simple and transparent. This is due to the simplicity of the model. Note however that the theory already contains the most prominent characteristics of quantum field theory. We have simple tree diagrams, but also infinite series of quantum correction in the form of loop diagrams (Feynman diagrams consisting of loops over which we have to integrate). The technique can be used in more physical theories. For quantum electrodynamics, quantum chromodynamics or the standard model, we simply use a more complicated Lagrangian and derive a more extended list of Feynman rules. See figure 15.1b for a Feynman diagram in quantum electrodynamics. Generally the vertices correspond to interactions while a the lines correspond to propagators. In chapter 16, we derive Feynman rules for standard perturbation theory. We will see that many properties of Feynman diagrams in quantum field theory can be translated to standard perturbation theory. This begs the question, whether these properties are really quantum mechanical and not an artifact of the methodology.

15.4 Effective field theory in quantum systems

Quantum field theory gives a good description of physics at the quantum scale. It allows us to calculate cross sections between the fundamental particles from the Lagrangian

(a) tree diagram in φ^4 theory

(b) Electron scattering in quantum electrodynamics
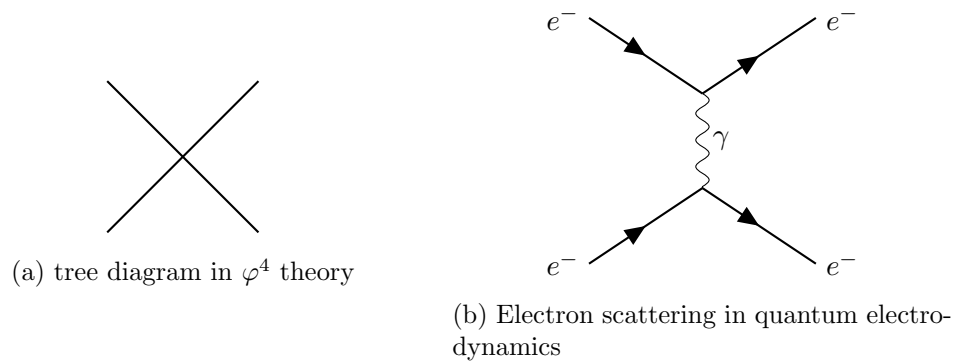
Figure 15.1: Feynman diagrams

of the standard model. It can predict the interactions between, leptons, quarks and bosons. However in some situations, we are not interested in or do not know the physics of the smallest scales. For example, in nuclear physics we do not want do deal with the individual quarks. We instead would like to deal with protons, neutrons and electrons. Another example is the standard model in the setting of string theory. In string theory, all fundamental particles are interpreted as vibrations of strings. If string theory is correct, it should reproduce the standard model in on the scale of quarks, or energy scales probed by collision experiments. In both situations we can use effective field theory.

An effective field theory can be obtained from a fundamental theory by integrating over specific scales. In practice we can start from the fundamental action and path integral, and integrate over the ultraviolet degrees of freedom. This results in a path integral over the interesting degrees of freedom with a modified action. This is the effective action. This effective theory is an approximation but will make it more easy to perform physical analysis.

Effective theories, in which the underlying theory is not well known have appeared in many stages during the development of high energy physics. The theories are normally phenomenological. They are constructed out of empirical data and help us find the underlying fundamental theory. We should however always keep the limitations of the theory in mind. On high energy scales, the effective theory is supposed to be inadequate.

In chapters 17 and 18, we consider effective field theory in large-scale structure formation. By integrating out the small scale structures, we obtain a theory of the large scale structures which includes the influence of the small scale on the large scale fluctuations.

Chapter 16

Standard and Effective Perturbation Theories of Large-Scale Structure

Standard perturbation theory expands the equation of motion in terms of some physical quantity. In Eulerian perturbation theory we expand in terms of the density perturbation. In Lagrangian perturbation theory we expand in terms of the displacement field. The expansion is valid as long as the small-scale non-linear behavior does not significantly influences the linear or mildly non-linear dynamics. In effective field theory we start with the equation of motion and integrate over the small scale physics. In this way we incorporate the influence of the small scale on the large scale, leading to a greater validity of the expansion. In this chapter we systematically develop standard perturbation theory and effective field theory. We follow the approach of Sean Carroll et al. [17].

16.1   Standard perturbation theory

Standard Perturbation Theory (SPT) can be used to approximate solutions of differential equations. In dynamical systems, this often implies approximating the equations of motion. Consider a set of differential equations, hereafter called the equations of motion, of the form

$$\mathcal{D}^i_j \phi^j - \frac{1}{2} M^i_{jk} \phi^j \phi^k - \frac{1}{3!} N^i_{jkl} \phi^j \phi^k \phi^l + \cdots = 0.$$

The 'vector'[1] ϕ contains all physically relevant quantities, such as position or density. In this chapter we will assume that ϕ contains the Fourier transform of the quantities of interest. The matrix $\mathcal{D}$ contains time derivatives and terms linear in ϕ. We here assume that $\mathcal{D}$ only contains first order derivatives. Higher order derivatives can always be implemented via extra parameters in ϕ. The matrices $M, N, \ldots$ contain the coefficients of the couplings between the different components of ϕ. Let $M^i_{jk}, N^i_{jk}, \ldots$, without loss of generality, be symmetric in the lower indices. The field ϕ can be written as a series

---

[1]The vector ϕ does not transform as a vector under rotations and translations.

in a perturbation parameter ϵ,

$$\phi^i_{SPT} = \epsilon \phi^i_{(1)} + \epsilon^2 \phi^i_{(2)} + \epsilon^3 \phi^i_{(3)} + \dots$$

Substituting the series in the equation of motion and sorting by powers of ϵ we obtain a set of differential equations

$$\mathcal{D}^i_j \phi^j_{(1)} = 0$$
$$\mathcal{D}^i_j \phi^j_{(2)} = \frac{1}{2} M^i_{jk} \phi^j_{(1)} \phi^k_{(1)}$$
$$\mathcal{D}^i_j \phi^j_{(3)} = \frac{1}{2} \left(M^i_{jk} \phi^j_{(1)} \phi^k_{(2)} + M^i_{jk} \phi^j_{(2)} \phi^k_{(1)} \right) + \frac{1}{3!} N^i_{jkl} \phi^j_{(1)} \phi^k_{(1)} \phi^l_{(1)}$$
$$= M^i_{jk} \phi^j_{(1)} \phi^k_{(2)} + \frac{1}{3!} N^i_{jkl} \phi^j_{(1)} \phi^k_{(1)} \phi^l_{(1)}$$
$$\dots$$

In large-scale structure formation problems we are interested in the evolution of density fluctuations, evolving due to gravity. We evolve an initial distribution ϕ^i_{in} at time τ_{in} to a distribution ϕ at time τ. The first equation can be solved by the retarded Green function

$$\phi^i_{(1)}(\tau) = G^i_j(\tau, \tau_{in}) \phi^j_{in},$$

with the Green function G satisfying the condition

$$\mathcal{D}^i_j G^j_k(\tau; \tau_{in}) = \delta^i_k \delta^{(1)}(\tau - \tau_{in}).$$

By substituting $\phi_{(1)}$ in the corresponding differential equation, we can easily check that this expression works. The second correction $\phi_{(2)}$ can be solved in terms of $\phi_{(1)}$ and the third correction can subsequently be solved by using the solution of $\phi_{(1)}$ and $\phi_{(2)}$. This leads to a tower of solutions,

$$\phi^i_{(2)}(\tau) = \frac{1}{2} \int_{\tau_{in}}^{\tau} \mathrm{d}\tau' G^i_j(\tau, \tau') M^j_{kl}(\tau') \phi^k_{(1)}(\tau') \phi^l_{(1)}(\tau'),$$
$$\phi^i_{(3)}(\tau) = \int_{\tau_{in}}^{\tau} \mathrm{d}\tau' G^i_j(\tau, \tau') M^j_{kl}(\tau') \phi^k_{(2)}(\tau') \phi^l_{(1)}(\tau')$$
$$+ \frac{1}{3!} \int_{\tau_{in}}^{\tau} \mathrm{d}\tau' G^i_j(\tau, \tau') N^j_{klm}(\tau') \phi^k_{(1)}(\tau') \phi^l_{(1)}(\tau') \phi^m_{(1)}(\tau'),$$

in which all corrections can be iteratively solved. In practice often only the lower order corrections are relevant.

16.1.1 Solutions and tree diagrams

Richard Feynman provided a systematic pictorial way to perform such an expansion in quantum field theory. We can perform an analogous derivation in the standard perturbation theory setting. The terms $\phi^i_{(1)}, \phi^i_{(2)}, \phi^i_{(3)}$, can be represented by the diagrams of
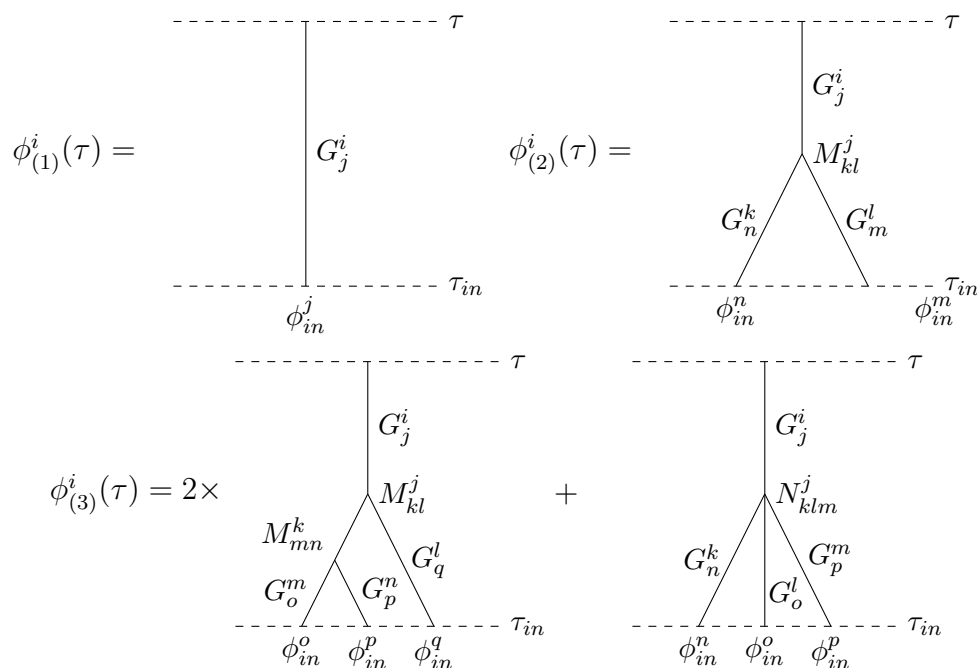
Figure 16.1: Feynman diagrams of first, second and third perturbations

figure 16.1. The lower and upper horizontal line represent ϕ_{in} and ϕ respectively. The vertices on the lower horizontal line correspond to the initial conditions ϕ_{in}. The line segments correspond to the Green function G and play the role of the propagator. The vertices in the diagram correspond to the interaction terms. The three point vertices correspond to M, the four point vertices to N. We finally integrate over the times at which the vertices are evaluated. Note that the number of vertices on the horizontal initial field line is equal to the order of the perturbation. The proportionality constants of the diagrams are symmetry factors.

16.1.2   Correlation functions and loop diagrams

So far, the framework of Feynman diagrams in standard perturbation theory is completely analogous to tree diagrams in quantum field theory. The evolution of an initial condition in time correspond to a onshell interaction[2]. In quantum field theory we are however not restricted to onshell interactions and can consider loop diagrams in which we integrate over the momentum 'running in the loop' (see figure 16.3). It turns out that the analogy extends further than tree diagrams. We here show how correlation functions in standard perturbation theory can be interpreted as loop diagrams.

  Using standard perturbation theory, we can approximate correlation functions. Up

---

[2]Interactions in which all momenta of the lines are fixed by the conservation of momentum.
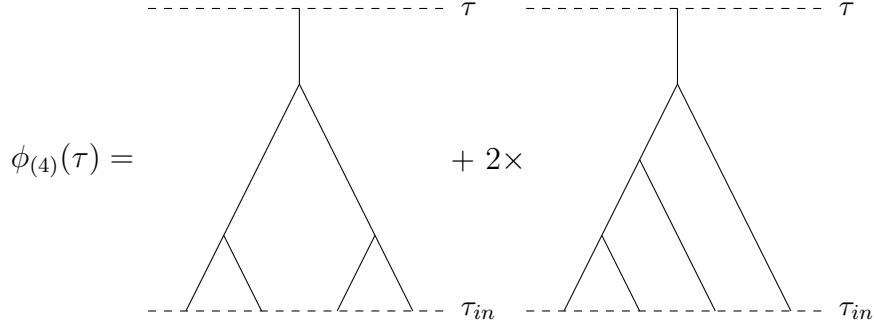
Figure 16.2: The Feynman diagram of the fourth perturbation, assuming $N^i_{jkl} = 0$ for all indices
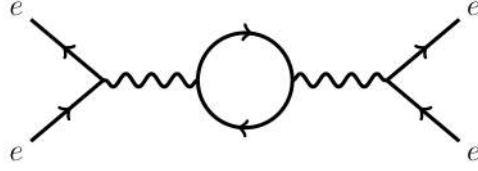

Figure 16.3: A loop diagram in quantum electro dynamics

to fourth order in ϵ, the two-point correlation function of ϕ is

$$
\begin{aligned}
\langle \phi_{SPT} \phi_{SPT} \rangle =& \langle (\epsilon\phi_{(1)} + \epsilon^2\phi_{(2)} + \dots)(\epsilon\phi_{(1)} + \epsilon^2\phi_{(2)} + \dots) \rangle \\
=& \epsilon^2 \langle \phi_{(1)}\phi_{(1)} \rangle + 2\epsilon^3 \langle \phi_{(1)}\phi_{(2)} \rangle + \epsilon^4 (2\langle \phi_{(1)}\phi_{(3)} \rangle + \langle \phi_{(2)}\phi_{(2)} \rangle) + \dots
\end{aligned}
$$

Lets first analyze the quadratic correction

$$
\langle \phi_{(1)}\phi_{(1)} \rangle.
$$

We can substitute the solution of $\phi_{(1)}$ in terms of the initial condition ϕ_{ln} and pull the expectation value brackets towards the initial conditions,

$$
\begin{aligned}
\langle \phi^i_{(1)}(\mathbf{k}_1)\phi^j_{(1)}(\mathbf{k}_2) \rangle =& \langle G^i_k(\tau, \tau_{in})\phi^k_{in}(\mathbf{k}_1)G^l_i(\tau, \tau_{in})\phi^l_{in}(\mathbf{k}_2) \rangle \\
=& G^i_k(\tau, \tau_{in})G^l_i(\tau, \tau_{in})\langle \phi^k_{in}(\mathbf{k}_1)\phi^l_{in}(\mathbf{k}_2) \rangle \\
=& (2\pi)^d\delta^{(d)}(\mathbf{k}_1 + \mathbf{k}_2)G^i_k(\tau, \tau_{in})G^l_i(\tau, \tau_{in})P^{ij}(\mathbf{k}_1),
\end{aligned}
$$

with P the power spectrum of the initial conditions and d the number of spatial dimensions. This term in the correlation function can be represented by two lines, connected by the power spectrum (see figure 16.4). By performing a similar analysis on the cubic correction

$$
\langle \phi_{(1)}\phi_{(2)} \rangle,
$$

we can show that it vanishes. This is due to the fact that the expectation value for the product of an odd number of Gaussian statistics is zero. The fourth order correction turn out to be more complex. First consider the two-point correlation between the first and third order correction

$$\langle \phi_{(1)} \phi_{(3)} \rangle.$$

We can again substitute the solutions and pull the expectation value brackets towards the initial conditions. Under the assumption that $N = 0$, the correlation function turns out to be

$$
\begin{aligned}
\langle \phi_{(1)}^i(\mathbf{k}_1) \phi_{(3)}(\mathbf{k}_2) \rangle =& (2\pi)^d \delta^{(d)}(\mathbf{k}_1 + \mathbf{k}_2) \\
& \times \int_{\tau_{ln}}^{\tau} \mathrm{d}\tau' \int_{\tau_{ln}}^{\tau'} \mathrm{d}\tau'' \int \frac{\mathrm{d}\mathbf{q}}{(2\pi)^d} G_k^j(\tau, \tau') M_{lm}^k(\mathbf{k}_1, \mathbf{q}, \mathbf{k}_1 - \mathbf{q}) G_n^m(\tau', \tau'') \\
& \times M_{op}^n(\mathbf{k}_1 - \mathbf{q}, -\mathbf{q}, \mathbf{k}_1) G_q^i(\tau, \tau_{ln}) G_r^p(\tau'', \tau_{ln}) P^{qr}(\mathbf{k}_1) \\
& \times G_s^l(\tau', \tau_{ln}) G_t^o(\tau'', \tau_{ln}) P^{st}(\mathbf{q}).
\end{aligned}
$$

In terms of Feynman diagrams, this expression can be expressed as the contraction between first and third order correction, as illustrated in figure 16.4. One of the legs of the third order correction is connected with the first order correction while the other two legs are connected with each other. We subsequently integrate over the momentum running in the loop. In our example we integrate over the momentum $\mathbf{q}$ and weight it with the power spectrum. Another interesting correlation function is the two-point correlation function of the second order corrections

$$\langle \phi_{(2)} \phi_{(2)} \rangle.$$

The corresponding loop diagram, assuming $M = 0$ is illustrated in figure 16.4. We again integrate over the momentum running in the loop. Note that not all diagrams can be completely contracted in this fashion. We need an even number of vertices on the lower horizontal line. It can however be proven that the correlation function of diagrams with an odd number of vertices on the lower horizontal line are zero for Gaussian random field initial conditions.

16.2   Effective equation of motion

In the previous section we developed standard perturbation theory in a systematic fashion using Feynman-like diagrams. In this section we smooth the equations of motion with a kernel W_Λ and determine the corresponding perturbation theory. We only take into account the linear and quadratic terms in the equation of motion, i.e. only $\mathcal{D}$ and M can be nonzero. It is straightforward to extend the approach to higher orders.

In this chapter we will use the smoothing kernel

$$\hat{W}_\Lambda(\mathbf{k}) = \Theta(\Lambda - |\mathbf{k}|)$$
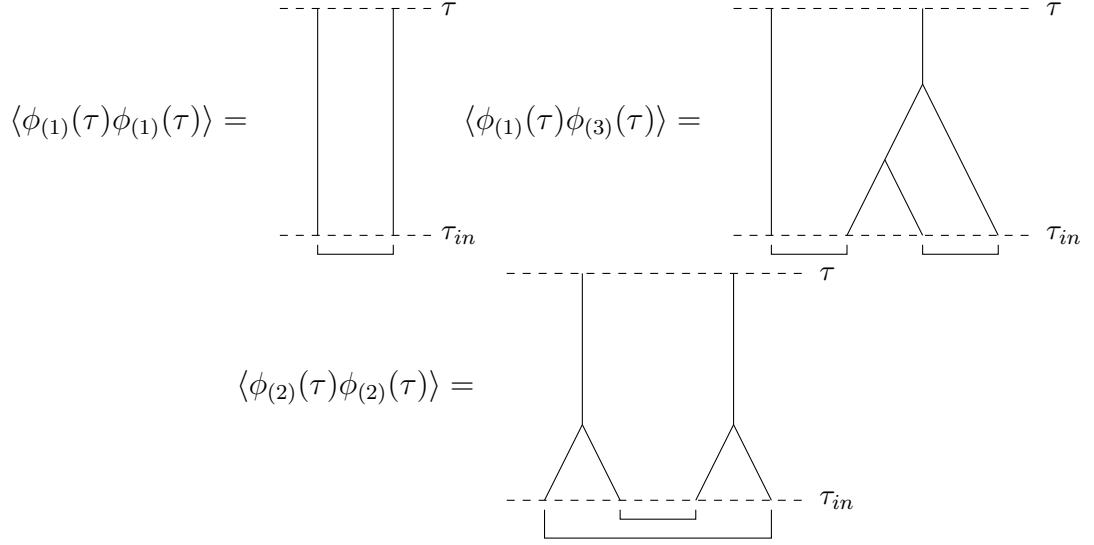
Figure 16.4: The Feynman diagram of the two-point correlation function of the second and third perturbation

although other kernels can easily be implemented. For variables ϕ^i we define the long wavelength fluctuations to be

$$\phi_L^i(\mathbf{k}) = \hat{W}_\Lambda(\mathbf{k})\phi^i(\mathbf{k})$$

for all $\mathbf{k}$ and the sort wavelength fluctuations as

$$\phi_S = \phi - \phi_L.$$

Assuming the operator $\mathcal{D}$ is diagonal in momentum space

$$
\begin{aligned}
0 =& \mathcal{D}_j^i \phi_L^i - \frac{1}{2}\hat{W}_\Lambda M_{jk}^i \phi^j \phi^k \\
=& \mathcal{D}_j^i \phi_L^i - \frac{1}{2}\hat{W}_\Lambda M_{jk}^i \phi_L^j \phi_L^k - \hat{W}_\Lambda M_{jk}^i \phi_S^j \phi_L^k - \frac{1}{2}\hat{W}_\Lambda M_{jk}^i \phi_S^j \phi_S^k.
\end{aligned}
$$

The first two terms represent dynamics of long wavelength physics. The third term the interaction between long and short and the fourth self interactions of sort-wavelength physics. So far we have only rewritten the equation of motion. In an effective field theory we want to express ϕ_S in terms of ϕ_L and integrate over the short-wavelength physics. In order to do this, consider the difference between the equation of motion and the equation above

$$0 = \mathcal{D}_j^i \phi_S^j - \frac{1}{2}(1 - \hat{W}_\Lambda)M_{jk}^i \phi_S^j \phi_S^k - (1 - \hat{W}_\Lambda)M_{jk}^i \phi_L^j \phi_S^k - \frac{1}{2}(1 - \hat{W}_\Lambda)M_{jk}^i \phi_L^j \phi_L^k.$$

If we let ϕ_L be a background field we can write the short wavelength field ϕ_S as a function of the long wavelength field $\phi_S[\phi_L]$ and substitute this equation in the equation of motion

derived above. If we could analytically obtain $\phi_S[\phi_L]$, there would be no reason to use effective field theory. We would have solved the complete non-linear problem, and have simultaneously solved one of the millennium problems. We can however write ϕ_S as a Taylor series in ϕ_L and obtain coefficients from observations or N-body simulations. The Taylor series reads

$$\phi_S^i(\tau) = \phi_{S0}^i(\tau) + \int_{\tau_{in}}^{\tau} \frac{\partial \phi_S^i(\tau)}{\partial \phi_L^j(\tau')}\bigg|_{\phi_L=0} \phi_L^j(\tau')\mathrm{d}\tau' + \dots,$$

with $\phi_S[\phi_L = 0] = \phi_{S0}$ the solution of the differential equation for ϕ_S with $\phi_L = 0$ leading to the condition

$$0 = \mathcal{D}_j^i \phi_S^j - \frac{1}{2}(1 - \hat{W}_\Lambda)M_{jk}^i \phi_S^j \phi_S^k.$$

The integral in the second term of the expansion runs from the initial time τ_{in} to the time τ at which it is evaluated. This integral contains the history of small scale fluctuations as a function of large scale. This is one of the fundamentally different properties of effective field theory for large-scale structures with respect to effective field theory in particle physics in which no such integral appears.

   We can include higher-order terms, but will in this thesis restrict our calculation to the linear order. Cutting of the Taylor expansion to linear order and inserting the equation in the equation of motion we obtain the effective equation of motion

$$\begin{aligned}
0 =& \mathcal{D}_j^i \phi_L^j - \frac{1}{2}\hat{W}_\Lambda M_{jk}^i \phi_L^j \phi_L^k - \hat{W}_\Lambda M_{jk}^i \phi_{S0}^j \phi_L^k - \frac{1}{2}\hat{W}_\Lambda M_{jk}^i \phi_{S0}^j \phi_{S0}^k \\
& - \hat{W}_\Lambda M_{jk}^i \phi_{S0}^j \int_{\tau_{in}}^{\tau} \frac{\partial \phi_S^k(\tau)}{\partial \phi_L^l(\tau')} \phi_L^l(\tau')\mathrm{d}\tau' - \hat{W}_\Lambda M_{jk}^i \phi_L^j \int_{\tau_{in}}^{\tau} \frac{\partial \phi_S^k(\tau)}{\partial \phi_L^l(\tau')} \phi_L^l(\tau')\mathrm{d}\tau',
\end{aligned}$$

in which the differentials are evaluated at $\phi_L = 0$.

16.2.1 Effective perturbation theory

We now use the standard perturbation theory developed in the section above to derive a perturbative solution of the effective field equation of motion derived above. The long wavelength field can be written as

$$\phi_L^i = \epsilon\left(\phi_{L(1)}^i + \Delta\phi_{L(1)}^i\right) + \epsilon^2\left(\phi_{L(2)}^i + \Delta\phi_{L(2)}^i\right) + \epsilon^3\left(\phi_{L(3)}^i + \Delta\phi_{L(3)}^i\right) + \dots$$

in which $\phi_{L(n)}^i$ is defined to be equal to the standard perturbation theory term $\phi_{(1)}^i$ with $M_{ij}^k \to \hat{W}_\Lambda M_{ij}^k$, and $\phi_{in}^i \to \hat{W}_\Lambda \phi_{in}^i$. The term $\Delta\phi_{L(n)}^i$ represents the influence of short-wavelength physics on the solutions. This is the effective field theory term which appears in the solution. If we now substitute this series in the effective equation of motion and

sort in terms of ϵ we obtain the set of equation of motion for $\Delta\phi^i_{L(n)}$,

$$\mathcal{D}^i_j \Delta\phi^j_{L(1)} = 0$$

$$\mathcal{D}^i_j \Delta\phi^j_{L(2)} = \hat{W}_\Lambda M^i_{jk} \phi^j_{S0} \phi^k_{L(1)} + \frac{1}{2} \hat{W}_\Lambda M^i_{jk} \phi^j_{S0} \phi^k_{S0}$$

$$\mathcal{D}^i_j \Delta\phi^j_{L(3)} = \hat{W}_\Lambda M^i_{jk} \phi^j_{S0} \left(\phi^k_{L(2)} + \Delta\phi^k_{L(2)} \right) + \hat{W}_\Lambda M^i_{jk} \left(\phi^j_{S0} + \phi^j_{L(1)} \right) \int_{\tau_{in}}^\tau \frac{\partial \phi^k_S(\tau)}{\partial \phi^l_L(\tau')} \phi_{L(1)}(\tau') \mathrm{d}\tau'$$

$$\cdots$$

with the differentials being evaluated at $\phi_L = 0$.

Since we have the initial conditions in the expression $\phi^i_{L(1)}$ we can solve $\Delta\phi^i_{L(1)}$ with the trivial solution

$$\Delta\phi^i_{L(1)} = 0.$$

The solutions of the second and third equations of motion are

$$\Delta\phi^i_{L(2)} = \int_{\tau_{in}}^\tau G^i_j(\tau, \tau') \left[\hat{W}_\Lambda M^j_{kl} \phi^k_{S0} \phi^l_{L(1)} + \frac{1}{2} \hat{W}_\Lambda M^i_{kl} \phi^k_{S0} \phi^l_{S0} \right],$$

$$\Delta\phi^i_{L(3)} = \int_{\tau_{in}}^\tau G^i_j(\tau, \tau') \left[\hat{W}_\Lambda M^j_{kl} \phi^k_{S0} (\phi^l_{L(2)} + \Delta\phi^l_{L(2)}) \right.$$
$$\left. + \hat{W}_\Lambda M^j_{kl} (\phi^k_{S0} + \phi^k_{L(1)}) \left[\int_{\tau_{in}}^{\tau'} \frac{\partial \phi^l_S(\tau')}{\partial \phi^m_L(\tau'')} [G(\tau', \tau'')^{-1}]^m_n \mathrm{d}\tau'' \right] \phi^n_{L(1)}(\tau') \mathrm{d}\tau'' \right],$$

where we used the inverse Green function G^{-1} in the expression of the short-wavelength effect. This inverse exists since large-scale structure formation is invertible. The term

$$\frac{\partial \phi_S}{\partial \phi_L},$$

cannot be determined from first principle. It should either be measured from direct observations or N-body simulations. Carroll et al. have extended the Feynman rules of standard perturbation theory, to include the effective corrections. In this thesis we do this implicitly by performing standard perturbation theory on the effective equations of motion.

Chapter 17

Perturbation Theory of Eulerian Large-Scale Structure Formation

In chapter 3 we studied the equations of motion which govern the formation of large-scale structure. In chapter 16 we studied the general framework of effective field theory. In this chapter we study standard perturbation theory and effective field theory of large-scale structure formation in the Eulerian setting. We follow the work of Sean Carroll et al. [17] and Carrasco et al. [16].

17.1   Eulerian equations of motion

In the Eulerian setting the evolution is governed by the conservation of mass, Euler and Poisson equations. In comoving coordinates they can be expressed as

$$
\begin{aligned}
0 &= \partial_\tau \delta + \partial_j((1+\delta)v^j), \\
0 &= \partial_\tau v^i + \mathcal{H} v^i + \partial^i \Psi + v^i \partial_j v^j, \\
0 &= \delta^{ij} \partial_i \partial_j \Psi + 4\pi G a^2 \rho_u \delta,
\end{aligned}
$$

with matter perturbation $\delta = \frac{\rho - \rho_b}{\rho_b}$, velocity v^i with respect to conformal time $\tau(t) = \int_0^t \frac{dt'}{a(t')}$, conformal Hubble parameter $\mathcal{H} = (\partial_\tau a)/a$, mean density ρ_u, scale factor a and gravitational potential Ψ. Using the convolution theorem, these equations can be expressed in Fourier space as

$$
\partial_\tau \hat{\delta}(\mathbf{k}) - i\mathbf{k} \cdot \hat{v}(\mathbf{k}) - \int \frac{d\mathbf{k}'}{(2\pi)^3} i\hat{\delta}(\mathbf{k}')\mathbf{k}' \cdot \hat{v}(\mathbf{k} - \mathbf{k}') = 0
$$

$$
\partial_\tau \hat{v}^i(\mathbf{k}) + \mathcal{H}\hat{v}^i(\mathbf{k}) - \int \frac{d\mathbf{k}'}{(2\pi)^3} [i\hat{v}^i(\mathbf{k}') \cdot (\mathbf{k} - \mathbf{k}')\hat{v}^i(\mathbf{k} - \mathbf{k}')] = ik^i \hat{\Psi}
$$

$$
-4\pi G \rho_u \frac{\hat{\delta}(\mathbf{k})}{k^2} = \frac{\hat{\Psi}}{a^2}.
$$

185

On large scales the dark matter fluid is assumed to have a gradient velocity field, i.e. vanishing curl. For this reason we work with the divergence of the velocity field $\theta = \partial_i v^i$, which is a scalar and contains the same information. In Fourier space θ can be written as $\hat{\theta} = -ik_i \hat{v}^i$. The equations of motion for this choice of parameters are

$$0 = \partial_\tau \hat{\delta}(\tau, \mathbf{k}) + \hat{\theta}(\tau, \mathbf{k}) + \int \frac{\mathrm{d}^3 q}{(2\pi)^3} \frac{\mathbf{k} \cdot \mathbf{q}}{q^2} \hat{\delta}(\tau, \mathbf{k} - \mathbf{q}) \hat{\theta}(\tau, \mathbf{q}),$$

$$0 = \partial_\tau \hat{\theta}(\tau, \mathbf{k}) + \mathcal{H} \hat{\theta}(\tau, \mathbf{k}) + \frac{3}{2} \mathcal{H}^2 \hat{\delta}(\tau, \mathbf{k}) + \int \frac{\mathrm{d}^3 q}{(2\pi)^3} \frac{k^2 \mathbf{q} \cdot (\mathbf{k} - \mathbf{q})}{2q^2 (\mathbf{k} - \mathbf{q})^2} \hat{\theta}(\tau, \mathbf{k} - \mathbf{q}) \hat{\theta}(\tau, \mathbf{q}),$$

where we have substituted the Poisson equation to obtain a system of two differential equations with two unknowns.

17.2 Standard perturbation theory

We can write the system of differential equations in a more condensed form as

$$0 = \mathcal{D}_j^i \phi^j - \frac{1}{2} M_{jk}^i \phi^j \phi^k,$$

with

$$\phi(k) = \begin{pmatrix} \hat{\delta}(k) \\ \hat{\theta}(k) \end{pmatrix}.$$

The fact that the differential equation only contains linear and quadratic terms in ϕ restrict our Feynman diagrams to three point vertices. The linear terms of the equation are written in terms of the tensor $\mathcal{D}$ given by

$$\mathcal{D}_j^i = \begin{pmatrix} \partial_\tau & 1 \\ \frac{3}{2} \mathcal{H}^2 & \partial_\tau \end{pmatrix},$$

while the quadratic terms are written in terms of the tensor M defined as

$$M_{ij}^\delta(k_1; k_2, k_3) = \begin{pmatrix} 0 & -\frac{k_1 k_3}{k_3^2} \\ -\frac{k_1 k_2}{k_2^2} & 0 \end{pmatrix},$$

$$M_{ij}^\theta(k_1; k_2, k_3) = \begin{pmatrix} 0 & 0 \\ 0 & -\frac{k_1^2}{k_2 k_3} \end{pmatrix}.$$

In order to perform standard perturbation theory on this equation, we determine the retarded Green function G. The Green function satisfies

$$\mathcal{D}_j^i G_k^j(\tau; \tau_{in}) = \delta_k^i \delta^{(1)}(\tau - \tau_{in}).$$

$$\phi^i_{(1)}(\tau) = \qquad\qquad G^i_j \qquad\qquad \phi^i_{(2)}(\tau) =$$
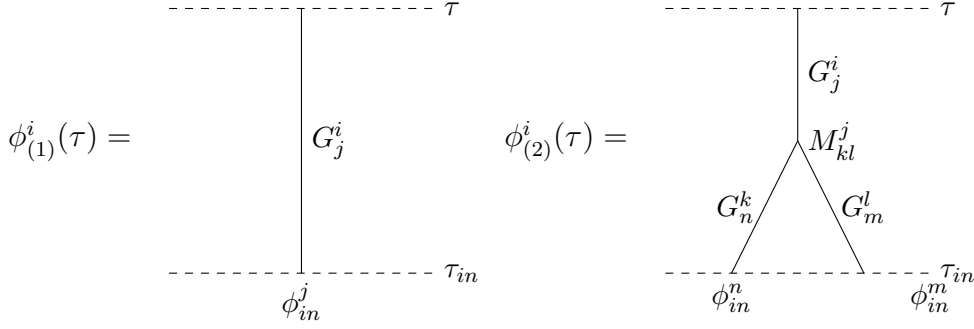
Figure 17.1: The first and second order approximation in standard perturbation theory

For a Einstein-de Sitter universe, this condition is solved by

$$G^i_k(\tau_1; \tau_2) = \begin{pmatrix} \frac{3\tau_1^5 + 2\tau_2^5}{5\tau_1^3\tau_2^2} & \frac{-\tau_1^5 + \tau_2^5}{5\tau_1^3\tau_2} \\ -\frac{6(\tau_1^5 - \tau_2^5)}{5\tau_1^4\tau_2^2} & \frac{2\tau_1^5 + 3\tau_2^5}{5\tau_1^4\tau_2} \end{pmatrix} \Theta(\tau_1 - \tau_2).$$

The propagator G and interaction matrix M allow us to perform standard perturbation theory. The first order correction is

$$\phi^i_{(1)}(\tau) = G^i_j(\tau, \tau_{in})\phi^j_{in}.$$

This corresponds to a Feynman diagram consisting of a vertical line, see figure **??**. Different Fourier modes evolve independently. The second order correction is of the form

$$\phi^i_{(2)}(\tau) = \int_{\tau_{in}}^{\tau} \mathrm{d}\tau' G^i_j(\tau, \tau') M^j_{kl}(\tau') \phi^k_{(1)}(\tau') \phi^l_{(1)}(\tau')$$

$$= \int_{\tau_{in}}^{\tau} \mathrm{d}\tau' G^i_j(\tau, \tau') M^j_{kl}(\tau') G^k_m(\tau', \tau_{in}) \phi^m_{in} G^l_n(\tau', \tau_{in}) \phi^n_{in}.$$

The interaction matrix M couples different Fourier modes and different components of ϕ. This corresponds to a vertex in the corresponding Feynman diagrams, see figure **??**. The integral over time represents different moments at which the coupling can take place. Higher order corrections will contain more vertices and have more involved couplings between different Fourier modes of δ and θ.

17.3   Eulerian effective field theory

In the standard perturbation theory we approximated solutions of the standard equation of motion

$$0 = \mathcal{D}^i_j \phi^j_L - \frac{1}{2} M^i_{jk} \phi^j_L \phi^k_L.$$

In an effective theory we integrate over small scale physics. This results in additional terms in the equations of motion. Formally up to linear order, the effective equation of motion is

$$
\begin{aligned}
0 =& \mathcal{D}^i_j \phi^j_L - \frac{1}{2}\hat{W}_\Lambda M^i_{jk}\phi^j_L\phi^k_L - \hat{W}_\Lambda M^i_{jk}\bigg[\phi^j_{S0}\phi^k_L + \frac{1}{2}\phi^j_{S0}\phi^k_{S0} \\
&+ \phi^j_{S0}\int_{\tau_{in}}^{\tau}\frac{\partial\phi^k_S(\tau)}{\partial\phi^l_L(\tau')}\phi^l_L(\tau')\mathrm{d}\tau' + \phi^j_L\int_{\tau_{in}}\frac{\partial\phi^k_S(\tau)}{\partial\phi^l_L(\tau')}\phi^l_L(\tau')\mathrm{d}\tau'\bigg],
\end{aligned}
$$

with the first two terms being the original equation of motion for long wavelength modes with long wavelength interactions. The remaining terms are the effective contributions. The effective contributions should be measured from observations or N-body simulations, since we do not know the behavior of

$$
\frac{\partial\phi^k_S(\tau)}{\partial\phi^l_L(\tau')}.
$$

It is a function of the times τ and τ' and expresses the influence of the small scale physics on the large scale fluctuations. One fundamental difference between effective field theory in large-scale structure formation and quantum field theory can be seen from this functional differential. It can in principle contain information of the past, i.e. the derivative can be large for $\tau' \ll \tau$. The evolution of the small scale physics in a cluster can depend nature of the inflow of matter in at an earlier time. The derivative can furthermore differ in different environments. This phenomenon does not occur in quantum field theory since all fundamental particles of the same species are identical and do not contain some form of hysteresis. Although promising and insightful, we do not yet know much about this differential. More research is needed to extend the use of this formalism.

There however exist different approaches to effective field theory of large-scale structure formation. Baumann et al. [9] and Carrasco et al. [16] performed analyses on the Boltzmann equation and derived similar corrections. They showed that the corrections can be interpreted as an imperfect fluid. Mercolli and Pajer [49] used Newtonian symmetries to derive effective corrections. Their corrections include the perfect fluid corrections of Baumann and Carrasco but are a bit more general. See appendix B for a sketch of the derivation. Carroll et al. [17] connected the effective corrections described above to the corrections of Mercolli and Pajer with the identification

$$
\begin{aligned}
&-\hat{W}_\Lambda M^i_{jk}\bigg[\phi^j_{S0}\phi^k_L + \frac{1}{2}\phi^j_{S0}\phi^k_{S0} + \phi^j_{S0}\int_{\tau_{in}}^{\tau}\frac{\partial\phi^k_S(\tau)}{\partial\phi^l_L(\tau')}\phi^l_L(\tau')\mathrm{d}\tau' + \phi^j_L\int_{\tau_{in}}\frac{\partial\phi^k_S(\tau)}{\partial\phi^l_L(\tau')}\phi^l_L(\tau')\mathrm{d}\tau'\bigg]\\
&=C^i_l(\tau,k)\phi^l(k),
\end{aligned}
$$

with

$$
C^i_l(\tau,k) = \begin{pmatrix} \chi^\delta & \chi^\theta \\ k^2 c_s^2 & -k^2\frac{c_v^2}{\mathcal{H}} \end{pmatrix}.
$$

The parameters $\chi^\delta, \chi^\theta, c_s$ and c_v are analogous to the heat conduction coefficients, viscosity and speed of sound of an imperfect fluid but can depend on time. In terms of these functions, the effective equations of motion are

$$0 = \mathcal{D}_j^i \phi_L^j - \frac{1}{2} \hat{W}_\Lambda M_{jk}^i \phi_L^j \phi_L^k + C_j^i(\tau, k) \phi_L^j(k)$$

$$= [\mathcal{D}_j^i + C_j^i(\tau, k)] \phi_L^j - \frac{1}{2} \hat{W}_\Lambda M_{jk}^i \phi_L^j \phi_L^k.$$

Hence in effective perturbation theory, up to linear order, we only modify the Green function.

Chapter 18

Perturbation Theory of Lagrangian Large-Scale Structure Formation

In chapter 3 we studied the equations of motion which govern the formation of large-scale structure. In chapter 16 we studied the general framework of effective field theory. In chapter 17 we applied standard perturbation theory to the Eulerian fluid equations. In this chapter we study standard and effective perturbation theory of large-scale structure formation in the Lagrangian setting. For the Lagrangian approach we follow Porto et al. [56]. We start with standard perturbation theory and then apply effective field corrections.

18.1 Lagrangian standard perturbation theory in single-flow regions

In 1970, Zel'dovich [72] derived a linear Lagrangian approximation of large-scale structure formation. Bouchet et al. in 1992 [12] and Buchert and Ehlers in 1993 [15] extended Zel'dovich's approach to second order and obtained what is now known as the 2LPT model (Second order Lagrangian Perturbation Theory). In 1994 and 1995, Buchert [14], Bouchet et al. [11] and Catelan [19] studied the third order approximation, known as 3LPT. The fourth order approximation, known as 4LPT, was investigated by Venselow [68], Shiraishi [62] and Sasaki and Kasai [61]. These approaches were mainly aimed at gradient displacement fields. Tatekawa [65] performed in 2013 a complete analysis of Lagrangian perturbations theory with a general displacement fields up to fourth order.

   In this chapter we follow the notation of Tatekawa and cast the Lagrangian perturbation theory in the Feynman diagram notation described in the previous chapter. The

Eulerian large-scale structure formation equations can be written as

$$\frac{\partial \delta}{\partial t} + \frac{1}{a}\nabla_x \cdot [\mathbf{v}(1 + \delta)] = 0,$$
$$\frac{\partial \mathbf{v}}{\partial t} + \frac{1}{a}(\mathbf{v} \cdot \nabla_x)\mathbf{v} + \frac{\dot{a}}{a}\mathbf{v} = \frac{1}{a}\mathbf{g},$$
$$\nabla_x \times \mathbf{g} = 0,$$
$$\nabla_x \cdot \mathbf{g} = -4\pi G \rho_b a \delta,$$
$$\delta = \frac{\rho - \rho_b}{\rho_b}.$$

In the Lagrangian framework we consider the evolution of infinitesimal fluid elements, displaced according to the map

$$\mathbf{q} \mapsto \mathbf{x} = \mathbf{q} + \mathbf{s}(\mathbf{q}, t)$$

with $\mathbf{q}$ the initial position, $\mathbf{x}$ the final position and $\mathbf{s}$ the displacement. The conservation of mass has a natural form in the Lagrangian perspective. Since the fluid elements flow with the fluid, a fluid element always contains the same mass. Mathematically, the volume of a fluid element can be obtained by multiplying with a Jacobian. The density goes as one over the Jacobian. As a consequence, we can write the conservation of mass as

$$\delta = 1 - J^{-1}$$

with for regions without shell crossing

$$J = \det\left(I + \frac{\partial s_i}{\partial q_j}\right).$$

Note that in multi-flow regions, we have to apply this formula to all flows and add over the densities of the flows. In this section we will only consider single-flow regions. This is one of the major restrictions of the perturbation theory derived in this section. In the rest of this chapter we will abbreviate partial derivatives with respect to Lagrangian coordinates by commas, i.e., $\partial s_i/\partial q_j = s_{i,j}$. The Euler and Poisson equations can be combined and form the central equations of this section

$$\nabla_x \cdot \left(\ddot{\mathbf{s}} + 2\frac{\dot{a}}{a}\dot{\mathbf{s}}\right) = -4\pi G \rho_b (J^{-1} - 1),$$
$$\nabla_x \times \left(\ddot{\mathbf{s}} + 2\frac{\dot{a}}{a}\dot{\mathbf{s}}\right) = 0.$$

In general the displacement field $\mathbf{s}$ can be decomposed in a longitudinal and transversal part

$$\mathbf{s} = \mathbf{s}^L + \mathbf{s}^T,$$

with

$$\nabla \cdot \mathbf{s}^T = 0 \text{ and } \mathbf{s}^L = \nabla S,$$

for some scalar field S. In this section we consider a gradient displacement field, i.e., $\mathbf{s}^T = 0$. Under this assumption we only have the divergence differential equation and can write the evolution equation as

$$\frac{\partial}{\partial x_i} \left(\ddot{S}_i + 2\frac{\dot{a}}{a}\dot{S}_i \right) = -4\pi G \rho_b (J^{-1} - 1).$$

The calculations presented here can however trivially be extended to include transversal component of $\mathbf{s}$, and the curl equation. In the divergence equation we still have a partial derivative in Eulerian $\mathbf{x}$-directions. This derivative can be traced back to the Poisson equation, which contains a Laplacian with respect to the Eulerian position. Fortunately we can use the definition of the displacement field to express partial derivatives with respect to Eulerian positions in terms of partial derivatives with respect to Lagrangian positions via the expansion

$$\begin{aligned}
\frac{\partial}{\partial x_i} &= \frac{\partial}{\partial q_i} - s_{j,i}\frac{\partial}{\partial x_j} \\
&= \frac{\partial}{\partial q_i} - s_{j,i}\frac{\partial}{\partial q_j} + s_{j,i}s_{k,j}\frac{\partial}{\partial x_k} \\
&= \frac{\partial}{\partial q_i} - s_{j,i}\frac{\partial}{\partial q_j} + s_{j,i}s_{k,j}\frac{\partial}{\partial q_k} - \dots
\end{aligned}$$

This transformation can be written more formally as

$$\frac{\partial}{\partial x_i} = (M^{-1})_{ij}\frac{\partial}{\partial q_j},$$

with the matrix M given by the components

$$M_{ij} = \delta_{ij} + S_{,ij},$$

with δ the Kronecker delta. In the sections below, we analyze the perturbation theory up to second order, assuming a gradient displacement field, in one-, two-, and three-dimensional models of the universe.

18.1.1   One-dimensional universe

In one dimension the Lagrangian evolution equation states

$$(1 - S_{,11} + S_{,11}^2 - S_{,11}^3 + \dots) \left(\ddot{S}_{,11} + 2\frac{\dot{a}}{a}\dot{S}_{,11} \right) = -4\pi G \rho_b (J^{-1} - 1),$$

with $J = 1 + S_{,11}$. Using the Taylor series around $x = 0$,

$$\frac{1}{1+x} = 1 - x + x^2 - x^3 + \dots,$$

the equation simplifies to

$$\ddot{S}_{,11} + 2\frac{\dot{a}}{a}\dot{S}_{,11} = 4\pi G\rho_b S_{,11}.$$

Note that this simplification follows directly from the alternative transformation from Eulerian to Lagrangian partial derivatives. This differential equation is a harmonic oscillator and allows solutions of the form

$$S(\mathbf{q}, t) = \left[C_1 e^{-it\left(\dot{a}/a + \sqrt{4\pi G\rho_b + (\dot{a}/a)^2}\right)} + C_2 e^{-it\left(\dot{a}/a - \sqrt{4\pi G\rho_b + (\dot{a}/a)^2}\right)} \right] \psi(\mathbf{q}),$$

with the constants C_1, C_2 and the function ψ. Both C_1, C_2, and ψ can be obtained from the initial conditions. In general one of the exponentials will decay, while the other grows in time. If we ignore the decaying mode and write the growing mode as $D_+(t)$, we get the Zel'dovich approximation

$$S(\mathbf{q}, t) = D_+(t)\psi(\mathbf{q}) \text{ and } s_i(\mathbf{q}, t) = D_+(t)\psi_{,i}(\mathbf{q}).$$

Hence we have proved that the Zel'dovich approximation is exact (neglecting the decaying mode) up to shell crossing. After shell-crossing the approximation of J is no longer valid, since we have to sum over the flows. The Lagrangian perturbation theory in one dimension, contains only a first order term. In higher dimensions, the increasing complexity of J introduces higher order corrections.

For completeness we write the second order equation as two first order equations in Lagrangian Fourier space

$$0 = \dot{\hat{S}} - \hat{T},$$

$$0 = \dot{\hat{T}} + 2\frac{\dot{a}}{a}\hat{T} - 4\pi G\rho_b\hat{S},$$

with $T = \dot{S}$. These equations can be written in Feynman notation

$$D^i_j \phi^j = 0$$

with

$$\phi = \begin{pmatrix} \hat{S} \\ \hat{T} \end{pmatrix}$$

and

$$D = \begin{pmatrix} \frac{\mathrm{d}}{\mathrm{d}t} & -1 \\ -4\pi G\rho_b & 2\frac{\dot{a}}{a} + \frac{\mathrm{d}}{\mathrm{d}t} \end{pmatrix}.$$

In the Feynman diagram notation, the Lagrangian standard perturbation theory in one dimension is a lines (see figure 13.3b), representing the Zel'dovich approximation.

18.1.2 Two-dimensional universe

In two dimensions we can perform a similar calculation. This time the density is given in terms of the Jacobian

$$J = 1 + S_{,ii} + \det(S_{,ij}) = 1 + S_{,ii} + \epsilon_{ij}S_{,1i}S_{2j},$$

with ϵ_{ij} the two dimensional Levi-Civita symbol[1]. The complete evolution equation reads

$$0 = \left(\frac{\partial}{\partial q_i} - S_{,ji}\frac{\partial}{\partial q_j} + S_{,ji}S_{,kj}\frac{\partial}{\partial q_k} - \dots \right) \left(\ddot{S}_{,i} + 2\frac{\dot{a}}{a}\dot{S}_{,i} \right)$$
$$+ 4\pi G\rho_b \left(\frac{1}{1 + S_{,ii} + \epsilon_{ij}S_{,1i}S_{2j}} - 1 \right).$$

After expanding the last term with the Taylor series

$$\frac{1}{1+x} = 1 - x + x^2 - x^3 + \dots,$$

we get a differential equation containing infinitely many terms. It is remarkable to note how the complexity increases while going form one to two dimensions. We can however perform standard perturbation theory on the equation. In order to do this, we write the differential equation in the form

$$\mathcal{D}^i_j\phi^j = \frac{1}{2!}M^i_{jk}\phi^j\phi^k + \frac{1}{3!}N^i_{jkl}\phi^j\phi^k\phi^l + \dots,$$

with

$$\phi = \begin{pmatrix} \hat{S} \\ \hat{T} \end{pmatrix},$$

with $\hat{S}$ the Fourier transform of S and $\hat{T} = \dot{\hat{S}}$, and $\mathcal{D}, M, N, \dots$, some tensors containing the information of the differential equation. In order to determine these tensors, we first sort the differential equation in linear, quadratic and higher orders in S

$$f^{(1)} = \ddot{S}_{,ii} + 2\frac{\dot{a}}{a}\dot{S}_{,ii} - 4\pi G\rho_b S_{,ii}$$

$$f^{(2)} = -S_{,ij}\ddot{S}_{,ij} - 2\frac{\dot{a}}{a}S_{,ji}\dot{S}_{,ij} + 4\pi G\rho_b[(S_{,ii})^2 - \epsilon_{ij}S_{,1i}S_{,2j}]$$

$$f^{(3)} = S_{,ij}S_{,kj}\ddot{S}_{,ik} + 2\frac{\dot{a}}{a}S_{,ij}S_{,kj}\dot{S}_{,ik} + 4\pi G\rho_b[2(S_{,ii})(\epsilon_{ij}S_{,1i}S_{,2j}) - (S_{,ii})^3]$$

$$f^{(4)} = -S_{,ij}S_{,kj}S_{,lk}\ddot{S}_{,il} - 2\frac{\dot{a}}{a}S_{,ik}S_{,kj}S_{,lk}\dot{S}_{,il} + 4\pi G\rho_b[(\epsilon_{ij}S_{,1i}S_{,2j})^2 - 3(S_{,ii})^2(\epsilon_{ij}S_{,1i}S_{,2j})]$$

$$f^{(5)} = \dots$$

---

[1]The Levi-Civita symbol $\epsilon_{i_1,\dots,i_d}$ is 1 if $(i_1,\dots,i_d)$ is en even permutation, -1 if it is an odd permutation of $(i, 1, 2, \dots, d)$, and 0 if it is no permutation of $(1, \dots, d)$.

We subsequently substitute S_{SPT} for S in the differential equation, defined as

$$S_{SPT} = \epsilon S^{(1)} + \epsilon^2 S^{(2)} + \epsilon^3 S^{(3)} + \dots,$$

with constant ϵ and scalar fields $S^{(i)}$. We moved the index to superscript, since partial derivatives are written in subscript notation. The differential equation in linear, quadratic and cubic order in ϵ are given by

$$
\begin{aligned}
\epsilon^1 : \quad & 0 = f^{(1)}(S^{(1)}), \\
\epsilon^2 : \quad & 0 = f^{(1)}(S^{(2)}) + f^{(2)}(S^{(1)}, S^{(1)}), \\
\epsilon^3 : \quad & 0 = f^{(1)}(S^{(3)}) + f^{(2)}(S^{(1)}, S^{(2)}) + f^{(2)}(S^{(2)}, S^{(1)}) + f^{(3)}(S^{(1)}, S^{(1)}, S^{(1)}), \\
\epsilon^4 : \quad & 0 = \dots
\end{aligned}
$$

where the jth argument of $f^{(i)}$ refer to the jth factor S in the products from the left, in the definition of $f^{(i)}$. Since our use of $f^{(i)}$ is symmetric, the order in the definition is irrelevant. In terms of S, we have the linear and quadratic term in ϵ

$$
\epsilon^1 : \quad 0 = \ddot{S}^{(1)}_{,ii} + 2\frac{\dot{a}}{a}\dot{S}^{(1)}_{,ii} - 4\pi G\rho_b S^{(1)}_{,ii}
$$

$$
\epsilon^2 : \quad 0 = \ddot{S}^{(2)}_{,ii} + 2\frac{\dot{a}}{a}\dot{S}^{(2)}_{,ii} - 4\pi G\rho_b S^{(2)}_{,ii} + 4\pi G\rho_b \left((S^{(1)}_{,11})^2 + S^{(1)}_{,11}S^{(1)}_{,22} + (S^{(1)}_{,12})^2 + (S^{(1)}_{,22})^2 \right)
$$

$$
\epsilon^3 : \quad 0 = \dots
$$

In Fourier space, with respect to the Lagrangian coordinates, these equations can be written as

$$
\epsilon^1 : \qquad 0 = \ddot{\hat{S}}^{(1)}(\mathbf{k}) + 2\frac{\dot{a}}{a}\dot{\hat{S}}^{(1)}(\mathbf{k}) - 4\pi G\rho_b \hat{S}^{(1)}(\mathbf{k})
$$

$$
\begin{aligned}
\epsilon^2 : \qquad 0 = {} & \ddot{\hat{S}}^{(2)}(\mathbf{k}) + 2\frac{\dot{a}}{a}\dot{\hat{S}}^{(2)}(\mathbf{k}) - 4\pi G\rho_b \hat{S}^{(2)}(\mathbf{k}) \\
& - \frac{4\pi G\rho_b}{k^2} \int \left(k_1' k_2'(k_1' - k_1)(k_2' - k_2) + (k_1')^2(k_1 - k_1')^2 \right. \\
& \left. + (k_1')^2(k_2 - k_2')^2 + (k_2')^2(k_2 - k_2')^2 \right) \hat{S}^{(1)}(\mathbf{k}')\hat{S}^{(1)}(\mathbf{k}' - \mathbf{k})\mathrm{d}\mathbf{k}'
\end{aligned}
$$

$$
\epsilon^3 : \qquad 0 = \dots
$$

The first equation, consisting of the linear terms in ϵ, which can be written as

$$\mathcal{D}^i_j \phi^{(1)j} = 0$$

by which

$$
\mathcal{D} = \begin{pmatrix} \frac{\mathrm{d}}{\mathrm{d}t} & -1 \\ -4\pi G\rho_b & 2\frac{\dot{a}}{a} + \frac{\mathrm{d}}{\mathrm{d}t} \end{pmatrix}.
$$

The $\mathcal{D}$ derived here coincides with the $\mathcal{D}$ derived in one-dimensional Lagrangian standard perturbation theory, and gives the Zel'dovich approximation in two dimensions. The second equation, proportional to ϵ^2, is in compact notation given by

$$\mathcal{D}^i_j \phi^{(2)j} = \frac{1}{2!} M^i_{jk} \phi^{(1)j} \phi^{(1)k}$$

by which the matrix M is zero for all elements other then the element M^2_{11} which is given by

$$M^2_{11} = -\frac{8\pi G \rho_b}{k^2} \big(k'_1 k'_2 (k'_1 - k_1)(k'_2 - k_2) + (k'_1)^2 (k_1 - k'_1)^2 + (k'_1)^2 (k_2 - k'_2)^2$$
$$+ (k'_2)^2 (k_2 - k'_2)^2 \big).$$

The third equation, proportional to ϵ^3, can be written in compact notation as

$$\mathcal{D}^i_j \phi^{(3)j} = M^i_{jk} \phi^{(1)j} \phi^{(2)k} + \frac{1}{3!} N^i_{jkl} \phi^{(1)j} \phi^{(1)k} \phi^{(1)l}$$

which gives N. The higher order tensors follow from similar calculations.

Using this method, we can write nLPT theory in Feynman notation. The Zel'dovich approximation, consists out of a line (see figure 13.3b). The 2LPT and 3LPT theory can be expressed as figure 13.3b and figure 13.3b.

18.1.3   Three dimensional universe

The calculation in three spatial dimensions is very similar to the two-dimensional calculation. The only difference is in the Jacobian, which in three dimensions reads

$$J = 1 + S_{,ii} + \frac{1}{2} \left[(S_{,ii})^2 - S_{,ij} S_{,ji} \right] + \det(S_{,ij})$$
$$= 1 + S_{,ii} + \frac{1}{2} \left[(S_{,ii})^2 - S_{,ij} S_{,ji} \right] + \epsilon_{ijk} S_{,1i} S_{,2j} S_{,3k}.$$

After writing the term $1/J$ as a series in $S_{,ii} + \frac{1}{2} \left[(S_{,ii})^2 - S_{,ij} S_{,ji} \right] + \epsilon_{ijk} S_{,1i} S_{,2j} S_{,3k}$, we obtain a differential equation containing infinity many terms. We can sort the differential equations in homogeneous terms

$$f^{(1)} = \ddot{S}_{,ii} + 2\frac{\dot{a}}{a} \dot{S}_{,ii} - 4\pi G \rho_b S_{,ii}$$
$$f^{(2)} = -S_{,ji} \ddot{S}_{,ij} - 2\frac{\dot{a}}{a} \dot{S}_{,ij} - 4\pi G \rho_b ((S_{,ii})^2 - S_{,ij} S_{,ji}) - (S_{,ii})^2)$$
$$f^{(3)} = S_{,ji} S_{,kj} \ddot{S}_{,ik} + 2\frac{\dot{a}}{a} S_{,ji} S_{,kj} \dot{S}_{,ik} - 4\pi G \rho_b (\epsilon_{ijk} S_{,1i} S_{,2j} S_{3k} + (S_{,ii})^3$$
$$- \frac{1}{2} (S_{,ii})[(S_{,ii})^2 - S_{,ij} S_{,ji}])$$
$$f^{(4)} = \dots$$

After substitution of

$$S_{SPT} = \epsilon S^{(1)} + \epsilon^2 S^{(2)} + \epsilon^3 S^{(3)} + \dots,$$

the differential equation can be sorted in equation linear, quadratic, cubic and higher order in ϵ,

$$\epsilon^1 : \qquad 0 = \ddot{S}_{,ii}^{(1)} + 2\frac{\dot{a}}{a}\dot{S}_{,ii}^{(1)} - 4\pi G\rho_b S_{,ii}^{(1)}$$

$$\epsilon^2 : \qquad 0 = \ddot{S}_{,ii}^{(2)} + 2\frac{\dot{a}}{a}\dot{S}_{,ii}^{(2)} - 4\pi G\rho_b S_{,ii}^{(2)} + 2\pi G\rho_b \left(S_{,ii}^{(1)}S_{,jj}^{(1)} - S_{,ij}^{(1)}S_{,ij}^{(1)} \right)$$

$$\epsilon^3 : \qquad 0 = \dots$$

In Fourier space with respect to the Lagrangian coordinates, these equations can be written as

$$\epsilon^1 : \qquad 0 = \ddot{\hat{S}}^{(1)}(\mathbf{k}) + 2\frac{\dot{a}}{a}\dot{\hat{S}}^{(1)}(\mathbf{k}) - 4\pi G\rho_b \hat{S}^{(1)}(\mathbf{k})$$

$$\epsilon^2 : \qquad 0 = \ddot{\hat{S}}^{(2)}(\mathbf{k}) + 2\frac{\dot{a}}{a}\dot{\hat{S}}^{(2)}(\mathbf{k}) - 4\pi G\rho_b \hat{S}^{(2)}(\mathbf{k})$$

$$+ \frac{2\pi G\rho_b}{k^2}\int [(k_i'k_i')(k_j - k_j')(k_j - k_j') - k_i'k_j'(k_i - k_i')(k_j - k_j')]$$

$$\hat{S}^{(1)}(\mathbf{k}')\hat{S}^{(1)}(\mathbf{k}' - \mathbf{k})d\mathbf{k}'$$

$$\epsilon^3 : \qquad 0 = \dots$$

In terms of the ϕ-notation, this gives

$$\mathcal{D} = \begin{pmatrix} \frac{\mathrm{d}}{\mathrm{d}t} & -1 \\ -4\pi G\rho_b & 2\frac{\dot{a}}{a} + \frac{\mathrm{d}}{\mathrm{d}t} \end{pmatrix}.$$

This again gives the Zel'dovich approximation. The matrix M is zero for all elements other then the element M_{11}^2 which is given by

$$M_{11}^2 = \frac{2\pi G\rho_b}{k^2}[(k_i'k_i')(k_j - k_j')(k_j - k_j') - k_i'k_j'(k_i - k_i')(k_j - k_j')].$$

18.2   Transversal displacement term in standard perturbation theory

When we include the transversal component of the displacement field $\mathbf{s}^T$ we have to add the curl differential equation

$$\nabla_x \times \left(\ddot{\mathbf{s}} + 2\frac{\dot{a}}{a}\dot{\mathbf{s}} \right) = 0,$$

to the analysis. We furthermore must include the transversal component in the Jacobian J. In one dimension, the displacement field cannot be decomposed in a longitudinal and a transversal component. In two dimensions we get

$$J = 1 + S_{,ii} + s_{i,j}^T + \det(S_{,ij} + s_{i,j}^T).$$

In three dimensions the Jacobian becomes

$$
\begin{aligned}
J =& 1 + S_{,ii} + \frac{1}{2}\left[(S_{,ii})^2 - S_{,ij}S_{,ji} - s_{i,j}^T s_{j,i}^T - 2S_{,ij}s_{j,i}^T\right] + \det\left(S_{,ij} + s_{i,j}^T\right) \\
=& 1 + S_{,ii} + \frac{1}{2}\left[(S_{,ii})^2 - S_{,ij}S_{,ji} - s_{i,j}^T s_{j,i}^T - 2S_{,ij}s_{j,i}^T\right] \\
& + \epsilon_{ijk}\left(S_{,1i} + s_{1,i}^T\right)\left(S_{,2j} + s_{2,j}^T\right)\left(S_{,3k} + s_{3,k}^T\right)
\end{aligned}
$$

We however do not make this extension in this thesis, since it greatly enlarges the expressions while rotation in large-scale structure formation only occurs after shell crossing.

18.3   Lagrangian standard perturbation theory with multi-flow regions

In the previous section, we derived a Lagrangian perturbation theory which follows the derivation of the Zel'dovich approximation and the 2LPT, 3LPT and 4LPT models. One of the major drawbacks of this approach is the density is only accurately approximated in single flow regions. There exist more sophisticated Lagrangian perturbation theories, which do not suffer from this problem. We here sketch the Lagrangian perturbation theory used by Rafael Porto et al. in 2013 [56] in deriving the first effective Lagrangian perturbation theory.

The differential equations of large scale structure formation can be written as

$$
\frac{\partial^2 \mathbf{x}(\mathbf{q})}{\partial \tau^2} + \mathcal{H}\frac{\partial \mathbf{x}(\mathbf{q})}{\partial \tau} = -\nabla_{\mathbf{x}}\Phi(\mathbf{q}),
$$

$$
\nabla_{\mathbf{x}}^2 \Phi = \frac{3}{2}\Omega_m \mathcal{H}^2 \delta(\mathbf{q}).
$$

The density can be approximated as

$$
\delta(\mathbf{x}, \tau) = \int \mathrm{d}q\, \delta^{(d)}(\mathbf{x} - \mathbf{x}(\mathbf{q}, \tau)).
$$

Note that $\mathbf{x}$ is a spatial coordinate, while $\mathbf{x}(\mathbf{q}, \tau)$ is the position a Lagrangian volume element , initially at $\mathbf{q}$, after time τ. This is the integral form of the Jacobian used in the previous section. The equations can be written in Fourier space, with respect to Eulerian coordinates. The Fourier transform of the density perturbations is

$$
\hat{\delta}(\mathbf{k}, \tau) = \int \mathrm{d}q\, e^{-i\mathbf{k}\cdot\mathbf{x}(\mathbf{q},\tau)},
$$

by which the Poisson equation can be written as

$$
\hat{\Phi}(\mathbf{k}, \tau) = -\frac{3}{2}\mathcal{H}^2\Omega_m \frac{1}{k^2}\int \mathrm{d}q\, e^{-i\mathbf{k}\cdot\mathbf{x}(\mathbf{q},\tau)}.
$$

By substituting this expression for the gravitational potential in the equations of motion, we obtain an explicit and exact form of the Lagrangian fluid equations

$$
\mathbf{x}''(\mathbf{q}, \tau) + \mathcal{H}\mathbf{x}'(\mathbf{q}, \tau) = \frac{3}{2}\mathcal{H}^2\Omega_m \int \mathrm{d}\mathbf{q}' \int \frac{i\mathbf{k}}{k^2} e^{i\mathbf{k}\cdot(\mathbf{x}(\mathbf{q},\tau)-\mathbf{x}(\mathbf{q}',\tau))}\frac{\mathrm{d}\mathbf{k}}{(2\pi)^d}.
$$

Matsubara [46] performed standard perturbation theory on this differential equation. Rafael Porto et al. in 2013 [56] extended it to include effective corrections to the equations of motion. The great advantage of this approach is that it works for both single and multi stream regions. In this thesis we however restrict our self to Lagrangian fluid dynamical approximation in which the displacement field is a gradient field.

18.4   Lagrangian effective field theory

In the previous chapter we considered effective field theory in the Eulerian setting. The effective equations of motion can be written as

$$\frac{\partial \delta}{\partial t} + \frac{1}{a}\nabla_x \cdot [\mathbf{v}(1+\delta)] + \chi^\delta \delta + \chi^\theta \partial_i v^i = 0,$$
$$\frac{\partial \mathbf{v}}{\partial t} + \frac{1}{a}(\mathbf{v} \cdot \nabla_x)\mathbf{v} + \frac{\dot{a}}{a}\mathbf{v} - c_s^2 \nabla \delta + \frac{c_v^2 a}{\dot{a}}\nabla^2 \mathbf{v} = \frac{1}{a}\mathbf{g},$$
$$\nabla_x \times \mathbf{g} = 0,$$
$$\nabla_x \cdot \mathbf{g} = -4\pi G \rho_b a \delta,$$
$$\delta = \frac{\rho - \rho_b}{\rho_b},$$

with $\chi^\delta, \chi^\theta, c_s^2$, and c_v^2 functions of time which should be empirically measured.

In the standard perturbation theory setting, we replaced the conservation of mass by the deformation of Lagrangian volume elements. We can now longer do this when χ^δ and χ^θ are nonzero. I however suspect that χ^δ and χ^θ will be small, since the conservation of mass is a very intuitive constraint on a dark matter fluid. The viscosities c_s, and c_v represent a stickiness of large scales, due to small scale physics. We could for example imagine that the generation of caustics and formation of stars in a galaxy will slow down large scale fluctuations.

An interesting case appears when we only take the viscosity c_v into account. In this model particles follow the Zel'dovich approximation up to shell crossing. After shell crossing they however turn around and virialize in filaments and clusters. In the limit $c_v \to 0$, we obtain the well known adhesion model. We studied the adhesion model in detail in chapter 3. It can be seen as one of the earliest effective models of Lagrangian large-scale structure formation.

Chapter 19

Statistics of Caustics in General Lagrangian Approaches

In chapters 12 and 13 of this thesis we analyzed the statistics of caustics appearing in the Zel'dovich approximation. In chapter 4 we observed that caustics exist in a more general setting. They are generated in any Lagrangian approach to structure formation, during shell crossing. In this chapter we extend the conditions for caustics in Lagrangian approaches presented in chapter 6. We furthermore show how these conditions can be used to calculate the statistics of caustics in standard and effective perturbation theory. We do not perform the calculations explicitly but do show how they can be executed.

19.1 Caustics conditions in Lagrangian approaches

In chapter 6 we observed that the Zel'dovich approximation predicts infinite densities when

$$D_+(t) = \frac{1}{\lambda_i},$$

with λ_i on of the eigenvalues of the deformation tensor. Using the fact that the deformation tensor is constant in the Zel'dovich approximation, we constructed an embryonic skeleton in Lagrangian space. We furthermore classified components of the skeleton using Lagrangian catastrophe theory. Specific conditions on the Lagrangian fluctuations could be specific features of the skeleton. We here generalize these conditions of generic Lagrangian approaches.

19.1.1 Caustics in one dimension

In one dimension, caustics in the Zel'dovich approximation can be classified as being fold and cusp catastrophes. The folds correspond to level crossings whereas the cusps correspond to maxima and minima of the initial density perturbation. In this thesis we often used the symbol λ_1 for the density perturbation, since the caustics conditions

are in principal conditions on the eigenvalue fields of the deformation tensor (T_{11}). In the one dimensional Zel'dovich approximation, there is only one eigenvalue field, which turns out to coincide with the density perturbation. The caustics conditions are

$$\text{fold} : \lambda_1 = \lambda \text{ and } \lambda_{11} \neq 0,$$
$$\text{cusp} : \lambda_1 = \lambda \text{ and } \lambda_{11} = 0,$$

with $\lambda = 1/D_+(t)$ the eigenvalue corresponding with shell crossing. In the Zel'dovich approximation, the deformation tensor is constant. In Lagrangian approaches beyond the Zel'dovich approximation, the deformation can change in time. In approaches with a gradient displacement field, the conditions however remain valid[1]. In this chapter we aways assume the displacement field to be a gradient field. Hence the folds and cusps occurring at time t are fully determined same eigenvalue conditions in the eigenvalues of the deformation tensor $(T_{11})(t)$ at that instant.

19.1.2   Caustics in two dimensions

In two dimensions, the conditions of point catastrophes change as in the one-dimensional case. The cusp, swallowtail, and umbilic catastrophes appearing at time t correspond to the same conditions on the eigenvalues of the deformation tensor $(T_{ij})(t)$ at that instant in time. The A_2-lines consist of the points which experience shell crossing at some fixed moment in time. Since the A_2-lines statistic do not explicitly depend on time, the A_2-lines correspond to the isocontours of the eigenvalue fields of $(T_{ij})(t)$.

The A_3-line conditions in generic Lagrangian models are a bit more involved, since the A_3-lines consist of the points which collapsed to cusp catastrophes at some time t. Hence formally the points on the A_3-lines corresponding to the first eigenvalue satisfy the conditions

$$\lambda_1(t) = \frac{1}{D_+(t)} \text{ and } \lambda_{11}(t) = 0,$$

for some time t, with $\lambda_i(t)$ the eigenvalue of the time evolved deformation tensor. The A_3-lines corresponding to the second eigenvalue field follows analogously.

19.2   Statistics of caustics in standard and effective perturbation theory

For the Zel'dovich approximation we expressed the statistics of caustics in terms of two point correlation functions of the initial density field and its derivatives. Since the geometric statistics developed in chapter 10, can be applied to any stationary random field, we can use the correlation functions of the evolved deformation tensor to calculate the statistics of caustics.

The statistics of point catastrophes correspond to correlation functions of products

---

[1]When the displacement field contains a transversal component more extended conditions are needed as we saw in chapter 6.

of eigenvalues and derivatives of eigenvalues of eigenvalues. We can subsequently rotate to the Hessian frame and substitute the expressions of the eigenvalues in terms of the deformation tensor. We now have the expectation value of a product of components of the deformation tensor and its derivatives. In standard and effective perturbation theory we can approximate these expectation expectation values by expanding the expectation value in terms of different corrections. Each correction in the resulting expectation corresponds to a Feynman diagram described in chapter 15.

The line statistics are bit more involved, since they consist out of the expectation value of the square root of a sum of squares of the eigenvalue field and their derivatives. We can tackle this problem by expanding the square root around the expectation of the argument. We here illustrate this expansion

$$\langle f(\mathbf{x}) \rangle = f(\langle \mathbf{x} \rangle) + \frac{1}{2!} \left\langle (\mathbf{x} - \langle \mathbf{x} \rangle)^T \mathcal{H} (\mathbf{x} - \langle \mathbf{x} \rangle) \right\rangle + \dots,$$

with $\mathcal{H}$ the Hessian of f being evaluated at $\langle \mathbf{x} \rangle$. For our case consider the function $f(x, y) = \sqrt{x^2 + y^2}$ with $\langle x \rangle = a$ and $\langle y \rangle = b$. The Hessian is of f is

$$\mathcal{H} = \frac{1}{(a^2 + b^2)^{3/2}} \begin{pmatrix} b^2 & -ab \\ -ab & a^2 \end{pmatrix}$$

by which

$$\langle \sqrt{x^2 + y^2} \rangle = \sqrt{\langle x \rangle^2 + \langle y \rangle^2}$$
$$+ \frac{1}{(a^2 + b^2)^{3/2}} \left[b^2 \langle (x - a)^2 \rangle - 2ab \langle (x - a)(y - b) \rangle + a^2 \langle (y - b)^2 \rangle \right] + \dots$$

The dots indicate higher order corrections. We have not calculated the statistics of caustics in standard perturbation theory explicitly. This remains to be done in further research.

Chapter 20

Conclusion

It is generally thought that the universe originated at the Big Bang. In the 10^{-36} to 10^{-32} seconds after its start, the universe experienced a great expansion. This period is know as the inflationary epoch. Inflation both flattened the curvature of space and homogenized the temperature in the universe. At the same time it generated tiny density fluctuations, which we can now observe as temperature anisotropies in the cosmic microwave background. Statistical analyses have shown these fluctuations to be well modeled by Gaussian random fields. It is thought that all structure in the universe originates from these density fluctuations.

At the time the universe became neutral, the matter particles in it were approximately uniformly distributed and at rest. As time evolved, they started moving. Overdense regions accumulated matter from their underdense surroundings. This process continued till the overdense regions became dense enough to form stars and galaxies. The resulting distribution of galaxies is no longer a uniform one. The gravitational collapse of the initial density fluctuations has resulted in an intricate structure, composed out of clusters, filaments, voids and walls. This has been observed in many high redshift galaxy surveys and is today known as the large-scale structure or the cosmic web.

In this process regions of infinite density, called caustics, emerged. These caustics can most easily be thought of if we model the matter in the universe as a fluid. The initial distribution of particles was uniform. This can be modeled as a homogeneous fluid. As time evolved, the fluid started to flow, towards overdense regions and away from underdense regions. At some moment in time different elements of the fluid started to cross and formed the first structures. This process is called shell crossing and during this process infinite densities or caustics emerged.

Caustics play a prominent role in large-scale structure formation. They are generated during gravitational collapse and stars can only form in dense regions. For this reason, stars can be seen as tracers of the underlying large-scale structure. A better understanding of the caustics in the universe may help us unravel the details of the cosmic web.

In this thesis we restrict ourself to one- and two-dimensional models of large-scale structure formation. In one-dimensional models of the universe, the caustics consist

of points. According to Lagrangian catastrophe theory, we can classify them as fold and cusp catastrophes. A cusp catastrophe is created at the start of a shell crossing after which it splits into two fold catastrophes. In this thesis we both numerically and analytically studied the statistics of these caustics in the framework of the Zel'dovich approximation. We furthermore extended the analytic study to standard and effective perturbation theory.

In two-dimensional models of the universe, the caustics consist of lines and points. According to Lagrangian catastrophe theory, we can classify them as umbilic, swallowtail, cusp and fold catastrophes. The fold catastrophes consist of lines, known as A_2-lines, on which for all points at a specific point in time shell crossing occurs. The A_2-lines consist of piecewise smooth curves. The singular points on the A_2-lines are the cusp catastrophes, also known as A_3 points. As time evolves the A_3 points follow trajectories through space. These trajectories are known as A_3-lines. The A_3-lines are on their turn again piecewise smooth curves. Its singular points are the swallowtail and umbilic catastrophes. In this thesis we both numerically and analytically study the statistics of these caustics in the Zel'dovich approximation. A further comparison of the caustics of the Zel'dovich approximation with an N-body simulation shows that the A_3-lines follow the filamentary structure of the cosmic web, while the swallowtail and umbilic catastrophes reside in the clusters.

Caustics play a prominent role in large-scale structure formation. A study in the framework of the Zel'dovich approximation indicates that we can use a caustics skeleton to follow the evolution of the cosmic web. In particular the length of the filaments in the cosmic web seems to be a property that may be studied in this fashion. We derived analytic statistics of the caustics in the Zel'dovich approximation and show how this approach can be extended to higher order standard perturbation theory and effective field models of large-scale structure formation. These theoretical derivations can be used to gain further insight in the properties of the cosmic web.

Chapter 21

Discussion

According to current cosmological models, all structure in the universe originates from quantum fluctuations rendered to classical density fluctuations by inflation. Quantum field theory and observational analyses indicate that these classical fluctuations can be modeled by Gaussian random fields. Since the information of Gaussian random fields is completely contained in their power spectrum, all statistical structural properties of the current universe can be expressed as a function of the power spectrum of these initial density fluctuations. From a physical perspective, moreover there is nothing more to be determined apart from these statistical properties, since also about the initial conditions only statistics are known.

Although elegant, expressing the statistics of structural properties in terms of the power spectrum is difficult due to the nonlinear nature of gravity. We can approximate the statistics numerically by means of N-body simulations. N-body simulations are however, expensive and are not free from numerical artifacts. This thesis should be seen as a first investigation to analytically estimate these properties. By means of caustics occurring in the Zel'dovich approximation in one and two dimensions, we constructed a skeleton and derived analytic formulas for the density of point catastrophes and the average line length in this skeleton. We furthermore in two dimensions compared the skeleton with an N-body simulation modeling a dark matter fluid, showing a great agreement of the cosmic web and the skeleton on mildly non-linear scales. The lines of the skeleton coincide with the filaments and the vertices are positioned in the clusters. On strongly nonlinear scales, the skeleton however starts to deviate from the structure observed in N-body simulations. In order to improve the skeleton we adapted the approach to Lagrangian standard perturbation and effective field theory. Although the approach seems promising, futher research is necissary to model reality more precisely. Then results might be compared to observational data and applications can be developed.

21.1 Extensions

The analytical calculations of the statistics of caustics, as described in this thesis, need to be extended in several ways before they can be applied to observations. We here

discuss the most prominent extensions that deserve further attention.

Three-dimensional models of structure formation

In this thesis, we restricted ourselves to one- and two-dimensional models of large-scale structure formation. In observations of large-scale structure we however are dealing with three spatial dimensions. An extra dimension induces complexity not present in one- and two-dimensional models. In the language of Lagrangian catastrophe theory, three spatial dimensions lead to two additional catastrophes, the A_5 and D_5 catastrophes. Furthermore, the nature of the catastrophes change. The A_2 catastrophes now form surfaces, at which shell crossing occurs. As time evolves, they sweep through space. The A_3 catastrophes, at a fixed point in time, form lines (not to be confused with the A_3-lines) at which shell crossing starts to take place. In time these lines move through space and trace surfaces. These surfaces are expected to correspond to the walls appearing in the cosmic web. Note that there exists only one type of wall in three dimensions. The A_4 and D_4 catastrophes correspond to points, that move through space as time evolves. The trajectories of these four-dimensional catastrophes correspond to filaments in the cosmic web. Potentially we can have three different types of filaments, i.e., the A_4, D_4^- and D_4^+ filaments. Each type corresponds to a different environment. However, remains an open question which type occurs in which environment. The additional A_5 and D_5 catastrophes occur on fixed instances of space-time. They occur at the singularities in the four-dimensional catastrophes and will probably represent the clusters of the cosmic web.

As explained above, a third spatial dimension adds a new layer of complexity to the analyzes. There are several ways to move forward in dealing with this additional complexity. I feel that we first should determine the role of caustics in the three-dimensional Zel'dovich approximation. This can be done by performing a three dimensional N-body simulation on a Gaussian random field and by then comparing the resulting structure with the caustics skeleton of the initial fluctuations. This will enable us to determine the accuracy of the skeleton in three dimensions. On the other hand we have to develop new catastrophe conditions for the newly added catastrophes. Since these conditions will be local, this will enable us to trivially extend the two-dimensional analytic analysis to the three dimensional Zel'dovich approximation.

Beyond the Zel'dovich approximations

In this thesis we derived a standard perturbation theory and effective field theory scheme for Lagrangian large-scale structure formation. We showed how to approximate correlation functions and derived statistics of caustics in one- and two-dimensions. Due to time limitations the framework has not yet been applied to calculate the statistics of caustics in these models. Such calculations when done could easily be adapted to more sophisticated Lagrangian perturbation schemes.

Beyond the gradient displacement field

The caustics conditions described in this thesis are based on the assumption that the displacement field of the dark matter particles is a gradient vector field, i.e., there exists a potential such that this gradient equals the displacement field. This assumption is supported by the result that any rotation initially present in the displacement field is suppressed by the expansion of the universe: the displacement field is rotationless till shell-crossing. When dark matter flows start to cross, vorticity is created. The caustics conditions presented here do not work for displacement fields with vorticity. The framework of Lagrangian catastrophe theory is however general enough to classify the caustics resulting form such displacement fields. Hence, further research could generalize the caustics conditions to this situation.

Beyond the skeleton

In this thesis we worked with a caustics skeleton. We used the truncated Zel'dovich approximation and tried to catch the structure of the cosmic web in terms of a skeleton, consisting of points of size zero and lines without thickness. In this process we suppressed small scale caustics. The observed cosmic web is, however, not a skeleton; the clusters have a finite size and the filaments do have a thickness. Moreover, the filaments and walls have a complex structure themselves. The cosmic web is a hierarchic, fractal-like object. The skeleton approach dismisses these details. The analysis proposed here can, however, be modified to include these statistical properties.

One potential way to probe these details is by gradually removing the suppression of the small scale caustics. By decreasing the smoothing scale, we include smaller scale structures which will result in more caustics. This principle can be interpreted as 'dressing the skeleton'; we add a size to the elements of the skeleton. Another fruitful approach would be to apply the present analysis on constrained Gaussian random fields. In this way we can specifically target an environment and determine its statistical properties. Both approaches will enable us to get more insight in the hierarchy of the cosmic web. It will, however, in practice be difficult to perform these calculations due to the restrictions of the Zel'dovich approximation. We have yet to see whether Lagrangian standard perturbation and effective field theory are able to model the small and large scale structure simultaneously.

21.2   Applications

If the analysis presented here can successfully be extended as described above, there are numerous applications. We here mention some interesting applications.

The length of filaments

One of the most promising statistical measures of the caustics skeleton is the average length of filaments. The curves of the skeleton have a good alignment with two-

dimensional N-body simulations and their average length is easily computable from the statistics of the initial conditions. In order to verify the validity of this approach, we could compare the length distribution in a skeleton with those in N-body simulations. We expect, however, that the concept of length needs adaptation in order to be an interesting measure. The skeleton is namely winded in the clusters, and this leads to overestimation of the distance between clusters. There are of course multiple ways to correct for this issue. I would propose to weight the line length by its curvature.

Classification of the cosmic web

The cosmic web consists of an extremely complex network, and the scientific community is still unable to unambiguously classify its structure. The caustics skeleton might help to in the future construct a more rigorous classification. We saw that the extension to three-dimensional models results in a skeleton with clusters represented by A_5 and D_5 catastrophes, filaments by A_4, and D_4 catastrophes and walls by A_3 catastrophes. Hence, this classification uniquely defines components of the cosmic web and differentiates between different types of filaments. It remains to be seen which type of filament will correspond to which environment. Type and environment will however be directly linked, since the difference between filaments results from the nature of the matter inflow generating the filament.

A classification like this is definitely feasible in N-body simulations, as the complete history of particles is known is this case. In observational data this will be more difficult, since the caustics skeleton relies on the phase-space distribution of particles. However, since new galaxy surveys are expected to measure the complete phase-space distribution of galaxies and reconstruction algorithms of large-scale structure are in rapid development, we might be able to perform this classification in the future.

Bibliography

[1] R. J. Adler and J. E. Taylor. *Random Fields and Geometry*. John Wiley & Sons, 2007.

[2] R. A. Alpher. A Neutron-Capture Theory of the Formation and Relative Abundance of the Elements. *Physical Review*, 74:1577–1589, December 1948.

[3] R. A. Alpher, H. Bethe, and G. Gamow. The Origin of Chemical Elements. *Physical Review*, 73:803–804, April 1948.

[4] V. I. Arnol'd. Normal forms of functions near degenerate critical points, Weyl groups A, D, E and Lagrange singularities. *FAA*, 6, June 1972.

[5] V. I. Arnold. *Catastrophe theory*. 1984.

[6] V. I. Arnold, S. F. Shandarin, and I. B. Zeldovich. The large scale structure of the universe. I - General properties One- and two-dimensional models. *Geophysical and Astrophysical Fluid Dynamics*, 20:111–130, 1982.

[7] V.I. Arnol'd. *Mathematical Methods of Classical Mechanics*. Graduate Texts in Mathematics. Springer, 1989.

[8] Vladimir Igorevich Arnol'd, Sabir Medzhidovich Gusein-Zade, and Aleksandr Nikolaevich Varchenko. *Singularities of differentiable maps I. Classification of critical points, caustics and wave fronts*. Mono. Math. Birkhäuser, Boston, MA, 1982. Trans from the Russian, Moscow, 1982.

[9] D. Baumann, A. Nicolis, L. Senatore, and M. Zaldarriaga. Cosmological nonlinearities as an effective fluid. *jcap*, 7:51, July 2012.

[10] F. Bernardeau, S. Colombi, E. Gaztañaga, and R. Scoccimarro. Large-scale structure of the Universe and cosmological perturbation theory. *physrep*, 367:1–248, September 2002.

[11] F. R. Bouchet, S. Colombi, E. Hivon, and R. Juszkiewicz. Perturbative Lagrangian approach to gravitational instability. *aap*, 296:575, April 1995.

[12] F. R. Bouchet, R. Juszkiewicz, S. Colombi, and R. Pellat. Weakly nonlinear gravitational instability for arbitrary Omega. *apjl*, 394:L5–L8, July 1992.

[13] T. G. Brainerd, R. J. Scherrer, and J. V. Villumsen. Linear Evolution of the Gravitational Potential: A New Approximation for the Nonlinear Evolution of Large-Scale Structure. *apj*, 418:570, December 1993.

[14] T. Buchert. Lagrangian Theory of Gravitational Instability of Friedman-Lemaitre Cosmologies - a Generic Third-Order Model for Nonlinear Clustering. *mnras*, 267:811, April 1994.

[15] T. Buchert and J. Ehlers. Lagrangian theory of gravitational instability of Friedman-Lemaitre cosmologies – second-order approach: an improved model for non-linear clustering. *mnras*, 264:375–387, September 1993.

[16] J. J. M. Carrasco, M. P. Hertzberg, and L. Senatore. The effective field theory of cosmological large scale structures. *Journal of High Energy Physics*, 9:82, September 2012.

[17] S. M. Carroll, S. Leichenauer, and J. Pollack. A Consistent Effective Theory of Long-Wavelength Cosmological Perturbations. *ArXiv e-prints*, October 2013.

[18] Domenico P. L. Castrigiano and Sandra A. Hayes. *Catastrophe theory. With a foreword by René Thom. 2nd ed.* Advanced Book Program. Boulder, CO: Westview Press. xvi, 264 p., 2004.

[19] P. Catelan. Lagrangian dynamics in non-flat universes and non-linear gravitational evolution. *mnras*, 276:115–124, September 1995.

[20] P. Coles. The clustering of local maxima in random noise. *mnras*, 238:319–348, May 1989.

[21] P. Coles, A. L. Melott, and S. F. Shandarin. Testing approximations for non-linear gravitational clustering. *mnras*, 260:765–776, February 1993.

[22] R. H. Dicke, P. J. E. Peebles, P. G. Roll, and D. T. Wilkinson. Cosmic Black-Body Radiation. *apj*, 142:414–419, July 1965.

[23] A. G. Doroshkevich. Spatial structure of perturbations and origin of galactic rotation in fluctuation theory. *Astrophysics*, 6:320–330, October 1970.

[24] A. G. Doroshkevich. The space structure of perturbations and the origin of rotation of galaxies in the theory of fluctuation. *Astrofizika*, 6:581–600, 1970.

[25] A. Einstein. Die Grundlage der allgemeinen Relativitätstheorie. *Annalen der Physik*, 354:769–822, 1916.

[26] R.P. Feynman and A.R. Hibbs. *Quantum mechanics and path integrals*. International series in pure and applied physics. McGraw-Hill, 1965.

[27] J. Foster and J. D. Nightingale. *A Short Course in General Relativity*. 2006.

[28] A. Friedmann. Über die Krümmung des Raumes. *Zeitschrift fur Physik*, 10:377–386, 1922.

[29] J. Gllmm, A. Jaffe, and F. Wilczek. Quantum Physics: A Functional Integral Point of View. *Physics Today*, 35:82, 1982.

[30] D. Gromoll and W. Meyer.

[31] F. Guerra, L. Rosen, and B. Simon. Statistical mechanics results in the P(phi) _2 quantum field theory. *Physics Letters B*, 44:102–104, April 1973.

[32] S. N. Gurbatov, A. I. Saichev, and S. F. Shandarin. The large-scale structure of the universe in the frame of the model equation of non-linear diffusion. *mnras*, 236:385–402, January 1989.

[33] J. Hidding, S. F. Shandarin, and R. van de Weygaert. The Zel'dovich approximation: key to understanding cosmic web complexity. *mnras*, 437:3442–3472, February 2014.

[34] Johan Hidding. PhD thesis, 2014.

[35] Johan Hidding, Rien van de Weygaert, Gert Vegter, Bernard J.T. Jones, and Monique Teillaud. The sticky geometry of the cosmic web. In *Proceedings of the Twenty-eighth Annual Symposium on Computational Geometry*, SoCG '12, pages 421–422, New York, NY, USA, 2012. ACM.

[36] E. Hubble. A Relation between Distance and Radial Velocity among Extra-Galactic Nebulae. *Proceedings of the National Academy of Science*, 15:168–173, March 1929.

[37] N. Kaiser A.S. Szalay J.M. Bardeen, J.R. Bond. The statistics of peaks of gaussian random fields. *Astrophysical journal part 1*, 304.

[38] B. J. T. Jones. The origin of scaling in the galaxy distribution. *mnras*, 307:376–386, August 1999.

[39] C. Kiefer and D. Polarski. Why do cosmological perturbations look classical to us? *ArXiv e-prints*, October 2008.

[40] C. Kiefer, D. Polarski, and A. A. Starobinsky. Quantum-To Transition for Fluctuations in the Early Universe. *International Journal of Modern Physics D*, 7:455–462, 1998.

[41] G. Lemaître. Un Univers homogène de masse constante et de rayon croissant rendant compte de la vitesse radiale des nébuleuses extra-galactiques. *Annales de la Societe Scietifique de Bruxelles*, 47:49–59, 1927.

[42] B. Little, D. H. Weinberg, and C. Park. Primordial fluctuations and non-linear structure. *mnras*, 253:295–306, November 1991.

[43] M.S. Longuet-Higgins. Mathematical analysis of random noise. *Philosophical transactions of the royal society london A*, 249:321, 1957.

[44] M. R. Lovell, V. Eke, C. S. Frenk, L. Gao, A. Jenkins, T. Theuns, J. Wang, S. D. M. White, A. Boyarsky, and O. Ruchayskiy. The haloes of bright satellite galaxies in a warm dark matter universe. *mnras*, 420:2318–2324, March 2012.

[45] S. Matarrese, F. Lucchin, L. Moscardini, and D. Saez. A frozen-flow approximation to the evolution of large-scale structures in the Universe. *mnras*, 259:437–452, December 1992.

[46] T. Matsubara. Nonlinear perturbation theory with halo bias and redshift-space distortions via the Lagrangian picture. *prd*, 78(8):083519, October 2008.

[47] A. L. Melott, J. Einasto, E. Saar, I. Suisalu, A. A. Klypin, and S. F. Shandarin. Cluster analysis of the nonlinear evolution of large-scale structure in an axion/gravitino/photino-dominated universe. *Physical Review Letters*, 51:935–938, September 1983.

[48] A. L. Melott, T. F. Pellman, and S. F. Shandarin. Optimizing the Zeldovich Approximation. *mnras*, 269:626, August 1994.

[49] L. Mercolli and E. Pajer. On the velocity in the Effective Field Theory of Large Scale Structures. *jcap*, 3:6, March 2014.

[50] D. Novikov, S. Colombi, and O. Doré. Skeleton as a probe of the cosmic web: the two-dimensional case. *mnras*, 366:1201–1216, March 2006.

[51] P. J. E. Peebles. *The large-scale structure of the universe*. 1980.

[52] A. A. Penzias and R. W. Wilson. A Measurement of Excess Antenna Temperature at 4080 Mc/s. *apj*, 142:419–421, July 1965.

[53] S. Perlmutter, G. Aldering, M. della Valle, S. Deustua, R. S. Ellis, S. Fabbro, A. Fruchter, G. Goldhaber, D. E. Groom, I. M. Hook, A. G. Kim, M. Y. Kim, R. A. Knop, C. Lidman, R. G. McMahon, P. Nugent, R. Pain, N. Panagia, C. R. Pennypacker, P. Ruiz-Lapuente, B. Schaefer, and N. Walton. Discovery of a supernova explosion at half the age of the universe. *nat*, 391:51, January 1998.

[54] M.E. Peskin and D.V. Schroeder. *An Introduction to Quantum Field Theory*. Advanced book classics. Addison-Wesley Publishing Company, 1995.

[55] D. Pogosyan, C. Pichon, C. Gay, S. Prunet, J. F. Cardoso, T. Sousbie, and S. Colombi. The local theory of the cosmic skeleton. *mnras*, 396:635–667, June 2009.

[56] R. A. Porto, L. Senatore, and M. Zaldarriaga. The Lagrangian-space Effective Field Theory of Large Scale Structures. *ArXiv e-prints*, November 2013.

[57] S.O. Rice. Mathematical analysis of random noise. *Bell system technology journal*, 23.

[58] A. G. Riess, A. V. Filippenko, P. Challis, A. Clocchiatti, A. Diercks, P. M. Garnavich, R. L. Gilliland, C. J. Hogan, S. Jha, R. P. Kirshner, B. Leibundgut, M. M. Phillips, D. Reiss, B. P. Schmidt, R. A. Schommer, R. C. Smith, J. Spyromilio, C. Stubbs, N. B. Suntzeff, and J. Tonry. Observational Evidence from Supernovae for an Accelerating Universe and a Cosmological Constant. *aj*, 116:1009–1038, September 1998.

[59] G. Rossi. Peaks and dips in Gaussian random fields: a new algorithm for the shear eigenvalues, and the excursion set theory. *mnras*, 430:1486–1503, April 2013.

[60] Barbara Ryden. *An introduction to cosmology*. Pearson Addison-Wesley, 2003.

[61] M. Sasaki and M. Kasai. Non-Linear Vorticity-Density Coupling in Lagrangian Dynamics. *Progress of Theoretical Physics*, 99:585–597, April 1998.

[62] J. Shiraishi.

[63] B. Simon. *The P(O)2 Euclidean (Quantum) Field Theory*. Princeton Series in Physics. Books on Demand, 1974.

[64] D. Sudarsky. Shortcomings in the Understanding of why Cosmological Perturbations Look Classical. *International Journal of Modern Physics D*, 20:509–552, 2011.

[65] T. Tatekawa. Fourth-order perturbative equations in Lagrangian perturbation theory for a cosmological dust fluid. *Progress of Theoretical and Experimental Physics*, 2013(1):010003, January 2013.

[66] S.T. Thornton and J.B. Marion. *Classical Dynamics of Particles and Systems*. Brooks/Cole, 2004.

[67] R. van de Weygaert and E. Bertschinger. Peak and gravity constraints in Gaussian primordial density fields: An application of the Hoffman-Ribak method. *Monthly Notices of the Royal Astronomical Society*.

[68] M. Venselow. Master's thesis.

[69] R. W. Wilson and A. A. Penzias. Isotropy of Cosmic Background Radiation at 4080 Megahertz. *Science*, 156:1100–1101, May 1967.

[70] A. Zee. *Quantum Field Theory in a Nutshell: (Second Edition)*. In a Nutshell. Princeton University Press, 2010.

[71] C. Zeeman. A Catastrophe Machine. pages 276–282, 1972.

[72] Y. B. Zel'dovich. Gravitational instability: An approximate theory for large density perturbations. *aap*, 5:84–89, March 1970.

[73] Y. B. Zeldovich. Structure (Topology) of the Universe. *Comments on Astrophysics and Space Physics*, 5:169, 1973.

[74] V. M. Zukalyukin. Lagrangian and Legendrian Singularities. *FAA*, 10, January 1976.

Appendix A

N-Body simulation

For the analysis of shell crossing in N-body simulations, we constructed a simple one- and two-dimensional N-body simulation. The simulation is discussed in chapter 4. On the subsequent pages you will find an implementation in Mathematica. The programs have been written in collaboration with Johan Hidding.

N - Body 1D

`PP[list_] :=`
  `Show[ListLinePlot[list, AspectRatio → 1, PlotRange → {{0, L}, {-3000, 3000}},`
    `PlotStyle → Black, ImageSize → 300], ListPlot[list, PlotStyle → Red]]`
`ZP[list_] := Show[ListPlot[list, AspectRatio → 1, PlotRange → {{0, L}, {0, L}},`
  `PlotStyle → Red], ListLinePlot[list, AspectRatio → 1,`
  `PlotRange → {{0, L}, {0, L}}, PlotStyle → Black]]`

`ℱ[f_] := Chop[Fourier[f, FourierParameters → {1, -1}]]`
`ℱℐ[f_] := Chop[InverseFourier[f, FourierParameters → {1, -1}]]`
`fftIndgen[n_, L_] :=`
  $\frac{2 \pi}{L}$ `Flatten[{Range[0., n / 2.], -Reverse[Range[1., n / 2. - 1]]}]`

Initial Conditions

`GRF[size_, pk_, L_, σ_] := Module[{noise, amplitude, Pk1, smooth, data},`
  `With[{pkt = pk},`
   `Pk1 = Compile[{{kx, _Real}}, If[kx == 0, 0, Sqrt[Abs[pkt[kx]]]]]];`
  `noise = Fourier[RandomVariate[NormalDistribution[], {size}]];`
  `amplitude = Map[Pk1, fftIndgen[size, L], 1];`
  `smooth = Map[`$e^{-(\sigma)^2 \#^2 / 2}$` &, fftIndgen[size, L], 1];`
  `data = InverseFourier[smooth * noise * amplitude];`
  $\frac{1}{\text{StandardDeviation[Flatten[data]]}}$ `data]`

Cosmology

`Cosmology[H0_, Ωm_, ΩΛ_, a_] := H0 a` $\sqrt{\Omega\Lambda + \Omega m\, a^{-3} + (1 - \Omega m - \Omega\Lambda)\, a^{-2}}$
  `H0 = 70.0; Ωm = 1; ΩΛ = 0;`

Mass deposition

`CIC[Data_] := Module[{BinL},`
  `BinL = Mod[BinLists[Mod[Data, L]` $\frac{\text{f2m n}}{L}$`, {0, f2m n}], 1];`
  `Map[w1, BinL] + Map[w2, RotateRight[ BinL, {1, 0}]]]`
`w1 = Compile[{{list, _Real, 1}}, If[Length[list] == 0, 0, Total[(1 - list)]]];`
`w2 = Compile[{{list, _Real, 1}}, If[Length[list] == 0, 0, Total[list]]];`

Integrator

```
In[29]:= LeapFrog[ai_, af_, da_] := Module[{X, P},
         {X, P} = Zeldovich[ai, ai + da / 2, Φ];
         Do[
          X += Drift[a, da, P];
          P -= Re[Kick[a + da / 2, da, X]];
          , {a, ai, af, da}];
         {X, P}
        ]
      Interp1D[Field_, x_] := Module[{X1, X2, xm, xn, rx, f1, f2, n},
         X1 = Floor[x];
         X2 = Ceiling[x];
         xm = Mod[x, 1.0];
         xn = 1.0 - xm;
         n = Length[Field];

         f1 = Table[Field[[Mod[X1[[i]], n] + 1]], {i, 1, Length[x]}];
         f2 = Table[Field[[Mod[X2[[i]], n] + 1]], {i, 1, Length[x]}];

         f1 * xn + f2 * xm
        ]
      Grad2[F_] := 1/12 RotateRight[F, 2] -
        2/3 RotateRight[F, 1] + 2/3 RotateLeft[F, 1] - 1/12 RotateLeft[F, 2]
```

Gravity

```
In[32]:=  Drift[a_, da_, P_] :=  da / (a² Cosmology[H0, Ωm, ΩΛ, a]) P

Kick[a_, da_, X_] := Module[{δ, invm, Φ, acc},
   δ = CIC[X] * m - 1.0;
   invm = Map[If[# == 0, 0, -1/#²] &, fftIndgen[f2m n, L], 1];
   Φ = 3 / 2 Ωm H0² ℱℐ[invm * ℱ[δ]] / a;
   acc = Interp1D[f2m n / L Grad2[Φ], Mod[X f2m n / L, f2m n]];
   da / Cosmology[H0, Ωm, ΩΛ, a] acc
  ]

Zeldovich[apos_, avel_, Φ_] := Module[{u, X, P},
   u = - n/L Grad2[Φ];
   X = Flatten[MapIndexed[L/n #2 + apos #1 &, u]];
   P = avel u;
   m = f2m;
   {X, P}
  ]
```

Run

```
In[45]:=  n = 2⁸; L = 2⁶; σ = 1; ai = 0.02; af = 1.02; ni = 50; da = (af - ai) / ni;
δ = 20 Chop[GRF[n, #^(-1/2) &, L, σ]];
invm = Map[If[# == 0, 0, -1/#²] &, fftIndgen[n, L]];
Φ = ℱℐ[invm * ℱ[δ]];

In[40]:=  n = 2⁷; L = 2⁶; σ = 1; ai = 0.03; af = 1.02; ni = 50; da = (af - ai) / ni;
δ = 5 Table[e^(-0.01 (x-L/2)²), {x, L / n, L, L / n}];
invm = Map[If[# == 0, 0, -1/#²] &, fftIndgen[n, L]];
Φ = ℱℐ[invm * ℱ[δ]];

In[44]:=  f2m = 2; {X, P} = LeapFrog[ai, 1.4, 0.02];
```

N - Body 2D

```mathematica
SetDirectory["C:\\Users\\J.L.
    Fel\\Documents\\Universiteit\\Master\\Master onderzoek (60)"]
```

C:\Users\J.L. Fel\Documents\Universiteit\Master\Master onderzoek (60)

```mathematica
ℱ[f_] := Chop[Fourier[f, FourierParameters → {1, -1}]]
ℱℐ[f_] := Chop[InverseFourier[f, FourierParameters → {1, -1}]]
fftIndgen[n_, L_] :=
  (2 π)/L Flatten[{Range[0., n/2.], -Reverse[Range[1., n/2. - 1]]}]

inv = Compile[{{kx, _Real}, {ky, _Real}}, If[kx == 0 && ky == 0, 0, -1/(kx^2 + ky^2)]];
```

Plotting

```mathematica
Area[{{x1_, y1_}, {x2_, y2_}, {x3_, y3_}}] :=
  Abs[1/2 (x1 y2 + x2 y3 + x3 y1 - x2 y1 - x3 y2 - x1 y3)]
trig[list_] := Module[{}, {Opacity[0.5], ColorData["LightTemperatureMap"][
      0.5 Log[Area[list]^-1]], ColorFunctionScaling → {0, 0.7}, Polygon[list]}];
Mozaic[X_] := Module[{x, T0, T1, T2, T3, Triang1, Triang2, n},

  n = √Length[X] ;
  x = Partition[X, n];
  T0 = Flatten[x, 1];
  T1 = RotateLeft[x, {1, 0}]; T1[[-1, All, 1]](*+=L*); T1 = Flatten[T1, 1];
  T2 = RotateLeft[x, {0, 1}]; T2[[All, -1, 2]] += L - L/n; T2 = Flatten[T2, 1];
  T3 = RotateLeft[x, {1, 1}]; T3[[All, -1, 2]] += L - L/n; T3 = Flatten[T3, 1];
  Triang1 = Transpose[{T0, T1, T2}, {2, 1}][[ ;; -n - 1]];
  Triang2 = Transpose[{T3, T2, T1}, {2, 1}][[ ;; -n - 1]];
  Graphics[Flatten[{Map[trig, Triang1], Map[trig, Triang2]}],
    AspectRatio → 1, ImageSize → 300]]
MP[data_] := MatrixPlot[data^T, DataReversed → {True, False}]
GridPlot[X_] := Show[(*ListPlot[X,PlotStyle→Red,AspectRatio→1],*)
  ListLinePlot[Partition[X, n], PlotStyle → Black, AspectRatio → 1,
    ImageSize → 500], ListLinePlot[Partition[X, n]^T, PlotStyle → Black]]
```

Initial Conditions

```
GRF[size_, Pk_, L_, σ_] :=
 Module[{noise, amplitude, smooth, Pk2, Sm2, kx, ky, data},
   Pk2 = Compile[{{kx, _Real}, {ky, _Real}},
     If[kx == 0 && ky == 0, 0, Sqrt[Pk[Sqrt[kx^2 + ky^2]]]]];
   Sm2 = Compile[{{kx, _Real}, {ky, _Real}}, e^(-(σ)^2 (kx^2+ky^2)/2)];
   noise = Fourier[RandomVariate[NormalDistribution[], {size, size}]];
   amplitude =
    Map[Pk2 @@ # &, Outer[List, fftIndgen[size, L], fftIndgen[size, L]], {2}];
   smooth = Map[Sm2 @@ # &, Outer[List, fftIndgen[size, L],
      fftIndgen[size, L]], {2}];
   data = InverseFourier[smooth * noise * amplitude] // Chop;
   1/Variance[Flatten[data]]^(1/2) data]
```

Cosmology

```
Cosmology[H0_, Ωm_, ΩΛ_, a_] := H0 a Sqrt[ΩΛ + Ωm a^-3 + (1 - Ωm - ΩΛ) a^-2]
H0 = 70.0; Ωm = 1; ΩΛ = 0;
```

Mass deposition

```
CIC[Data_] := Module[{BinL},
   BinL = Mod[BinLists[Mod[Data, L] (f2m n)/L, {0, f2m n}, {0, f2m n}], 1];
 Partition[Map[w1, Flatten[BinL, 1]] +
     Map[w2, Flatten[RotateRight[ BinL, {1, 0}], 1]] +
     Map[w3, Flatten[RotateRight[ BinL, {0, 1}], 1]] +
     Map[w4, Flatten[RotateRight[ BinL, {1, 1}], 1]], f2m n]
w1 = Compile[{{list, _Real, 2}},
    If[Length[list] == 0, 0, (1 - list[[All, 1]]) . (1 - list[[All, 2]])]];
w2 = Compile[{{list, _Real, 2}}, If[Length[list] == 0,
     0, list[[All, 1]] . (1 - list[[All, 2]])]];
w3 = Compile[{{list, _Real, 2}}, If[Length[list] == 0,
     0, (1 - list[[All, 1]]) . list[[All, 2]]]];
w4 = Compile[{{list, _Real, 2}}, If[Length[list] == 0,
     0, list[[All, 1]] . list[[All, 2]]]];
```

Integrator

```
LeapFrog[ai_, af_, da_] := Module[{X, P},
  {X, P} = Zeldovich[ai, ai + da / 2, Φ];
  Do[
   plot = (*GridPlot[X]*)ListPlot[X, AspectRatio → 1, ImageSize → 500,
     PlotStyle → {Black, PointSize[Tiny]}](*MP[Log[CIC[X]]]*);
   X += Drift[a, da, P];
   P -= Re[Kick[a + da / 2, da, X]];
   , {a, ai, af, da}];
  {X, P}
 ]
Interp2D[Field_, x_] := Module[{X1, X2, xm, xn, rx, f1, f2, f3, f4, n},
  X1 = Floor[x];
  X2 = Ceiling[x];
  xm = Mod[x, 1.0];
  xn = 1.0 - xm;
  n = Length[Field];

  f1 = Extract[Field, Mod[X1, n] + 1];
  f2 = Extract[Field, Mod[{X2〚All, 1〛, X1〚All, 2〛}ᵀ, n] + 1];
  f3 = Extract[Field, Mod[{X1〚All, 1〛, X2〚All, 2〛}ᵀ, n] + 1];
  f4 = Extract[Field, Mod[X2, n] + 1];

  f1 * xn〚All, 1〛 * xn〚All, 2〛 + f2 * xm〚All, 1〛 * xn〚All, 2〛 +
   f3 * xn〚All, 1〛 * xm〚All, 2〛 + f4 * xm〚All, 1〛 * xm〚All, 2〛
 ]
```

$$Grad2[F\_, i\_] := \frac{1}{12} RotateRight[F, \{2, 0\}] - \frac{2}{3} RotateRight[F, \{1, 0\}] +$$
$$\frac{2}{3} RotateLeft[F, \{1, 0\}] - \frac{1}{12} RotateLeft[F, \{2, 0\}] /; i == 1$$

$$Grad2[F\_, i\_] := \frac{1}{12} RotateRight[F, \{0, 2\}] - \frac{2}{3} RotateRight[F, \{0, 1\}] +$$
$$\frac{2}{3} RotateLeft[F, \{0, 1\}] - \frac{1}{12} RotateLeft[F, \{0, 2\}] /; i == 2$$

Gravity

```
Drift[a_, da_, P_] := da/(a^2 Cosmology[H0, Ωm, ΩΛ, a]) P

Kick[a_, da_, X_] := Module[{δ, invm, Φ, accx, accy, acc},
  δ = CIC[X] * m - 1.0;
  (*plot=MP[Log[(δ+1)/m]];*)
  invm = Map[inv @@ # &,
    Outer[List, fftIndgen[Length[δ], L], fftIndgen[Length[δ], L]], {2}];
  Φ = 3/2 Ωm H0^2 ℱℐ[invm * ℱ[δ]] / a;
  accx = Interp2D[n/L Grad2[Φ, 1], Mod[X (f2m n)/L, f2m n]];
  accy = Interp2D[n/L Grad2[Φ, 2], Mod[X (f2m n)/L, f2m n]];
  acc = {accx, accy}^T;
  da/Cosmology[H0, Ωm, ΩΛ, a] acc]

Zeldovich[apos_, avel_, Φ_] := Module[{u, X, P},
  u = -{n/L Grad2[Φ, 1], n/L Grad2[Φ, 2]};
  X = Flatten[MapIndexed[L/n #2 + apos #1 &, Transpose[u, {3, 1, 2}], {2}], 1];
  P = Flatten[Transpose[avel u, {3, 1, 2}], 1];
  m = f2m^2;
  {X, P}]
```

Run

```
n = 2^8; L = 50.0; σ = 0.0; ai = 0.02; af = 1.02; ni = 50; da = (af - ai)/ni;
δ = 10 Chop[GRF[n, #^(-0.5) &, L, σ]];
invm = Map[inv @@ # &,
   Outer[List, fftIndgen[Length[δ], L], fftIndgen[Length[δ], L]], {2}];
Φ = ℱℐ[invm * ℱ[δ]];
Grid[{{MP[δ], MP[Φ]}}]

{X, P} = Zeldovich[ai, ai, Φ];
f2m = 2; {X, P} = LeapFrog[ai, af, 0.02];
```

Appendix B

Effective Corrections From Newtonian Symmetries

We here describe the derivation of effective corrections using Newtonian symmetries presented by Mercolli and Pajer [49]. We start with the most general generalization of the conservation of mass and Euler equations and than constrain the equations with symmetries. The symmetries considered are

1. Statistical homogeneity and isotropy

2. Galilean invariance

3. Conservation of the total number of dark matter particles

4. Conservation of the total momentum

5. Equivalence principle

The statistical homogeneity and isotropy symmetry induces two constraints on corrections. Firstly, all numerical coefficients of effective corrections cannot depend on spatial coordinates. Secondly, all expectation values can only depend on the norm of the distance between the points where the operators in the expectation value are evaluated.

Galilean invariance is the invariance of the differential equations under the Galilean transformations $\mathbf{x} \to \mathbf{x} + \mathbf{u}t$ for all velocities $\mathbf{u}$ and times t. Note that under this transformation the density is invariant, $\delta \to \delta$ and the velocity of the dark matter fluid $\mathbf{v}$ transforms as $\mathbf{v} \to \mathbf{v} - \mathbf{u}$. The Eulerian time derivatives transform non trivially since $\partial_t \to \partial_t + \mathbf{u} \cdot \nabla$. From the transformation of the velocity of the dark matter fluid and Eulerian time derivative, it follows that the Lagrangian time derivative $\partial_t + \mathbf{v} \cdot \nabla$ is invariant. We for this reason will use Lagrangian derivatives.

The conservation of the total number of dark matter particles implies that $\int \mathrm{d}\mathbf{x} \partial_t \rho = 0$. Analogously, the conservation of total momentum can be written as $\int \mathrm{d}\mathbf{x} \partial_t (\mathbf{v}\rho) = 0$. The equivalence principle should be seen as the restriction that all particles in a gravitational field experience the same acceleration.

In physical space in terms of Galilean invariant combinations, we can write the most general linear extension of the conservation of mass and Euler equation as

$$(\partial_\tau + \mathbf{v} \cdot \nabla)\rho + C_\theta \theta + C_{\rho\theta}\rho\theta = C_\rho \rho + C_{\Delta\delta}\Delta\delta + C_{\Delta\theta}\Delta\theta,$$
$$(\partial_\tau + \mathbf{v} \cdot \nabla)\mathbf{v} + C_{\nabla\phi}\nabla\phi = C_{\nabla\rho}\nabla\rho + C_{\nabla\theta}\nabla\theta + C_{(\rho+\theta)}(\rho + \theta)\nabla\phi.$$

with $\theta = \nabla \cdot \mathbf{v}$. From the first symmetry, we conclude that all coefficients can only depend on time. From the third symmetry we can conclude that $C_\rho = 0$ and $C_{\rho\theta} = 1$. The fourth symmetry leads to $C_\theta = 1$, while the fifth symmetry induces $C_{(\rho+\theta)} = 0$ and $C_{\nabla\phi} = 1$. Hence the five symmetries reduce the extension to

$$(\partial_\tau + \mathbf{v} \cdot \nabla)\rho + \theta + \rho\theta = C_{\Delta\delta}\Delta\delta + C_{\Delta\theta}\Delta\theta,$$
$$(\partial_\tau + \mathbf{v} \cdot \nabla)\mathbf{v} + \nabla\phi = C_{\nabla\rho}\nabla\rho + C_{\nabla\theta}\nabla\theta.$$

In comoving coordinates we can write these equations as

$$\partial_t \delta + \partial_i[(1+\delta)v^i] = -\chi_1 \frac{\Delta\delta}{\mathcal{H}} + \chi_2 \frac{\Delta\theta}{\mathcal{H}^2}$$
$$\dot{v}^i + \mathcal{H}v^i + \partial^i\phi + v^j\partial_j v^i = -c_s^2\partial^i\delta + \frac{3}{4}\frac{c_{sv}^2}{\mathcal{H}}\Delta v^i + \frac{4c_{bv}^2 + c_{sv}^2}{4\mathcal{H}} + \frac{4c_{bv}^2 + c_{sv}^2}{4\mathcal{H}}\partial^i\nabla \cdot \mathbf{v}.$$